Out-Of-Equilibrium Dynamics and Locality in Long-Range Many-Body Quantum Systems

Lorenzo Cevolani

NNT : 2016SACLO011

THESE DE DOCTORAT
DE L'UNIVERSITE PARIS-SACLAY

préparée à

L'INSTITUT D'OPTIQUE GRADUATE SCHOOL

ÉCOLE DOCTORALE N°572
Ondes et Matière (EDOM)

Spécialité de doctorat : Physique

par

Lorenzo Cevolani

Out-Of-Equilibrium Dynamics and Locality in Long-Range Many-Body Quantum Systems

Thèse présentée et soutenue à Palaiseau, le 2 décembre 2016

Composition du jury :

Mme Patrizia Vignolo	Rapporteur	Institut non-lineaire de Nice
M. Salvatore R. Manmana	Rapporteur	Georg-August-Universität Göttingen
M. Luca Tagliacozzo	Examinateur	University of Strathclyde
M. Guillaume Roux	Examinateur	Université Paris-Saclay
M. Laurent Sanchez-Palencia	Directeur de thèse	Institut d'Optique Graduate School
Mme Leticia F. Cugliandolo	Presidente	Université Pierre et Marie Curie

a mio nonno

Contents

Introduction

Statistical mechanics is one of the most precise theories in modern physics. Despite its age (it is almost 150 years old) the statistical approach is still the fundamental tool to deal with systems made of a macroscopic number of particles. In the presence of the interactions, the microscopic dynamics is impossible to be determined analytically due to the complexity of the equation of motions. In turn, the statistical approach is able to predict averages of macroscopic observables at thermal equilibrium and to connect relevant quantities, such as volume, pressure, temperature, etc..., to the microscopic Hamiltonian without knowing the dynamics of microscopic constituents. Mathematically, this simplification is due to the ergodic hypothesis which allows to compute time averages as phase-space ones.
If the system is slightly out of thermal equilibrium, but still connected to a heat reservoir, the statistical approach is still reliable. The larger system absorbs the excess of macroscopic observables of the smaller one helping it to reach equilibrium. Anyway, The statistical approach fails completely to describe the time evolution of closed systems driven far from equilibrium. Many protocols exist to drive a system out-of-equilibrium, the mostly used one is the so called quantum quench. The system is prepared in the ground state of an initial Hamiltonian $\mathcal{H}_i$ and at $t = 0$ the Hamiltonian is suddenly changed, from $\mathcal{H}_i$ to $\mathcal{H}_f$ modifying one coupling constant. This drives the system far from equilibrium because its initial state is a highly excited state of the final Hamiltonian. The fact that the system is isolated makes the time evolution unitary and the equilibration after long times not always possible.
The time evolution following a quantum quench is far from being ergodic, and the statistical approach no longer holds. The dynamics of macroscopic observables can then be determined just by an explicit solution of the microscopic equations of motion. In the field of out-of-equilibrium dynamics, two are the crucial questions: how local observables time evolve and how the system thermalizes (if it does) long time after the quench.
In the last decade, the realization of cold atomic clouds has pushed the experimental research in this field. These systems can be used to reproduce different Hamiltonians (fermionic, bosonic or spin ones) with a great freedom in the geometry of the system, in the type of interactions and in their strength. The possibility to change the parameters of the Hamiltonian faster than any internal time scale allows us to realize the quench protocol in these experiments. Most important, the fact that these clouds are trapped using electromagnetic fields makes them extremely well decoupled from the environment. The isolated-system hypothesis is then well satisfied over the experimental times and the dynamics of the system is indeed unitary.

Lieb-Robinson bounds Even if it has been possible to obtain crucial results for both the time evolution and thermalization in different experimental situations, much work remains to be done to interpret these complicated phenomena. Many of the theoretical tools used to describe systems at equilibrium cannot be adapted to the out-of-equilibrium. The research on general principles to understand the time evolution is one of the most exciting and difficult problems in modern physics. One of the few results existing in this field are general bounds on the dynamics of local observables, as correlations. They constrain the time evolution of specific observables inside precise portions of the space-time plane. The most famous one is the Lieb-Robinson bound, which applies to lattice models interacting via finite-range potentials, such as nearest-neighbor or contact terms. The authors find a bound on the commutator between two local operators defined over two disjoints set of the lattice. The bound divides the space-time plane in two regions. One where the commutator can be significant and the other where it is exponentially small. It defines then a position-dependent activation time $t^\star\left(R\right) \sim R/v_{lr}$.
The fact that this activation time scales linearly with R points out that it is a straight line in the space-time plane. Two local operators, in order to have a non-zero commutator, need to wait a time proportional to their distance. No surprise then if this is called "light-cone" effect, in analogy to special relativity. It has to be noticed, however, that in this case the correlations are not exactly zero for $t < t^\star$, as in special relativity, but just strongly suppressed.
The quantity studied by Lieb and Robinson in their paper is not accessible in modern experiments. There, the quantities of interest are rather equal-time correlations between local observables, $\langle A_X(t)B_Y(t)\rangle - \langle A_X(t)\rangle\langle B_Y(t)\rangle$, where the expectation value is computed using the initial state of the system $|\Psi_0\rangle$. A bound on this quantity can be derived if we assume rapidly decaying correlations on this state. This bound takes the same form as the previous one and we can say that correlations are created in the system following a linearly increasing light-cone.
This effect has been found in several experimental and numerical works: lattice bosons in different phases, spin models and fermionic systems. There, the velocity of the light-cone can be extracted from the data but it cannot be compared directly to the theory because the value of v_{lr} is not fixed by the bound.
v_{lr} is determined by the so-called microscopic theory. In a system with well defined long-lived excitations, as quasi-particles or other fundamental excitations, with a well defined spectrum, the light-cone velocity for correlations is given by $v_{lc} = 2\max V_k$, where V_k is the group velocity, derived as usual from the energy spectrum. This result provides an easy schematic approach to interpret the spreading of correlations. Following a quantum quench, the sites of the system act as sources of quasi-particles and these are responsible for the dynamics of the observables. Correlations, as well as other local observables, need to wait for the arrival of the fastest quasi-particle to be activated at a given distance. The fastest quasi-particles are then responsible for the first signal in the correlations, i.e. the actual light-cone.

Long-range interacting systems While the situation is rather well understood for short-range interacting systems, many questions remain open for long-range potentials. For instance, for algebraic interactions of the form $V(R) \sim 1/R^{\alpha}$, the Lieb-Robinson bound has been extended. For $\alpha < D$ no bound is known. It means that correlations can a priori be activated at arbitrary large distances in arbitrary short times. For $\alpha > D$, the commutator can be bounded by a potential-dependent expression which gives an activation time of the form $t^{\star} \sim \alpha \ln(R)$. Compared to the short-range case, this bound allows faster-than-ballistic propagation.
This bound has been improved for $\alpha > 2D$. In this case, it becomes algebraic $t^{\star} \sim R^{\beta}$, with $\beta < 1$ which also allows faster-than-ballistic propagation.
These bounds have to be checked in order to see if they are able to reproduce correctly the propagation of correlations or if they have to be improved again. The realization of quantum systems interacting via long-range potentials is possible using trapped ions. They interact like spins with long-range exchange term. These systems respect the general hypothesis of the bounds presented before. The study of the dynamics of different observables points toward the violation of the short-range Lieb-Robinson bounds and faster-than-ballistic propagation appears for sufficiently small values of α. However, such systems are not large enough to be free from finite-size effects and they cannot follow the dynamics for sufficiently long times to have a precise description of the propagation. The typical system size is in fact around 9 ions but the technological improvement is pushing forward to obtain larger chains: at the present moment the maximal length is already 22. Future works will better characterize the propagation of correlations in long-range interacting systems, but for the moment it is fair to say that a quantitative experimental measurement is lacking.
Numerical approaches have then been used to deal with these systems out of equilibrium, in particular, the time-dependent density matrix renormalization group (t-DMRG), the time-dependent variational Monte Carlo (t-VMC), and the truncated Wigner approximation (DTWA). These approaches can be used to explore larger systems for longer times than the ones in experimental set-ups. The results obtained by these methods for one-dimensional spin systems exhibit a richer dynamics than the one expected from the known bounds. In particular, the existence of three regimes of propagation has been pointed out, including an instantaneous (non-local) regime, an algebraically propagating (quasi-local) regime and a ballistic (local) regime. It is then clear that it is necessary to go beyond the present general bounds.

Scope and main results of the thesis The aim of this thesis is to develop analytic approaches to determine the actual behavior of space-time dynamics of correlations in long-range interacting systems. This way, we have been able to reproduce previous results for the long-range Ising model, to give a clear physical picture of the origin of these three regimes, and to predict (surprisingly) slower-than-ballistic propagation of correlations in the quasi-local regime. The latter is confirmed by numerical time-dependent Monte Carlo calculations. Moreover, we have generalized these results to dimension higher than one ($D > 1$) where we find: (i) ballistic (local) propagation for $\alpha > D + 1$, (ii) slower-

than-ballistic (quasi-ballistic) for $D < \alpha < D + 1$, and (iii) instantaneous for $D > \alpha$. The existence of the last two of them is associated to second and first order divergences in the many-body excitation spectrum.
We then focus on a different model: lattice bosons interacting via a long-range potentials (long-range Bose-Hubbard model) in one dimension. We aim to understand if the previous results which determine a connection between the regime of propagation and the energy spectrum of excitations are universal. We start from the density-density correlations and their time evolution that presents a ballistic spreading for every value of α. This is completely unexpected from the general bounds and the analysis of the Ising model, where a transition from a bounded to an unbounded propagation occurs at $\alpha = 1$. We then use again the analytic approach to explain these data. The bosonic model allows again long-lived excitations known as Bogoliubov quasi-particles. They are created following the quantum quench and they spread in the system creating correlations and other observables. For $\alpha > 1$, the excitation spectrum has a finite maximum group velocity. This is compatible with a ballistic propagation and it explains the data of the numeric for these values of α. In turns, for $\alpha < 1$ the maximum group velocity is infinite and one may expect non-ballistic spreading. Studying carefully the observable it is anyway possible to see that not all the modes contribute the same way to the time evolution. Due to the long-range interactions, some parts of the spectrum have a vanishing contribution to the dynamics. Using the quasi-particle picture and the stationary-phase approximation we quantified this contribution and we concluded that the modes with infinite velocity have a completely negligible effect on the dynamics. To prove this argument we compare the velocity of the light-cone extracted from time-dependent Monte Carlo data to the one of the quasi-particles with the largest contribution, finding a perfect agreement.
The previous discussion has showed that the inhomogeneous contribution of quasi-particles has strong effects on the space-time dynamics of quantum correlations. Since the distribution of contributions obviously depends on the observable, one may expect that the correlation dynamics is observable-dependent. We then study another observable, namely one-body correlation function, and its time evolution. There, the quasi-particles that contribute stronger to the time evolution are the ones with infinite velocity. We find then that for $\alpha < 1$ the propagation is algebraic and faster-than-ballistic, meaning that in this case the effect of the infinite velocity modes is not negligible. This last work then allows us to conclude that the energy spectrum is not the only quantity to determine the dynamics of correlations. The role played by the specific observable is completely unexplored in the general bounds but it can be encoded naturally using the quasi-particles picture.

Content of the manuscript

Chapter 1 We start with a comparison between quantum systems at- and out- of equilibrium. Reviewing different results in the literature, we describe how different models are realized in cold atomic gases as well as in other systems and how they can be probed using different techniques. We introduce the reader to the two main problems of the out of-equilibrium dynamics: the spreading of correlations and

the thermalization problem. The latter is described in more details at the end of the chapter. Its classical and quantum descriptions are given and, finally, the experimental observations of thermalization or its absence are discussed.

Chapter 2 This chapter is dedicated to the universal bounds on the dynamics of many-body quantum system as well as the experimental, numerical, and theoretical understandings of short-range interacting models. We review the bounds on these systems on both the commutator and the correlation function starting from the literature works where they are derived. We revise the microscopic approach and the main experimental and numerical observations of the light-cone dynamics of correlations. We finally review several extensions of the previous bound in presence of long-range interactions.

Chapter 3 In this chapter we present the study of long-range interacting spin models, in particular the long-range Ising model in transverse field. We start with a review of its experimental realizations in trapped-ion experiments. We then revise different numerical methods used to study the time evolution of this system. They point out a strong dependence on the interaction decay. This study is based on the quasi-particles approach described before for short-range models. W present then my results based on this method. We provide an analytical description of the three different regimes found in the time evolution. We connect the propagation of correlations to the divergences of the energy spectrum of fundamental excitations of the system. We compare these expressions to the Monte-Carlo results obtained by a collaborator and published in a joint publication. A good agreement between my analytic predictions and the numerical results is found.

Chapter 4 In this chapter we study a system of lattice bosons interacting via a long-range potentials. We want to determine what is universal in the time evolution and what it is not. Numerical simulations find that the propagation of two-body (density-density) correlations in this model is always ballistic. This result cannot be understood as before using the energy spectrum of excitations. In fact, surprisingly, the finite propagation takes place also in the presence of quasi-particles with infinite velocity. We demonstrate that this can be understood looking at the part of the spectrum that contributes most to the time evolution of the observable. This can be used to see that the large velocities present in the spectrum do not contribute to the time evolution. We then study a different observable, namely one-body correlations, finding a faster-than-ballistic propagation. This can be understood using the quasi-particles picture and it opens the door for an observable-dependent definition of locality. We then demonstrate that the time evolution in long-range quantum systems cannot be understood looking just at the energy spectrum, but more quantities have to be involved. Also in this case, we find that the general bounds are not able to reproduce the behavior of the time evolution. The analytical expressions have been obtained by the author and they are compared to Monte-Carlo simulations realized by a collaborator and published in a joint publication.

Introduction en français

La mécanique statistique est l'une des plus importantes théories de la physique moderne. Même si elle a presque 150 ans, l'approche statistique est encore un instrument fondamental pour décrire les systèmes avec un nombre macroscopiquement grand de particules. En présence des interactions, la solution des équations du mouvement est extrêmement compliquée et une solution explicite pour la dynamique du système manque toujours. Par contre la description statistique est capable de décrire les moyennes des observables macroscopiques à l'équilibre thermique et de connecter différentes quantités comme le volume, la pression, la température, etc... sans résoudre complètement les équations du mouvement pour les constituants fondamentaux. Mathématiquement la condition qui assure l'équivalence entre les moyennes statistiques et les moyennes temporelles est appelée condition d'ergodicité. Si le système est très peu hors de l'équilibre thermique et en contact avec un réservoir, le méthode statistique est encore capable de décrire le comportement du système. Dans ce cas, le réservoir absorbe l'excès des quantités macroscopiques présentes dans le système et, le stabilise, et le conduit à l'équilibre. La description statistique est de toute façon complètement inutile si le système est très loin de l'équilibre thermique et est isolé. Un grand nombre de protocoles peut être utilisé pour pousser un système hors de l'équilibre. Le plus utilisé est le quantum quench. Le système est préparé dans l'état fondamental d'un Hamiltonien initial $\mathcal{H}_i$ et à $t = 0$ l'Hamiltonien est changé $\mathcal{H}_i \to \mathcal{H}_f$ selon un changement rapide d'une constante de couplage. Ce changement pousse le système hors de l'équilibre parce que l'état initial est un état énergétiquement très loin de l'état fondamental du Hamiltonien final. En plus, le fait que le système est isolé force l'évolution temporel à être unitaire et la thermalisation aux temps longs n'est pas du tout assurée. Dans ce cas, l'évolution temporelle est loin d'être ergodique et, par conséquent, l'évolution temporelle n'est pas du tout décrite par une simple moyenne statistique. La seule façon de déterminer l'évolution temporelle des différentes observables est de la calculer explicitement à partir des équations de mouvement microscopiques. Les deux questions principales pour ce problème sont : quel est le comportement des observables locales pendant l'évolution temporelle et comment le système thermalise, s'il thermalise. La réalisation de nuages d'atomes ultra froids a revigoré la recherche de nouveaux effets dans la physique hors de l'équilibre. Ces systèmes peuvent être utilisés pour modéliser différents Hamiltoniens (fermioniques, bosoniques et aussi de spin) avec une grande liberté sur le choix de plusieurs paramètres : la géométrie du système, le type et l'intensité des interactions. En particulier, la possibilité de changer l'intensité des interactions extrêmement rapidement, comparé à toutes les échelles de temps internes des nuages, a permit de réaliser avec une grande précision le protocole du quantum quench. Plus important, les nuages sont piégés en utilisant des champs magnétiques ou électriques et ils sont donc presque parfaitement isolés du laboratoire. L'hypothèse d'isolation, fondamentale pour le protocole du quench, est donc bien satisfaite, de sorte que l'évolution temporelle est unitaire.

Borne de Lieb-Robinson Même si plusieurs expériences ont étés menés pour explorer et l'évolution temporelle, et la thermalisation, en obtenant des résultats cruciaux pour les deux champs de recherche, un grand travail reste à faire du coté théorique pour expliquer en profondeur ces phénomènes. En fait, la plupart des approches théoriques et numériques utilisées pour étudier les systèmes quantiques à l'équilibre sont complètement inutiles quand on est hors de l'équilibre. La recherche des principes généraux pour comprendre precisament la dynamique des systèmes quantiques en interaction est donc devenue l'un des plus intéressants et difficiles problèmes pour la physique moderne. Un des rares résultats généraux pour la dynamique des corrélations est la présence de bornes sur leur évolution temporelle. Ces bornes forcent la dynamique dans des régions spécifiques du diagramme d'espace-temps. Le plus connue de ces bornes est la borne de Lieb-Robinson qui s'applique aux systèmes de spins sur réseau avec interactions à courte portée, comme les interactions premier-voisin. Les auteurs trouvent une borne sur le commutateur entre deux observables localisés sur deux parties disjointes du réseau. La borne détermine une séparation entre deux parties du diagramme espace-temps. Une zone où le commutateur est grand et une autre zone où il est exponentiellement petit. La séparation entre ces deux zones définit un temps d'activation qui est proportionnel à la distance entre les deux zones $t^\star \sim R/v_{lr}$. Le fait que ce temps d'activation dépend linéairement de la distance R définit cette ligne de séparation comme une droite. Donc, deux observables localisées dans deux zones distantes R, doivent attendre un temps fini $t^\star$ proportionnel à R pour avoir un commutateur significativement différent de zéro. Par analogie avec la relativité restreinte, cet effet est appelé cône de lumière. Il faut noter que les commutateurs pour temps précédents au temps d'activation n'est pas exactement zéro, comme dans la relativité restrainte, mais simplement extrêmement petit.
La quantité étudiée par Lieb et Robinson dans leur papier n'est pas accessible aux expériences. Dans ce cas, les quantités mesurées sont les corrélations au même temps $\langle A_X(t)B_Y(t)\rangle - \langle A_X(t)\rangle\langle B_Y(t)\rangle$ où la valeur moyenne est calculée pour l'état initial du système $|\Psi_0\rangle$. Cette quantité peut être bornée en utilisant le résultat de Lieb et Robinson si on suppose que le corrélations présentes avant le quench décroissent exponentiellement avec la distance. La borne sur les corrélations dans ce cas prend la même forme que pour le commutateur. Les corrélations donc sont activées avec un cône balistique qui se propage à vitesse finie.
Ce effet a été trouvé dans plusieurs expériences et travaux numériques : bosons sur réseau dans les phases isolante et superfluide, modèles de spin et systèmes fermioniques. Les donnés peuvent être utilisées pour déterminer expérimentalement la vitesse de propagation des corrélations. Cette vitesse ne peut être comparée directement à la borne parce que elle ne détermine pas la valeur de la vitesse de Lieb-Robinson.
La vitesse de propagation peut être fixée en utilisant la théorie microscopique. Si dans le système il y a des excitations bien définies, comme des quasi-particules ou des magnons, avec une spectre E_k, la vitesse du cône est déterminée par $v_{lc} = \max V_k$, où V_k est la vitesse du groupe des excitations $V_k = \partial_k E_k$. Ce résultat nous donne une façon simple d'interpréter physiquement le phénomène de la propagation des corrélations. Après un quench, les sites du réseau émettent ces excitations qui se propagent dans tout le sys-

tème en transportant les corrélations et autres observables locales. Pour avoir un signal à une distance fixée dans une observable, on doit attendre l'arrivée des excitations les plus rapides qui créent le premier signal. Ces excitations sont donc responsables du cône et leur vitesse détermine la vitesse du propagation des corrélations.

Interactions à longue portée La dynamique des corrélations dans des systèmes avec interactions de courte portée est donc bien comprise. Pour la dynamique en présence d'autres types d'interactions, en particulier les interactions à longue portée, la physique n'est pas du tout claire. La forme typique de ces interactions est une décroissance algébrique avec la distance $1/R^{\alpha}$. Pour cette forme d'interactions la borne de Lieb-Robinson a été etendue. Pour $\alpha < D$, où D est la dimension du système, aucune borne a été trouvée pour systèmes infinis pour l'instant. Cela nous permet de supposer que les corrélations et autres observables locales peuvent être activées arbitrairement loin en un temps arbitrairement petit. Pour $\alpha > D$, le commutateur entre deux observables locales est borné par une expression qui dépend explicitement du potentiel. Il est possible de définir un temps d'activation qui dans ce cas dépend logarithmiquement de la distance $t^{\star} \propto \alpha \ln(R)$. Comparé avec le cas des interactions à courte portée, quand les interactions sont à longue portée la propagation peut être beaucoup plus rapide que balistique. Cette borne a été améliorée pour $\alpha > 2D$ où le temps d'activation prend une forme algébrique $t^{\star} \propto R^{\beta}$ avec $\beta < 1$ qui détermine aussi une propagation plus rapide que balistique.
Ces bornes doivent être testées pour confirmer si elles sont capables de décrire correctement la propagation des corrélations ou elles doivent être encore améliorées. En laboratoire est possible réaliser des systèmes des ions avec interactions à longue portée et les pousser hors de l'équilibre pour étudier l'évolution temporelle de différents observables expérimentalement. L'analyse des donnés expérimentales pour la propagation des corrélations dans ces systèmes confirme la violation des bornes de Lieb-Robinson pour des systèmes de courte portée. En plus, un horizon dans le temps d'activation est présent et pour des valuers de α suffisamment petites cet horizon est algébrique et super-balistique. Ces systèmes ne sont pas assez grands pour être exempts des effets de taille finie. Le nombre d'ions typique dans ces systèmes est $9 \sim 10$, ce qui rend ces systèmes plutôt petits, en particulier pour des interactions de longue portée. Le développement technologique est en train d'améliorer les techniques expérimentaux et au moment présent, il est possible de réaliser des systèmes de 22 ions, qui ont été utilisés pour étudier la thermalisation dans ces systèmes. C'est donc probable que les travaux futurs sur la propagation des corrélations dans ces systèmes amélioreront considérablement les mesures, mais pour le moment il est juste d'affirmer que des mesures quantitatives manquent.
Différentes méthodes numériques ont été développées pour étudier ces systèmes hors de l'équilibre : le Density Matrix Renormalization Group dépendant du temps (t-DMRG), le Monte Carlo variationnel dépendant du temps (t-VMC) et l'approximation de Wigner (DTWA). Ces méthodes peuvent simuler l'évolution temporelle de systèmes un ordre de grandeur plus grands de ceux réalisés en laboratoire. Les premiers résultats obtenus par ces méthodes présentent une dynamique beaucoup plus riche que celle envisagée par les bornes. Trois régimes sont en fait présents dans la propagation : un régime instantané

(non local), un régime où les corrélations se propagent algébriquement (quasi-local) et un régime où les corrélations se propagent balistiquement (local). Ces résultats montrent la nécessité d'une description plus précise que celle donnée par les bornes.

But et résultats principaux de la thèse Le but de cette thèse est de présenter une méthode analytique pour déterminer le comportement de la propagation des corrélations dans des systèmes avec interactions de longue portée. Avec cette méthode nous avons reproduit les résultats présents dans la littérature pour le modèle de Ising, donné une interprétation claire de l'origine des trois régimes présents dans la dynamique et démontré qu'une propagation sub-ballistique est présente dans le régime quasi-local. Bien qu'une propagation sub-balistique soit surprenante en présence d'interactions de longue portée, ce résultat est confirmé par des simulations Monte Carlo. Nous avons ensuite généralisé nos résultats analytiques en dimension quelconque et trouvé encore trois régimes : (i) un régime balistique pour $\alpha > D + 1$, (ii) un régime sub-ballistique pour $D < \alpha < D + 1$ et (iii) un régime instantané pour $\alpha < D$. L'existence des deux derniers est associée aux différents divergences dans le spectre d'excitations.
Nous avons ensuite étudié un modèle de bosons sur réseau avec interactions de longue portée (long-range Bose-Hubbard model) en une dimension. Cette étude veut comprendre si la relation entre le spectre d'excitations et le régime des propagation démontrée pour le modèle de Ising est universel ou non. Nous étudions les corrélations densité-densité et nous trouvons que le propagation de cet observable est balistique pour toutes les valeurs de α. Ce résultat n'est pas prévu si on regarde juste les bornes. L'analyse faite sur le modèle de Ising montre en effet,une transition entre un régime instantané et un régime avec un forme de localité à $\alpha = 1$. On utilise donc encore une méthode analytique pour expliquer ces donnés. Les excitations fondamentales pour ce modèle sont les particules de Bogoliubov. Ces quasi-particules sont créées après le quench et elles se propagent dans le système avec les observables locales. Pour $\alpha > 1$, le spectre des excitations a une vitesse de groupe bornée et cela est en accord avec une propagation balistique avec une vitesse finie. Par contre, pour $\alpha < 1$, la vitesse maximale est infinie et une propagation non balistique est attendue. Une étude plus approfondie de l'observable permet de comprendre que la contribution des différentes quasi-particules à l'évolution temporelle de l'observable n'est pas la même pour tous. En utilisant les quasi-particules, il est possible de quantifier la contribution des différents modes à l'observable et de déterminer que la contribution des quasi-particules avec une vitesse infinie est complètement négligeable comparée aux autres. Nous avons ensuite comparé la vitesse extraite des données Monte Carlo et la vitesse des quasi-particules qui donnent la contribution majeure à l'observable et nous avons trouvé un accord parfait entre les deux.
L'analyse des corrélations densité-densité a confirmé que les inhomogénéités des contributions des différentes parties du spectre ont un effet très important sur la propagation des observables. Les poids qui quantifient les différents contributions des différentes quasi-particules dépendent fortement de l'observable et on peut donc conclure que la propagation dépend de l'observable. Nous avons donc étudié une observable différente, les corrélations à un corps, et son évolution temporelle. Pour ce observable spécifique,

la contribution majeure vient des modes de vitesse infinie. Nous avons trouvé que pour $\alpha < 1$ la propagation est algébrique et plus rapide que balistique, ce qui confirme que les quasi-particules avec une vitesse infinie contribuent à la propagation. Ce dernier travail nous permet de confirmer que le spectre des excitations n'est pas toujours la seule quantité qui détermine la propagation des observables. Les observables même jouent un rôle fondamental pour la détermination de l'évolution temporelle. Ce rôle est complètement inexploré par les bornes générales mais il peut être pris en compte très facilement en utilisant le méthode analytique développée dans cette thèse.

1 Out-of-Equilibrium dynamics of many-body quantum systems

1.1 From equilibrium to out-of-equilibrium physics

Statistical mechanics [1] is one of the most precise and powerful techniques in modern theoretical physics. It explains how to describe a variety of systems made of a huge number of degrees of freedom using just a small number of macroscopically measurable parameters. In particular, we deal with systems at the equilibrium once these parameter do not change appreciably in time.
On the one hand, the thermodynamics was able to well describe the properties of fluids and gases at equilibrium in terms of some simple quantities such as pressure, volume, and moles without a microscopic theory [2].
On the other hand, classical mechanics describes the motion of classical particles and more complicated rigid objects as points in the phase-space, a mathematical space defined by the positions and the momenta of all the classical particles. The state of the system moves in this space according to the Hamilton equations of motion, which are extremely precise [3]. Moreover, the atomistic theory infers that all the macroscopic objects are composed by more fundamental constituents, say atoms or molecules, that fulfill these equations of motion. Statistical mechanics determines the macroscopic behavior of liquids and gases from the microscopic behavior of atoms, connecting the atomic lengths and time scales to the macroscopic ones of the typical systems studied in thermodynamics.
The dimension of the phase-space for N point-like classical particles in a three dimensional space is equal to $6N$, that is $3N$ spatial coordinates and $3N$ momenta. Thanks to statistical mechanics, it is possible to describe the system on a macroscopic scale in terms of just a small number of parameters. It is in fact clear that the motion of atoms at a microscopic level is much faster than the macroscopic one. This difference in length and time scales makes it possible to average out these microscopic degrees of freedom and to find an effective and simpler description at larger scales.
The discovery of quantum mechanics sparked a dramatic revolution in the way we see the microscopic world and its behavior. A system is described by a wave-function, which is mathematically a vector in a Hilbert space, and its time evolution is given by the Schrödinger equation [4]. This new description of the microscopic theory is anyway naturally encoded in statistical mechanics using the same hypothesis as in the classical case, i.e. ergodicity. Anyway, at the quantum level, a huge distinction between two different types of particles have to be done: bosons and fermions. The difference between them relies on the microscopic level: two bosonic particles can be exchanged without changing

the wave-function while the same process involving two fermions changes the sign of the wave-function.
This imposes a constraint to the number of particles that can occupy a single quantum state: if they are bosons this number can range from zero to infinity while just one fermion can occupy a state at most. The consequences of these statistics are not only at the microscopic level but also at the macroscopic one. Even if differences between these two types of particles are usually small at large temperatures, when the system is at absolute zero temperature, or at extremely low temperatures, bosonic and fermionic systems have different behaviors. On one hand, the ground state of a bosonic system is defined as the state where all the particles occupy the lowest single-particle energy state. This effect is known as Bose-Einstein condensation and it has been observed experimentally in 1995 in [5, 6]. The system in this state has a macroscopically large wave-function thanks to its huge coherence length. This state exhibits features typical of the quantum world on macroscopic length scales, such as superfluidity, which was, at the beginning, not distinguished from Bose-Einstein condensation.
On the other hand, the ground state of a system of N non-interacting fermions has a completely different structure because of the Pauli exclusion principle. Fermionic particles cannot condensate in the lowest energy state and they occupy the N lowest single-particle energy levels. This state is called a Fermi sea and it is fundamental to describe many physical properties like the atomic structure and the consequent stability of matter, metals, semiconductors, and also the physics of massive stars such as supernovae.
Previous examples are meaningful when interactions between particles vanish, but they can significantly change the physics of both bosons and fermions. If interactions between fundamental constituents are small, bosonic and fermionic systems can be described using different perturbative approaches. Bosonic systems are described by accurate quadratic theories, such as the Bogoliubov theory of superfluidity [7]. On the other hand, when interactions between fermions are allowed at zero temperature, extreme effects appear. The most studied one is superconductivity, discovered in Leiden in early 1900, and explained by Bardeen Cooper and Shrieffer [8] after almost 50 years. This effect is induced by the interaction between the vibration of the metallic crystal and the electrons in the conducting band and it consists in a vanishing resistance of some metals at extremely low temperature.
All the results obtained in equilibrium statistical mechanics, both classical and quantum, rely on the assumption that the dynamics of the system is ergodic. Ergodicity allows to get rid of the microscopic dynamics of the constituents of the system and to compute expectation values simply as averages over a defined surface. In Sec. 1.5.1 we will give more details about ergodicity and how it is not always present when the systems are out of equilibrium.

The reader could anyway say that equilibrium physics is quite rare, usually a nontrivial time evolution is present in physical systems at any scale. Not all the results of statistical theory fail to describe such situations. If we think about the simple problem of two systems with different macroscopic parameters in contact, we know that there

is a transport of energy, particles, and other quantities between them in order to reach a new equilibrium for the global system. If the amount of "quantities", like energy for example, exchanged is small compared to its total amount, then the system can still be described by statistical mechanics using linear response theory [9]. If this is not the case, then statistical mechanics fails to describe the dynamics and the system is "far-from-the-equilibrium".
Once far from equilibrium, the full dynamics of the microscopic constituents has to be solved in order to infer the macroscopic one. The time dependence of the observables has to be computed explicitly from the microscopic equation of motion [10]. Driving a system out-of-equilibrium in a controlled way and measuring microscopic quantities with a high degree of precision have been impossible tasks until recent times. Thanks to new cold atomic setups, now it is possible to engineer different types of systems and, in particular, to realize close quantum systems [11]. In Sec. 1.3 we will describe in detail these cold atomic setups. This is almost impossible in standard condensed-matter systems because of the presence of the phononic degrees of freedom or of the environment which cannot be neglected. The presence of a thermal bath tends to destroy the quantum nature of the microscopic quantum time evolution, making it more classical.
A deep understanding of this far-from-equilibrium dynamics in both classical and quantum systems is fundamental to describe properly the physical world we observe. Physics, at all scales, shows strong out-of-equilibrium effects from the time evolution of the Universe after the big-bang to the dynamics of small clouds of atomic gases in cold atomic experiments. Moreover, several technological applications of the dynamics of quantum many-body systems are possible, the most important one is related to the quantum computer. This device will perform local operations on quantum q-bits and clearly, these processes are all out-of-equilibrium ones. No-one would ever buy a computer without the possibility to change its internal state, i.e. the information contained in it.

1.2 Open questions in far-from-equilibrium quantum dynamics

1.2.1 A simple example: The Kapitza pendulum

The out-of-equilibrium dynamics is sometimes impossible to predict from the mere knowledge of the equilibrium one. Completely new effects appear during the time evolution of physical systems far-from-equilibrium. A simple example where this occurs is the Kapitza pendulum [12, 13]. Here, a simple time-dependent perturbation of an extremely simple physical system gives rise to an drastic change in its physics. Before describing the Kaptiza pendulum, we briefly review the physics of the standard pendulum at equilibrium.
The mechanical energy of the system, represented in Fig. 1.1, is

$$E = m\frac{l^2}{2}\dot{\theta}^2 - mg\cos(\theta)$$

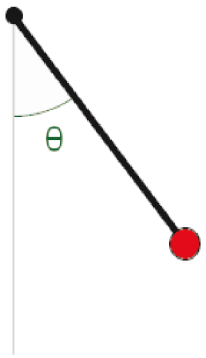

Figure 1.1: Representation of the physical pendulum. Two equilibrium positions are present as function of θ: a stable one at $\theta = 0$ and an unstable one at $\theta = \pi$. From Wikipedia.

where θ is the angle describing the amplitude of oscillations, m is the mass of the particle, l is the distance from the fulcrum, and g is the gravitational acceleration. The equilibrium position of the system can be found imposing $\partial_\theta E = 0$ at $\dot{\theta} = 0$. We find that $\theta = 0$ and $\theta = \pi$ are the two equilibrium positions. Anyway, these are not of the same type: $\theta = 0$ is a stable equilibrium position, while $\theta = \pi$ is an unstable one. In the first case a force always points to the equilibrium position forcing the pendulum to oscillate around it. In the second case the force pushes the point far away from the unstable equilibrium position. This respects the everyday intuition: if the pendulum is placed at $\theta = \pi$ a small perturbation is sufficient to push it far away from it. The situation drastically changes when the system is driven out-of-equilibrium. This can be done inducing oscillations of frequency Ω and amplitude a of the fulcrum. A schematic representation is presented in Fig. 1.2 where now the angle θ is referred to the vertical line.
If Ω is small compared to the typical frequency of the pendulum ω, then the system can be described again using the equilibrium physics. At every time t the system can be considered at equilibrium and it has oscillations of frequency ω around the point where the fulcrum is. In this case the out-of-equilibrium protocol affects the system as a modulation.
When the frequency Ω becomes much larger than ω the situation drastically changes. In this case the system is far from equilibrium and the effects of the oscillations of the fulcrum cannot be simply taken into account as simple modulations and here it is the point where our intuition fails. Averaging over the extremely fast and small oscillations of the fulcrum, represented by $a/l \ll 1$ and $\omega/\Omega \ll 1$ with $a\Omega/l\omega$ finite, we obtain an effective potential

$$V_{eff} = -mgl\cos(\theta) + \left[\frac{1}{2}ma\Omega\sin(\theta)\right]^2,$$

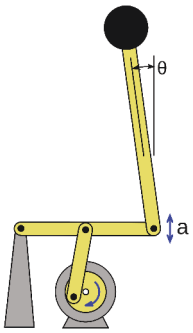

Figure 1.2: Schematic representations of the Kaptiza pendulum. The Kapitza pendulum is a standard pendulum where the fulcrum oscillates with frequency Ω and amplitude a, as represented in the figure. When Ω is sufficiently larger (see text for details) the upper equilibrium position $\theta = 0$ in this figure, $\theta = \pi$ using the reference of the previous figure, becomes stable. This effect is due to the fact that the system is driven out of equilibrium using an oscillating drive. From Wikipedia.

where a is the amplitude of the oscillations of the fulcrum that has to be much smaller than l. The equilibrium positions of the effective potential are then

$$\partial_\theta V_{eff} = m \sin(\theta) \left[gl + \frac{a^2\Omega^2}{2} \cos(\theta) \right] = 0.$$

$\theta = 0$ and $\theta = \pi$ are again the equilibrium positions, but if we compute the second derivative of the effective potential we have

$$\partial_\theta^2 V_{eff} = m \left[gl \cos(\theta) + \frac{a^2\Omega^2}{2} \left(2\cos^2(\theta) - 1 \right) \right].$$

For the equilibrium position at $\theta = \pi$ its value is

$$\partial_\theta^2 V_{eff}(\theta = \pi) = -mgl + \frac{ma^2\Omega^2}{2},$$

which is larger than zero, meaning a stable equilibrium point, if

$$\frac{a^2\Omega^2}{\omega^2 l^2} > 2.$$

This stabilization of the upper equilibrium point is completely unpredictable from the study of the system at equilibrium. This effect depends also on the protocol used to drive the system out of equilibrium. Different protocols, or the same protocol with different parameters, do not lead to the same physical results. In our example this is represented by the two different behaviors for small and large values of Ω compared to ω.

1.2.2 A difficult problem

The specific problem of the Kapitza pendulum points out that an ad hoc description for out-of-equilibrium physics is needed. Different types of innovative methods have been developed in last years [14, 11], and many more will be created in the future. The aim is to create a comprehensive set of theoretical, numerical, and experimental tools to study and understand out-of-equilibrium physics.
The dynamics of a many-body quantum system, which is the topic of this manuscript, is always extremely difficult to solve analytically. The complexity of the mathematical problem grows exponentially with the number of constituents if they are interacting. However, some models are exactly solvable [15], and they play a key-role in the theoretical analysis of out-of-equilibrium physics. Examples of these systems are the ones described by quadratic Hamiltonians, or others solvable by more complicated methods as the Bethe ansatz [16]. Even if the number of such models is quite small, they are important to push the research in model-independent results that can be applied to more complicate situations.
In order to check the validity of these more general results, new numerical and experimental methods have been developed. Quantum Monte Carlo (QMC) [17] and Density Matrix Renormalization Group (DMRG) [18] are two excellent and extremely precise tools to study the physics at the equilibrium. Anyway, they are not suited for the out-of-equilibrium physics in their usual form. Extensions of these methods have been proposed to make them reliable and suitable for this new challenge. In particular, the DMRG has to deal with the strong increasing of the entanglement during the time evolution. This effect has been corrected in the time-dependent DMRG (t-DMRG [19, 20] and TEBD [21]) algorithm which is now able to study the time-evolution of many out-of-equilibrium problems. We will present some results obtained using this method later, see Sec. 2.3.1 and 3.2. The time-Variational Monte Carlo [22, 23] is the extension to time-dependent problems of the Quantum Monte Carlo. This methods is based on an ansatz of the wave function of the Jastrow type [24] with time-dependent complex parameters. The time-evolution of these parameters is described by a first-order differential equation that gives the dynamics of the wave function and the observables. This method will be described in detail later in this manuscript 2.3.1.

The experimental tools play also a key-role in the research in out-of-equilibrium physics, the goal of this study is to use experimental setups as quantum simulators [25]. The idea behind a quantum simulator is to use a quantum system to simulate the behavior of a much more complicated model. This is a conceptual breakthrough in the way we used to see an experimental setup.
A quantum simulator can:

- reproduce single- and many-particle physics, from the kinetic to the interaction terms
- be prepared in a generic state with a high degree of precision

- perform precise manipulations on the state of the system
- access the result of the simulation probing the system

Even if these requirements are extremely difficult to satisfy, modern cold atomic gases are the perfect examples of quantum simulators. We will see how these systems are prepared and how they are used to study the out-of-equilibrium dynamics, in between other extremely important problems, in Sec. 1.3.
While we have powerful numerical methods available, t-DMRG and t-VMC, and extremely versatile experimental setups it is useful to develop new analytical methods as well. The importance of the theoretical works for this field relays in their possibility not to solve just one specific problem, but to generalize its solution to a more general class of them. This will help to build a consistent physical picture that can be used to interpret also numerical and experimental results obtained in more complicated situations.

1.2.3 Open challenges

In this manuscript we will focus on the dynamics of many-body quantum physics driven out of equilibrium. As we saw in the Kapitza pendulum example: the protocol is a crucial part of the description of out-of-equilibrium physics 1.2.1.
We will choose the simplest available protocol: the quantum quench. It consists in preparing the system in an eigenstate of an initial Hamiltonian $\mathcal{H}_i$ and then performing a sudden change to a new one $\mathcal{H}_i \to \mathcal{H}_f$. This change is obtained by varying the value of one of the coupling constants in the Hamiltonian. After the change in the Hamiltonian, the system is decoupled from the environment and it evolves in time with a unitary evolution. We will focus on instantaneous variations of the parameters but it is possible to take into account also slow quenches, where the change takes place over a finite time.
The perfect isolation of the system, crucial for the quench protocol, is extremely challenging to be realized in a laboratory. Such condition is anyway present in modern cold atomic gases (see Sec. 1.3.4). These systems are able to simulate different types of interacting models and they can follow the time evolution on different times scales.
Even if many different works are published every day in the field of out-of-equilibrium physics, they can be classified in two general macro-categories:

- The time evolution of observables during and right-after the out-of-equilibrium protocol.
- The description of the state reached by the system long time after the out-of-equilibrium protocol.

The first question is the main topic of this manuscript and it will be discussed in detail in next chapters. In particular, the role played by the range of interactions during the time evolution will be extensively discussed. When interactions are short-range, the perturbation induced by a local observable spreads in the system linearly in time and space, see Sec. 2.1. In the case of "long-range" interactions, different regimes appear depending on the model and the observable.

For what concerns the thermalization problem, it is an extremely interesting and exciting field of study. We will give a brief description, far from being complete, in Sec. 1.5 but it will not be further discussed in the rest of the manuscript.

1.3 Ultracold atoms as model systems

As we said, cold atomic gases are systems used to mimic the behavior of different classes of many-body quantum systems. We are now going to discuss in detail, how it is possible to realize these systems and to use them to explore the out-of-equilibrium behavior of quantum systems.

1.3.1 Gaseous systems at low temperatures

As first, we want to put the gas in a regime where quantum effects are dominant. This is called the quantum degenerate regime. The crossover between the classical and degenerate regime in three dimensions is defined by the condition

$$\lambda^3 n \sim 1, \tag{1.1}$$

where n is the density of particles, and λ is the de Broglie wave-length of a particle of mass m at temperature T

$$\lambda = \frac{h}{\sqrt{2\pi m k_B T}}.$$

The value of λ determines the length scale where quantum effects are relevant. If its value is much smaller than the typical inter-particle distance, $(1/n)^{1/3}$, then quantum effects do not affect the classical motion. On the contrary, if $\lambda \gg (1/n)^{1/3}$, the quantum nature of particles cannot be neglected. Quantum statistics as the Bose-Einstein or Fermi-Dirac distributions has to be taken into account. The separation between the classical and the quantum regime is then defined by relation (1.1).

1.3.1.1 Quantum gases in the degenerate regime

We want now to describe how it is possible to obtain this regime in an experimental setup. Many different experimental techniques have been used and they improve quickly trying to obtain better and better results. The aim of all of them is to obtain compressed and cold atomic clouds in the quantum degenerate regime.

Laser-cooling Generally, the atoms are extracted from a source, which releases an atom cloud traveling pretty fast, its velocity is around a few hundred meters per second. The atoms are usually extracted at room temperature or even higher temperatures, depending if they come from an oven or not. In both cases, they are extremely far from the quantum degenerate regime.
The first process to enter in this regime is the laser cooling of atoms [26]. It consists in

the application of six counter-propagating laser beams, two for every spatial direction, to slow down the atoms. The lasers act as a viscous force

$$F_{Lasers} = -\alpha v,$$

where α is the effective viscosity and v is the velocity of atoms.
In order to confine atoms in the region hit by the lasers, a magnetic field B is applied inducing a linear force

$$F_{trap} = -Bx$$

which traps the atoms along the direction x.
This step aims at loading the trap with a sufficiently large number of atoms and starting to slow them down with the lasers. The slow-down process cannot go on forever. It is balanced by cycles of absorption-emission of photons by the atoms inducing dissipative forces on the atoms, hence producing heating effects. When the slow-down and absorption-emission processes balance each others, the temperature of the cloud is around some millikelvin. The magnetic confinement is then turned off and the cloud then is cooled down to tens of hundreds of microkelvin thanks to the lasers alone.

Trapping The cloud is now extremely cold but it is not sufficiently dense to enter in the degenerate regime. Instead of decreasing the temperature, i.e. increasing λ, the degenerate regime is achieved compressing the cloud, i.e. increasing the value of n. This is done using the force induced on the atoms by the laser beams.
An oscillating electric field $\mathbf{E}(\mathbf{r}, t)$, as the one created by a laser beam acts on the electrons inside the atoms polarizing them. Due to their interaction with the electric field the atoms gain a dipole moment $\mathbf{d}$. In the case of a laser beam with frequency ω_L, the components of the vector $\mathbf{d}$ can be written as

$$d_i = \sum_j \alpha_{ij}(\omega_L) E_j(\mathbf{r}, t),$$

where i and j label the components in three dimensional space [27] and ω_L is supposed far from atomic transitions.
The energy shift value ΔE is given by the Stark effect [28]

$$\Delta E = \sum_{i,j} \alpha_{ij}(\omega_L) \langle E_i^*(\mathbf{r}, t) E_j(\mathbf{r}, t) \rangle,$$

where the average $\langle \ldots \rangle$ is performed over several oscillations of the field. The dominant contribution to the summation is the term where the energy $E_1 = \hbar\omega_1$ is closest to the laser $\Delta = \omega_L - \omega_1$. The polarizability tensor α_{ij} can then be approximated by

$$\alpha_{ij}(\omega_L - \omega_1) \propto \frac{\delta_{ij}}{\Delta}$$

and the energy shift

$$\Delta E \propto \frac{1}{\Delta} \langle |\mathbf{E}(\mathbf{r}, t)|^2 \rangle \propto \frac{I(\mathbf{r})}{\Delta},$$

where $I(\mathbf{r}) = \langle |\mathbf{E}(\mathbf{r},t)|^2 \rangle$ is the intensity of the laser.
The effective potential induced on the atoms is then

$$V_{opt}(\mathbf{r}) \propto \frac{I(\mathbf{r})}{\Delta},$$

which follows the intensity profile of the laser beams and it can be attractive or repulsive depending on the sign of Δ. If $\Delta < 0$ the laser is red detuned and the atoms are attracted by the region where the intensity is larger. Conversely, when the laser is blue detuned $\Delta > 0$ the atoms are pushed away from the same regions. Different geometries can be realized changing the shape of $I(\mathbf{r})$.
In the standard case, $I(\mathbf{r})$ has a gaussian shape

$$I(\mathbf{r}) \sim I_0 e^{-\frac{|\mathbf{r}|^2}{2\sigma^2}},$$

where $I_0 > 0$ is the maximal intensity and σ is its typical size. If I_0 is larger than any intrinsic energy scale of the atomic cloud, then it will lay at the bottom of the potential created by the laser. There, the potential can be approximated by an harmonic shape

$$V(\mathbf{r}) = \frac{I(\mathbf{r})}{\Delta} \approx \frac{I_0}{\Delta} - \frac{I_0}{\Delta\sigma^2}\frac{|\mathbf{r}|^2}{2}. \tag{1.2}$$

Different potentials can be obtained by shaping $I(\mathbf{r})$ at will.

Evaporative cooling At this stage, it is sufficient to decrease again the temperature of the cloud to enter the degenerate regime. This is achieved using evaporative cooling techniques [29]. In this process, we lower the value of I_0 in Eq. (1.2) at the energy of the most energetic particles in the potential well. In this way we let the atoms with large velocities, i.e. the part of the cloud with a high temperature, escape out of the trap. The residual part of the cloud, composed by the slowest particles, thermalizes at the bottom of the trap. This process needs scattering between the remaining atoms in the trap to reach a well definite temperature. The residual cloud inside the trap has then a temperature smaller than the initial one. Even if loosing atoms is not helping our gas entering the degenerate regime, it decreases n, the loss of a small amount of energetic atoms is compensated by the huge decreasing in the temperature. At this stage the gas is now at the quantum degenerate regime, where $n\lambda^3 \gg 1$, and the temperatures are $1 \sim 500$ nK. The atomic cloud in these conditions is fully dominated by quantum effects.

1.3.1.2 Measurements in cold atomic gases

Once our system has been prepared in the degenerate regime, it is important to have methods to probe it. Different ways allow to measure different observables in the atomic cloud, in particular densities in real and momentum space. The most simple way to do that is to shine the cloud with a laser beam and to analyze the resulting shadow. The decreasing of the intensity of laser depends on the density of the cloud and we can

then reconstruct the position of the every atom. These measurements are called *in-situ* measurements and they are used to obtain the spatial density $n(\mathbf{r})$ of the cloud. These are destructive measurements, the states of the atomic cloud before the measure are completely different. For lattice models, which we will describe in Sec. 1.3.2, the precision of modern measurements of this type can reach the single-site resolution or even single-excitation precision [30].
The density in momentum space are obtained using *time-of-flight* measurements. There, the trap confining the atoms is suddenly turned off and the atomic cloud expands while falling. Shining the cloud during its expansion and comparing it to the initial state allows to determine the momentum distribution $n(\mathbf{k})$. Since the cloud can be assumed to expand freely, at least for some small times after its release, the momentum is given by $\mathbf{k} = m\mathbf{R}/t$ where $\mathbf{R}$ is the position of the cloud. Clearly, this method is also destructive because once the cloud is released and shined with leaser beams, the system has to be regenerated from the very beginning.
A third method that is used in many out-of-equilibrium experiments is the matter-wave interference [31] technique. It consists in preparing the system inside a trap, as we described before, and then splitting the cloud in two identical parts. This is possible thanks to an extremely fast change of the intensity $I(\mathbf{r})$ of the laser from a single to a double potential-well configuration. The potential barrier can be set in a way that the two systems in the two potential wells do not interact and they evolve independently. At a certain time both the potential-wells are then turned off and the two clouds expand. While falling, they interact and the interference pattern between them is measured. It gives information about the local phase difference between the two clouds. This process is again destructive and the atoms are completely lost after the measurement.
Our description of the cold-atom experiments is extremely general, and we did not enter in all the details that an experimentalist has to solve in order to obtain good measurements. These details depend on the specific atomic specie used, and on the specific setup. What we described here was a paradigmatic example of how a cold-atom experiment is structured and how it works. We hope that the interested reader may find all the information in the references we gave [32, 33, 25, 34].

1.3.1.3 Observation of the ground states of Bose and Fermi gases

Bose-Einstein condensation The first experiment we want to present is the observation of a Bose-Einstein condensate in a cold atomic gas [35]. This has been obtained by the group of Cornell et Weiman at JILA in 1995 [6] and, in the same year, by the group of W. Ketterle [5], all of them have been awarded of the Nobel Prize in 2001.
The energy distribution $n(E)$ of a non-interacting gas of bosonic particles, i.e. the number of particles occupying the same energy level, is determined by the Bose-Einstein distribution

$$n\left(E_k\right) = \frac{1}{e^{\beta(E_k-\mu)}-1},$$

where $\beta = 1/k_B T$, E_k is the single particle energy, and μ is the chemical potential. The Hamiltonian for a non-interacting system can be written as

$$\mathcal{H} = \sum_{\mathbf{k}} (E_{\mathbf{k}} - \mu)\, b^{\dagger}_{\mathbf{k}} b_{\mathbf{k}},$$

where the operator $b_{\mathbf{k}}$ destroys a particle of momentum $\mathbf{k}$ while its adjoint creates a particle of the same momentum. The dispersion relation is the free one $E_{\mathbf{k}} = \frac{|\mathbf{k}|^2}{2m}$.
In order to ensure that the wave-function fulfills the right properties under exchange of two particles, the $b_{\mathbf{k}}$ and $b^{\dagger}_{\mathbf{k}}$ operators have to be

$$\left[b_{\mathbf{k}}, b^{\dagger}_{\mathbf{k}'}\right] = \delta_{\mathbf{k},\mathbf{k}'}.$$

At extremely low temperatures, the state of the system is the one that minimizes the total energy, i,e, its ground state. This is possible if all the particles occupy the state with $\mathbf{k} = 0$. The Bose-Einstein condensation is then determined by a macroscopic occupation of the lowest energy state

$$n\,(E_0) = N_0 \sim N.$$

It is clear that the condensation is in the momentum space, where one of the momenta is macroscopically occupied while the others are microscopically occupied. The condensation happens also in real space if our single-particle Hamiltonian is not translational invariant. In the case of an harmonic trap, the single-particle Hamiltonian is given by the standard harmonic oscillator one. In this case the condensation in $\mathbf{k}$-space state determines also the one in real space because the wave-functions of all the particles are concentrated at the bottom of the trap.
In their experiment [6], Cornell et his collaborators used a could of ^{87}Rb atoms cooled down at $170nK$ in an optical harmonic trap and a phase-space density $n\lambda^3 \sim 10^5 - 10^6$. In this case, the presence of the condensate is detected through the velocity distribution, Fig. 1.3, where a macroscopic occupation of the $\mathbf{v} = 0$ appears under a critical temperature.

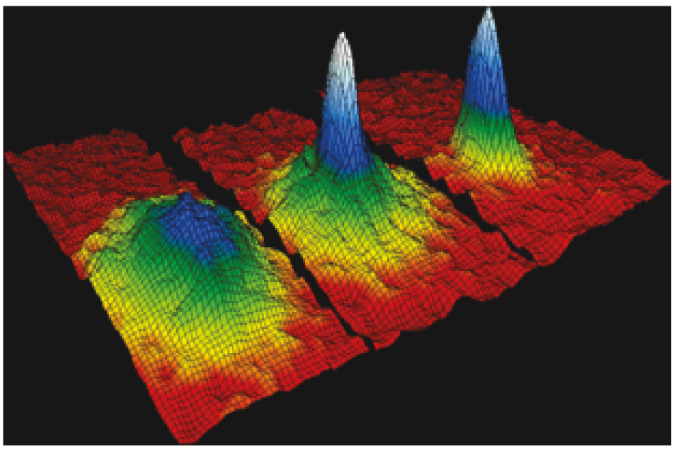

Figure 1.3: Velocity distribution $\mathbf{v}$ of a Bose-Einstein condensate for, from left to right, $T > T_C$ where the distribution of atoms at $\mathbf{v} = 0$ is of the same order of magnitude of the other values of $\mathbf{v}$, $T < T_C$ where a strong peak at $\mathbf{v} = 0$ signals the condensation of a large number of particles in this state and for the same value of temperature but after a stronger evaporative cooling that suppress the influence of $\mathbf{v} \neq 0$ enhancing the effect of Bose-Einstein condensation. Figure from Ref. [36].

This study has been a huge breakthrough in the observation of the equilibrium properties of matter at extremely low temperatures. In particular, it pointed out that cold atomic systems are perfect to realize isolated quantum systems.

Fermi-sea Cold atoms have also been used to explore the microscopic properties of fermionic gases at low temperatures [33, 37, 38]. Fermions compose the standard matter, and the exclusion principle, which is their intrinsic characteristic, is used to explain the stability of matter, the evolution of supernovae, and the properties of metals and semiconductors.
The ground state of a fermionic system reflects the exclusion principle and it is completely different from the bosonic one. Bosons can all occupy the same state, meaning that the minimal energy configuration for a system of N bosons is the one where all of them are in their lowest-energy state. In contrast, Fermions cannot occupy the same energy level, and the minimal energy configuration of the system is then different. In a system made of N fermions, with single particle spectrum E_n, the ground state is defined as the state where the N lowest energy states, from $E_0 \leq E_1 \leq \cdots \leq E_{N-1}$, are occupied. If the Hamiltonian is a free and translational invariant Hamiltonian, it can be written in Fourier space as

$$\mathcal{H} = \sum_{\mathbf{k}} \left(E_{\mathbf{k}} - \mu\right) f_{\mathbf{k}}^{\dagger} f_{\mathbf{k}}$$

where again $E_k = \frac{k^2}{2m}$ is the dispersion relation, and μ the chemical potential. The particle operator $f_{\mathbf{k}}$ $\left(f_{\mathbf{k}}^{\dagger}\right)$ destroys (creates) a particle of momentum $\mathbf{k}$ and they fulfill

anti- commutation rules

$$\left\{ f_{\mathbf{k}}, f^{\dagger}_{\mathbf{k}'} \right\} = \delta_{\mathbf{k},\mathbf{k}'}.$$

This ensure the right symmetry of the wave-function under particle exchange.
The ground state in Fourier space is then described as a step function where the first N lowest energy levels are occupied

$$|GS\rangle \propto \prod_{\mathbf{k}\leq\mathbf{k}_F} f^{\dagger}_{\mathbf{k}} |0\rangle ,$$

where $|0\rangle$ is the vacuum state. The key parameter to describe this state is the Fermi momentum $\mathbf{k}_F$ and the associated Fermi energy E_F. The first corresponds to the wave-vector of the particles with largest energy and the latter to its energy. It is important to notice that this state has a discontinuous structure in $\mathbf{k}$-space, with all the momenta occupied for $\mathbf{k} \leq \mathbf{k}_F$ and all empty otherwise, this density distribution is called a Fermi-step. Indirect proofs of the existence of such a state have been found in many physical systems, e.g. the pressure of the supernovae. A direct observation of the Fermi distribution at zero temperature has anyway been possible just using cold atomic gases.
In Ref. [39], a cloud of 9×10^4 ^{40}K has been first trapped, and then cooled down to reach the quantum degenerate regime. The momentum distribution has been measured using time-of-flight techniques, described in Sec. 1.3.1.2. In order to avoid density changes due to the harmonic confinement, the data has been taken just from the central part of the trap. There, the local density approximation gives meaningful results for translational invariant systems. The observed momentum distribution is not a perfect Fermi step. This is due to the fact that even if the gas is at extremely low temperatures, the Fermi step is reached just at exactly zero temperature. In Fig. 1.4 the values of the occupancy $n(k)$ as a function of k are plotted. It is possible to see that the occupation number has a sharp cut exactly at $k = k_F$ as expected. The distribution does not go exactly to zero because of the temperature effects, but anyway it can be fitted using the theoretical temperature dependence of the Fermi-Dirac distribution

$$n\left(E_k\right) = \frac{1}{e^{\beta(E_k-\mu)}+1}$$

at $T = 1/\beta k_B = 0.12 T_F$ where $T_F = E_F/k_B$. The solid line in the same figure is obtained from the previous equation at the temperature of the cloud and using k_F as fitting parameter.

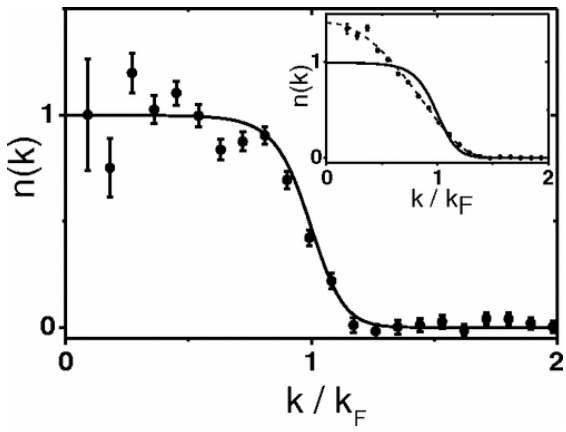

Figure 1.4: Occupation number $n(k)$ as function of the momentum k measured in units of k_F in a non-interacting Fermi gas [33, 37, 38]. The points are the experimental results and the line is obtained using the Fermi-Dirac distribution at the temperature of the gas and then fitting using k_F as single free parameter. In order to obtain a result comparable to the theory of homogeneous gases, the experimental data are obtained using just the internal 16% of the trap. The temperature T is fixed using the data from the full average over the trap.
In the inset the results obtained by all the trap are shown. It is possible to see how the homogeneity condition affects the results: the points are the experimental results obtained averaging over six images and the dotted line is the fit for an harmonically trapped Fermi gas. The fit, as before is performed just using k_F as free parameter. The solid line is the Fermi-Dirac distribution for a free homogeneous gas at the same conditions, the difference between the two points out the huge effect of inhomogeneity of the trap. Figure from Ref. [39].

Many other complex behaviors have been detected with a great accuracy using cold atomic gases which now are a fundamental tool to explore and open new frontiers in physics. In the previous examples, anyway, a huge simplification is used: the particles are not interacting. Even if this condition makes the theoretical description easier, a lot of physical effects are neglected in this way. We will see now how interactions are taken into account.

1.3.1.4 Engineering and controlling interactions in cold atomic gases

In cold atomic systems different types of interactions can be engineered. The first idea is to use the interactions that naturally take place between two atoms at the microscopic level. Even if they are really complicated, since they involve many sub-atomic details, usually these interactions are extremely short-ranged and isotropic at the energy scales involved in experiments.
This introduces a huge simplification in their theoretical description because atoms can be modeled as soft spheres with a coupling constant g_s, determined by the scattering

length a_s via the relation

$$g_s = \frac{4\pi\hbar a_s}{m}$$

and the potential may be replaced by a pure contact potential

$$V(\mathbf{r}) = g_s \delta(|\mathbf{r}|). \tag{1.3}$$

Theoretically, this imposes some conditions on the typical energy scales accessible, for example the energy of a collision has to be not large enough to excite internal degrees of freedom. Moreover, the spherical symmetry of the previous expression is given by the $s-$wave scattering which is the only one contributing to the collisions at low energies. The higher momentum collisions, as the $p-$waves scatterings, are suppressed because the energy of the colliding particles is not large enough to overcome the centrifugal barrier. At low energies these processes are then neglected, leaving a spherically symmetric effective scattering.
The introduction of interactions in both fermionic and bosonic systems can then be used to explore new physics in cold atomic gases. Effects range from the fermionization of one-dimensional interacting bosons to high-temperature superconductivity in metals, which seems to be catched by the Fermi-Hubbard model.
Creating interactions is anyway not really useful if it is not possible to control them. This is fundamental both at equilibrium and out-of-equilibrium. In the first case, the exploration of physics at different interaction strengths can be used to study the phase-diagram of the model, detecting different states of matter and phase transitions. In the latter, we want to induce a change in the system to create a time evolution. As we said, a sudden change in the interactions between particles is the best way to induce a non trivial dynamics.
The easiest way to achieve that takes advantage of the specific form of Eq. (1.3). In order to change the strength of interactions is sufficient to modify the scattering length a_s. This can be done coupling the atoms to a magnetic field and creating a Feshbach resonance [40]. The physical meaning of such a phenomenon can be understood using a simple picture. We can consider a scattering between two atoms which has a "background" channel potential $V_{bg}(R)$ and "closed" channel $V_c(R)$. $V_{bg}(R)$ has a free state for large distances R, and $V_c(R)$ allows a bound state. The Feshbach resonance occurs when, for a small collision energy E, a resonance occurs between the bound state of energy E_c in the closed channel and the free state in the background potential. This resonance can be tuned with a magnetic field used to control the energy difference between the two states if they have different magnetic moments. The importance of this process is its effect on the scattering length, which can be written, close to the resonance, as

$$a_s(B) = a_{bg}\left(1 - \frac{\Delta}{B - B_0}\right) \tag{1.4}$$

where a_{bg} is the scattering length of the background potential alone, B_0 is the value of the potential where the resonance occurs and a diverges and Δ is the width of the resonance. Eq. (1.4) provides a powerful method to tune the interaction strength to

almost any value from infinitely repulsive to infinitely attractive. $a_s(B)$ ranges from $-\infty$ to $+\infty$ depending on sign of Δ and the difference $B - B_0$.
Even if this method allows us to change the intensity of the potential, it does not allow us to change its form. In this manuscript we will focus on interactions not of the same type of Eq. (1.3): the long-range ones.
The prototype of such potential is

$$V(R) \propto \frac{1}{|R|^\alpha}$$

which is isotropic and with a long-range tail determined by α. It is possible to realize long-range interactions using dipolar molecules [41] or trapped ions [42]. At the fundamental level, dipolar interactions are also not spherically symmetric. They are repulsive along one direction and attractive along the others, creating a strong dependence of the physics to the geometry of the trap. Moreover, in optical lattices, the extension of the Bose-Hubbard model, see Sec. 1.3.2, with such interactions exhibits different exotic solid phases as super-solids, check-board states or superfluid phases [43, 44, 45, 46].
Long-Range interacting quantum systems will be intensively studied in this manuscript. In particular the consequences of long-range interactions on the time evolution of correlations will be discussed. It is then important to know that they can be realized in experimental setups to allow the possibility to check theoretical results in real experiments [47, 48].

1.3.1.5 Most important systems realizable in cold atomic experiments

Cold atomic setups give us the possibility to realize many different types of systems which we briefly review here.

Low-dimensional systems The most striking example of such a freedom is the realization of one and two dimensional systems thanks to the optical techniques we described before. The confinement along any of the three directions is obtained thanks to a couple of counter-propagating laser beams. They act on the atoms as a static potential. Eq. (1.2) can be generalized to anisotropic $I(\mathbf{r})$ with inhomogeneous σ_i, namely

$$I(x,y,z) = I_0 e^{-\frac{x^2}{2\sigma_x^2}} e^{-\frac{y^2}{2\sigma_y^2}} e^{-\frac{z^2}{2\sigma_z^2}}.$$

This generates an anisotropic potential

$$V(x,y,z) = \frac{I_0}{\Delta}\left[1 - \frac{1}{2}\left(\frac{x^2}{\sigma_x^2} + \frac{y^2}{\sigma_y^2} + \frac{z^2}{\sigma_z^2}\right)\right].$$

We can then tune σ_z, for example, to be extremely small compared to the other two. In this way the excitations along the z direction are energetically expensive. This constraints the motion into the $x-y$ plane, where it is energetically favorable, and we obtain a perfect bi-dimensional system. If we do the same for two directions, $\sigma_x \ll \sigma_y = \sigma_z$, then the

motion will be forced along a tube and we obtain an effective one-dimensional system. These one-dimensional systems are extremely interesting from the theoretical point of view. It is known that quantum fluctuations become dominant in one dimension. Many exact theoretical tools to solve the Schrödinger equation, like the Bethe ansatz or the inverse scattering methods [49, 50], can provide exact solutions for many-body quantum systems. Moreover, many approximation methods are available such as bosonization or Luttinger-liquid theory [51]. Also numerical methods are available, such as the Density Matrix Renormalization Group (DMRG) [18] and its derivations.
These low-dimensional geometries are realized in cold atom setups with both Fermi and Bose particles. They can explore different phenomena as the microscopic properties of Luttinger liquids [52, 53, 54, 55] and the fermionization of bosons in the Tonks-Girardeau regime [56, 57, 58, 59, 60].

Optical lattices Cold atoms can be used also to realize perfect lattices, as we will discuss in details in Sec. 1.3.2. Periodic potentials are fundamental to describe condensed-matter models. They occur in almost all solids and in particular in metals and crystals. Even if these structures are present in Nature and they can be realized in different shapes thanks to crystal growth techniques, in all condensed-matter systems crystals have some defects. These defects need to be described using ad hoc theoretical methods, which are not always easy to handle. Moreover, crystal lattices allow the presence of phononic excitations that act on the particles as a thermal bath. This makes hardly possible to drive these systems out of equilibrium in a controlled way. For the quench protocol described before the presence of such a bath is even more dangerous because it makes the time evolution non unitary.
These two problems can be solved using cold atomic gases. Lattices can be realized using laser beams with spatially ordered intensity profile. The effective model describing the motion of atoms in a lattice is the so-called Hubbard model discussed in detail in the next section 1.3.2. The main feature of these systems is the perfect realization of the lattice without any defect and without any phononic excitation. In this sense, cold atomic gases are the only possibility to realize an unitary evolution in a lattice model for sufficiently long times. The quantum quench requires in fact a complete isolation of the system from the environment.

Further examples Many other interesting effects can be simulated and probed in cold atomic gases, which versatility is the key to their success in the last decades. Disorder plays a central role in condensed-matter physics. It leads to striking effects as the localization of the waves in a disordered potential, known as Anderson localization [61]. If weakly repulsive interactions are then allowed between the particles, their effect tends to delocalize the wave function. In contrast, disorder tends to localize it. It is then important to understand how interactions and disorder interplay and how to compute the critical values of the couplings that separate the Anderson insulator from the superfluid and the superfluid from the Mott Insulator. Disorder can be created in optical lattices superimposing different optical potentials with incommensurate wavelengths [62, 63, 64].

Tuning the parameters in different ways it is possible to explore different regimes ranging from Anderson-Bose glass to the transition between the Anderson-glass and the Mott-Insulator taking also into accounts the effects of the trap [65, 66, 67, 68]. The signature of the Anderson localization can be also detected by the analysis of the weak nonlinear effects in the BEC, as proposed by different theoretical works [67, 69, 70, 71, 72, 73, 74, 75], which is a promising field of study that can be applied to experiments in the future [76].
Another field where cold atomic gases are intensively used is the study of high-temperature superconductivity. The fundamental nature of this phenomenon represents a mystery for modern physics. However it seems that some hints can arrive from the study of the $D = 2$ Fermi Hubbard model with spin 1/2 [77]. This system is difficult to simulate numerically and the results obtained are still hardly debated. Its realization using cold atomic atoms with spin or pseudo spins [78, 79], or with fermions [80, 81] or with fermions-bosons mixtures [82, 83] will give crucial hints for the solution of the high-temperature superconductivity problem.
The realization of a large zoology of spin systems with topological order is possible in cold atoms and they could be used in quantum computation [84, 85]. These models are obtained using excited molecules with strong dipolar interactions, which are supposed to be a good to realize a toolbox for quantum computation thanks to the anisotropy in the dipole-dipole interaction [86, 87].
Last but not least, the fractional quantum Hall effect has been intensively studied in condensed-matter physics and a huge theoretical effort has been done to deepen its understanding [88, 89]. Nevertheless, the experimental observation of the features of strongly-correlated states, as the anyonic nature of the excitations determining this effect, is still missing. In order to clarify these questions, it has been proposed to study these effects in a rotating Bose-Einstein condensate, where the rotation acts like the presence of a constant magnetic field along the axis [90, 91, 92, 93]. This can be simulated in the Bose-Hubbard model where particular hopping matrices can lead to Hall states [94, 95, 96, 97].
In this section we presented a small number of the applications of cold atomic gases. The list is far from being complete and it is increasing in time at a large rate extending the fields where cold atomic gases are a crucial tools to deepen the understandings of quantum physics.
In the next section we will focus on the most known lattice model that can be realized in cold gases: the Hubbard model. This model is per se an extremely interesting model for the fact that it shows effects of an extremely correlated systems as the Mott insulator-superfluid transition, observed in [98], but it can be used to simulate more complicated models as spin models. It will be at the heart of the discussion of the next chapters.

1.3.2 Lattice systems and Hubbard models

We can now discuss more intensively one of the most important models that have been realized in cold atoms: the Hubbard model, which aims to describe interacting particles on a lattice.
A lattice is created using the same optical techniques used for the trapping process 1.3.1.1.

A standing wave creates a potential proportional to its intensity. If this takes the form $I(\mathbf{r}) = I_0 \sin^2(\mathbf{k} \cdot \mathbf{r})$ we create an effective spatially ordered potential which acts on the particles as a lattice.

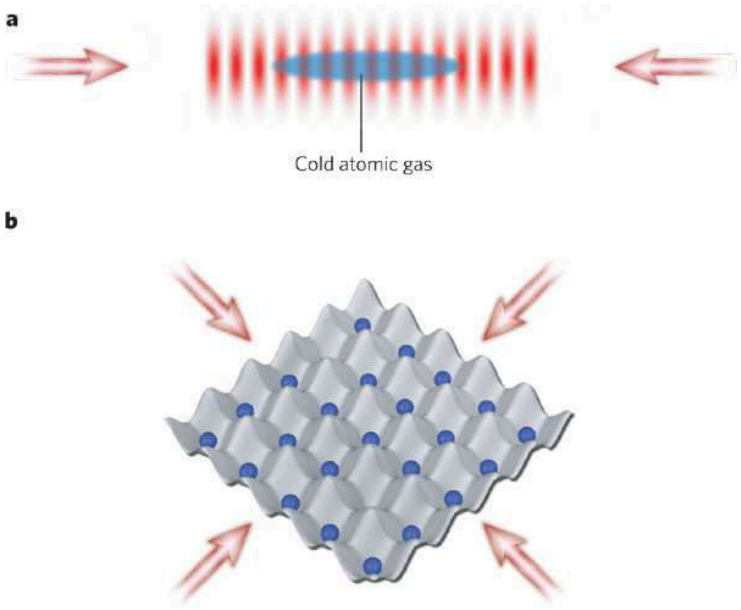

Figure 1.5: Schematic representation of how it is possible to create lattices using counter-propagating laser beams. The interference between lasers creates a spatially oscillating patter that acts like a periodic effective potential on atoms. a) Two counter-propagating beams along one direction create an effective one dimensional lattice. b) two couples of counter-propagating beams along two directions, x and y, create a spatially ordered potential along the two directions that induces a two dimensional lattice.
Lattices create this way do not allow phononic excitations and no impurities are present. These two effects affect all the lattices in condensed matter systems, as metals or crystals, and they can lead to drastic consequences in the physical behavior of the systems. Figure from Ref. [99].

Since the gas is extremely cold, it occupies the lowest accessible energy states. This

means that the wave-function is located at the minimum of the lattice potential. The natural basis to describe the state of the system is the Wannier one. These functions are peaked at the bottom of the lattice sites and they decay algebraically outside.
Physically, two main effects occur in the system: a hopping between nearest-neighbor sites and an interaction between particles occupying the same site. The first is due to the tunneling effect between a site and the neighbor one. The latter occurs because of the extremely short range of the interactions between particles, see Eq. (1.3).
We can then built a Hamiltonian using the particle operators a_i and $a_i^\dagger$, that respectively destroys and creates a particle at the site i , and they fulfill the (anti-) commutation relation depending on the (fermionic) bosonic nature of the chosen particles.

The Bose-Hubbard Model We start our discussion from the simplest case of a lattice loaded with a single specie of bosonic atoms. As we said, the particles can hop between nearest neighbor sites and they interact when they are on the same site.
The hopping term takes into account the process that destroys a particle at site i and creates another one at site $i+R$. The tunneling process decays rapidly with the distance because of the fast suppression of the Wannier functions. The most important process is the one between nearest neighbors sites, $R=1$, which probability is J:

$$\mathcal{H}_{hop} = -J \sum_{\langle i,j \rangle} \left(a_i^\dagger a_j + a_j a_i^\dagger \right).$$

The value of J is determined by the transition matrix between the Wannier function at the site i and the one at the site $i+1$ mediated by the kinetic potential acting on the cloud.
The interactions between particles is determined by the same point-like interaction potential described before. Because of its extremely short range nature, this process is allowed just if two particles occupy the same site i. We can write it as if every of the n_i particles at the site i interacts with the other $n_i - 1$ with a uniform cost U. The number of interaction processes is then $\frac{1}{2} n_i (n_i - 1)$ where the factor $1/2$ corrects double counting. This yields to an interaction Hamiltonian of the form

$$\mathcal{H}_{int} = \frac{U}{2} \sum_i n_i \left(n_i - 1 \right)$$

Summing these two fundamental pieces, in the case of a single bosonic species, we find the celebrated Bose-Hubbard Hamiltonian

$$\mathcal{H}_{BH} = -J \sum_{\langle i,j \rangle} \left(a_i^\dagger a_j + a_j a_i^\dagger \right) + \frac{U}{2} \sum_i n_i \left(n_i - 1 \right).$$

It is then possible to add a confinement potential, which depends on the on-site energies ϵ_i, and a chemical potential that takes into account the energetic cost of adding or removing particles. The full Hamiltonian then reads

$$\mathcal{H} = -J \sum_{\langle i,j \rangle} \left(a_i^\dagger a_j + a_j a_i^\dagger \right) + \frac{U}{2} \sum_i n_i \left(n_i - 1 \right) + \epsilon_i \sum_i n_i - \mu \sum_i n_i. \tag{1.5}$$

The ground state of the Hamiltonian is determined by the competition between the hopping, which tends to delocalize the wave function letting atoms spread around the lattice, and the on-site interaction term, which tends to localize the wave function.
We study a homogeneous system ($\epsilon_i = 0$) and we analyze the two opposite cases where $U = 0$ or $J = 0$ respectively. In the first case the Hamiltonian describes simply a pure hopping

$$\mathcal{H} = -J \sum_{\langle i,j \rangle} \left(a_i^\dagger a_j + a_j a_i^\dagger \right) - \mu \sum_i n_i.$$

The ground state of this Hamiltonian is simply a Bose-Einstein condensate [100]. It can be found rewriting it in the Fourier space, using the operators $a_{\mathbf{q}} = \frac{1}{N} \sum_{\mathbf{R}} e^{-\imath \mathbf{R}\cdot\mathbf{q}} a_{\mathbf{R}}$, we get

$$\mathcal{H} = \sum_{\mathbf{q}} \left(\epsilon_{\mathbf{q}} - \mu \right) a_{\mathbf{q}}^\dagger a_{\mathbf{q}}.$$

The ground state for a N-particle system is simply the minimal energy configuration

$$|GS\rangle \propto \left(a_{\mathbf{q}=\mathbf{0}}^\dagger \right)^N |0\rangle = \left(\sum_i a_i^\dagger \right)^N |0\rangle$$

where $|0\rangle$ is the vacuum state. This ground state represents a completely delocalized state where the particles form a cloud of atoms, each occupying the entire lattice. Naively, this is represented by the fact that the state is sharp in $\mathbf{k}$-space, consequently it is broad in $\mathbf{R}$-space.
The ground state of the system with $J = 0$ has a completely different structure, determined by the Hamiltonian

$$\mathcal{H} = \frac{U}{2} \sum_i n_i \left(n_i - 1 \right) - \mu \sum_i n_i.$$

This Hamiltonian can be diagonalized simply using the local Fock basis of every site $|n_i\rangle$ and obtaining a pure local description where all the sites are decoupled. The ground state is then a fully localized state at zero temperature where all the particles are in one of these states. In the specific case of $\langle n \rangle = \bar{n} \in \mathbb{N}$, where an integer number of particles occupies every site, the state is a Mott insulator. Now, if we allow small hopping between nearest-neighbor sites, setting $J \neq 0$, the high energetic cost due to the on-site interactions U cannot be payed by the hoping term $J \ll U$. The motion of particles is then completely suppressed creating an insulating state. If the mean number of particles per site is not an integer$\langle n \rangle \neq \bar{n}$ then we have a superfluid state over a Mott insulator with $[\bar{n}]$ particles per site, where [.] is the integer fraction. In every site we have a portion of particles that localizes and forms the insulator. The excess of particles per site, $\bar{n} - [\bar{n}]$, forms a superfluid.
The competition between these two phases is determined by the ratio U/J. A quantum phase transition between the superfluid regime ($U/J \ll 1$) and the Mott insulator ($U/J \gg 1$) occurs at a critical value U_c/J_c. This phase transition has been studied

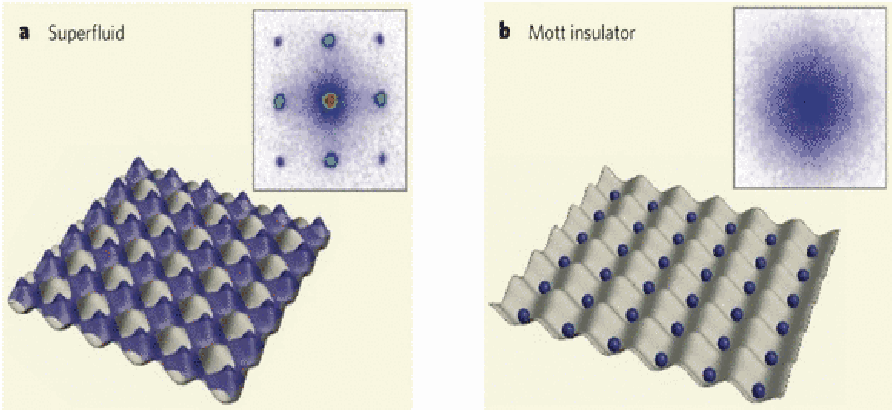

Figure 1.6: Experimental observation of the momentum distribution $n(\mathbf{k})$ in a Bose-Hubbard model in two dimensions. a) In its superfluid phase where the particles are delocalized. In this state the particles act as coherent sources of signals for the measurements. The fact that they are coherent creates the ordered pattern observed in the $n(\mathbf{k})$. b) In the Mott insulator phase where an integer number of particles occupies every site and the hopping between nearest-neighbor sites is suppressed. In this case, atoms in different sites act as incoherent sources for the measurements. These incoherence destroys every signal in the momentum distribution and consequently no ordered structure is present in this observable. Figure from Ref. [104].

and detected in cold atomic gases in one [101, 102, 55], two [101], and three dimensions [98, 103]. For the two dimensional case, the results are shown in Fig. 1.6. The structure of the two different ground states is in fact completely different once observed in k-space. The small U regime, i.e. superfluid state, has an organized structure in $\mathbf{k}$ space with ordered peaks. The coherence between the signals coming from all the delocalized atoms creates this ordered pattern. On the other side, when J is small, the system is in a Mott insulating state where atoms in different sites are not correlated. This destroys the interference patter seen in the superfluid case and a cloud without any structure in $\mathbf{k}$ space is detected.

Fermi-Hubbard model The Bose-Hubbard Hamiltonian we presented before is not the only example of Hamiltonians of the Hubbard type. A first simple change can be introduced using fermionic particles instead of bosonic ones. In this case the creation and destruction operators are respectively $f_i^\dagger$ and f_i and they anti-commute $\left\{f_i^\dagger, f_j\right\} = \delta_{ij}$ [105]. The hopping term clearly represents the same physical effects as in the bosonic case: a particle can tunnel through the potential barrier and appear on the other side and it is represented as

$$-J \sum_{\langle i,j \rangle} \left(f_i^\dagger f_j + f_j^\dagger f_i \right).$$

The fact that the same site cannot be occupied by more than one fermion is ensured by the anti-commutation relation.
The interaction term has anyway to be changed since $n_i(n_i - 1) = 0$ because of the fermionic statistics. We can consider an interaction term that involves the overlap between two nearest neighbor sites, which is not zero. It is due again to the small leaks outside the single site of the Wannier wave-function

$$V \sum_{\langle i,j \rangle} n_i n_j,$$

where these are the number of atoms at nearest-neighbor sites i and j. Even if this term has been studied in many theoretical works on the Fermi-Hubbard model, its detection in cold atomic experiments is still missing.
If we want to allow on-site interaction for fermions we need to overcome the Pauli exclusion principle. This can be achieved using internal degrees of freedom of the atomic species. New particles operators $f_{i,\sigma}$, depending now on the internal state σ are now defined. The anti-commutation relations are then

$$\left\{ f^\dagger_{i,\sigma}, f_{j\sigma'} \right\} = \delta_{\sigma\sigma'}\delta_{i,j}.$$

In the case of spin-1/2 particles we have two internal states $\sigma = \{\uparrow, \downarrow\}$, two particles can share the same site if they have opposite spins. The interaction term is then

$$\mathcal{H}_{int} = U \sum_i n_{i,\downarrow} n_{i,\uparrow}.$$

Terms of these type can be induced and controlled in cold atomic systems and their effect can be measured [106].

Extended Hubbard models We can then generalize the previous results to include different internal degrees of freedom with different interaction strengths which can depend also on single site i labeled as $U_{i\sigma\sigma'}$. This gives generalized on-site interactions of the type

$$\mathcal{H}_{int} = \sum_{i,\sigma,\sigma'} U_{i\sigma\sigma'} n_{i,\sigma} n_{i,\sigma'}.$$

More complicated interactions can be used, as the long-range ones we briefly described before [41]. These interactions depend on the distance $|i - j|$ between sites and on the internal states σ and σ' of the particles

$$\mathcal{H}_{int} = \sum_{i,j,\sigma,\sigma'} V_{\sigma,\sigma'}(|i - j|)\, n_{i,\sigma} n_{j,\sigma'}.$$

From the theoretical point of view, it is possible to include in the model also a long-range version of the hopping term. It destroys a particle at the site i and creates it at site j, and it takes the form

$$\mathcal{H}_{hop} = \sum_{i,j,\sigma,\sigma'} t_{\sigma,\sigma'}(|i - j|) \left[a_{i,\sigma} a^\dagger_{j,\sigma'} + a_{j,\sigma'} a^\dagger_{i,\sigma} \right]$$

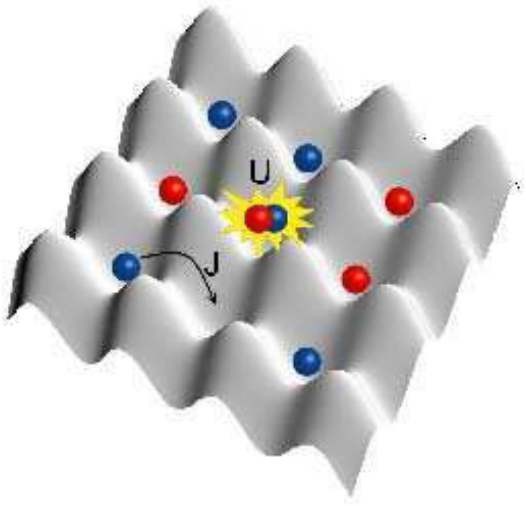

Figure 1.7: Schematic representation of a $D = 2$ Hubbard model. It is possible to load into the lattices different atomic species to create more exotic systems, as Fermi-Fermi or Bose-Fermi Hubbard models. In this figure it is possible to see a system with two species, red and blue. The interactions between them are on-site, with coupling U, and the motion on the lattice is induced via hopping between nearest-neighbor sites with coupling J. This is one example of the variety of systems can be described by Hubbard-like Hamiltonians. Figure from Ref. [82].

these terms are anyway impossible to realize in state of art experimental setups and they can be explored just numerically and theoretically.

Mixed systems, see Fig. 1.7, can also be realized. Loading the lattice with two different atomic species, like two fermionic or two bosonic or Bose-Fermi mixtures, it is possible to explore even more complicated phases of matters.

Clearly, the difficult in the realization and control of these Hamiltonians grows with the complexity of the added terms, in particular when interactions are present. These Hubbard type Hamiltonians are anyway able to reproduce different physical effects in lattice models from the Mott-Superfluid transition, we observed before, to the superconductivity for the fermionic version [99, 107, 108, 34, 109].

1.3.3 Spin models

Spin models [110] are used to understand the magnetism in complex materials and they can be used to engineer different quantum states [85]. Such systems can be realized in the laboratory using the Hubbard model. Different spin systems can be obtained using internal degrees of freedom or specific limits of that Hamiltonian.

Implementation of the XY model We can provide an explicit example: the XY model. We start from the homogeneous Bose-Hubbard model described by Hamiltonian (1.5) where $\epsilon_i = 0$ for simplicity

$$\mathcal{H}_{BH} = -J \sum_{\langle i,j \rangle} \left(a_i^\dagger a_j + a_i a_j^\dagger \right) + \frac{U}{2} \sum_i n_i \left(n_i - 1 \right) - \mu \sum_i n_i.$$

The XY model is a spin 1/2 model. Two possibles states are needed: one for the spin up and another for the spin down. The easiest way to obtain this condition is to use the $n_i = 0$ eigenstate as down spin and the $n_i = 1$ one as the up spin. We then have to limit the number of possible particles per site to $N = 1$. This condition is satisfied exactly if the on-site interaction energy U is larger than all other energy scales μ and J. In this way, the possibility that two atoms are on the same site is extremely small and every site has the same local Hilbert space of a spin-1/2. For this specific regime, called hard-core limit, using the transformations

$$\begin{aligned} a_i^\dagger &= \frac{1}{2} \sigma_i^\dagger \\ a_i &= \frac{1}{2} \sigma_i^- \\ n_i &= \frac{1}{2} \left(\sigma_i^z + 1 \right) \end{aligned}$$

it is possible to map the Bose-Hubbard Hamiltonian onto the spin-1/2 XY Hamiltonian

$$\mathcal{H}_{XY} = -\frac{J}{4} \sum_{\langle i,j \rangle} \left(\sigma_i^\dagger \sigma_j + h.c. \right) - \frac{\mu}{2} \sum_i \left(\sigma_i^z + 1 \right),$$

where $\sigma_i^\pm = \left(\sigma_{x,i} \pm \imath \sigma_{y,i} \right) / 2$, $\sigma_{\gamma,i}$ where $\gamma = x, y, z$ are the Pauli matrices. The hopping term with energy scale J acts as an exchange term between spins while the chemical potential μ represents a magnetic field.

Other spin models

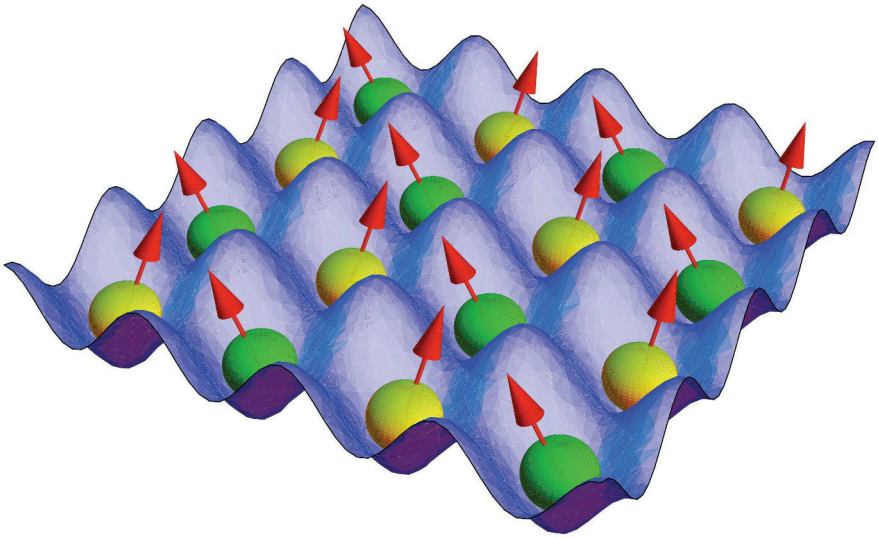

Figure 1.8: Representation of a spin model in optical lattices. Spin models can be realized in cold atomic experiments using internal degrees of freedom of the atomic species loaded into the lattice. Using atoms with N internal states we can obtain an Hamiltonian for effective spin of magnitude $S = (N-1)/2$. The understanding of spin models is fundamental in many field of condensed matter physics from magnetism to quantum Hall effect. Cold atomic gases provide perfect spin models which can be used to simulate a wide range of Hamiltonians. Figure from Ref. [111].

Spin systems can also be realized using internal states of the atoms , every internal state represents a spin component. As we said in the description of the Hubbard model, atoms in different internal states can be loaded in the optical lattices. These N internal states create an effective spin $S = (N-1)/2$ that can be used to reproduce spin Hamiltonians. More complicated mixtures of species of bosons can be used to obtain more exotic Hamiltonians. For example, a Bose-Bose mixture can be reduced to the XXZ model and the Bose-Fermi mixture can simulate a spin model just for 1D systems, where it simulates a XXZ model in external field [112, 113, 114]. All the previous proposals are extremely complicated to realize in an experimental setup and many different new cooling protocols have been proposed to reach the ranges of temperatures where the interesting physics appears [115, 116, 117, 118].

Trapped ions A specific class of systems that can be used to simulate quantum spin chains are trapped ions [42]. They are made of ions loaded into linear radio-frequency trap [119, 120, 121]. In these traps, the competition between the repulsive electric force and the trapping force, attracting the atoms at the bottom of the trap, creates a natural crystal. Laser-light-mediated interactions can be created between the ions in the trap.

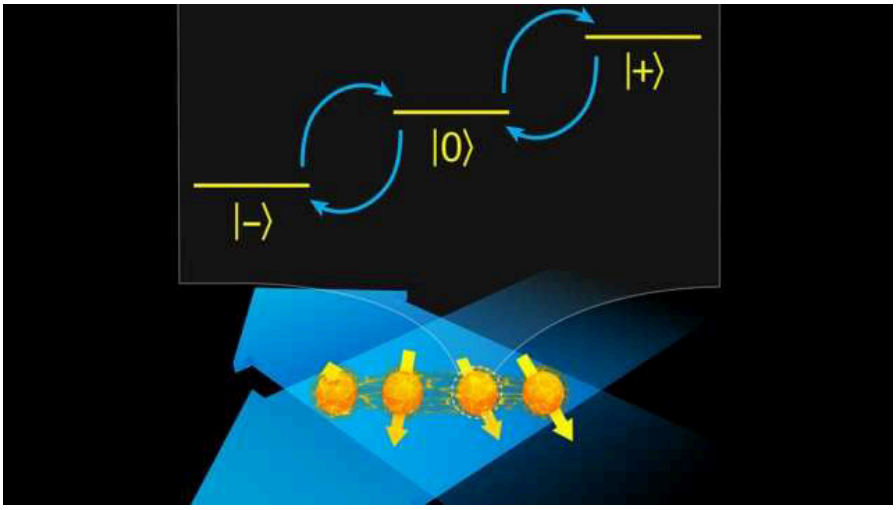

Figure 1.9: Schematic representation of the internal states of a trapped ionic system. The interactions between the particles can be engineered thanks to beams of lasers. This model can also be used to obtain long-range exchange terms between spins at different sites. Figure from Ref. [111].

Different models can then be simulated inducing different interactions.
In [122, 123] it has been presented how the following Hamiltonian can be realized in trapped ions

$$\mathcal{H} = \frac{1}{2}\sum_{i,j} J^{\alpha}_{i,j}\sigma^{\alpha}_{i}\sigma^{\alpha}_{j} + \sum_{i} B^{\alpha}_{i}\sigma^{\alpha}_{i}.$$

The spin-spin interaction is realized by coupling the spins to off-resonant radiation in a regime where the energy scale that controls the motion of the ions is negligible compared to the detuning of the laser. In 2008 the previous Hamiltonian has been implemented to simulate a one dimensional Ising chain, where

$$J^{\alpha}_{ij} = J\frac{\delta_{j,i+1} + \delta_{j,i-1}}{2}.$$

The pramagnetic to ferromagentic transition has been observed setting the exchange coupling between spins in presence of magnetic field to different values. In Fig. 1.10, the average magnetization of crystals composed by $N = 2$ and $N = 9$ ions of $^{171}Yb^{+}$ is presented as function of B and J [124, 125]. It is possible to see how both the set of data are in good agreement with exact theoretical predictions for the studied observable. It is also possible to see how, around $B = J$, the magnetization has a pronounced change which becomes sharper increasing the number of atoms. This is a signature of the phase transition occurring at this point in the thermodynamic limit $N \to \infty$.
This model is not the only one that can be simulated using ions crystal and more complicated J^{α}_{ij} functions can be engineered, even if the system sizes are still not huge.

However the experimental control over the system is improving, and in some years it will be possible to control sufficiently big systems to compete on classical computers.

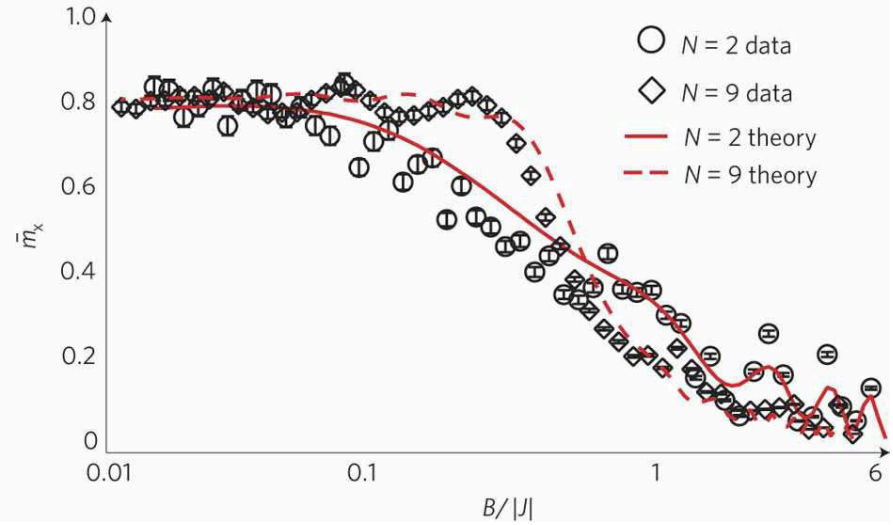

Figure 1.10: Average magnetization as function of the couplings for the one dimensional Ising model realized in a system composed by $N = 2$ and $N = 9$ trapped ions, see text and [42]. It is possible to see how both the data sets are in good agreement with exact numerical simulations of the same model. The derivative of the magnetization around $B = J$ becomes steeper passing from $N = 2$ to $N = 9$. This is due to the fact that in that point a quantum phase transition occurs in the thermodynamic limit [126]. Figure from Ref. [42].

1.3.4 Cold atoms out of equilibrium

In the previous sections we discussed how cold atomic gases are used to implement different Hamiltonians in atomic clouds at extremely low temperatures. These temperatures are obtained using evaporative cooling and magnetic or optical confinement allowing great flexibility, see Sec. 1.3.1.1and Refs. [127, 128, 129, 130, 131, 99, 32]. Moreover, it is possible to engineer directly the quantum state of the system loading selected atoms in selected states [132, 133] controlled by the experimentalists.
The great freedom we have in the realization of Hamiltonians and quantum states, the extremely weak coupling between the cloud and the external environment have allowed the study of many out-of-equilibrium phenomena in these systems. As we said, the protocol we want to use to drive quantum systems out of equilibrium is the quantum quench. This relays on two fundamental hypothesis:3

1. An instantaneous variation of one of the microscopic parameters of the Hamiltonian
2. A unitary time evolution, i.e. the system has to be completely decoupled from the external environment.

Both these conditions can be satisfied in cold atomic gases. Interaction strengths can be changed via Feshbach resonance, see Sec. 1.3.1.4, and the cloud can be isolated from the environment that is peculiar feature of these systems. In ^3He experiments, for example, the liquid was contained in a metallic container and the absorption of the helium atoms by this barrier made impossible to achieve a perfect isolation. If interactions between the system and the environment are still present the time evolution of the system is far from being unitary. The atomic clouds have decoherence times of the order of hundreds of milliseconds, which are much longer than the typical microscopic time scales, order of milliseconds.
Many groups have analyzed and studied different out-of-equilibrium situations using different techniques. We will briefly review the most important ones. The group of Bloch [98, 134] studied the dynamics of trapped bosons in an optical lattice. They performed a sudden change within the superfluid regime in the potential barrier of the lattice, which controls the interaction potential and the hopping term, and they studied the presence of collapses and revivals in the wvae-function. These effects are due to the fact that, after a quench, the time evolution can be written on the Fock space, where every component has a time and energy dependent phase that periodically dephase and rephase the field.
The setups of Weiler et al. [135] and Lemporesi et al. [136] focused on the formation of a Bose-Einstein condensate using evaporative cooling. As we described in Sec. 1.3.1.1, during the evaporative cooling the most energetic part of the atomic cloud escapes from the trap. Using radio-frequency transitions it is possible to control the rate of atoms escaping the trap for unit of time. In this way, the velocity at which the system enters in the degenerate regime can be fixed. This can be interpreted as a slow quench, where a parameter of the Hamiltonian changes smoothly over a finite amount of time. In such situation, the formation of defects can be observed while creating the Bose-Einstein condensate. The dependence of the density of defects on the escaping rate can be compared to the Kibble-Zurek theory [137] finding a perfect agreement between theory and experimental data. In this case, experimental coherence times are so long that they overcome the computational time accessible by classical numerical simulations [138].
In these experiments, measurements are obtained using the standard techniques already used for the equilibrium: "time-of-flight" measurements for the density in the Fourier space and "in-situ-imaging" to detect atoms positions in real space, see Sec. 1.3.1.2. Both of them are extremely precise to study the system during its time evolution. When combined with fluorescence and high-resolution optics, they also can reach precision up to the level of single atoms [139, 98, 140].
In [141], Bucker at al. achieved the single atom sensibility in fluorescence time-of-flight letting the atoms pass through a resonant laser beam. A proposal improving this mechanism is discussed in [30]. This method aims at measuring not only single atoms but also single excitations in the system. The same technique is used to observe parametric amplification dynamics which consists in studying the decay of excited states of the atoms due to interactions. The highly instable initial state where all atoms are in the first excited sate is realized making two beams of atoms collide with proper impulse as

described in [142, 143, 144].
Another measurement obtained in cold atomic gases is the matter-wave interference we described before and it has been applied in out-of-equilibrium [145, 146, 147]. In particular, it has been applied in [148] to show that a cloud of ^{87}Rb atoms has memory of its initial state for sufficiently long times. This confirms the fact that thermalization in closed quantum systems is not as simple as in other cases. The study of the interference pattern of matter-waves [149, 150, 151] reveals that the system does not thermalize immediately to a thermal state but long-lived pre-thermalization plateau, different from the thermal equilibrium state, are present [152, 148, 149].
Out-of-equilibrium protocols, as the quantum quenches or the ramps, relay on the fact that it is possible to change some parameters of the Hamiltonian without altering the state of the system. As for the equilibrium physics, the value of the scattering length that defines the typical interactions between atoms in cold atomic gases is determined by the Feshbach resonance, see Sec. 1.3.1.4. An example of interaction quench is the one described in [153], where ^{133}Cs are prepared as a bidimensional superfluid state into a highly deformed optical trap. The interaction between particles is instantaneously changed performing a quantum quench. The time evolution of this system reveals two things: on short time scale the density fluctuations are generated by the sound waves of the final Hamiltonian and on longer time scales the density profile converges to the one of the post-quench Hamiltonian at equilibrium.
As we said before, spin systems can be realized using cold atoms and it is also possible to drive them out-of-equilibrium. The one-dimensional Ising model has been realized loading the atoms in a tilted optical lattice [154, 155, 156]. The system has been prepared in its ground state and then, using Feshbach resonances again, a quench in the vicinity of the phase transition [126] has been performed. The presence of coherent oscillations in the spins has been observed together with the tunneling between nearest neighbor sites [157].

The previously presented results are just some of the most important experiments realized in cold atomic gases to explore the out-of-equilibrium dynamics of many-body quantum systems. In Sec. 2.3.2 we will analyze in detail the experimental observation of the propagation of correlations in short-range interacting quantum systems, while the same analysis in presence of long-range interactions will be discussed in Sec. 3.1. At the end of this chapter, Sec. 1.5.3, we will analyze two important experimental works on thermalization in closed quantum many-body systems.

1.4 Propagation of information

As we said in Sec. 1.2, there are two main research fields related to the time evolution of quantum systems:

- how it is possible to describe the time evolution itself
- how to describe the state reached by the system long time after the quench.

Here we want briefly to introduce the first point, which will be extensively discussed in the next chapters, the second point will be briefly discussed in Sec. 1.5. As we briefly presented before, many experimental tools have been developed to study the dynamics of many-body systems. It is then important to understand what the theory can infer on these phenomena.
Usually, the out-of-equilibrium dynamics of systems connected to a thermal bath can be treated using linear-response theory [9]. The excess of energy and other quantities in the system is rapidly absorbed by the thermal bath, which state is not significantly altered by this absorption due to its size. The system then rapidly termalizes thanks to the thermal bath and the physical description can be easily represented in the framework of statistical mechanics.
The situation considered here is much more complicated. We assume that the system is far from equilibrium and it is closed. The excess of energy or other quantities are now forced to stay inside the system and they give rise to different physical effects. The system cannot be described statistically and then its description is purely microscopic. The physical state is then described by a wave vector $|\Psi\rangle$, defined in some Hilbert space. Its time evolution is given by the Schrödinger equation [4]

$$\imath\partial_t |\Psi\rangle = \mathcal{H}(t) |\Psi\rangle$$

where $\mathcal{H}(t)$ is a time-dependent Hamiltonian. As it is well known, the explicit form of the time evolution operator for a generic time-dependent Hamiltonian is impossible to write in a closed form, and approximation methods have to be used.
In the case where the Hamiltonian is time-independent, an explicit solution can be found expressing the state of the system in the basis of the eigenstates of the Hamiltonian

$$|\Psi(t)\rangle = \sum_n e^{-\imath E_n} \langle \Phi_n | \Psi_0 \rangle |\Phi_n\rangle .$$

There, the complications come from the sum over an arbitrary large number of terms and the scalar products between the eigenstates and the initial state. Even in the cases where the eigenstates are known, these tasks are usually too though to be done. Because of these problems, an explicit expression for the time evolution of generic observables is extremely difficult to find also for models where the spectrum is known.

Lieb-Robinson bounds It is anyway possible to extract more general results from the previous equation, as found by Lieb and Robinson in 1972 [158] and it will be discussed in Sec. 2.1. They analyze the problem from a more general point of view, looking for something as much universal as possible, that can be applied to the widest class of models. They find that if the interactions between sites have a finite range the effect of a local operator located in a finite set of the lattice takes a finite amount of time to affect another region at distance R. This amount of time $t^\star$ is called activation time and they find that it is proportional to the distance between R the two sets. The proportionality constant between $t^\star$ and R has the dimensions of a velocity and it is called the *Lieb-Robinson velocity*, $R = v_{lr} t^\star$. In the region $t < t^\star$ the effects of the perturbation are extremely

small.
In other words, the propagation of signals during the time evolution is bounded by a ballistic cone in the space-time diagram. The similarity between this effect and the propagation of information in special relativity motivates the name "light-cone" effect. As it is well known, relativity does not allow signals traveling with a velocity faster than c, the velocity of light in the vacuum. So, two points in the space-time diagram, for instance (R_1, t_1) and (R_2, t_2), can be connected just if

$$\frac{R_2 - R_1}{t_2 - t_1} \leq c.$$

This equation imposes a strict bound on the part of the (R, t) plane accessible to physical signals.
This bound on the maximum velocity is preserved also using quantum entangled states. These states are able to affects instantaneously two arbitrary distant points in space [159] but they cannot be used to send signals because of the probabilistic nature of quantum measurements [160]. It is well known that the quantum theory allows non-local and instantaneous effects. This can be done preparing the system in particular systems like Bell pairs. However, these particular states cannot be used to send communicate. Indeed, the first measurement on the Bell pair is probabilistic and it projects the state on an undetermined one. Therefore the pair cannot be used to send a chosen message.
The theorem demonstrated by Lieb and Robinson is anyway an *effective light-cone*. The effect of a local observable is extremely small outside the "light-cone" region but it is not strictly zero, as for a signal outside the real light-cone in a relativistic theory. Moreover, the result [158] provides just a bound and not an exact theorem, in this sense it has to be clear that the signals are suppressed in the outside-cone region. No clue is given by the theorem about what happens inside, where the bound is order $O(1)$ or larger. The Lieb-Robinson bound provides a universal result obtained without solving the equation of motion. However, the price to pay is the sacrifice of the knowledge of the structure inside this "light-cone".
The theorem is not able to determine in a clear and physical way the velocity v_{lr} which appears then just as a mathematical parameter with the dimensions of a velocity. It can depend on the specific form of the interactions, which do not enter in the scaling between $t^\star$ and R. The quantification of this parameter is fundamental to give to the entire bound a more practical use. These questions can be studied using the microscopic theory.

Cardy-Calabrese approach The first study of the connection between the velocity of the light-cone and the microscopic theory is due to Cardy and Calabrese in [161]. There, they studied how different observables evolve in time following a quantum quench to a point of the parameter space where the system is described by a conformal field theory [162]. In these theories, the model acquires scale invariance and, consequently, the dispersion relation $E_k = \lambda k$ is linear. The relevant velocity to describe the propagation of local observables, correlations in their case, is the group velocity $\lambda = \partial_k E_k$. More important than the result itself, an interpretation scheme is proposed in the paper. It states that the

spreading of correlations and other local observables following a quantum quench can be seen as the spreading of quasi-particles with a velocity determined by the group velocity $v_k = \partial_k E_k$. The light cone effect is generated by the fastest quasi-particles, because they are the first to connect two points.
The velocity of the light-cone is then simply determined by the microscopic theory as the maximum group velocity multiplied by two

$$v_{lc} = 2max_k \partial_k E_k.$$

How this factor 2 appears will be explained in detail in Sec. 2.2. Naively if we are observing correlations between two points, x_1 and $x_2 > x_1$, they both act as source of quasi-particles. Quasi-particles coming from x_1 to x_2 and vice-versa will meet half-way because they have the same velocity v_k. The effective distance to cover is then not R but $R/2$ which means that the particles effectively travel as the double of the velocity.
This is an important step. It connects directly the microscopic theory and the macroscopic one, provided by the Lieb-Robinson bound. Both of them agree on the scaling of the activation time $t^\star$, which is linear in R, and the microscopic theory determines exactly the light-cone velocity.
The Cardy and Calabrese argument has found to be able to predict the spreading of correlations also in situations not exactly described by the Lieb-Robinson bound. On the one hand ,the first just needs that the final Hamiltonian allows well-defined excitations with a finite maximum group velocity. On the other hand, the Lieb-Robinson result is a bound over the commutator between two local observables and its rigorous extension to the correlation function requires strict hypothesis on the pre-quench state.

Long-Range interactions The previous results hold for short-range interacting quantum systems. As we discussed in Sec. 1.3.1.4, different types of interactions can be realized in cold atomic gases, e.g. long-range interactions. The main question is: "Is it possible to find a macroscopic general bound if the interactions are long-range?". The answer is yes, as found in [163, 164] and we will discuss in Sec. 2.4. The result is anyway extremely different from the short-range case.
In the specific case of a lattice spin model with long-range interactions, it is possible to impose a bound on the commutator between local observables just if the long-range potential decays sufficiently fast. In this case, the bound depends explicitly on the form of the interactions. In particular, the activation time $t^\star$ is no longer proportional to R but one finds $t^\star \propto \ln[V(R)]$, where $V(R)$ is the potential. This changes drastically the scenario from the short-range point of view, mainly because it seems that the universality present in the short-range bound is completely lost.
Approaches to improve this logarithmic bound have been proposed. For example in [165] an extension of the previous theorem for finite systems with generic long-range interactions has been formulated. Another proposition [166, 167] has improved the light-cone shape, from a logarithmic bound to an algebraic one. We will analyze all these results in detail in Sec. 2.4 presenting their predictions on the time evolution of quantum systems. Since many different bounds are present, it is then important to study the time evolution

of long-range interacting quantum systems from the microscopic point of view. It will be possible to determine which of the proposed bounds, if any, describes correctly the time evolution. The study of exactly-solvable models with such interactions and their dynamics following a quantum quench is then crucial. Several works in the literature demonstrate the presence of different regimes in the propagation of correlations depending on the decay of the potential [168, 169, 170, 23, 171]. We will use the name "regime" to identify these behaviors to be consistent with the other works in the literature. They range from an instantaneous propagation for slow decaying interactions to a ballistic spreading for fast decaying interactions. These have been observed in t-DMRG [168], DTVP [169], t-VMC [23], DTWA [172]. Also, they have been observed analytically for exactly solvable models [173, 23, 170, 169]. On the other side, the extended Bose-Hubbard model, studied both with the t-VMC and the quasi-particles approach [23], exhibits a ballistic propagation for all the long-range potentials studied. We will review the most important literature works in Chap. 3 and 4, where we will also present my results published in [23, 170].
None of the results found in these works violates the macroscopic bounds proposed in [166, 163]. Anyway, it is clear that these are not able to predict the correct time evolution found in the numerical simulations and analytic computations.
It is then crucial to study and understand which are the key quantities to interpret properly the dynamics in the presence of such interactions. These results will be useful to lead the discovery of new, more precise, bounds which will be able to describe correctly the dynamics of quantum systems with long-range interactions that can be then extended to non-solvable models.

1.5 Thermalization

We briefly discuss now the thermalization problem. We give more details than about propagation of information since we will not discuss it again in this manuscript.

1.5.1 Ergodicity in closed quantum systems

Equilibrium is a fundamental condition in physics and the process that leads a system from an out-of-equilibrium state to an equilibrium one is called equilibration. This is a natural process in systems coupled to a bath or an external system because the exchange of quantities between the two leads to a stabilization of the macroscopic properties of smaller systems. For closed quantum systems anyway the system has to redistribute the excess of energy and other quantities alone. Internal interactions are then the only way for the system to restore equilibrium and this means to satisfy the ergodic condition.
The concept of ergodicity is clear in classical physics: it means the equivalence between time and phase-space averages. During its time evolution, the system explores all the accessible phase-space [1]. This portion is defined as the hyper-surface where the points have the same energy as the initial state. Mathematically, given the initial condition X_0, this hyper-surface is defined as $E = H(X_0) = H(X(t))$ where $X(t)$ is the time

evolution of the system.
The time evolution of a generic observable A in the phase-space can be written as

$$A(X(t)) = \int dY A(Y)\rho_{ps}(Y(t)),$$

where $\rho_{ps} = \delta(Y - X(t))$. This is the time-dependent density of points in the phase space. Since the time scales of the microscopic motion are extremely fast compared to the macroscopic ones, we can average this distribution over time in order to obtain a result independent on the microscopic dynamics. The result will depend just on the hyper-surface through E

$$\bar{\rho}_{ps} = \overline{\delta\left[Y - X\left(t\right)\right]} \equiv \lim_{T\to\infty} \frac{1}{T}\int_0^T dt\delta\left[Y - X\left(t\right)\right] = \rho_{mc}(E),$$

where $\bar{} = \lim_{T\to\infty}\frac{1}{T}\int_0^T dt$ and the density $\rho_{mc}(E)$ is the micro-canonical distribution. If we want a meaningful definition of phase-space averages, the memory of the initial condition X_0 has to be lost after a finite time smaller than the macroscopic time scales. This is true if the trajectory $X\left(t\right)$ covers uniformly the energy surface, meaning that we can start from every initial condition and span the entire surface, which is the definition of an ergodic system. In the case where this is true then it is possible to compute observables as phase-space averages instead of time averages.
In the domain of quantum physics the concept of quantum ergodicity is still not fully understood, even if its study has begun almost a century ago (in 1929 [174]). We can start from the microcanonical density matrix $\hat{\rho}_{mc}$. We can express this operator using the eigenstates $|\Psi_i\rangle$ and the eigenvalues E_i of the Hamiltonian $\mathcal{H}$. We can then define suitable energy shells of width δE around the mean values E, where δE is sufficiently small compared to macroscopic scales, but sufficiently large to contain enough microscopic energy levels. In this way, the average will be computed using a sufficiently large number of terms in order to obtain a meaningful result.
The microcanonical ensemble density matrix is then written as

$$\hat{\rho}_{mc} = \frac{1}{N_E}\sum_{i\in\mathcal{G}_E} |\Psi_i\rangle\langle\Psi_i|$$

where the sum is restricted to the set $\mathcal{G}_E$ defined by the N_E energy levels between E and $E + \delta E$.
Now we have to ask if every initial normalized state $|\Psi_0\rangle$, written in the $|\Psi_i\rangle$ basis

$$|\Psi_0\rangle = \sum_{i\in\mathcal{G}_E} c_i |\Psi_i\rangle \quad \sum_i |c_i|^2 = 1,$$

converges to the distribution $\hat{\rho}_{mc}$ for every set of coefficients c_i after a time average. If the system is closed, the time evolution is unitary and it gives

$$|\Psi(t)\rangle = e^{-\imath\mathcal{H}t}|\Psi_0\rangle = \sum_{i\in\mathcal{G}_E} c_{i,E}e^{-\imath E_i t}|\Psi_i\rangle\,.$$

We average over the time evolution as we did before, obtaining

$$\overline{|\Psi(t)\rangle\langle\Psi(t)|} \equiv \lim_{T\to\infty}\frac{1}{T}\int_0^T dt \sum_{i,j\in\mathcal{G}_E} c_i^* c_j e^{-\imath t(E_j-E_i)} |\Psi_j\rangle\langle\Psi_i|$$

the time average can be computed easily, giving

$$\lim_{T\to\infty}\frac{1}{T}\int_0^T dt e^{-\imath t(E_j-E_i)} = \delta(E_i - E_j)$$

Plugging this result in the previous equation we get the so called diagonal ensemble

$$\overline{|\Psi(t)\rangle\langle\Psi(t)|} = \sum_{i\in\mathcal{G}_E} |c_i|^2 |\Psi_i\rangle\langle\Psi_i| = \hat{\rho}_{diag}.$$

The ergodic condition is then satisfied if the equality $\hat{\rho}_{mc} = \hat{\rho}_{diag}$ holds. We need to request $|c_i|^2 = 1/N_E$ which is extremely stringent condition on the initial state. It is then almost impossible to realize quantum ergodicity simply "quantizing" the same concept already seen for classical systems [174, 175].
The problem can be solved focusing on the observables instead of on quantum states [176, 177, 174]. If we choose a set of macroscopic observables $\mathcal{M}_\beta$, we expect that, in the long-time limit, the expectation value tends to the one of the microcanonical ensemble

$$\lim_{t\to\infty}\langle\Psi(t)|\mathcal{M}_\beta|\Psi(t)\rangle \to Tr[\mathcal{M}_\beta\hat{\rho}_{mc}] \equiv \langle\mathcal{M}_\beta\rangle_{mc}. \tag{1.6}$$

The limit procedure have to be taken carefully because of the presence of revivals in finite systems [178]. This means that the thermodynamic limit has to be taken before the long-time limit, if we invert these two, no thermalization will be present. A rigorous way to define the equality (1.6) consists in computing the mean square difference between the two sides and observe if this goes to zero with time [179].
In other case, a simpler solution consists in evaluating the time average of Eq. (1.6) and verifying that

$$\overline{\langle\Psi(t)|\mathcal{M}_\beta|\Psi(t)\rangle} = Tr[\mathcal{M}_\beta\hat{\rho}_{diag}] \to \langle\mathcal{M}_\beta\rangle_{mc}.$$

If this holds, the diagonal ensemble and the microcanonical ensemble give the same expectation values, i.e. they are equivalent. This is true if the observables $\mathcal{M}_\beta$ depend just on the macrostate and not on the microstate of the system. Mathematically this forces the observables $\mathcal{M}_\alpha$ to commute and to be coarse grained over the surface $\mathcal{G}_E$. This means that if we take two eigenstates $|\Psi_i\rangle$ and $|\Psi_{i+1}\rangle$ so that $|E_i - E_{i+1}| \sim \delta E$, then

$$|\langle\Psi_i|\mathcal{M}_\beta|\Psi_i\rangle - \langle\Psi_{i+1}|\mathcal{M}_\beta|\Psi_{i+1}\rangle| \sim \frac{1}{\sqrt{D}} \quad \forall\beta,$$

where D is the dimension of the Hilbert space. This forces the observables to have almost the same expectation value over the surface $\mathcal{G}_E$. If the previous hypothesis are satisfied then it is possible to demonstrate that the diagonal ensemble and the microcanonical one are equivalent for non pathological initial state $|\Psi_0\rangle$. The system is then ergodic.

1.5.2 The generalized Gibbs ensemble

All the previous discussion is purely mathematical and it is then important to find examples where ergodicity is explicitly found.
The discussion in the previous section seems to state that ergodicity is present in every quantum system, many experimental works, as [180], tell us a completely different story: ergodicity is not at all guaranteed in a quantum system. If It is described by an integrable or nearly-integrable Hamiltonian, thermalization can be absent. An integrable Hamiltonian is a theory where an infinite number of conserved charges is present. The absence of thermalization in these systems has been predicted in several works [181, 182, 183]. The presence of these conserved charges constraints the motion of the system in a portion of the Hilbert space which is much smaller than the one needed to satisfy ergodicity. This condition is then absent and the state of the system cannot relax to a thermal state but only possibly to a different ensemble. The conserved charges have to respect the same hypothesis as the operators $\mathcal{M}_\beta$ we saw before. This automatically excludes the projector operators. Any Hamiltonian has an trivial infinite set of conserved operators: $P_j = |\Psi_j\rangle \langle\Psi_j|$ where $|\Psi_j\rangle$ is the eigenstate of the Hamiltonian. These operators are in fact not coarse grained over the surface $\mathcal{G}_E$. If we take two states $|\Psi_i\rangle$ of energy E_i and $|\Psi_{i+1}\rangle$ of energy E_{i+1}, the difference between their expectation values is not going to zero

$$| \langle\Psi_i|P_j|\Psi_i\rangle - \langle\Psi_{i+1}|P_j|\Psi_{i+1}\rangle | = \begin{cases} 1 & j \in \{i, i+1\} \\ 0 & \text{otherwise} \end{cases}$$

The projector operators, even if they are always conserved during the time evolution, are not meaningful operators to describe thermalization.
In the next examples we will see practical cases in quantum and classical mechanics where these conserved quantities are explicitly found.

Integrability in classical systems To discuss this point, we can give more details using a simple toy model of classical integrable system which is the periodic harmonic chain, which Hamiltonian reads

$$\mathcal{H} = \sum_{i=0}^{M-1} \left[\frac{p_i^2}{2m} + \frac{m\nu^2}{2} (x_j - x_{j+1})^2 \right]$$

where x_j are the deviations from the equilibrium positions, p_i are the momenta of the particles and M is the number of particles, and we assume periodic boundary conditions on the chain. We drive the system out of equilibrium displacing some of the particles from their equilibrium positions. We can then study the time evolution of this out-of-equilibrium state. The Hamiltonian can be diagonalized in the Fourier space. It describes excitations of quasi momenta $q_n = 2\pi n/M$ with $n \in \mathbb{N}$ and the dispersion relation $\omega_n = 2\nu \sin(q/2)$. The absence of thermalization in this case is due to the fact that no exchange of energy is present between the q_n modes, but the system can reach an asymptotic state at very long times [184, 185].

This can be understood from the explicit expression of the displacement of one of the particles, which can be written in Fourier space as

$$x_j(j) = \sum_{n=0}^{M-1} x_{q_n}(t) e^{-\imath q_n j},$$

and

$$x_q(t) = A_q \cos(\omega_q t),$$

where A_q is the complex amplitude determined by the initial conditions. If we assume that just the small momenta $q \ll \pi$ are excited, it is then possible to linearize the dispersion relation around $q \approx 0$, where $\omega_q \approx \nu q$. Since the spectrum is linear, the state of the system is periodic of period $T = M/\nu$. The motions persists for infinite time and the system does not thermalize to a steady state. Thermalization appears if the linear approximation does not hold. In that case, a time scale is identified by

$$\tau(\omega_{\bar{n}+1} + \omega_{\bar{n}-1} - 2\omega_{\bar{n}}) \sim 1,$$

where $\bar{n}$ is the maximum of A_q. For the model we are interested in it is possible to compute explicitly as $\tau \sim M^2/\nu$ and this defines the long-time limit. For $t \gg \tau$ all the modes are completely dephased and the different modes are uncorrelated due to non-linear effects in the spectrum. This final state is completely determined by the modules of the amplitudes, $|A_q|$, which are M real-valued numbers representing the occupancies of the respective modes and which are conserved during the time evolution.

Integrability in quantum systems If we now try to extend the previous argument to the quantum case, we can consider a simple many-body integrable model as the Ising chain in transverse field [126]. Its Hamiltonian reads

$$\mathcal{H} = -\sum_i \left(\sigma_i^x \sigma_{i+1}^x + g\sigma_i^z\right),$$

where σ_i^x and σ_i^z are the local spin operators at the site i, and g is the interactions strength of the magnetic field normalized to the spin exchange coupling. This model has a simple phase transition at $g_c = 1$ where the spectrum of excitations becomes gapless. For values of $g < g_c$ the system is ferromagnetic and for $g > g_c$ the system is paramagnetic. Both these phases are gapped. The system can be diagonalized mapping it to a free fermionic model using the Jordan-Wigner transformations [186] and then writing the Hamiltonian in the Fourier space

$$\mathcal{H} = 2\sum_{k>0} \left[(g - \cos(k)) \left(c_k^\dagger c_k - c_{-k} c_{-k}^\dagger\right) + \imath \sin(k) \left(c_k^\dagger c_{-k}^\dagger - c_{-k} c_k\right)\right],$$

where $k = 2\pi n/L$ where L is the length of the chain. Using a standard Bogoliubov transformation, $c_k = \cos(\theta_k)\gamma_k - \imath \sin(\theta_k)\gamma_{-k}^\dagger$ [7], and choosing $\tan(2\theta_k) = \sin(k)/[g - \cos(k)]$ the previous Hamiltonian becomes diagonal

$$\mathcal{H} = \sum_k E_k \gamma_k^\dagger \gamma_k,$$

where $E_k = 2\sqrt{[g-\cos(k)]^2+\sin^2(k)}$ is the dispersion relation of the Bogoliubov quasi-particles. The time evolution of the system can then be easily written from the equation of motion of the γ_k which diagonalize the Hamiltonian $\gamma_k = \exp(-\imath E_k t)\,\gamma_k(0)$. As for the harmonic chains, the time-dependent phases are incommensurate and they become completely uncorrelated after long times. Anyway, the occupation of every energy level, namely $\langle\gamma_k^\dagger\gamma_k\rangle$, is constant during the time evolution. We can study the time evolution of the total magnetization following a sudden quench in the parameter g [10], which a global operator and it reads

$$\begin{aligned} M^x(t) = \sum_i \sigma_i^x &= -2\sum_{k>0}\Big[\cos(2\theta_k)\left(\gamma_k^\dagger\gamma_k - \gamma_{-k}\gamma_{-k}^\dagger\right) \\ &\quad + \imath\sin(2\theta_k)\left(\gamma_{-k}\gamma_k e^{-\imath 2E_k t} - \gamma_k^\dagger\gamma_{-k}^\dagger e^{\imath 2E_k t}\right)\Big]. \end{aligned}$$

If we take the time average of this expression, we find that its expectation value over a generic initial state $|\Psi_0\rangle$ is

$$\overline{\langle M^x(t)\rangle} = -2\sum_{k>0}\cos(2\theta_k)\left(\langle\gamma_k^\dagger\gamma_k\rangle - \langle\gamma_{-k}\gamma_{-k}^\dagger\rangle\right)$$

so its thermalization value depends just on the initial occupation number. Looking at this peculiarity, Rigol et al. [187] suggested that the steady state of the system is described by an ensemble of the type

$$\rho_G = \frac{1}{Z}e^{-\sum_k \lambda_k\gamma_k^\dagger\gamma_k},$$

which is a generalization of the Gibbs ensemble to the case of L conserved quantities $\gamma_k^\dagger\gamma_k$.
The form of ρ_G can then be used to compute expectation values of local observables. As for the standard ensembles the Lagrange multipliers λ_k are fixed by the conditions

$$\langle\Psi_0|\,\gamma_k^\dagger\gamma_k\,|\Psi_0\rangle = Tr\left[\rho_G n_k\right] = \langle\gamma_k^\dagger\gamma_k\rangle_G$$

The Generalized Gibbs Ensemble (GGE) The ensemble ρ_G is exactly the one presented in [188] to describe the behavior of a system with N conserved quantities I_α. In this case the maximization of the entropy has to be done introducing N Lagrange multipliers λ_α. The subsequent ensemble has the density matrix

$$\rho_G = \frac{e^{-\sum_\alpha \lambda_\alpha I_\alpha}}{Z}.$$

It is usually assumed that all integrable theories thermalize to a GGE. It has then to be determined the nature of the quantum charges to include in the exponent of the summation. This opens several problems on the set of observables that have to be chosen because in principle the projectors on the eigenstates of the Hamiltonian are always conserved for all systems, both integrable and non-integrable. The answer to this question can be found studying the case of the Gibbs ensemble. There, the explicit form

of the probability density comes from the fact that sufficiently large subsystems have to behave as statistically independent. This assumption and the fact that the conserved quantities have to be additive are crucial for the determination of the Gibbs ensemble as the exponential of the energy and not of another function of the energy. In the same way, the conserved charges I_α have to be chosen to be additive when the subsystem considered is sufficiently large. For the specific case of the Ising model, the operators $\gamma_k^\dagger \gamma_k$ have been found to respect these conditions in [187]. The relaxation of different integrable models to the GGE has been tested explicitly in many different models as: Luttinger Liquids [189, 190], free bosonic theories [191, 192], hardcore bosons [187], Lieb-Lininger model [193, 194], spin models [195, 196, 197, 198] and Hubbard-like models [199, 200]. The previous discussion is more an argument than a real theorem, even if thermalization has been found in some classes of models, a general theorem that states how different systems thermalize is still missing. Moreover, the exploration of long-time dynamics of many-body interacting quantum systems is, from the numerical point of view, extremely challenging. The possibility to simulate different Hamiltonians in experimental cold atomic gases plays then a key role in the exploration of the thermalization problem in such systems. As we said in Sec. 1.3, cold atomic gases can be used to engineer different Hamiltonians and to drive them out of equilibrium. Moreover it is also possible to constraint systems in reduced dimensionality, as one or two dimensional geometries. Integrability is in fact an extremely delicate characteristic of the system, a fine tuning of all parameters of the Hamiltonian is needed to observe it. Extra terms in the Hamiltonian drive the system away from integrability and produce drastically different results. In classical physics the role of perturbations in an integrable theory is well understood using the KAM theory [3]. At the quantum level, however, this is not the case. Even small perturbations produce pre-thermalisation plateau [201, 148, 202] described by the GGE before that real thermalization occurs. Anyway, it is still not known how to define "small" and "large" in the context of perturbation around the integrable case.

1.5.3 Experimental study of thermalization in closed quantum systems

As we said in the last section, integrability is an extremely delicate peculiarity of some Hamiltonians and, anyway, its effects on the physical behavior of quantum systems are drastic, in particular on their thermalization. We want now to discuss two main experiments on thermalization in closed quantum systems, in integrable and non-integrable models. The first one is the observation of the absence of thermalization in a many body quantum systems due to its integrability. The second one is the experimental observation of thermalization in the Bose-Hubbard model. We present these two examples between many others because they are two milestones in this topic. They exhibit how cold atomic gases can be used to explore these systems that demand an extremely fine tuning of all the parameters which can be achieved just in these setups.

Absence of thermalization: the quantum Newton cradle. The "quantum Newton cradle" realized by T. Konishita and his collaborators in 2006 [180] is one of the most beautiful examples of how cold atoms can study time evolution for extremely long times.

The system is a bosonic one dimensional gas described by the Lieb-Liniger [203] Hamiltonian

$$\mathcal{H}_{LL} = -\frac{\hbar^2}{2m}\sum_i \partial_i^2 + g\sum_{i<j}\delta\left(x_i - x_j\right).$$

It represents bosons with point-like interactions of coupling constant g. The system has two different regimes controlled by the parameter $\gamma = mg/\hbar n_{1D}$, where m is the mass of the particles, and n_{1D} is the one-dimensional density of the confined bosonic gas [203, 204]. When γ is small, the system is can be described as weakly-interacting bosons. In the opposite the limit, $\gamma \gg 1$, the system is described by a symmetric wave function: Tonks-Girardeau wave-function [205]. This wave-function is obtained by the modulus of a determinant of anti-symmetric wave functions of spinless fermions.
In the experiment, the one-dimensional system is weakly confined using a harmonic trap and it is prepared in the ground state of the Hamiltonian. At $t = 0$ the wave-function is then split in two equal parts with equal and opposite momentum. This is obtained pulsing a $3,2\,THz$ optical lattice along the tubes which acts as a phase grating [206]. Two pulses of intensity $11 W cm^{-2}$, time length $23\mu s$, and time separation $33\mu s$ deplete the region at $k \approx 0$ momentum and populate the states of momentum $\pm k$, the wave-vector of the superimposed optical lattice. The two split wave functions oscillate in the trap, colliding again at its center. During the collision they exchange momentum and energy as in the famous Newton cradle. The astonishing fact is that these oscillations are persistent and a relaxation is found just for extremely long time, see Fig. 1.11.

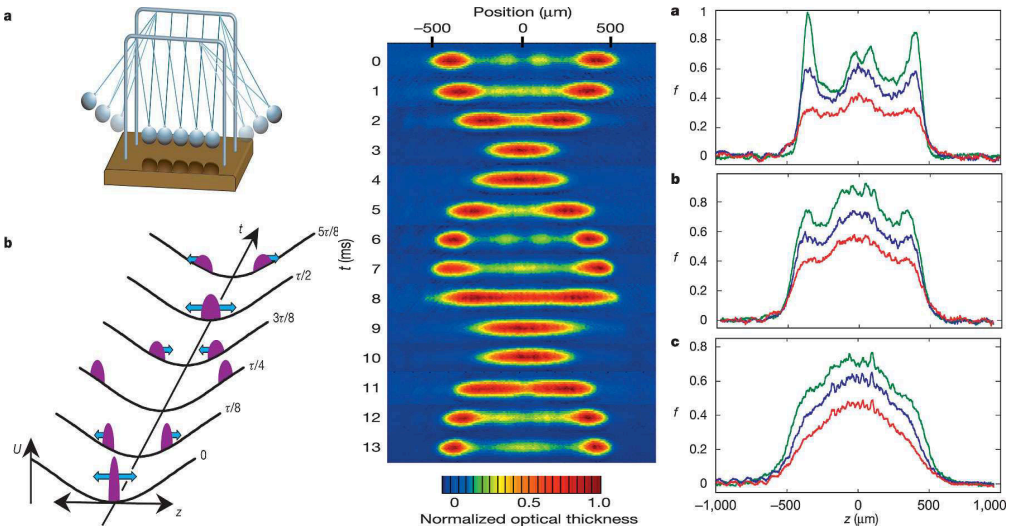

Figure 1.11: Left: Pictorical representation of the quantum Newton's cradle experiment. Center: Data from the time evolution of the experiment with the $n(x)$. Right: plot of the momentum distribution at different times, the memory of the initial state remains for extremely long times as predicted by thermalization for nearly integrable models. Figures from Ref. [180].

This effect has been found for all the values of γ studied, and it is due to the fact that the Lieb-Lininger Hamiltonian is integrable in one dimension [50]. Once the experiment is reproduced in a 2 or 3 dimensional trap the system thermalizes to an equilibrium distribution after some collisions of the two wave-functions. This effect is a signature of the absence of integrability of the Hamiltonian in dimensions higher than one [207]. Thermalization can be detected looking at the momentum distribution, measured using time-of-flight techniques. In 1D the momentum distribution comes back always to the initial value while in 3D it thermalizes to the Gaussian equilibrium function after some collisions, Figs. 1.11. This experiment is particularly important because of the presence of a weak confinement along the axis of motion which explicitly breaks the integrability of the Hamiltonian. This absence of integrability creates pre-thermalization plateaus where the system behaves as an integrable system. The system is supposed to thermalize to the standard thermal distribution for larger times. These time scales are not accessible by this experiment.

Thermalization: the Bose-Hubbard Hamiltonian The experiment performed by Trotzky et al. [208] explores on the other hand the relaxation in systems with non-integrable Hamiltonians. They study the relaxation in a Bose-Hubbard chain with harmonic trap, described by the Hamiltonian

$$\mathcal{H} = \sum_i \left[-J \left(\hat{a}_i^\dagger \hat{a}_{i+1} + \hat{a}_i \hat{a}_{i+1}^\dagger \right) + \frac{U}{2} \hat{n}_i \left(\hat{n}_i - 1 \right) + \frac{K}{2} j^2 \hat{n}_i \right]$$

where J controls the short-range hopping between nearest-neighbor sites, U the on-site interactions, and K the interaction between the particles and the confinement potential. As we said in Sec. 1.3.2, this Hamiltonian can be implemented in modern cold atomic gases.

The out-of-equilibrium protocol is the following, see Fig. 1.12:

1. The initial state of the system at $t = 0$ is

$$|\psi\left(t = 0\right)\rangle = |\ldots, 1, 0, 1, 0, \ldots\rangle \tag{1.7}$$

   where just the "even" sites are occupied and the "odd ones are empty. The couplings J and U are such that no tunneling between nearest neighbor sites is allowed.

2. At $t = 0$ the quench is performed to a set of values J, U, and K such that tunneling is allowed and the state $|\psi\left(t = 0\right)\rangle$ evolves according to the Hamiltonian.

3. After a time t the time evolution is frozen suppressing the tunneling. The state $|\psi(t)\rangle$ is probed measuring the density in the odd-sites thanks to band-mapping techniques.

The initial state is prepared creating a set of one dimensional systems using a three dimensional lattice of wave length $\lambda_{xl} = 1,530$ nm. The motion along the y and z directions is suppressed using laser beams of wave-length $\lambda_{y,z} = 844$ nm. This configuration

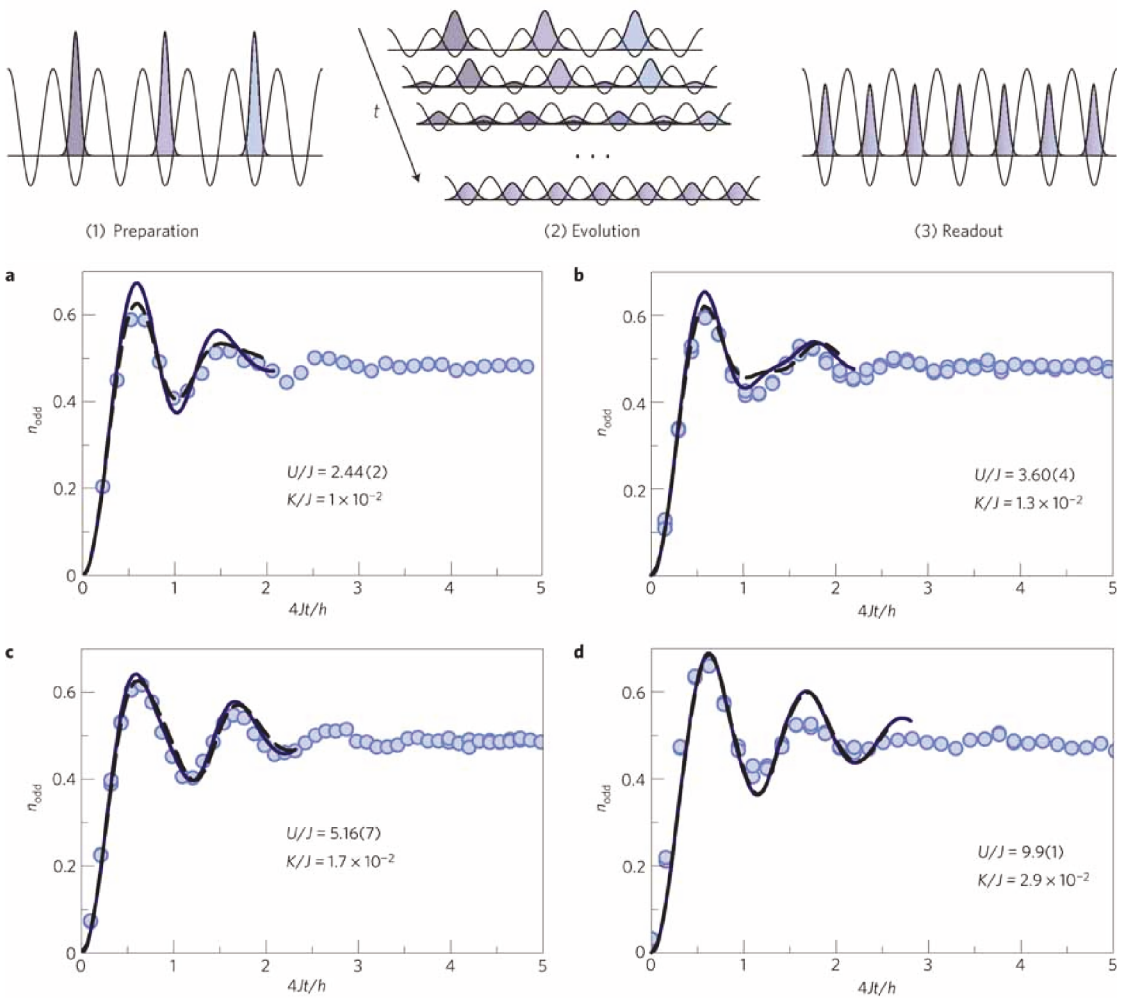

Figure 1.12: Top panel: Schematic representation of the Out-of-Equilibrium protocol performed in [208]. In the stage (1) the system is prepared in the state with an ordered state with one particle every two sites, the tunneling between the sites is suppressed thanks to the enhancement of the barrier. In the second stage (2), the tunneling between ties is allowed and the particles can jump from a site to the other one. In th final stage (3), the system is frozen again enhancing the potential barriers and the state of the system is read using fluorescence. Bottom panel: Results for the quantity n_{odd} presented in [208]. The solid line represents the t-DMRG results with just nearest-neighbor hopping while the dashed one represents the same computations with next-to-nearest-neighbor interactions obtained by the same method. Figure from Ref. [208].

of the couplings creates a set of 1D Mott insulators with an average of one atom per site, see Sec. 1.3.2. The systems are not all equal: the average number of particles for every $1D$ system is 31 while the maximum number of particles is 43.
A shorter lattice of wave length $\lambda_{x,s} = 2\lambda_{x,l}$ is added along the x-direction. This lattice creates empty sites in between of the already present ones. After that, the lasers of wave length $\lambda_{x,l}$ are turned off and the initial state of (1.7) is realized. Since the values of the hopping are extremely small, the system is completely frozen.
At time $t = 0$, step 2 is performed allowing the dynamics of the particles along the x direction, the hopping along the other two directions is still suppressed. After a time t the intensity of the laser is ramped up to the initial value and the dynamics stops. The system is now ready to be probed. Clearly, the measures are performed at the same time on all the 1D tubes and the results of the experiment are the averages over all the tubes. The time evolution of the density of the odd sites is measured using band-mapping technique [209, 210] and they are compared to accurate t-DMRG simulations for the same systems and geometry. A good agreement between numerics and experimental results is found for $U/J \lesssim 6$. The difference between the two for larger values of U/J is due to next-to-nearest neighbor hopping. These processes are represented by

$$\mathcal{H}_{hop}^{NN} = -J_{NNN} \sum_i \left(\hat{a}_{i+2}^\dagger \hat{a}_i + \hat{a}_{i+2} \hat{a}_i^\dagger \right),$$

which, once included in the numerical simulations, improves the agreement between numerical and experimental data, see Fig. 1.12. For even larger values, $U/J \gtrsim 10$, larger deviations are observed and they are due to the residual hopping between different tubes which is not taken into account in numerical simulations.
The density of odd sites exhibits oscillations of period $T \simeq h/4J$ and it damps to its equilibrium value, $n_{odd} = 1/2$, after less than 5 oscillations. In the absence of the trap, $K = 0$, the time evolution can be computed analytically in the cases of $U/J \approx 0$ or $U/J \to \infty$ using different types of perturbative approaches [211, 212]. Since both these approaches are based on free-quasi-particles, the correlation functions are algebraically suppressed as $1/\sqrt{t}$. The measured ones decay as $1/t^\gamma$ with $\gamma > 1/2$ because of the residual interactions between quasi-particles neglected in the theoretical models. Interactions between fundamental excitations helps to redistribute the energy and momentum between the degrees of freedom. This leads to a faster relaxation than in the free case. The numerical results obtained by t-DMRG are again in agreement with the experimental ones, showing a faster decay than the analytic case.

The two previous examples illustrate how integrability drastically affects the out-of-equilibrium dynamics. Integrability, in fact, reduces the portion of the Hilbert space accessible to the dynamics of system. The system is not able to explore the whole portion of the Hilbert space necessary to satisfy ergodicity. Absence of integrability allows a much faster exploration of the Hilbert space. This effect is stimulated by the presence of interactions, they are responsible for the exchange of energy between the degrees of freedom and they lead to a faster relaxation than in the free case.

2 Lieb-Robinson bounds and light-cone-like dynamics

In the previous section we briefly introduced the problem of the out-of-equilibrium dynamics in many-body quantum systems and then we discussed the thermalization problem. In this chapter we will revise the most important literature results on the dynamics of correlations we briefly outlined in Sec. 1.4.
At first, we start from the bound on short-range interacting lattice spin models known as the Lieb-Robinson bound (LR) [158] and its consequences on the correlation function [163, 213]. Both these results predict that the correlations between two local observables need a finite amount of time to be activated when the system is out-of-equilibrium. This activation time scales linearly with the distance between the two observables, creating an effective light-cone in the time-space plane. We then analyze the quasi-particle picture as explained by Calabrese and Cardy (CC) in Ref. [161]. We will see how the microscopic point of view (CC) is consistent with the macroscopic bound (LR) and moreover how it fixes some of its free parameters, as the light-cone velocity. We then review some of the numerical and experimental main results that confirm the presence of a light-cone structure in the evolution of correlations like the one performed by M Cheneau et al. [214] and the numerical results provided by t-DMRG [215] and t-VMC that we will discuss in more details [216].
We will then present several extension of the LR theorem to other types of interactions, such as long-range ones [163, 164, 166, 165]. Most important, we will see how the bound drastically changes its physics compared to the short-range case. For the long-range case the correlated region is no longer linear but its shape depends on the long-range potential. It thus exhibits a much faster propagation of correlations than in the short-range case.
The effects of these interactions on the time evolution of local observables will be the main topic of the rest of the manuscript.

2.1 Lieb-Robinson bound

2.1.1 Time-dependent dynamics

The time evolution of a closed quantum mechanical system is governed by the Schrödinger equation

$$\imath\partial_t |\Psi\rangle = \mathcal{H} |\Psi\rangle$$

where we set $\hbar = 1$, $|\Psi\rangle$ is the state of the system described by a vector in an Hilbert space, $\mathcal{H}$ is the Hamilton operator that can be a generic Hermitian operator defined in

the same Hilbert space as the state.
If the Hamiltonian is time independent, $\partial_t \mathcal{H} = 0$, then the previous equation has a simple solution

$$|\Psi\rangle = e^{-\imath t\mathcal{H}} |\Psi_0\rangle ,$$

We can then expand the previous expression on the basis of the eigenvectors of the Hamiltonian

$$\mathcal{H} |n\rangle = E_n |n\rangle ,$$

to obtain

$$|\Psi(t)\rangle = \sum_n e^{-\imath t E_n} |n\rangle \langle n|\Psi\rangle .$$

The time evolution of the state depends just on the spectrum of the Hamiltonian and the overlaps between the eigenvalues $|n\rangle$ and the initial state $|\Psi_0\rangle$.
In the context of quantum quenches, see Sec. 1.3.4, the time evolution is exactly given by the exponential time evolution because the post-quench Hamiltonian is time-independent as the initial one. The initial state, $|\Psi_0\rangle$, is not an eigenstate of the final Hamiltonian and then a non-trivial dynamics may show up.
The time evolution of expectation values of a generic operator A follows naturally by

$$\langle A\rangle(t) = \langle \Psi(t)| A |\Psi(t)\rangle = \sum_{n,m} e^{-\imath t(E_n - E_m)} \langle \Psi_0|m\rangle \langle n|\Psi_0\rangle \langle m| A |n\rangle . \tag{2.1}$$

Apparently this solves completely the problem of the time evolution in a generic quantum mechanical following a quantum quench.
Apparently, because the previous expression hides some insidious problems to solve:

1. The exact solution of the Hamiltonian can be done just for simple models. For a generic many-body interacting quantum system it is almost impossible to solve it. Anyway, even when this solution is available, a clear physical interpretation is difficult to extrapolate from the previous exact expressions.

2. The overlaps between the initial state $|\Psi_0\rangle$ and the eigenstates of the Hamiltonian are extremely complicated to write as function of the parameters of the problem, in particular in the case of a many-body system.

3. The summation over all the quantum numbers n and m is extremely difficult and actually almost impossible to be carried out exactly for generic systems.

The previous tasks can be done in just several specific cases like solvable models for a small number of particles and taking an initial specific initial state. An example is shown in Ref. [217] for the exactly solvable Lieb-Lininger model where the quench can be computed exactly just for less than 10 particles and starting from a non-interacting state. In these cases, numerical approaches are fundamental, because they are the only method able to compute the time evolution. We will review the most important methods, as t-DMRG and t-VMC later in this chapter.
The situation becomes much more complicated if we allow the Hamiltonian to be time

dependent, $\mathcal{H}(t)$. In this case the solution of the Schrödinger equation has to be expressed implicitly using the time evolution operator $\mathcal{U}(t_1, t_0)$ which has the following general properties

$$\begin{aligned} \mathcal{U}(t_1, t_1) &= \mathbb{I} \\ \mathcal{U}(t_2, t_1)\mathcal{U}(t_1, t_0) &= \mathcal{U}(t_2, t_0) \\ \imath\partial_t \mathcal{U}(t, t_0) &= \mathcal{H}\mathcal{U}(t, t_0) \end{aligned}$$

If the system is prepared in an initial state $|\Psi_0\rangle$at a time t_0, the time evolved state is

$$|\Psi(t)\rangle = \mathcal{U}(t, t_0)\,|\Psi_0\rangle\,.$$

Using the previous properties the time-evolution operator can then be written as a power series in the following form

$$\mathcal{U}(t, t_0) = \mathbb{I} + \sum_{n\in\mathcal{N}^\star} (-\imath)^n \int_{t_0}^{t} dt_1 \int_{t_0}^{t_1} dt_2 \ldots \int_{t_0}^{t_{n-1}} dt_n \mathcal{H}(t_1)\mathcal{H}(t_2)\ldots\mathcal{H}(t_n)$$

It seems like the only way to obtain a solution of the problem in a generic case is a numerical exact diagonalization of the Hamiltonian and a subsequent numerical evaluation of the equation (2.1). Clearly these results will be extremely size- and model-dependent and they will not give any hint about the real physics taking place at different scales during the time evolution. Luckily, some bounds on the time evolution of a wide class of Hamiltonians have been demonstrated. These results have the strong point to be extremely general and they provide general bounds on the dynamics of different observables. The first one of these results is the Lieb and Robinson bound on short-range interacting lattice Hamiltonian. It states that the dynamics of the commutator between two local observables is constrained inside a region in the R and t plane. The result has been demonstrated for the first time in Ref. [158] and then it has been extended to more general lattices in other papers [164, 163, 218].

2.1.2 Lieb-Robinson bound

In this section we do not want to give full details of the mathematical demonstration of the theorem but we will simply sketch its most important passages. Our aim is to give the most clear physical interpretation as possible. The theorem holds for lattice systems with short-range interactions and finite local Hilbert space, the prototype of such a system is a one dimensional Ising model in transverse field, the Hamiltonian of which reads

$$\mathcal{H} = -J\sum_{j=1}^{N-1} S_j^z S_{j+1}^z + B\sum_{j=1}^{N} S_j^x, \tag{2.2}$$

with open boundary condition (OBC). The local Hilbert space of every site j has dimension 2, spin up and spin down. It means that the entire system is represented in a space

of dimension 2^N. For a more generic situation with local Hilbert space of dimension d, the total Hilbert space is given by d^N where N is the total number of the sites.
Hamiltonian (2.2) is composed by two parts: the one involving the interaction between a spin and the external field B, which acts just on the local Hilbert space of the j-th site independently from the others. The spin exchange part is represented by the $S_i^x S_{i+1}^x$ term, which creates interaction between nearest-neighbor spins. It has a finite range because its effect involves just spins at finite distance $R = 1$. In the future, we will refer to these interactions as "short-range". We will apply this terminology to all the interactions acting on a finite set of sites of the lattice. Other examples of "short-range" interactions are next-to-nearest-neighbor interactions as $S_j^x S_{j+2}^x$ and all the other types of Hamiltonians acting on a site i and on the $i + R$ with finite R.
What we want to demonstrate is that local operators in different disjoint regions of the lattice need time to be in contact due to the fact that local interactions take a finite time to connect them. An example of this process can be done using Hamiltonian (2.2). Since the interactions are restricted to nearest-neighbor sites, a spin flip at site i takes a finite time to affect the site $i + \delta$. In fact, this spin-flip has to interact with all the sites in between i and $i + \delta$. The velocity of this spreading is not simply the $\hbar/J$, determined by the nearest-neighbor coupling, but a more complicated one we will present in Sec. 2.2. Assuming that interactions are just local we can prove that the effects of a local operator are exponentially suppressed outside a linearly increasing region of the lattice.
This result fixes the concept of "locality" for many-body quantum systems when they are out-of-equilibrium. The perturbation introduced by a generic local operator located in a region of the lattice spreads with a constant fixed velocity. The previous sentence needs to be associated to a distance, in order to define what is "near" and "far" from a site and define also properly which are "short-range" interactions and which are not. The natural distance defined on a lattice system is the Manhattan metric [219]

$$M(x, y) = \sum_{i=1}^{D} |x_i - y_i|,$$

where x_i and y_i are the components along different directions of the two position vectors x and y. Furthermore, the theorem holds for all the generic types of distance which can be defined over the lattice. We will refer to the distance between the site i and j simply as $\mathrm{dist}(i, j)$, assuming that it fulfills all the geometrical requirements for this quantity and it scales linearly with the distance between the two points.
The distance between two sets of the lattice X and Y is then defined as

$$\mathrm{dist}(X, Y) = \min_{i \in X, j \in Y} dist(i, j)$$

which represents simply the shortest path between the two in the chosen metrics. In the same way we can write the diameter of a region A as

$$\mathrm{diam}(A) = \max_{i \in A, j \in A} dist(i, j),$$

which is the maximal distance between two points of the set.
We can then define what is a "short-range" Hamiltonian as

$$\mathcal{H} = \sum_{Z} \mathcal{H}_Z \tag{2.3}$$

where every term in the sum has support just over a finite set Z and is zero outside the set $diam(Z)$ for every Z, assuming diam(Z) bounded by a constant. In this section we will assume the Hamiltonian to be time-independent in order to have simpler expressions but it is clear that the following argument can be applied to every Hamiltonian with a little effort.
Even if this concept seems to be really abstract, Hamiltonian (2.2) can be written simply in the form of Eq. (4.1). The model we are studying is in one dimension and many simplifications comes from this fact, for example the Manhattan metrics described before is equal to the standard Cartesian metrics, $dist(i,j) = |i-j|$. All the interaction terms $S_i^z S_{i+1}^z$ are zero outside a region of diameter $diam(S_i^z S_{i+1}^z) = 1$, the interaction between the spins and the external spins has zero diameter $diam(S_i^z) = 0$ because it involves just one site. The importance of the metrics arises in the case of periodic boundary conditions, which can be obtained adding a term to (2.2)

$$\mathcal{H} = -J \sum_{j=1}^{N-1} S_j^z S_{j+1}^z - J S_N^z S_1^z + B \sum_{j=1}^{N} S_j^x. \tag{2.4}$$

If we compute the range of the new interaction term using the standard distance for open boundary we obtain $diam(S_N^z S_1^z) = |N-1| = N-1$ which is clearly a wrong answer. The problem is due to the fact that the metrics $|i-j|$ describes the distance between the points just if the system has open boundary condition, see Fig. 2.1. If the boundary conditions are periodic then two paths connect two points and the correct distance is the shortest one of them, namely

$$d_{PBC}(i,j) = \min\left(|i-j|, |i-j \pm N|\right).$$

Using this definition we find that all the spin-spin terms have diameter 1 while the field-spin terms have all diameter 0. In conclusion, the choice of the metric, which means the way we measure space, has to be compatible with the physical problem we are looking at and for the phenomenon we want to study. The concept of "short-range" Hamiltonian, which means that just near sites can interact, is represented by the fact that $\mathcal{H}_Z$ has to decay fast with its range, $diam\,(Z)$. Mathematically, this is written as

$$\sum_{Z \ni i} \|\mathcal{H}_Z\| |Z| e^{\mu(\mathrm{diam}(Z))} \leq s < \infty \tag{2.5}$$

for all sites i and where μ and s are some finite real constants. The term $\|\mathcal{H}_Z\|$ represents the operator norm of $\mathcal{H}_Z$ and it corresponds to its larger eigenvalue. The previous expression holds if $\|\mathcal{H}_Z\|$ decays at least exponentially in the interaction diameter which

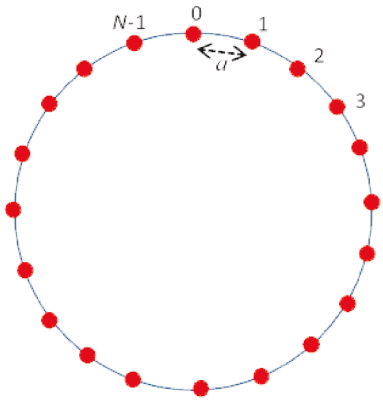

Figure 2.1: Schematic representation of a spin system with periodic boundary conditions (PBC), where the $N-1$-th spin interacts with the 0-th. It is possible to see how the distance we use in the case of open boundary conditions (OBC) gives completely wrong results. The distance between the initial and the last site using OBC distance is $d(0, N-1) = |N-1|$. If we analyze the problem more physically we understand that this picture is wrong because the two are just aside. The right definition of distance in this case is $d(0, N-1) = \min(|N-1|, |N-1-N|) = 1$ which is the right result we see in the picture. Figure from internet.

defines the slowest interaction decay that satisfies the hypothesis of this theorem.
If the previous condition is satisfied, we take two disjoint sets X and Y, $dist(X,Y) > 0$, and two local operators A_X and B_Y defined over them, we can write the following bound over the time evolution

$$\|[A_X(t), B_Y]\| \leq 2|X|\|A_X\|\|B_Y\|e^{-\mu dist(X,Y)}\left[e^{s|t|}-1\right], \tag{2.6}$$

where we used the time evolved operator $A_X(t)$ in the Heisenberg picture

$$A_X(t) = e^{\imath\mathcal{H}t}A_X e^{-\imath\mathcal{H}t}.$$

The expression (2.6) holds anyway also in the time dependent case, where the time evolution of the operator has a more complicated expression that the interested reader can derive by him/herself.
The physical meaning of the bound of Eq. (2.6) is striking: the time evolution of local observables is constrained inside a region that increases linearly with time. We can then introduce a useful simplification: If we want to study the time evolution of an operator as $A_X(t)$ we can restrict it to a region of the lattice. The time evolution of the operator affects in fact the whole system, but it is extremely small outside an effective light-cone. We can then introduce the restricted operator $A_X^l(t)$ [213] which differs from the identity just on a set X_l, which is the set containing all the spins which distance from X is less than l. Outside this region the operator is equal to the identity. Mathematically is

defined as

$$A_X^l(t) = \frac{1}{\mathrm{Tr}_Y(\mathbb{I}_Y)} \mathrm{Tr}_Y [A_X(t)] \otimes \mathbb{I}_Y,$$

where Y is the set containing all the spins not in X_l, Tr_Y is the trace over the region Y, and $\mathbb{I}_Y$ is the identity on the same space. Using the LR bound of Eq. (2.6) it is then possible to demonstrate that the difference between the $A_X(t)$ and $A_X^l(t)$ is exponentially small

$$\|A_X^l(t) - A_X\| \leq c|X| e^{-\frac{l-vt}{\xi}}, \tag{2.7}$$

where c is a constant, ξ is $1/\mu$, $v = \xi s$, and $|X|$ is the number of sites in the region X. We rewrote the previous expression in a slightly different way from Eq. (2.6) to make the Lieb-Robinson velocity v appears explicitly. We can then see that a generic operator $A_X(t)$ is well approximated by its restricted counterpart $A_X^l(t)$ during the time evolution.

2.1.3 Bound on the correlation functions

Let us see now how the bound (2.6) affects the time evolution of correlations, in the following we will follow the computations by Brevyi et al. presented in Ref. [213]. Up to here we never specified the state of the system: the presence of operator norms in fact makes the previous statements true for every vector in the Hilbert space. If we want to study the time evolution of connected correlation functions as

$$\langle A_X(t) B_Y(t) \rangle_c \equiv \langle A_X(t) B_Y(t) \rangle - \langle A_X(t) \rangle \langle B_Y(t) \rangle,$$

the properties of the state $|\Psi_0\rangle$ can play a great role in the determination of a bound on this quantity. In the following, we will assume that the expectation value $\langle A_X(t) B_Y(t) \rangle$ computed over the state $|\Psi_0\rangle$ has an exponential decay for every time t and any local operators

$$\langle A_X(t) B_Y(t) \rangle_c \leq \tilde{c} e^{-\frac{L}{\chi}} \tag{2.8}$$

where we normalized the operator norms $\|A_X\|$ and $\|B_Y\|$ to be smaller than 1 and L is the separation between the sets X and Y. We want now to bound the equal-time connected correlation function $\langle A_X(t) B_Y(t) \rangle_c$, where all the hypotheses of the Lieb-Robinson theorem are satisfied.

We can then find a bound on the connected correlation function at any time approximating any operator $A_X(t)$ by its restricted $A_X^l(t)$ constrained into X_l. We can consider then the difference

$$\langle A_X(t) B_Y(t) \rangle_c - \langle A_X^l(t) B_Y^l(t) \rangle_c = \langle \delta A_X(t) \delta B_Y(t) \rangle - \langle \delta A_X^l(t) \delta B_Y^l(t) \rangle$$

where we used the short-hand notation $\delta A_X \equiv A_X - \langle A_X \rangle$ for all the operators to express connected correlation functions as standard expectation values.

We can then apply Eq. (2.7) to the operator $\delta A_X \delta B_Y$ approximating it by $\delta A_X^l \delta B_Y^l$ as

$$|\langle \delta A_X(t) \delta B_Y(t) \rangle - \langle \delta A_X^l(t) \delta B_Y^l(t) \rangle| \leq \|\delta A_X(t) \delta B_Y(t) - \delta A_X^l(t) \delta B_Y^l(t)\| \leq c\,(|X| + |Y|)\, e^{-\frac{l-vt}{\xi}}.$$

Using the triangular inequality and remembering that $\langle \delta A_X \delta B_Y \rangle = \langle A_X B_Y \rangle_c$ we get

$$|\langle A_X(t) B_Y(t) \rangle_c| \leq |\langle A_X^l(t) B_Y^l(t) \rangle_c| + c\,(|X| + |Y|)\, e^{-\frac{l - vt}{\xi}}.$$

Using then the hypothesis (2.8) we can bound

$$|\langle A_X^l(t) B_Y^l(t) \rangle_c| \leq \tilde{c} e^{-\frac{L-2l}{\chi}},$$

where we used the distance $\mathrm{dist}\,(X_l, Y_l) = \mathrm{dist}\,(X, Y) - 2l = L - 2l$. Finally, we obtain a bound on the time evolution of the expectation value, as

$$|\langle A_X(t) B_Y(t) \rangle_c| \leq \tilde{c} e^{-\frac{L-2l}{\chi}} + c\,(|X| + |Y|)\, e^{-\frac{l - vt}{\xi}}.$$

We can then fix the value of l to

$$l = \frac{\chi v t + \xi L}{\chi + 2\xi},$$

which makes the two exponents equal.
We can then write the final result as

$$|\,\langle \Psi_0|\, A_X(t) B_Y(t)\, |\Psi_0\rangle_c\,| \leq [\tilde{c} + c\,(|X| + |Y|)]\, e^{-\frac{L - 2vt}{\xi'}}, \tag{2.9}$$

comparing it with (2.7), we can see that here we have $\xi' = \chi + 2\xi$, instead of χ, and $2v$, instead of v.
Several considerations have to be done on the expression (2.9):

1. It divides the L and t plane in two regions: for $t < L/2v$ the correlation function is exponentially suppressed and for $t > L/2v$ no bound is present on the correlation function. It means that there significant correlations can be present

2. For every distance L between the two observables, an activation time $t^\star$ exists which is defined as the moment when the correlation function is no longer bounded, i.e

   $$e^{-\frac{L - 2vt^\star}{\chi'}} \sim O(1).$$

   $t^\star$ scales linearly with the distance L and the proportionality constant is $v_{lc} = 2v$. Note that it is twice the velocity we found for the commutator, namely v.

3. The information that we get from this expression is universal because this results holds for all "short-range" Hamiltonian but it is partial because it just specifies that, for short times and sufficiently large distances, the effect of local operators is small. It is important to note that it does not tell us more than this.

2.1.4 Beyond the Lieb-Robinson bound hypothesis

The previous result is exact and extremely powerful but it has some strict hypothesis to be satisfied: the "short-range" interactions, the exponential decay of the initial expectation value, the underlying lattice, and the bound on the local Hilbert space. These hypothesis are exactly satisfied in spin systems and lattice fermions. The theorem assures that the correlation functions exhibit a horizon in their time evolution, and this horizon scales linearly in time. Many examples of these works can be found in the literature for different spin models and for different local observables [220, 221, 215, 222, 223].
The previous hypothesis are all fundamental for a rigorous mathematical application of the theorem but they are not all physically relevant to find a ballistic horizon. The first hypothesis that can be relaxed is the bound on the local Hilbert space. Physically, this is useful when a bosonic lattice system instead of a spin one is studied. While the number of local states is limited for a spin as well as fermionic models. In the bosonic case there is no upper bound on the number of bosons occupying a single site in the thermodynamic limit, the local Hilbert space of the system is then unbounded. Even if this is theoretically true, the probability of having n bosons in the same site i decreases exponentially with n. The states violating explicitly the Lieb-Robinson bound are practically never present. Numerical and analytical results for quantum quenches in the Bose-Hubbard model find a light-cone in different local observables as the $\langle b_i^\dagger b_{i+R}\rangle$ and the density-density correlation function $\langle n_i n_{i+R}\rangle$ [224, 225, 214, 216] in both finite and infinite systems. Some of the previous references perform quenches in the gapless phase of the Bose-Hubbard Hamiltonian. In that specific case the initial correlation function decays algebraically instead of exponentially because of long-range or quasi-long-range correlations. Even if (2.8) and the bound (2.6) are no longer satisfied, the presence of a light-cone has been detected [226, 227, 52, 216].
The extension of the theorem to interactions more complicated than the "short-range" ones breaks completely the picture, as we will see later in this chapter, allowing a faster-than-linear propagation of information. Surprisingly, some models still exhibit ballistic propagation of correlations also when extremely long-range interactions are involved [170, 171]. We will discuss the Bose-Hubbard chain with long-range interactions in Chapt. 3 and 4 because it needs a specific discussion.
We can conclude that a short-range interacting many-body quantum system on a lattice will exhibit a light-cone in the time evolution of expectation values of local observables, the decay of the initial state and the dimension of the local Hilbert space do not change drastically this result.

2.2 The quasi-particle approach

In the previous section we presented how short-range interactions on a lattice model give rise to a linearly increasing light-cone in the time evolution of local observables. The main result of the previous section is the presence of an activation time proportional to

the distance between the operators

$$t^\star = \frac{R}{v_{lc}}. \tag{2.10}$$

The proportionality constant has the dimension of the inverse of a velocity and it is called light-cone velocity in analogy to the special relativity.
Even if the Lieb-Robinson theorem fixes the qualitative dependence of the activation time on the distance R, it does not give a method to compute the light-cone velocity v_{lc}. This quantity that defines the maximum velocity at which correlations can spread over long distances is important and it has to be extracted from numerical or experimental data.
In order to determine this crucial parameter it is then important to change the point of view: Instead of looking at the time evolution from the macroscopic point of view, we start from the microscopic one and then we try to extract a physical meaning for the dynamics of correlations. As we said before, the solution of a quantum many-body problem cannot be done for all the systems, and we will use then a specific class of models, namely conformal-invariant ones.
We assume that the system is prepared in an initial state $|\Psi_0\rangle$ which is the ground state of an initial Hamiltonian $\mathcal{H}_i$. Then, at $t > 0$ we let this state evolve under the influence of another Hamiltonian $\mathcal{H}$. This is exactly the quantum quench protocol described in Sec. 1.3.4. We will study a particular case of the previous protocol, when the initial Hamiltonian has a mass gap m_0 and the final Hamiltonian is at, or closed to, a critical point, where the results acquire a great degree of universality. This way, the mass gap determines an exponential decay of local observables in the initial state, which is one of the hypothesis for Eq. (2.9).
In an extremely general way, we can write the time evolution of a generic local observable $\mathcal{O}(t, \{\mathbf{r}_i\})$ after a quantum quench as

$$\langle \mathcal{O}(t, \{\mathbf{r}_i\})\rangle = Z^{-1} \langle \Psi_0 | \, e^{\imath \mathcal{H} t - \epsilon \mathcal{H}} \mathcal{O}(\{\mathbf{r}_i\}) \, e^{-\imath \mathcal{H} t - \epsilon \mathcal{H}} \, |\Psi_0\rangle \,, \tag{2.11}$$

where the damping factor $e^{-\epsilon \mathcal{H}}$, with a small ϵ, has been included to ensure the absolute convergence of the integral in the path-integral formulation. The normalization factor Z is determined fixing to 1 the expectation value of $\mathbb{I}$, which gives

$$Z = \langle \Psi_0 | \, e^{-2\epsilon \mathcal{H}} \, |\Psi_0\rangle \,.$$

The expectation value (2.11) can be written using the path-integral formulation of quantum mechanics [228]

$$\langle \mathcal{O}(t, \{\mathbf{r}_i\})\rangle = \frac{1}{Z} \int \mathcal{D}\phi e^{-S[\phi]} \mathcal{O}(0, \{\mathbf{r}_i\}) \langle \Psi_0 | \phi(\tau_1, \mathbf{r})\rangle \langle \phi(\tau_2, \mathbf{r}) \, |\Psi_0\rangle \tag{2.12}$$

where we performed a Wick rotation and then the action is computed from an initial time $\tau_1 = -\epsilon - \imath t$ to a final time $\tau_2 = \epsilon - \imath t$ and it reads

$$S = \int_{\tau_1}^{\tau_2} d\tau \, \mathcal{L},$$

where $\mathcal{L}[\phi]$ is the lagrangian in imaginary time.
We want to study the expectation value on length and time scales much larger than the microscopic ones. In this regime it is possible to apply the renormalization group. We can the use the fact that the Hamiltonian $\mathcal{H}$ is at a critical point of the renormalization flow. The effect of the renormalization group on the state $|\Psi_0\rangle$ makes it flows to an invariant state $|\Psi_0^*\rangle$. In order to evaluate all quantities at the critical point, we can compute all the expectation values on the invariant state $|\Psi_0^*\rangle$ instead of the initial one. This procedure is safe if we rescale the time taking into account the initial mass gap, namely $\epsilon \to \epsilon + \tau_0$ where $\tau_0 \sim 1/m_0$. We can then take the limit $\epsilon \to 0^+$ without encountering divergences [229]. We can then translate the origin of time by the imaginary plane of $\tau_0 + \imath t$, so that $\tau_1' = 0$ and $\tau_2' = 2\tau_0$. The operator $\mathcal{O}$ is now inserted at $\tau = \tau_0 + \imath t$. Written in this way, Eq. (2.12) takes the form of an equilibrium expectation value of a $D+1$ dimensional system with a particular slab geometry and boundary conditions determined by the initial and final times written before.
The previous argument is valid for every quench from any point to the critical point in a D-dimensional system. We can now restrict ourselves to the specific case of a one-dimensional system described at its critical point by a conformal-invariant action in the limit of large distances. Even if the field of conformal invariant theories is extremely interesting for its application in condensed matter physics, we do not have space to list here its main results and we suggest to the interested reader to read Refs. [162, 230]. Conformal invariance is generated by the simultaneous presence of Lorentz invariance and scale invariance. This symmetry is sufficiently strong to fix exactly the two- and three-point functions, which are algebraically decreasing, while the four-point function is known up to a function of the anharmonic ratios, we will define later.
The scale-invariance of the action imposes the theory to be massless. In fact, if our theory is massive, we could measure distances using the inverse of its mass. The spectrum for a massless and Lorentz-invariant theory is then simply a linear spectrum

$$E_k = ck,$$

where c is the intrinsic velocity of the theory. In the case of photons this is the velocity of light and in the case of phonons is the velocity of sound for example.
The operators of the theory, as we were saying before, are all defined on a slab geometry in the (x,t) plane representing the strip $0 < \Im w < 2\tau_0$ in the complex plane . It can be mapped in the upper-half plane of the complex plane using the transformation

$$z = e^{\frac{\pi}{2\tau_0} w}.$$

The change in the coordinates affects the correlation function as described by [162] and for the simple case of product operators as $\mathcal{O} = \prod_i \Phi_i(w_i)$ it is simply written as

$$\langle \mathcal{O}(r_i) \rangle = \langle \prod_i \Phi_i(w_i) \rangle_{SLAB} = \prod_i |\frac{dw}{dz}|^{-\Delta_i} \langle \Phi_i(z_i) \rangle_{UHP}$$

where the $\langle \ldots \rangle_{SLAB}$ is computed on the slab geometry, labeled by w_i, while the $\langle \ldots \rangle_{UHP}$ is computed over the upper-half-plane, labeled by z_i. The parameters Δ_i are the holomorphic dimensions of the operator Φ_i and they are fixed by the scaling properties of

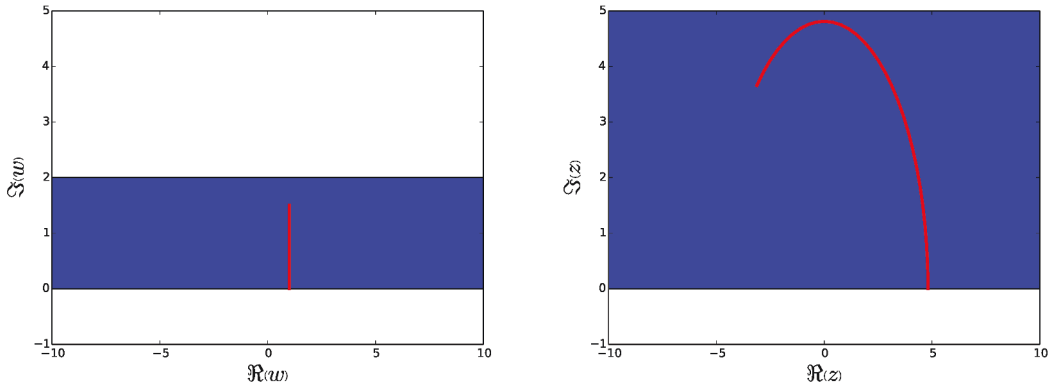

Figure 2.2: Different geometries involved in the computation of the correlation function. On the right: the strip geometry $0 < \Im(w) < 2\tau_0$ where we set $\tau_0 = 1$ where the parameter w is defined. On the left: the space where the variable z is defined, $0 < \Im(z)$. These two quantities are connected through the conformal transformation $z = e^{\frac{\pi}{2\tau_0} w}$. In red: the transformation of a line parallel to the $\Im(w)$ axis. This line physically represents the world line from $t = 0$ to $t = 3/2$ of the point $x = 1$. This line is transformed into a circumference arc in the z-complex plane. Using the polar representation of the complex plane $z = |z|e^{\imath\phi}$ it is defined by $|z| = e^{\frac{\pi}{2\tau_0}}$ and $\phi \in [0, \frac{\pi 3}{4\tau_0}]$.

the operator $\mathcal{O}$. An example of how it is possible to extract them in the Ising model can be found in [126] where a more physical interpretation of this parameters is given.
We can now analyze the specific case of two-point functions, which is the case studied in the previous section for the equal-time local operators

$$\langle \Phi(w_1) \Phi(w_2) \rangle.$$

This quantity is defined in the SLAB geometry described before. We can then map it into the upper half plane using the previous conformal transformation. It yields

$$\langle \Phi(w_1) \Phi(w_2) \rangle = \left(\frac{z_{1\bar{2}} z_{2\bar{1}}}{z_{12} z_{\bar{1}\bar{2}} z_{1\bar{2}} z_{\bar{1}2}} \right)^{\Delta} F(\eta),$$

where we used the definitions $z_{ij} = z_i - z_j$ and $z_{i\bar{j}} = z_i - \bar{z}_j$, $\eta = z_{1\bar{1}} z_{2\bar{2}} / z_{1\bar{2}} z_{\bar{1}2}$ is the anharmonic ratio, and $F(\eta)$ is a model-dependent function.
Writing everything back as a function of r and t in the combination $w = r + \imath t$, the correlation function in the large time and large distance limit is

$$\langle \Phi(0,t) \Phi(r,t) \rangle \cong \left(\frac{\pi}{2\tau_0} \right)^{2\Delta} \left(\frac{e^{\frac{\pi r}{2\tau_0}} + e^{\frac{\pi t}{\tau_0}}}{e^{\frac{\pi}{2\tau_0}(r+2t)}} \right)^{\Delta} F(\eta),$$

where

$$\eta \sim \frac{e^{\frac{\pi t}{\tau_0}}}{e^{\frac{\pi r}{2\tau_0}} + e^{\frac{\pi t}{\tau_0}}}.$$

We can then study two relevant limits for this expression: $r - 2t \gg \tau_0$ and $r - 2t \ll \tau_0$, where η can be written respectively as a $\eta \sim e^{\frac{\pi}{2\tau_0}(r-2t)} \ll 1$ and $\eta \sim 1$.
The first case, determined by the condition $r \gg \tau_0/2$, defines the pre-light-cone zone. In this region the function $F(\eta)$ can be written as a power expansion

$$F(\eta) \sim \left(A_b^{\Delta}\right)^2 \eta^{\Delta_b},$$

where A_b^{Δ} and Δ_b are fixed by the boundary conformal field theory [161]. The correlation function is then written as

$$\langle \Phi(0,t)\, \Phi(r,t) \rangle = \left(A_b^{\Delta}\right)^2 e^{-\frac{\pi\Delta}{\tau_0} t} \times e^{-\frac{\pi\Delta_b}{2\tau_0}(r-2t)},$$

which has the same expression of the bound (2.6) with an exponential decay for short times and long distances determined by the initial decay τ_0.
The other case is determined by $t > r/2$, post-light-cone, where $F \sim 1$ where we get

$$\langle \Phi(0,t)\, \Phi(r,t) \rangle \sim e^{-\frac{\pi\Delta}{2\tau_0} t}$$

meaning that the correlation function decays in time exponentially on the other side of the light-cone.
The previous explicit computation shows that it is possible to derive the correlation function exactly for a general class of theories with conformal invariance. Starting from a state with a mass gap m_0, which defines a time scale $\tau_0 \sim 1/m_0$, we can then write the exact value of the correlation function using results of the boundary conformal field theory. The correlation function has then two distinct regimes as a function of distance and time that can be written, restoring the velocity c. The separation line is $r = 2ct$ which defines the light-cone and where we can recognize Eq. (2.10) with $v_{lc} = 2c$. The velocity surprisingly depends just on the final Hamiltonian through c while the details of the initial Hamiltonian are contained all in the initial mass gap.
This result provides the connection between the general theory exposed in the previous section for an undetermined light-cone velocity and the microscopic velocity obtained in this one, i.e. c. The only microscopic quantity we then need is the dispersion relation of the final Hamiltonian E_k. The effect of the quench is spread around the system by the fundamental excitations of the final Hamiltonian, with spectrum $E_k = ck$. These excitations are created by the effect of the final Hamiltonian on the initial state $|\Psi_0\rangle$, which is not its eigenstate. The quasi-particles spread inside the system carrying correlations from a point to another one with velocity c. It is then clear that, in order to create correlation at distance r, we need to wait a time $t = r/2c$ which is the time needed by these fundamental excitations to meet halfway between the two points at distance r. The same quasi-particle picture holds in the same way in a more generic final Hamiltonian with a more complicated spectrum E_k, see Fig. 2.3. In this case, the velocity of the light-cone will be determined by the fastest quasi-particles responsible for the first enhancement in the signal. The key quantity is the group velocity defined as $V_k = \partial_k E_k$, the light-cone velocity will be then

$$v_{lc} = 2 \max_k V_k.$$

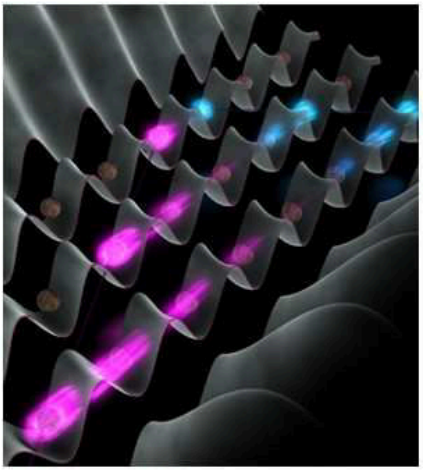

Figure 2.3: Schematic representation of the spreading of quasi-particles in a one-dimensional following a quantum quench. For different values of k the quasi-particles spread with a velocity $\partial_k E_k$ determined by the final Hamiltonian. Figure from the site of the LMU.

It means that the first signal appearing in a generic correlation function is given by the fastest quasi-particle in the spectrum.
This picture, called the quasi-particle picture, is the key approach used to understand how the perturbation due to a local observable spreads inside the system following a quantum quench. Here, what matters is just the final spectrum, and its derivative, while the initial state just provides a substrate with a non zero overlap with all the modes of the final Hamiltonian. The light-cone velocity can then be computed through the spectrum simply taking the maximum of its derivative.
The result and the picture proposed by Cardy and Calabrese are extremely useful to analyze the data from a quantum quench because they state that all the dynamical properties of the light-cone, and in particular its velocity and scaling, are determined by the spectrum of the final Hamiltonian.

2.3 Confirmations of the Lieb-Robinson bounds

In the previous section we described two different approaches to interpret the time-evolution of local observables following a quantum quench in short-range interacting quantum systems. A macroscopic one relaying on the bound of the time evolution operator (Lieb-Robinson bound) and a microscopic one proposed by Cardy and Calabrese.
These two methods predict both a linear spreading of correlations and other local observables in distance and time. From the microscopic method it is possible to extract the value of the light-cone velocity as the maximum group velocity of the final Hamiltonian.

2.3.1 Numerical proofs

2.3.1.1 Time Dependent Density Matrix Renormalization Group (t-DMRG)

We start from two numerical approaches: the Density Matrix Renormalization Group (DMRG) and the Variational Monte Carlo (VMC) which can be used to study both equilibrium and out-of-equilibrium dynamics for various Hamiltonians. For the DMRG and the t-DMRG (time dependent DMRG) many reviews are in the literature that can be of interest to the reader, as Ref. [18]. The DMRG is the most used method to study one-dimensional lattice models with short-range interactions. The dimension of the Hilbert space of a lattice model with a finite local Hilbert space grows exponentially in the system size. For instance, if we use again the Ising chain as an example, a chain with L sites with one spin 1/2 each has an Hilbert space of size 2^L, which grows exponentially in the system size. The idea behind DMRG is to describe the state of the system in this Hilbert space just using a fraction of possible states and this fraction grows slower than exponentially. The DMRG describes the state of the system decomposing it on a basis and erasing the states with the smaller amount of entanglement in the Schmidt decomposition. This procedure works at its best when we have a group of states with a large entanglement and another one which entanglement is negligible compared to the first ones. In this case the second group is erased during the numerical process and we get a description just as function of the first group. In the worst case we have a lot of states which contributions are of the same order of magnitude and it is not possible to erase states without affecting drastically the final results. Usually this happens when the system has a large amount of entanglement and, in particular, when it is close to a quantum phase transition due to the long-range correlations. If the system has short-range correlations, the error is well controlled because the entanglement entropy is bounded by a constant thanks to the area laws [231].

Quench in the Fermi-Hubbard model The DMRG can be changed in order to study time-dependent problems (t-DMRG) with both long- and short-range interactions Ref. [21, 20, 232]. In Ref. [215], Manmana et al. use the t-DMRG algorithm to study the evolution of correlations following a quantum quench of the spinless Fermi-Hubbard model at half-filing

$$\mathcal{H} = -J \sum_j \left(c_j^\dagger c_{j+1} + h.c. \right) + V \sum_j n_j n_{j+1}.$$

This system is of the same class of Hubbard Hamiltonians we already discussed in Sec. (1.3.2). When the system is at half-filling, it is integrable. It can be mapped into an anisotropic XXZ chain, using the Jordan-Wigner transformation [186] and it can then be exactly solved via a Bethe ansatz [233]. The phase diagram of the model shows a phase transition at $V_c = 2J$. For $V < V_c$ the ground state of the system is described by the Luttinger liquid theory while for $V > V_c$ it is a charge-density-wave insulator. In this phase, the translational invariance of the system is broken and two degenerate ground states appear.

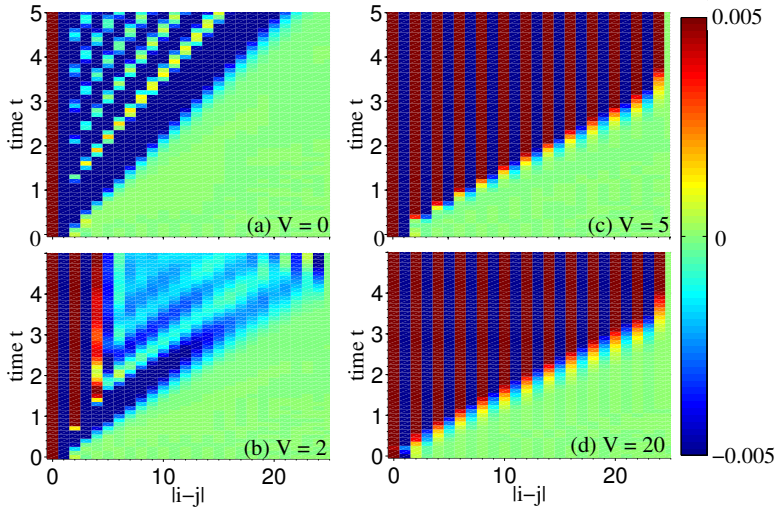

Figure 2.4: Time evolution of the quantity $G_{i,j}(t)$ for a quench $V_0 = 10J \to V_f$ where $V_f = 0, 2J, 5J, 20J$. The time is measured in units of $1/J$, as usual $\hbar = 1$. The "light-cone" structure in the R and t plane is clear for all the studied final Hamiltonians. Figure from Ref. [215].

The t-DMRG is then used to follow the time-evolution of density-density correlations

$$G_{i,j}(t) = \langle n_i(t) n_j(t) \rangle - \langle n_i(t) \rangle \langle n_j(t) \rangle$$

following different quenches from and to different regions of the phase diagram. The time-evolution for a propagation time $t \leq 5$ and for systems of length $L = 49$ or $L = 50$ and $N = 25$ fermions is shown in Fig. 2.4 for quenches starting from the insulating phase to several final values of the couplings. The initial state is the ground state of the Hamiltonian with $V = 10J > V_c$, which describes a gapped phase. This initial state has exponentially decaying correlations with distance as required by the result presented in Sec. 2.1.3. Starting from this state, different quenches are performed to the points $V/J = 0, 2, 5, 20$ respectively in the non interacting state, at the critical point, and to other points in the gapped phase. The time evolution of $G_{i,j}(t)$ for different distances and times is presented in Fig. 2.4. For all the studied cases, a "light-cone" appears in the considered time evolution of $G_{i,j}(t)$. Indeed, it can be seen on Fig. 2.4, two sites at distance $R = |i - j|$ remain uncorrelated up to a time t_R that is proportional to R. The proportionality constant is the light-cone velocity $v_{lc} = R/t_R$. These results are in perfect agreement with the bound on correlations presented in Sec. 2.1.3. We have a lattice model, with a finite local Hilbert space due to the fermionic statistic, finite-range interactions and an initial state with exponentially decaying correlations. The propagation of local operators is then constrained inside a linearly increasing region. At this point we can focus on the determination of the velocity of the light-cone extracted

from the numerical data. For quenches in the gapless phase, as $V = 0$ in Fig. 2.4 (a), the post-quench Hamiltonian describes spinless non-interacting fermions and the maximum velocity for this system, at half-filling, is the Fermi velocity $2J$. The light-cone velocity is then $v_{lc} = 2v_{max} = 4J$ as predicted by the Cardy-Calabrese approach. In the same figure it is possible to notice other fronts with lower velocities appearing at later times inside the light-cone. While the linear part of the spectrum, located in the phononic branch, determines the light-cone velocity, the other parts of the spectrum determine these later fronts which are due to the full spectrum of excitations. The same considerations can be made at the critical point $V = 2J$ where the same inner structure of the light-cone is present. The same structure can be found for the quench to the phase transition, Fig. 2.4 (b).
For quenches in the gapped phase, see Fig. 2.4 (c) and (d), the theoretical description is different because there is no linear part of the spectrum that is described by a conformal field theory, as in the gapless phase. However, a light-cone in the activation of the correlation function is present anyway. In this case, the inner structure is completely different: an alternating pattern is present instead of other slower fronts, see Fig. 2.4 (c) and (d). In Fig. 2.5 the time evolution of correlations for quenches from $V_0/J = 1/2$ to $V/J = 5$ and $V/J = 40$ are shown. In this case, the initial state contains algebraically decreasing correlations, typical of the Luttinger liquids, and not all the hypothesis of the bound presented in Sec. 2.1.3 are satisfied. A light-cone dynamics is anyway still present, meaning that the exponential decay of correlations in the initial state is not a fundamental hypothesis from the physical point of view. Comparing Fig. 2.5 with Fig. 2.4, the internal structure of the light-cone changes due to the different initial states used. After an initial light-cone due to the creation of correlations at the center of the chain, other slower ones appear with a velocity which is almost half of the "light-cone" one. These are due to the open boundary conditions. The inner structure of the light-cone in this case has a behavior somehow mixed between the two seen before. The authors interpret these regions as moving domains due to the passage through the phase transition and they are described by next-to-leading order Kibble-Zurek mechanism [234].
As exemplified by these results, the t-DMRG is a really powerful method to explore the time-evolution of quantum many body systems. However errors appear due to the truncation of the density matrix which introduces errors. Because of that, the simulations are reliable just for $t \sim 10/J$ even if some pieces of information about the long-time behavior can be extracted from these data. In addition to this problem, the t-DMRG is not naturally able to study bi-dimensional system or continuous systems, these have to be studied using particular adaptation of the one-dimensional algorithm [235, 236].

2.3.1.2 Time-dependent variational Monte Carlo

Another powerful numerical method that is not affected by the problems of the t-DMRG is the time dependent variational Monte-Carlo (t-VMC) that we discuss in this paragraph. This method can be used to study the time-evolution of quantum many-body systems with generic interactions and in generic dimensions. For this method we make an ansatz

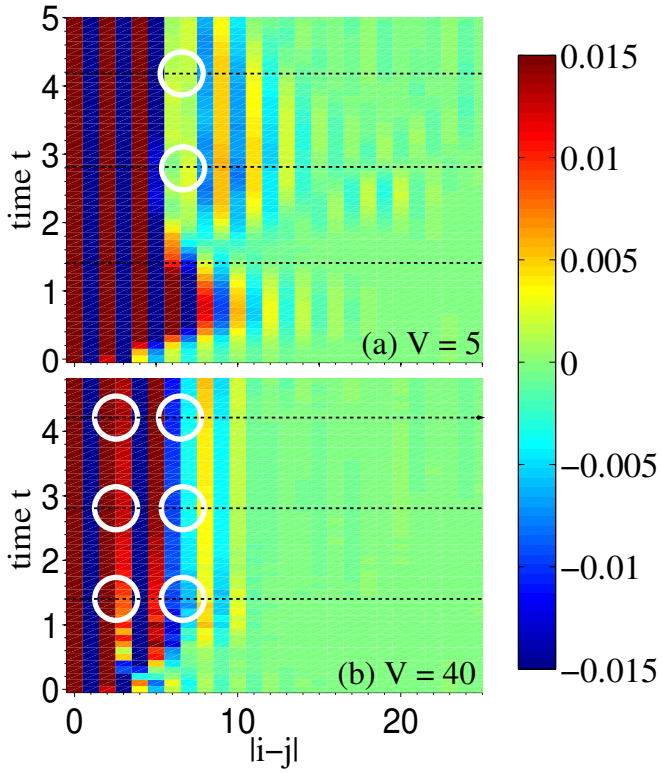

Figure 2.5: Time evolution of the density-density correlations following a quantum quench from the gapless phase, $V = J/2$, to the gapped phase, in figure (a) $V = 5J$ and in figure (b) $V = 40J$. It is possible to see how a light-cone is present also if the phase transition is crossed. The internal structure presents a mixed behavior: inner fronts with smaller velocity and alternating patters typical respectively of the gapless and gapped phases. Figure from Ref. [215].

on the wave function, taking it of the Jastrow type [24],

$$|\Psi(t)\rangle = e^{\imath \sum_\alpha \lambda_\alpha(t) O_\alpha} |\Phi_0\rangle ,$$

where the $\lambda_\alpha(t)$ are complex functions depending on time, O_α are operators that are chosen appropriately to describe the wave function, and $|\Phi_0\rangle$ is the initial state. The only constraint on the operators O_α is that they have to be diagonal in the basis chosen to describe the time evolution. We can then write a differential equation for the parameters $\lambda_\alpha(t)$ imposing that $\| (\imath\partial_t - \mathcal{H}) |\Psi\rangle \|$, where $\|.\|$ is the norm in the Hilbert space, is minimal for every value of time. This corresponds to minimize the distance, in the Hilbert space, between the real time evolution generated by the Hamiltonian, and the one of our anstaz. The minimization of the previous expression yields a differential

equation for the functions λ_α,

$$\sum_\alpha \dot{\lambda}_\alpha \langle O_\alpha O_\beta \rangle = -\imath \langle \mathcal{H} O_\beta \rangle \quad \forall \beta.$$

The solution of this first-order differential equation involves the computation of the expectation values $\langle \ldots \rangle$ on the Jastrow wave function. The expectation values are computed using a basis where the O_α operators are diagonal. This is done using Monte-Carlo techniques. It is possible to demonstrate that the norm of the wave function is exactly conserved if the λ_α parameters respect the previous equation, and also the energy is conserved if the Hamiltonian is time-independent. Moreover, we do not need any assumption for the type of interactions and the dimensionality of the system, the Jastrow ansatz is completely independent on these details. Reliable results heavily rest on the appropriate choice of the set of diagonal operators O_α. The numerical error of the method is due to the Monte Carlo errors in the computation of the expectation values, the numerical resolution of the differential equation, and the choice of O_α.

Quench in the Bose-Hubbard model The t-VMC was used to study the time evolution of correlations following a quantum quench in the superfluid regime of the Bose-Hubbard model [216],

$$\mathcal{H} = -J \sum_{\langle i,j \rangle} \left(a_i^\dagger a_j + h.c. \right) + \frac{U}{2} \sum n_i \left(n_i - 1 \right). \tag{2.13}$$

As discussed in Sec. 1.3.2, the Bose-Hubbard Hamiltonian has a superfluid phase for $J \gg U$ and a Mott-insulating phase for $U \gg J$. If we study these two regimes from the point of view of relevant fundamental excitations, the superfluid regime is dominated by Bogoliubov excitations while the Mott insulator by doblons and holons moving on a insulating state. In [216], Carleo et al. studied the time evolution of correlations following a quantum quench inside the superfluid regime. The fundamental excitations of the system are density-density excitations which are represented by $O_\alpha = n_k n_{-k}$ in the Jastrow wave-function.
From the point of view of the bound on correlations presented in Sec. 2.1.3, the system does not satisfy all the hypothesis because of the algebraically decreasing correlations in the initial state and because the local Hilbert space is infinte, due to the bosonic nature of the particles. This last property violates also the hypothesis of the Lieb-Robinson bound presented in Sec. 2.1.2.
A linearly increasing light-cone is anyway present in the time evolution of correlations, as presented in Fig. 2.6(a). In Fig. 2.6(b) the time evolution of the correlation function for different values of R is shown, and in Fig. 2.6(c) the dynamics of the quantity

$$\sqrt{\frac{\langle \mathcal{H}^2 \rangle_t - \langle \mathcal{H} \rangle_t^2}{\langle \mathcal{H}^2 \rangle_0 - \langle \mathcal{H} \rangle_0^2}}$$

is presented. This quantity is an indicator of the reliability of the simulation: if it is close to 1, the simulation is trustable. It is possible to see how this indicator is always close to

one except for a small amount of time, $0.1 \leq t \leq 1$, where it is bigger but anyway inside the 20% of the ideal value.

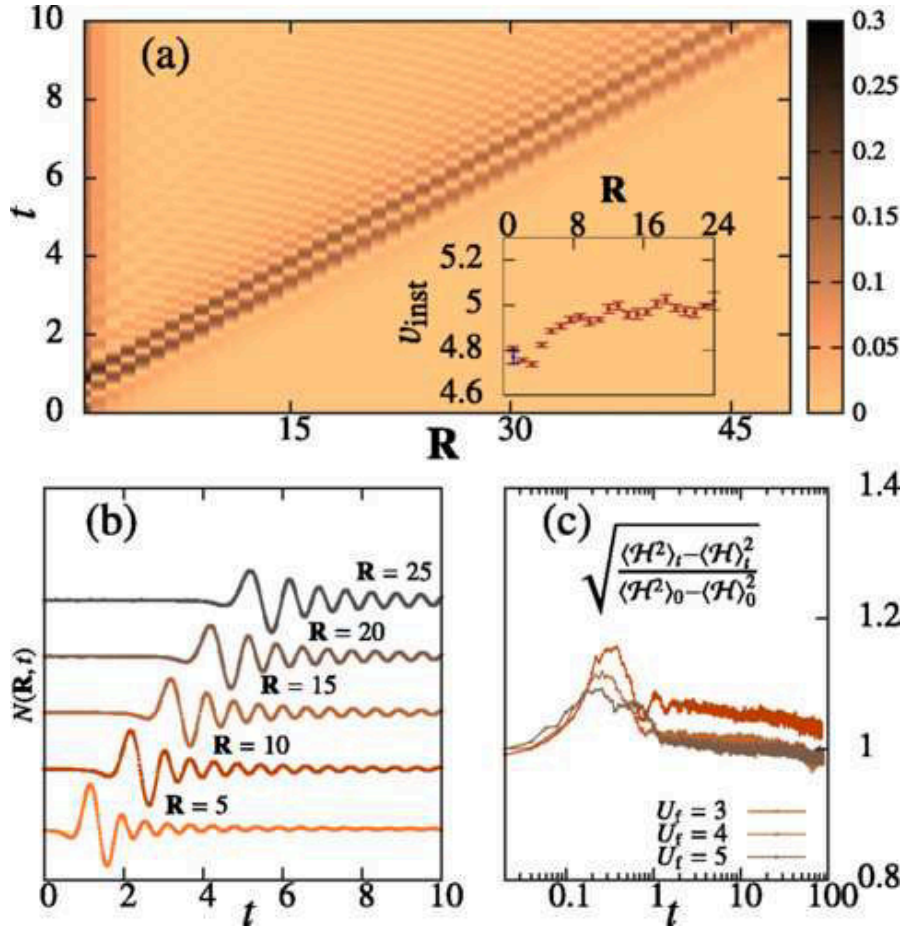

Figure 2.6: Time-evolution of correlations following a quantum quench $U_i = 2 \to U_f = 4$ in the superfluid regime of the Bose-Hubbard model (2.13). (a) Absolute value of the correlation function as a function of R and t. A "light-cone" shape is present in this time evolution. Inset: the instantaneous velocity of the absolute maximum is presented (red points) together with one point computed using exact diagonalization over a 12-sites system. (b) Vertical cuts of (a) for different values of R. (c) Log-log plot of the indicator $\langle H^2 \rangle - \langle \mathcal{H} \rangle^2$ normalized at the initial value. It is possible to see that this indicator is maximum the 20 % of the ideal value for a small amount of time and it then goes down rapidly to values close to 1. It has to be notice that in this last plot the times arrive at $t \sim 100$ which is one order of magnitude larger than the ones of the t-DMRG. Figure from Ref. [216].

Since the system allows long-lived free excitations, it is possible to compare the velocity extracted numerically from the data with the one computed from the theoretical model. It has been found that the first is slower than the latter. This arises from the fact that

the velocity extracted numerically is computed following the absolute maximum of the correlation function. The absolute maximum of the correlation function is not always the first maximum, resulting in a measure of the velocity which is slower than the theoretical one. I demonstrated that the velocity computed following the absolute maximum and the one computed from the first maximum are not the same and they can be predicted by the quasi-particle approach [237].
The t-VMC can be used also to simulate the time-evolution of quantum systems in dimensions higher than one. The time-evolution of correlations following a quantum quench in a bi-dimensional Bose-Hubbard Hamiltonian has been studied in the same paper. In Fig. 2.7 the results for the time-evolution of correlations in the bi-dimensional Bose-Hubbard model are shown.

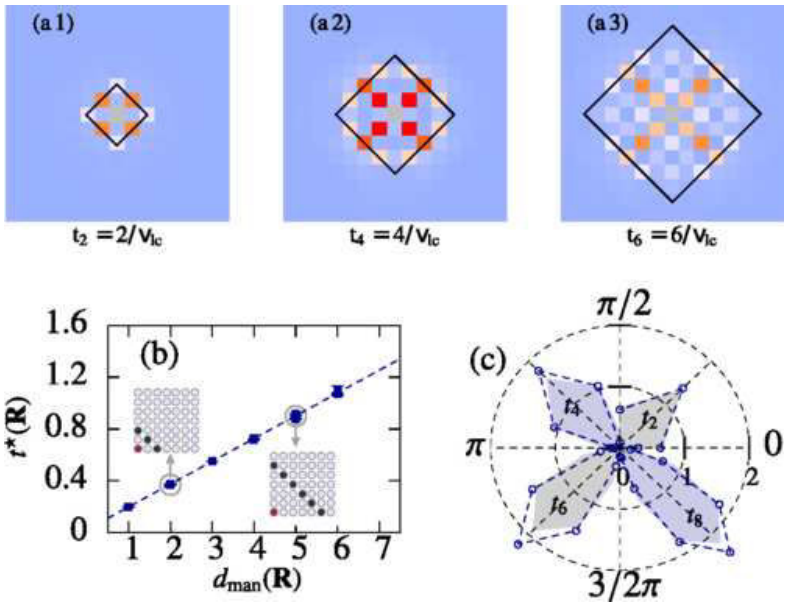

Figure 2.7: Time evolution of correlations in a 20×20 sites Bose-Hubbard model following a quantum quench inside the superfluid regime. (a) Time evolution of correlations as function of x and y for different times (a1), (a2) and (a3). A propagation of correlation is clear in the time evolution: correlations at a distance R are activated at a time $t^\star$ which increases with the distance. (b) The time $t^\star$ depends linearly on $d_{man}(R)$ which is the Manhattan metric. This means that it is possible to define a "light-cone" in this metric because there is a linear dependence between the distance and the activation time. The slope of this linear dependence defines the light cone velocity. (c) The figure shows the angular position of the maximum of the correlation function. They do not follow circles in the Cartesian metric but circles in the Manhattan does, which is an effect of the underlying lattice. The angular distribution shows that the signal is enhanced on the bisectrix of the plane de to the fact that many path on the lattice go on these lines compared with other points. Figure from Ref. [216].

Also in this case a causal structure is present in the correlation function where correlations need a time $t^\star$ to activate. In order to study the dependence of $t^\star$ on the distance, it is important to specify which type of distance is compatible with our physical problem. The cartesian distance is a not good indicator for distances on a lattice. The paths followed by the particles are different from a straight line. In turn, a more appropriate distance is defined by the Manhattan metric, which follows the paths of the particles moving on the lattice. It is defined as

$$d_{man}(x, y) = |x| + |y|$$

If we now plot the activation time $t^\star$ as function of this distance we see that they are proportional and the proportionality constant can be defined as the inverse of the light-cone velocity, see Fig. 2.7 (b).
t-VMC will be used in the next section to study the time-evolution of local observables in long-range interacting quantum systems. Anyway the t-VMC and t-DMRG are the two most important methods to simulate the time-evolution of many-body quantum systems and they are constantly improved to obtain better and more precise results.

2.3.2 Experimental proofs

In this section we want to discuss two of the most important experimental observation of the light-cone effect in the time evolution of local observables. As we already discussed in Sec. 1.3.4, cold atomic gases are the perfect systems to study these phenomena. They allow to engineer different Hamiltonians, to set the system in different initial state, to drive the system out-of-equilibrium, and to measure different observables during the time evolution.

2.3.2.1 Light-cone propagation in the Bose-Hubbard model

The first experiment is the one realized by M. Cheneau et al. in the group of I. Bloch [214]. There, several one-dimensional Bose-Hubbard chains are realized in a elongated optical trap with a ratio U/J compatible with a strong Mott insulator regime with one particle per site.
The quench protocol is performed changing that ratio to a new one U/J still in the Mott regime. This is done by lowering the intensity of the lasers creating the lattice and the change takes place in less than $100\mu s$. This time interval is shorter than any microscopic time scale of the system and a quantum quench is realized. During the time evolution, the initial state can be seen as a source of excitations that spread through the chain. As already mentioned above, the relevant excitations for the Mott state are doblons and holons, see Fig. 2.8.

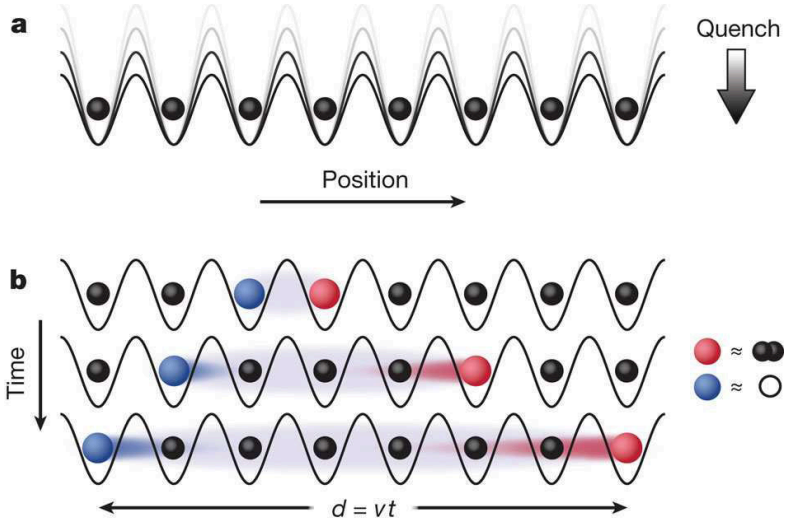

Figure 2.8: Representation of the quasi-particles spreading in a Mott insulator following a quantum quench. In the upper figure a Mott state with one particle per-site which the initial state of the system. At the time $t = 0$, a quantum quench is performed changing the final lattice depth. The initial state is not an eigenstate of the final Hamiltonian and then a non-trivial time evolution takes place. The time evolution of local observables is then given by the spreading of the fundamental excitations of the final Hamiltonian. We can then see in the lower panel how doblons, represented in red, composed by two particles and holons, represented in blue, spread in the system with different velocities. Figure from Ref. [214].

We can think at the Mott state as a state composed by 1 particle per site, where the probability of hopping between the nearest-neighbor site is extremely weak compared to the on-site energy, see Fig. 1.3.2. If we allow now particle hopping from a site to another, then one has two particles (a doblon) and the other one zero particles (holon). These states can be seen as fundamental excitations over a "vacuum" represented by the initial Mott state. These excitations are responsible for the spreading of correlations in the post-quench time-evolution, in agreement with the Cardy and Calabrese picture.
The post-quench time-dependent state can be written as a superposition of doblon and holons with their dispersion relations

$$|\Psi(t)\rangle \approx |\Psi_0\rangle + \imath\sqrt{8}\frac{J}{U}\sum_k \sin(ka_{lat})\left[1 - e^{-\frac{t}{\hbar}\imath(E_h+E_d)}\right] d_k^\dagger h_{-k}^\dagger |\Psi_0\rangle$$

where $|\Psi_0\rangle$ is the Mott insulating state with 1 particle per site, E_h and E_d are the dispersion relations of the holons created by $h_k^\dagger$ and doblons created by $d_k^\dagger$.
The observable accessible by the experimental setup is the correlation function of the parity operator,

$$C_d(t) = \langle s_i(t) s_{i+d}(t)\rangle - \langle s_i(t)\rangle\langle s_{i+d}(t)\rangle,$$

where $s_i = e^{\imath\pi(n_i - \bar{n})}$. The latter measures the parity of the excitations in the site i. If the site is occupied by a quasi-particle, doblon or holon, then $s_i = 1$, if it is not $s_i = 0$.

The initial state is a Mott state with almost 0 excitations, $P_{i,j}(0) \simeq 0$, for all the values of i and j.
In practice, the system is actually composed by a series of quasi-one-dimensional tubes due to the splitting of a 3D atom cloud using the same techniques presented in Sec. 1.3.2. It is realized starting from a degenerate gas of ^{87}Rb atoms which are confined in a bi-dimensional region using a laser with $a_{lat} = 532\,nm$ along the z- and y-axis. This splits the initial cloud in 10 nanotubes along the x-axis which are approximately one-dimensional systems. A lattice is then created along the x-axis using two counter-propagating lasers and realizing the one-dimensional Bose-Hubbard model. The intensity of these lasers can be tuned to obtain $U/J \approx 40$. For this value of the parameters the system is in an insulating regime of one atom per site. The temperature of the 1D tubes can be measured and it gives $T = 0.1U/k_B$ where k_B is the Boltzmann constant. The system can then be considered at zero temperature. As we said, a quench to a different U/J is realized changing the intensity of the lasers. After a variable time t, the system is then frozen, increasing the lattice depth in all the directions to a value $80E_r$. A fluorescence image with site-resolved precision is then performed, and the parity of the different sites can be detected directly. This procedure, repeated for different evolution times t, gives the time evolution of the observable $C_d(t)$.

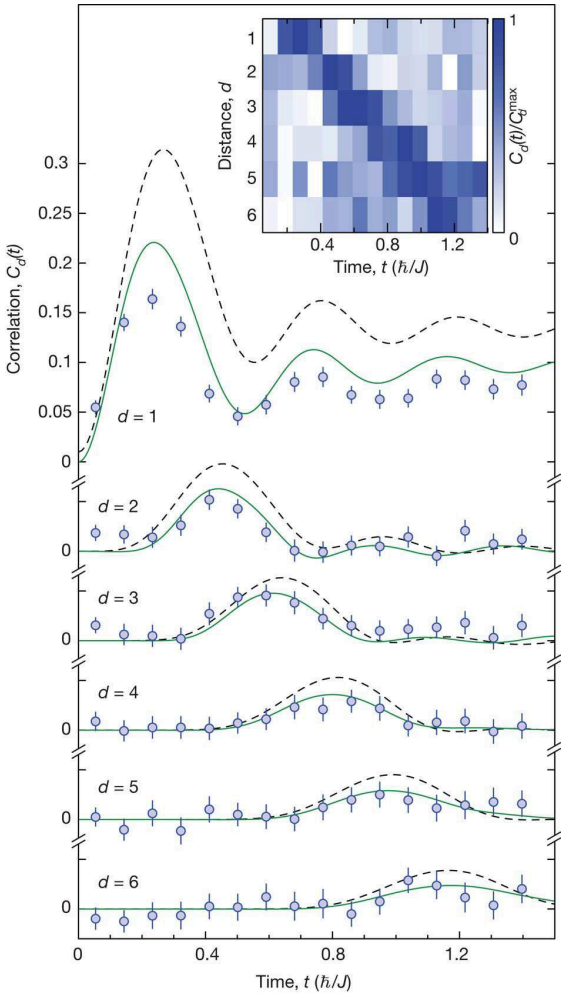

Figure 2.9: After the quench, a positive correlation signal propagates with increasing time to larger distances. Main figure, the experimental values for a quench from $U/J = 40$ to $U/J = 9.0$ (open circles) are in good agreement with the corresponding numerical simulation for an infinite, homogeneous system at zero temperature (continuous green line). Our analytical model (dashed black line) also qualitatively reproduces the observed dynamics. Inset, experimental data displayed as a color map (color scale at right), revealing the propagation of the correlation signal with a well defined velocity. The experimental values result from the average over the central N sites of more than 10^3 chains, where N equals 80% of the length of each chain. Figure from Ref. [214].

The results for the quench $U/J = 40 \rightarrow U/J = 9$ are presented in Fig. 2.9. A clear linearly increasing horizon is present in the time evolution of the parity operators as function of R and t. The propagation velocity can be extracted from these data. They are then compared with t-DMRG simulation at $T = 0$ temperature and to the theoretical model, finding a good agreement between these three independent approaches.

Qualitatively, the same results are obtained for the quenches to $U/J = 7$ and $U/J = 5$. For these values of the couplings a larger number of quasi-particles is generated. The theoretical model is consequently less accurate, but a linear light-cone is anyway present in the dynamics.
The velocity of the light-cone extracted from the data in the range $2 \leq R \leq 6$ is in agreement with the one extracted from the t-DMRG, considering the error-bars. These velocities are always smaller than the maximum velocity predicted by the theoretical model.
This experiment has been a milestone in the study of the out-of-equilibrium dynamics of closed quantum systems. It demonstrates that it is possible to perform a quantum quench in a strongly interacting quantum system and then follow its dynamics with a high degree of accuracy. Here, it points out the validity of the Lieb-Robinson theorem in a real experimental situation. It has then to be noticed how cold atoms are crucial to perform this experiment because they provide the only experimental setup where a real closed evolution is possible and it can be used to study length scales comparable to the numerical and analytic works.

2.3.2.2 Detection of the light-cone using matter-wave interference techniques

Another "light-cone" structure has been found in [238], where the authors study thermalization of a one-dimensional bosonic system following a quench. Even if this light-cone is not the same as in the previous case, it is anyway an important proof og the quasi-particle approach.
The experiment is realized this way: A system of thousands ^{87}Rb atoms is trapped in a $1D$ geometry at a temperature of $30 - 110nK$. The trapping is obtained by a magnetic trap realized $100\mu m$ under the wires of an atom-chip. The application of an additional magnetic field changes abruptly the shape of the trap from a single-well to a double-well geometry dividing the system in two equal parts inside two tubes. This procedure is the matter-wave analogous of a beam-splitter for photons. The double-well potential separates the two subsystems for a time t. Then, the two clouds are released from the trap and they interfere during their expansion. Using time-of-flights measurements it is possible to access the relative phase $\phi\left(z,t\right) = \theta_1(z,t) - \theta_2\left(z,t\right)$. This out-of-equilibrium protocol can be seen as a quench because the initial state, the Bose-Einstein condensate at the bottom of the single-well potential, is not an eigenstate of the time evolution Hamiltonian, represented by a double-well geometry.
The observable studied in this work is the phase difference between the two clouds,

$$\mathcal{C}(\bar{z} = z_1 - z_2, t) = \Re\langle e^{\imath\phi(z_1,t) - \imath\phi(z_2,t)}\rangle$$

where the measures are repeated 150 for every value of t in order to compute the expectation value.

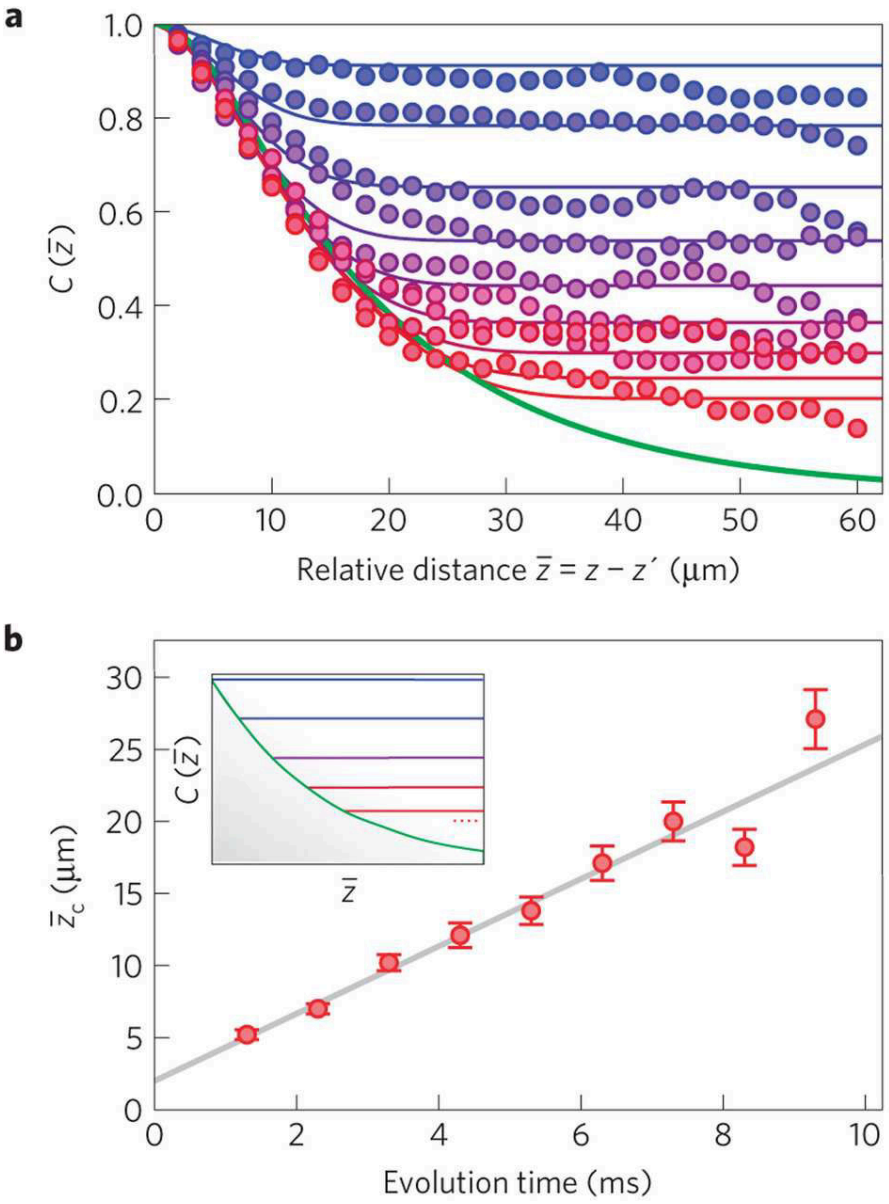

Figure 2.10: a) Plot of the function $C(\bar{z})$ as function of $\bar{z}$ for different times t. It is possible to see how the function reaches a plateau at different values of $\bar{z}^\star$ that increase linearly in time. The green line represents the relaxation value extracted theoretically using a Luttinger liquid theory, as the time increases the measured $C(\bar{z})$ approaches this line.
b) Plot of the values $\bar{z}^\star$ as function of time, the linear dependence between these two quantities allows to extract the slope with dimensions of a velocity which can be compared to Luttinger liquid theory. Figure from Ref. [238].

We can see that this observable decays exponentially in $\bar{z} = z_1 - z_2$ towards an equi-

librium value, for examples the ones plotted in Fig. 2.10. The exponential decay stops at $\bar{z} = \bar{z}_c$ and the function remains then constant, $\mathcal{C}(\bar{z} > \bar{z}_c, t) = \mathcal{C}(\bar{z}_c, t)$, as it is shown in Fig. 2.10 (b). The analysis of different values of $\bar{z}_c$ for different times exhibits a linear proportionality between the two quantities, $\bar{z}_c = 2ct$, as it is shown in the bottom panel of the same figure.

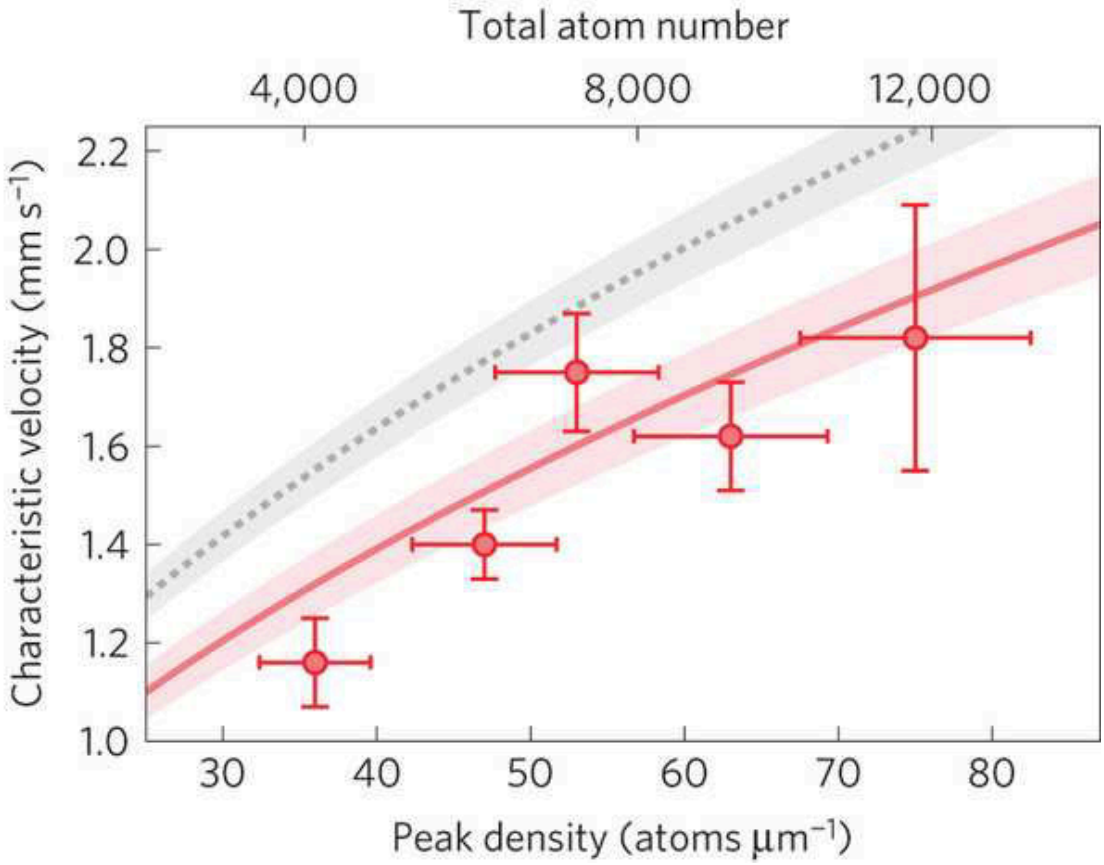

Figure 2.11: Comparison between the velocity extracted from the experimental points with error-bars and the one of the Luttinger liquid lines. The gray line is computed in the case of an homogeneous system while the red one in the case of a trapped one. The experimental data and the theory for trapped systems are in agreement taking into account the error bars due to the experimental conditions and resolution, see Supplementary Material of Ref. [238]. This confirms that thermalization takes place per quasi-particle spreading in the system and it is another proof of the validity of this picture in the interpretation of post-quench dynamics. Figure from Ref. [238].

It is possible to compare the velocity extracted from the experimental data to the one provided by a Luttinger liquid model. This model has a linear continuum dispersion relation, $\omega_k = c_0 k$, i.e. all the excitations have a group velocity $v_k = c_0$. A good agreement between the two quantities is found, as shown in Fig. 2.11.

In this case we do not find a standard light-cone in the activation time of local observables. The Hamiltonian of the system is in fact defined in continuum space, and the Lieb-Robinson bound does not hold for these systems. Anyway, a "light-cone" structure is present in the thermalization value of the studied observable. Even if this is not connected to the Lieb-Robinson bounds, it is anyway connected to the quasi-particle approach because the "velocity" of the thermalization is given by the velocity of these excitations.

2.4 Extension of the Lieb-Robinson bound to different types of interactions

As we saw in the previous sections, many-body systems interacting via short-range interactions have to respect some universal bounds on the time evolution. The Lieb-Robinson bound is completely general and it states that local observables can propagate just inside a "light-cone" structure. This effect has been observed in several numerical and experimental works.
We want now to focus on a different type of interactions: namely long-range interactions. Even if it is possible to extend the Lieb-Robinson theorem to different short-range interactions, as exponentially decaying ones, it is not possible to extend it to long-range ones, as $1/R^{\alpha}$, without drastic changes.

Logarithmic bound for $\alpha > D$ The simplest and most used long-range model is the long-range Ising chain in transverse field(LRTI). In $1D$, its Hamiltonian reads

$$\mathcal{H} = \frac{V}{2} \sum_{i \neq j} \frac{S_i^z S_j^z}{|i-j|^{\alpha}} + B \sum_{j=1}^{N} S_j^x,$$

where V is the long-range coupling. B is the magnetic field and $S_i^{\beta} = \frac{1}{2}\sigma_i^{\beta}$ is the spin-1/2 local operator.

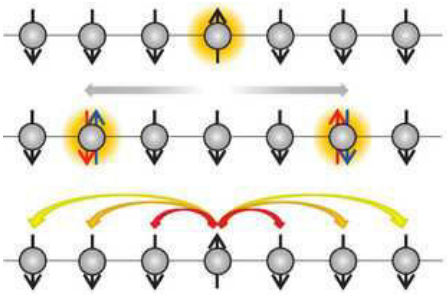

Figure 2.12: Graphical representation of a long-range interacting spin systems such as the LRTI chain. As it is possible to see, thanks to long-range interactions, all spins are connected and it is in principle possible to send signals at arbitrary large distances. This is the main reason why standard Lieb-Robinson bounds may not apply. Figure from Ref. [47].

We can notice that the argument we used in Sec. 2.1.2 for the short-range Ising model does no longer hold for its long-range version. In fact, if we want to analyze how a local spin-flip evolves in time, we find that it affects all the sites due to the long-range term

$$\sum_{i\neq j}\frac{S_i^z S_j^z}{|i-j|^\alpha}.$$

This means that the simple argument used before is no longer valid and a more technical discussion is needed.
Following Ref. [163, 164], it is possible to find a bound if interactions decay sufficiently fast. Intuitively, if the value of α is large we should recover the standard Ising model with short-range interactions. It is then natural to look for a bound in the region where interactions decay sufficiently fast. This condition over the long-range interaction is called *the self-reproducibility* condition. For a generic long-range potential $V(i,j)$, it reads

$$\sum_k V(i,k)\,V(k,j) \leq \lambda V(i,j)\,, \tag{2.14}$$

for a given constant $\lambda > 0$ and for every sites i and j. For the specific case of $V(i,j) = 1/|i-j|^\alpha$ it imposes $\alpha > D$. The time evolution operator can be written as power series of t, which involves the summation of terms of the type

$$e^{\imath t\mathcal{H}} \sim \sum_n \frac{t^n}{n}\sum_{i_1}\sum_{i_2}\cdots\sum_{i_n} V(i_1,i_2)\,V(i_2,i_3)\ldots V(i_{n-1},i_n)\,.$$

Terms of this type can be bounded using using (2.14) iteratively, which yields

$$\frac{t^n}{n}\sum_{i_1}\sum_{i_2}\cdots\sum_{i_n} V(i_1,i_2)\,V(i_2,i_3)\ldots V(i_{n-1},i_n) \leq V(i_1,i_2)\,\frac{t^n\lambda^n}{n!}. \tag{2.15}$$

The bound on the commutator of two local operators comes directly from the previous inequality summed over n. As we already did in Sec. 2.1.2, we take two operators $A_X(t)$ and B_Y which are defined over two disjoints sets X and Y. The time evolution of the operator A_X can be expressed as a power series and then it can be bounded using (2.15). In the specific case of $V(i,j) = 1/|i-j|^\alpha$ this bound reads

$$\|\,[A_X(t)\,,B_Y]\,\| \leq \mathcal{C}_{A_X,B_Y}\frac{1}{|i-j|^\alpha}\left(\frac{e^{\lambda t}-1}{\lambda}\right). \tag{2.16}$$

This bound predicts a finite activation time $t^\star$, which becomes evident once the previous equation is written this way

$$\|\,[A_X(t)\,,B_Y]\,\| \leq \mathcal{C}_{A_X,B_Y}e^{-\alpha\ln(|i-j|)}\left(\frac{e^{\lambda t}-1}{\lambda}\right).$$

The horizon of correlations is then given by

$$t^\star = \frac{\alpha}{\lambda}\ln(|i-j|)\,,$$

which increases logarithmically with the distance R. For $t < t^\star(R)$, the commutator is algebraically suppressed.

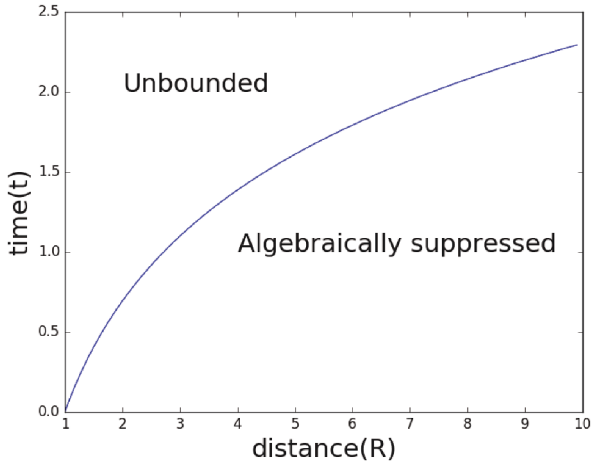

Figure 2.13: Shape of the horizon found in Ref. [163]. The activation time is $t^\star \propto \ln(R)$ and it divides the R, t plane into two regions: a region for $t < t^\star$ where correlations are algebraically suppressed and another region for $t > t^\star$, where they are unbounded.

It has to be noticed that, depending on the value of α, the commutator can be bounded, $\alpha > D$, or unbounded, $\alpha < D$. The fact that no bound is present for extremely long-range interactions can suggest that in this case the propagation is instantaneous, or that the result presented before has to be improved mathematically.
We will see in the next section that this logarithmic bound can be improved in different ways but, anyway, still no bound is present for infinite systems and $\alpha < D$.

Logarithmic bound in finite systems For finite systems it is possible to find a bound, dependent on the system size L, for every value of α, as found by Storch et al. in Ref. [165].
The authors start from the self-reproducibility condition

$$\sum_{k\in\Lambda} \frac{1}{[d(i,k)+1]^\alpha} \frac{1}{[d(k,j)+1]^\alpha} \leq \lambda \frac{1}{[d(i,j)+1]^\alpha},$$

where they used a long-range potential of the form $V(R) = [1+\mathrm{dist}(i,j)]^{-\alpha}$ where $\mathrm{dist}(i,j)$ is a generic distance. If $\alpha < D$ the convolution of the two functions on the left-hand-side can grow more and more with L. In the thermodynamics limit, it is then impossible to satisfy the self-reproducibility condition.
For finite systems it is possible to overcame the problem multiplying the left-hand-side

by a size dependent factor $\mathcal{N}_\Lambda$ in order to balance its divergence, namely

$$\mathcal{N}_\Lambda \sum_{k\in\Lambda} \frac{1}{[d\,(i,k)+1]^\alpha} \frac{1}{[d\,(k,j)+1]^\alpha} \leq \lambda \frac{1}{[d\,(i,j)+1]^\alpha}, \tag{2.17}$$

where we define

$$\mathcal{N}_\Lambda = \frac{1}{\sup \sum_{k\in\Lambda} [d\,(i,k)+1]^\alpha}.$$

We can then determine the scaling of $\mathcal{N}_\Lambda$ with the system size as

$$\mathcal{N}_\Lambda = \begin{cases} c_1 L^{\frac{\alpha}{D-1}} & 0 \leq \alpha < D \\ c_2 \ln(L) & \alpha = D \\ c_3 & \alpha > D \end{cases}$$

where c_i are all positive and non-zero constants. The function $\mathcal{N}_\Lambda$ has also the property to make the energy of the system extensive.
We can rewrite then rewrite Eq. (2.17) as

$$\sum_{k\in\Lambda} \frac{1}{[d\,(i,k)+1]^\alpha} \frac{1}{[d\,(k,j)+1]^\alpha} \leq \lambda_\Lambda(L) \frac{1}{[d\,(i,j)+1]^\alpha},$$

where $\lambda_\Lambda(L) \equiv \lambda/\mathcal{N}_\Lambda$. This equation has the same form of Eq. (2.14) but with $\lambda_\Lambda(L)$ instead of λ. We can then write a bound on the commutator between $A_X(t)$ and B_Y as

$$\| [A_X\,(t)\,, B_Y] \| \leq \mathcal{C}_{A_X,B_Y} \frac{1}{|i-j|^\alpha} \left(\frac{e^{\lambda_\Lambda(L)t} - 1}{\lambda} \right).$$

We can write the combination $\lambda_\Lambda(L)t = \lambda\,(t/\mathcal{N}_\Lambda)$ and introduce the rescaled time $\tau = t/\mathcal{N}_\Lambda$. The previous equation takes now the same form of Eq. (2.16) with τ instead of t

$$\| [A_X\,(t)\,, B_Y] \| \leq \mathcal{C}_{A_X,B_Y} \frac{1}{|i-j|^\alpha} \left(\frac{e^{\lambda\tau} - 1}{\lambda} \right).$$

In conclusion this bound predicts that, for all values of α, the commutator between two local operator in a finite system is bounded once expressed in a rescaled time variable τ which depends on the system size. We will come back on this result again in Sec. 3.6.3.

Algebraic bound for $\alpha > 2D$ The logarithmic bound we presented before can be improved. In particular, in Ref. [166] the authors derive a more stringent bound than the one we discussed before for $\alpha > 2D$.
The authors study a long-range system of the type

$$\mathcal{H} = \frac{1}{2} \sum_{i,j,\mu} S_{\mu,i} V_\mu(i,j) S_{\mu,j},$$

where $S_{\mu,i}$ is the component μ of the spin at site i and $V_\mu(i,j)$ is the interaction potential, assumed to decay as $1/d(i,j)^\alpha$. For $\alpha > 2D$ the authors demonstrate that it is possible to derive a more stringent bound, namely

$$\| [A_X(t), B_Y] \| \leq K \left[e^{(vt - r/t^\gamma)} + \frac{t^{\alpha(1+\gamma)}}{r^\alpha} \right], \tag{2.18}$$

where K is a positive constant depending on the specific operators, v is a constant depending on the Hamiltonian, and $\gamma = (D+1)/(\alpha - 2D) \geq 0$.
The activation time $t^\star$ can be found imposing the exponent to be zero

$$vt^\star - r/t^{\star\,\gamma} = 0 \rightarrow r \sim vt^{\star\,1+\gamma}$$

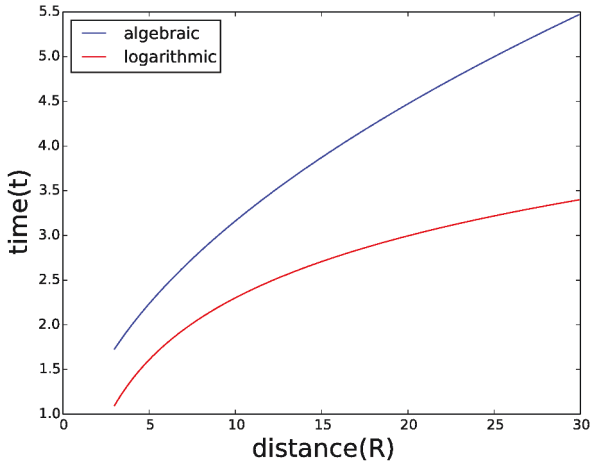

Figure 2.14: Comparison between the algebraic bound proposed in [166] and the algebraic one proposed in [163] it is possible to see how the first one is a more stringent bound that limits the accessible region of the R and t plane to the time evolution.

From the previous equation we can then derive how the activation time scales with the distance, finding a faster-than-ballistic dependence

$$t^\star \propto R^\beta,$$

where

$$\beta = \frac{1}{\gamma + 1} = \frac{\alpha - 2D}{\alpha + 1 - D} \leq 1.$$

This result is a more stringent bound on the time evolution of local observables than the one proposed in Ref. [163] and discussed in Eq. (2.16), see Fig. 2.14 for a direct

comparison. The importance of this result lies also in another fact. We expect that, as α grows, the behavior of the system becomes more and more similar to the one of a short-range model. For finite values of α the light-cone scales faster-than-ballistic but, if we take the limit $\alpha \to \infty$, we recover the Lieb-Robinson result $t^\star \propto R$.
Recently a new bound of the same form has been proposed in Ref. [167] which derives it for more general long-range Hamiltonians. If this bound is applied to two-body long-range interactions, the result of Foss-Feig et al. (2.18) is recovered.

In the next section we will discuss a more important characteristic that these bounds have to satisfy: they have to be able to predict the correct time evolution. The Lieb-Robinson bound presented in Sec. 2.1.2 predicts a ballistic scaling of the activation time with the distance for short-range interacting Hamiltonians. This has found to be true in experimental and numerical works as the ones presented before and many others.

3 Long-range Ising model in arbitrary dimensions

In this chapter we present experimental, numerical and analytic results for the time evolution of spin-spin correlations in long-range interacting quantum spin models. We start reviewing the most important experimental and numerical results in the literature on the dynamics of local observables in long-range interacting systems. We then present our results for the long-range transverse Ising model. We start from the Monte-Carlo simulations performed by G. Carleo, in collaboration with me, and then we derive in detail my analytical results based on the quasi-particle approach.
We focus on long-range Hamiltonians describing spin models in generic dimensions, written in the form

$$\mathcal{H} = \frac{1}{2} \sum_{\mathbf{R} \neq \mathbf{R}'} \sigma^{\lambda}_{\mathbf{R}} J^{\lambda\rho}_{|\mathbf{R}-\mathbf{R}'|} \sigma^{\rho}_{\mathbf{R}'} - h \sum_{\mathbf{R}} \sigma^{x}_{\mathbf{R}}. \tag{3.1}$$

This describes a system of three dimensional spins, represented by the Pauli matrices σ^{λ}_i, on a generic D dimensional lattice where the sites are labeled by their distance $\mathbf{R}$, and $|\mathbf{R}-\mathbf{R}'|$ is the Cartesian distance between two sites. The labels ρ and λ correspond to the directions of the spins in the 3D space λ, $\rho = x, y, z$. We will assume that the interaction between spins decays algebraically in space as

$$J^{\lambda\rho}_{|\mathbf{R}-\mathbf{R}'|} = \frac{J_{\lambda\rho}}{|\mathbf{R}-\mathbf{R}'|^{\alpha}},$$

where the constants $J_{\lambda\rho}$ can be positive or negative. The system can then be polarized using a constant magnetic field of intensity h. We define the direction of the magnetic field as x-direction for the spins.
This Hamiltonian is of the same type of the one already discussed in Sec. 2.4. We know then that the commutator between local observables can be bounded for sufficiently large values of α dependent on the dimensions. If $\alpha < D$, no bound is known and the propagation can in principle be instantaneous. For $D < \alpha$ the propagation is bounded and a finite activation time $t^{\star}$, scaling logarithmically with the distance between the points [163], is found

$$t^{\star} \propto \alpha \ln(|\mathbf{R}|).$$

This bound can then be improved for $\alpha > 2D$, where $t^{\star}$ takes an algebraic form [166]

$$t^{\star} \propto R^{\beta}$$

where $\beta < 1$ allows a faster-than-ballistic propagation.
The propagation of correlations induced by Hamiltonians of the type (3.1) has been

studied numerically and experimentally in different situations. The results obtained provide a strong dependence on the explicit form of the Hamiltonian used, on the initial state, and on the value of α. Many of these results cannot be guessed a priori by the general bounds on long-range interactions presented in Sec. 2.4. It has to be kept in mind that the bound on the commutator and the bound on the correlations take the same form just in specific cases. As we see Sec. 2.1.3 for the short-range case, this happens just on particular states, where correlations decay sufficiently fast.
After an introduction to the main results found in the literature we will focus on my work on the long-range transverse Ising model (LRTI), which corresponds to Hamiltonian (3.1) with long-range coupling of the type

$$J_{\rho\lambda} = V\delta_{\rho,z}\delta_{\lambda,z}.$$

The results we obtain are based on the mapping between the excitations of the Ising Hamiltonian in the strongly polarized state and bosonic particles. Thanks to this particular mapping, it is possible to define excitations called magnons and derive their dispersion relation. Our results can be easily extended to generic interacting bosonic quantum systems with long- and short-range interactions.
We provide the equations for the time evolution of the spin-spin correlation function, which can be easily generalized to more generic cases. Then we study the first- and second-order divergences of the energy spectrum as a function of α and D, and precisely relate them to the dynamical behavior of the correlations by computing analytically the dominant contributions.
For strong decay of interactions, $\alpha > D+1$, the group velocity of the quasi-particle excitations is bounded, which yields a linear conic causal region. This behavior is similar to that found for short-range interactions and corresponds to a dynamics significantly slower than the known bounds [163, 166]. For weak decay of interactions, $\alpha < D$, the energy spectrum diverges in the infrared limit. It provides a vanishing characteristic time, independent of the distance R, for the activation of correlations. The latter can be associated with instantaneous propagation of correlations and the breakdown of causality. This is compatible with the absence of known finite bound in this regime. Finite-size scaling of the typical times precisely confirms this behavior. For intermediate decay of interactions, $D < \alpha < D+1$, we find a bent-cone causal region determined by a sub-ballistic algebraic bound, $t^\star \sim R^\beta$, where β is some function of the exponent α and the dimension D. This again corresponds to a dynamics that is significantly slower than the known bounds. We study the full space-time dynamics of the spin-spin correlations for various values of α. Taking into account the contributions of all quasi-particles, we confirm the three regimes. We then characterize each regime in detail. For $\alpha < D$, we perform finite-size scaling of the correlation function, which confirms our analytical predictions for both the bound and the amplitude of the correlations at the propagation front, and the breaking of causality. For $\alpha > D+1$, we find a clear linear cone. We determine the associated velocity and find excellent agreement with the expected value of twice the maximum group velocity [161]. For $D < \alpha < D+1$, we find a clear algebraic bound, $t^\star \sim R^\beta$ for all tested cases and extract numerically the exponent $\beta(\alpha)$ in dimensions $D = 1$ and 2.

Finally we study the shape of the correlation front in dimension $D > 1$ and discuss its symmetries which are related to the spectrum.
The theory proposed in this chapter for the specific case of the LRTI can be anyway extended to more general systems. The Hamiltonian of the magnons is a quadratic bosonic Hamiltonian, and many different systems can be described by using this class of operators. We will see in Chap. 4 that the same Hamiltonian can be used to describe long-range interacting bosons in the superfluid regime.

3.1 Experimental realizations

Various versions of Hamiltonian (3.1) have already been realized in the laboratory using trapped ion techniques, see Sec. 1.3.3. In ion crystals it is possible to set a specific initial state and then drive the system out of equilibrium performing a spin-flip. This triggers a time evolution acting as a local quantum quench.

3.1.1 Innsbruck experiment

Jucevic et al. used this protocol, see Ref. [48], to drive out of equilibrium a long-range interacting spin chain. The system is realized using $^{40}Ca^{+}$ ions. The hyperfine states of the atomic structures can be used to map it into a spin-1/2 system. The two states $|S_{1/2}, m = 1/2\rangle$ and $|D_{5/2}, m' = 5/2\rangle$ are in fact coupled using Zeeman fields and they correspond to $|\uparrow\rangle$ and $|\downarrow\rangle$. The $|\uparrow\rangle$ is a metastable state and it decays into $|\downarrow\rangle$ in $1.16\,s$ thanks to a quadrupole transition of characteristic wavelength $\lambda = 729\,nm$. The crystal structure is formed naturally once the ions are trapped because of the electric repulsion. The initial state is set to $|\downarrow\rangle$ using optical pumping techniques with a $99,9\%$ precision. The presence of the trap slightly changes the energy levels making the system slightly inhomogeneous. However this effect can be quantified in a difference of $20\,Hz$, which is negligible compared to the typical energy scales of the Hamiltonian.
Interactions between the two spin states are obtained using a laser shining the chain. The laser is set to carry two frequencies $\omega_{\pm} = \omega_0 \pm \Delta$, where ω_0 is the energy difference between $|\uparrow\rangle$ and $|\downarrow\rangle$, and Δ is a positive detuning. The momentum exchange between the ions and the laser creates an effective potential between the hyperfines states that can be written as

$$\mathcal{H} = \sum_{i,j} J_{i,j} \sigma_i^x \sigma_j^x,$$

where the spin-exchange couplings are given by

$$J_{i,j} = \Omega_i \Omega_j \frac{k^2}{2m} \sum_n \frac{b_{i,n} b_{j,n}}{\Delta^2 - \nu_n^2}.$$

Ω_i denotes the Rabi frequencies of the bi-chromatic laser beam on the ions, labeled by $i = 1, \ldots, N$, $k = 2\pi/\lambda$, n is the wave-number, λ is the laser wavelength, and the mass of the ions is m. The ν_n coefficients are the oscillation frequencies of the atoms around their equilibrium positions. The coefficients $b_{i,n}$ are the Lamb-Dicke factors that depend on

the displacement of the ions from their equilibrium position [122]. This way it is possible to map the motion of the ions into an effective interaction at the spin level.
Increasing the detuning Δ to a value larger than any transition, it is possible to engineer a long-range anti-ferromagnetic interaction the form

$$J_{i,j} \propto \frac{1}{|i-j|^{\alpha}},$$

where α can be tuned from extremely small $\alpha \sim 0$ to quite large $\alpha \lesssim 3$, hence realizing a fast decaying interaction of the dipolar type.
The local magnetic field is then created using a shift in the frequency of the laser beam of a value $\delta = 2B$, which creates the requested interaction term

$$B \sum_i \sigma_i^z.$$

The experiment is carried out in the strongly correlated regime, $B \gg J_{i,j}$, where processes like

$$|\uparrow\rangle |\uparrow\rangle \rightarrow |\downarrow\rangle |\downarrow\rangle$$

are suppressed and the only ones still present are

$$|\uparrow\rangle |\downarrow\rangle \rightarrow |\downarrow\rangle |\uparrow\rangle$$

which conserves the magnetization along the z-axis.
We can then write the Ising Hamiltonian using the $\sigma_i^x = \sigma_i^+ + \sigma_i^-$ to obtain an effective Hamiltonian

$$\sigma_i^x \sigma_j^x = \left(\sigma_i^+ + \sigma_i^-\right)\left(\sigma_j^+ + \sigma_j^-\right) = \sigma_i^+\sigma_j^+ + \sigma_i^+\sigma_j^- + \sigma_i^-\sigma_j^+ + \sigma_i^-\sigma_j^-.$$

Since the transition of the type $|\uparrow\rangle |\uparrow\rangle \rightarrow |\downarrow\rangle |\downarrow\rangle$ are not allowed, the terms $\sigma_i^+\sigma_j^+$ and $\sigma_i^-\sigma_j^-$ can be dropped on this sub-space. The effective Hamiltonian is then of the XY type

$$\mathcal{H} = \frac{1}{2}\sum_{i,j} J_{i,j}\left(\sigma_i^+\sigma_j^- + \sigma_j^+\sigma_i^-\right).$$

From Hamiltonian (3.1), it can be derived taking the limit $B \rightarrow \infty$ and using V as the unit of energy.
The system is made of 15 ions and is prepared in the fully polarized state

$$|\Psi_0\rangle = \otimes_{i=1}^{15} |\downarrow\rangle_i.$$

The central spin is then flipped to $|\uparrow\rangle$ driving the system out of equilibrium and creating a non-trivial time evolution. The effect of the local perturbation spreads over the system thanks the fundamental excitations defined in this system, called magnons. In the weakly-interacting regime, these excitations are independent and they contribute to the time-evolution of the magnetization. The observable followed during the time evolution is the

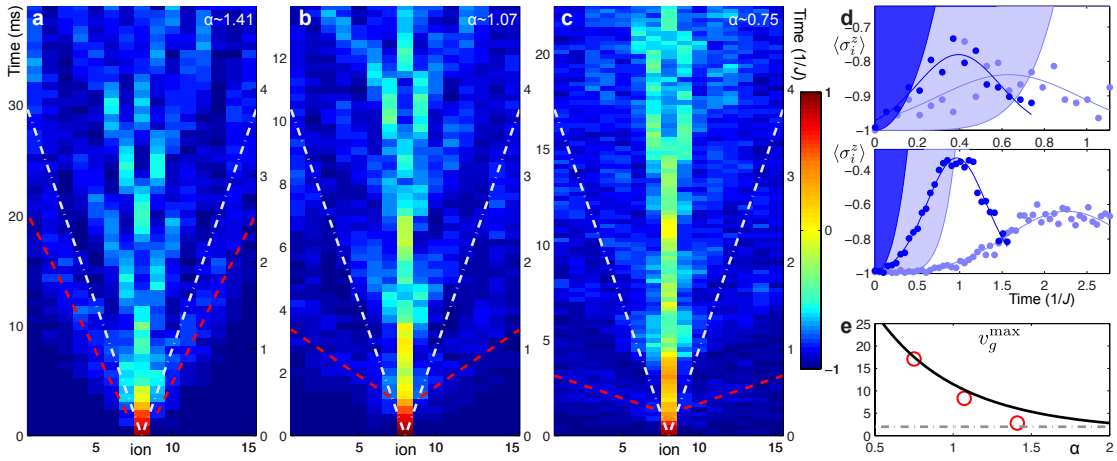

Figure 3.1: Time evolution of $\langle \sigma_i^z(t) \rangle$ following a local quench at the center of the chain for different values of α, in red, and a comparison to the short-range case, in white. a) for $\alpha = 1.41$ the behavior of the model is extremely close to the one from the dispersion relation of the short-range model. The model is then approximatively short-range for the regime we are looking at. b) and c) show the same plot for $\alpha = 1.07$ and $\alpha = 0.75$, where the interaction range becomes larger and larger and consequently the behavior of the model is becoming more and more long-range. The difference between these two regimes is even more accentuated in panel d) where the correlation function for $\alpha = 0.75$ of the spins $i = 6$ and $i = 13$ are shown and they are compared with the Lieb-Robinson bounds for short-range systems. In the top panel a clear violation of this bound is present for both the set of data, the signal arises in the region of small times violating the Lieb-Robinson bound. In the bottom panel the same quantities for $\alpha = 1.41$ are plotted. It is possible to see how the violation of the Lieb-Robinson bounds is almost impossible to detect and the system behaves almost as a short-range interacting system. Finally, in panel e) there is a comparison of the velocity of the light-cone. The solid line is the maximum velocity of the long-range model as function of α while the dashed one is the maximum velocity of the short-range model. The measured velocity, red circles is compatible with the maximum group velocity of the long-range model and it converges to the one of the short-range interacting increasing the values of α showing that the model becomes the more and more short-range interacting as the value α is increased. Figure from Ref. [48].

mean magnetization along the x-axis, $\langle \sigma_i^x(t) \rangle$, as a function of the distance between the ion i and the central site, where the local quench occurs. For different values of the decay α the dynamics is compared with the one of the short-range model, $\alpha \to \infty$.

In Fig. 3.1 the time evolution of $\langle \sigma_i^z(t) \rangle$ is plotted as a function of the site i and of the time t for three different values of α. In panel a) the time evolution for $\alpha = 1.41$ is shown with its front in red. It is then compared to the dynamics in the same local quench protocol for the short range model (white lines). It is possible to see how these two are close and how the short-range model is able to capture the dynamics of the long-range one.
If the value of α decreases, panels $\alpha = 1.07$ b) and $\alpha = 0.75$ c), a signal appears earlier and earlier in the long-range model and the difference in the activation time between the long- and the short-range models become larger. Moreover, the two differ also in the way the correlation function behaves outside this wave-front signal, i.e. leaks. While in the short-range case a sharp horizon is present, a more persistent one appears in the long-range case. This difference in the leaks is perfectly captured by the bounds presented in Sec. 2.4. For the short-range case the bound is in fact exponential, i.e. the signal falls off really quick outside the correlated region. For the long-range case it is algebraic, i.e. it falls down quite slowly outside the region where correlations are created. A clear violation of the short-range bound presented in Sec. 2.1.3 is present and it points out that the time-evolution in presence of short- and long-range interactions is very different. Since quasi-particles are well defined in this model it is possible to check the predictions of the Cardy-Calabrese argument, see Sec. 2.2. In panel e), the maximum group velocity of the magnons as a function of α (dashed line) is compared with the one of the short-range model (solid line). These can then be compared to the velocity extracted from the experimental data. It is possible to see how the data for small values of α are consistent with the long-range model and far from the short-range ones. Increasing α the velocities extracted from the long-range model approach the ones of the short-range one. Physically, this effect is motivated by the fact that, as α increases, its long-range behavior disappears.

3.1.2 JQI experiment

The previous experiment proved that a violation of the Lieb-Robinson bound is present when the interactions are sufficiently long-range. However it does not focus on the shape of the correlated region. The shape of the correlated region is the key difference between the long-range and the short-range interactions. In the presence of sufficiently long interactions, see Sec. 2.4, the shape of the horizon of the correlation function is algebraic

$$t^\star \propto R^\beta,$$

with $\beta \leq 1$. In contrast to the linear ballistic light-cone in the short-range interacting systems, $\beta = 1$, predicted by the Lieb-Robinson bound.
The work of P. Richerme et al presented in Ref. [47] address this question. The procedure is the same as in the previous experiment but $^{171}Yb^+$ ions are used. As before, the spin

model is obtained using two hyperfine states, namely the $|^2S_{1/2}, F = 0, m = 0\rangle$ and the $|^2S_{1/2}, F = 1, m = 0\rangle$, which are the $|\uparrow\rangle$ and $|\downarrow\rangle$ along the z-axis. The ion crystal is formed naturally by the Coulomb repulsive force between the ions and the trapping one. After that the long-range interactions are created using laser fields. These interactions map the motion of the ions into an effective long-range potential between the spins. The initial state can be set using optical pumping in the fully polarized state. In the experiment of Ref. [47], a global quench is performed letting the system time evolve using the LRTI Hamiltonian

$$\mathcal{H} = \sum_{i,j} J_{i,j}\sigma_i^x\sigma_j^x,$$

the coupling $J_{i,j}$ fall down as a power law $|i-j|^{-\alpha}$ with tunable parameter α between 0 and 3.
These long-range interactions are obtained using a dipole laser interaction as described for the experiment at Innsbruck. The initial state is the product state where all spins are down

$$|\Psi_0\rangle = \bigotimes_i |\downarrow\rangle_i\,,$$

obtained using optical pumping. The initial state is not an eigenstate of the Ising Hamiltonian and then a non trivial time-evolution appears. In the microscopic picture, every site of the chain acts now as a source of quasi-particles.
After a time t the interaction Hamiltonian is shut down and the system is probed using a CCD camera with a single site resolution. This is able to measure the state of every site and spin-spin correlations, namely

$$\mathcal{C}_{ij} = \langle\sigma_i^z(t)\sigma_j^z(t)\rangle - \langle\sigma_i^z(t)\rangle\langle\sigma_j^z(t)\rangle, \tag{3.2}$$

can then be extracted. These measurements are repeated 4000 times for every value of the evolution time t in order to get the dynamics of the averaged observable.

In Fig. 3.2 it is possible to see the time evolution of the spin-spin correlation function (3.2) as function of the distance $i-j$ and for different values of α. For all the values of α an algebraic and faster-than-ballistic light-cone is found. The parameter β extracted from the data goes to one as the parameter α is increased, in agreement with literature results [166, 167]. The shape of the light-cone is computed imposing a threshold for the quantity $\mathcal{C}_{ij}$ equal to $\mathcal{C}_{thres} = 0.1\mathcal{C}_{ij}^{max}$. It is then possible to extract the local velocity for these points and see that it is always faster than the Lieb-Robinson one. The only exception is $\alpha = 1.19$, where the velocity is constant and it is slower than the one of the short-range chain. The authors anyway do not repeat the same calculus for lower values of $\mathcal{C}_{thres}$, even if it is possible to see, for example in the case $\alpha = 1.19$, that a faster signal appears. They explain this faster-than-ballistic light-cone using the indetermination principle. A process defined by the time scale $\tau \sim 1/E_{ij}$ is determined by $E_{ij} \sim 1/|i-j|^\alpha$ which determines a bent light-cone $\tau \sim |i-j|^\alpha$. The small size of the system makes anyway difficult to determine the real velocity of the front. This measure can be extracted from a fit of the correlation front in a region where $\mathcal{C}_{thres}$ goes to zero which requires long times and large systems, as we will explain in Sec. 3.6.3 using

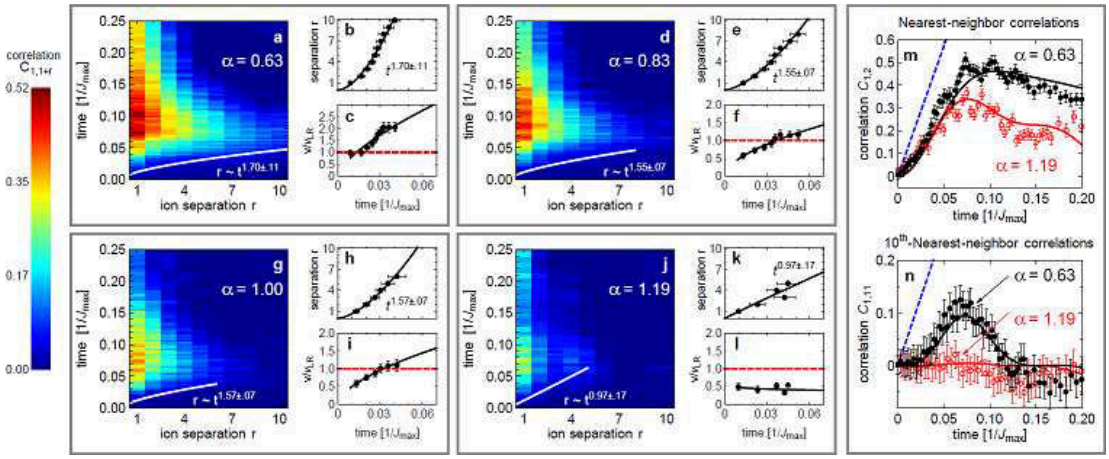

Figure 3.2: Time evolution of the correlation function (3.2) for the Ising chain with different values of α. for every value of α the light-cone shape is computed, finding a faster-than-ballistic propagation in every case. The instantaneous velocity is extracted from the numerical data and compared with the one of the short-range model finding that the first is alway larger than the latter. Figure from Ref. [47].

analytic computations.
As for a local quench, also for the global one features a violation of the Lieb-Robinson results when long-range interactions are present between different sites. The violation of the Lieb-Robinson bound is then important to compute new bounds on the dynamics of long-range interactions.
In the two cases already discussed, many of the values of the parameter α are extremely small. They are usually not in the range where a bound on the correlations is present and where, in principle, correlations can be unbounded. The fact that here they seem to be bounded may be due to the relatively small size of the system, not enough large to have a strong violation.
It is then important to study larger systems in order to discriminate from the finite size effects in the experimental setups. Modern numerical methods can access larger systems compared to experimental setups. They allow to simulate tens (t-VMC and DTWA methods) to almost a thousand (t-VMC) sites. Long-range interacting systems are anyway quite tricky to analyze due to their size effects and the thermodynamic limit is not always well defined. These numerical methods have to be compared then to analytical results computed in the regimes where they are available. These analytic results can be used to find the real behavior of the long-range interacting systems in the thermodynamics limit.

3.2 Theoretical results

We are now going to analyze the results on the propagation of correlations following a quantum quench for one and two dimensional LTRI models using two numerical approaches.

3.2.1 TDVP in the one-dimensional Ising model

We start discussing Ref. [169], where Hauke et al. study the dynamics of magnetization and entanglement in a LRTI chain (1D) following a local quench. This study has been done using the time dependent variational principle (TDVP) algorithm applied to matrix product states (MPS). A description of the method can be found in Ref. [169] and references therein. This method is similar to the t-DMRG which has already been used in [215] and other works for short-range interacting systems and here it is extended for long-range ones. The numerical results are then compared to the ones obtained by the quasi-particle picture.

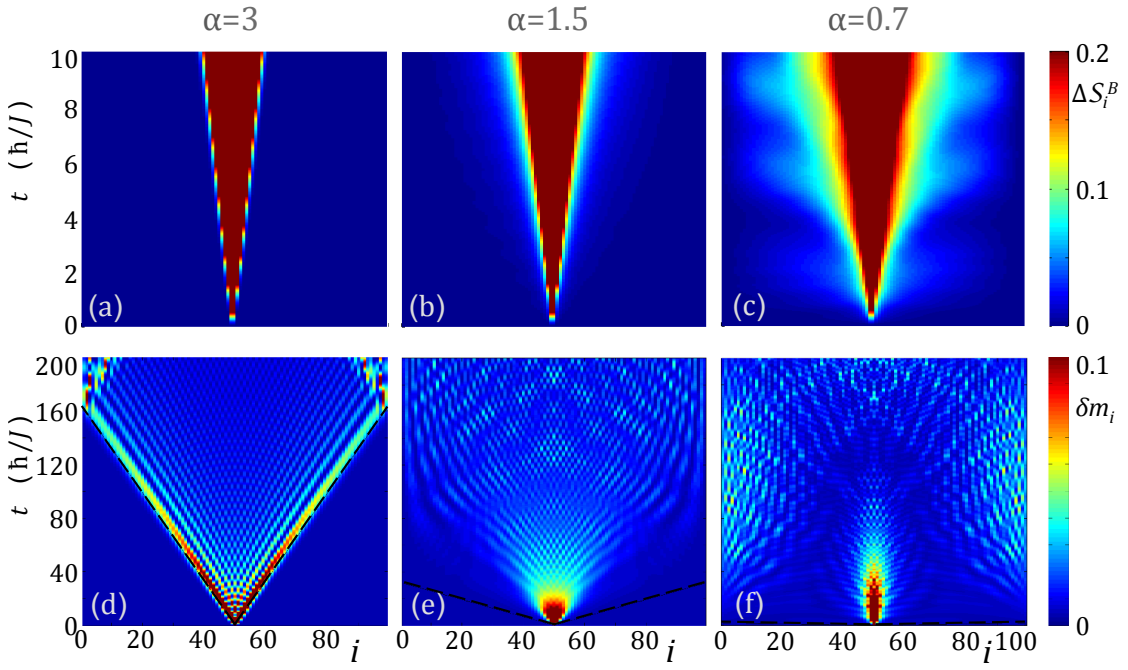

Figure 3.3: Time evolution of the magnetization following a local quench in the center of a LRTI chain computed for different values of α using TDVP, upper panel, and the quasi-particles approach, lower panel. The computations performed using the spin wave approximation can reach longer times. The regimes are then much clearer in these data compared to the TDVP ones. Left column: time evolution for $\alpha = 3$ computed with TDVP (a) and quasi-particle approach (d). A Clear ballistic light-cone appears in both of them. Central column: time evolution for $\alpha = 3/2$ computed using TDVP (b) and quasi-particles approach (e). In this case the time evolution is not ballistic, but it represents an algebraic increasing light-cone. Right column: time evolution for $\alpha = 0.7$ computed using the TDVP (c) and the quasi-particle approach (f). For this values a clear instantaneous propagation is present in the quasi-particle data. In the TDVP this instantaneous behavior is present even not so strong as in the other data. In this case, the analytic approach is fundamental to determine the right propagation regime. Figure from Ref. [169].

In Fig. 3.3 the time-evolution of $\langle \sigma_i^x \rangle(t)$ values in a one-dimensional LRTI chain following a local quantum quench for different value of α is presented. The data are obtained using the TDVP (upper panel) and a quasi-particle approach (lower panel).
We start from the TDVP results which are computed for $\alpha = 3$, 1.5, and 0.7. In the first case Fig. 3.3 (a), a ballistic propagation is found. For $\alpha = 1.5$, Fig. 3.3 (b), we can still see a strong signal propagating ballistically. Anyway, outside this region, a smaller signal is present. This is not propagating ballistically: its front is clearly bent and it suggests a slower-than-ballistic propagation. For $\alpha = 0.7$, Fig. 3.3 (c) a signal appears at small times in a large region of the system following the quench. In the inside, a strong ballistic propagating signal is still present as in the other cases.

The TDVP can anyway access relatively small times before that the growth of entanglement in the system is too large and the dynamics for further times cannot be explored. The authors then compare these numerical results with the ones obtained using a quasi-particles approach. This is based on the linear spin wave theory and we will describe it in full detail in Sec. 3.4. These results are presented in the lower panel of Fig. 3.3. In Fig. 3.3 (d) the propagation for $\alpha = 3$ is presented and it exhibits again a ballistic propagation of the front. For $\alpha = 1.5$,Fig. 3.3 (e), the propagation is not completely clear. It seems to have a faster-than-ballistic spreading for small times, then a linear one and finally a slower-than-ballistic one when it reaches the border of the system. For $\alpha = 0.7$, Fig. 3.3 (f), the propagation is then clearly instantaneous in the system. Magnetization is activated at the borders of the system right after the quench.
The authors then conclude that three regimes are present in the propagation of correlations depending on the value of α

- an instantaneous regime $\alpha < 1$, where correlations are activated instantaneously everywhere in the system right after the quench
- a quasi-local regime $1 < \alpha < 2$, where correlations are not instantaneous but they propagate algebraically. Even if it is not clear if they are faster- or slower-than-ballistic.
- a local regime $\alpha > 2$, where the propagation of correlations is ballistic.

The LSWT allows to access the energy spectrum of the fundamental excitations of the system, which reads

$$E_k = 2\sqrt{h\left(h + VP(k)\right)}$$

where $P(k)$ is the Fourier transform of the long-range potential

$$P_k = \sum_R \frac{e^{-\imath kR}}{R^\alpha}$$

which depends on the exponent α.
The three regimes are explained using the different divergences appearing in the dispersion relation as a function of α:

- For $\alpha < 1$ the dispersion relation is divergent around $k \approx 0$ corresponding to the non-local regime.
- For $1 < \alpha < 2$ the group velocity $\partial_k E_k$ is divergent around $k \approx 0$ corresponding to the quasi-local regime.
- For $\alpha > 2$ both the dispersion relation and the group velocity are finite and the propagation is ballistic. The light-cone velocity extracted from the numerics can be compared with the one extracted from the spectrum of excitations finding a perfect agreement between them. This is presented in Fig. 3.3 (d), where the dashed line is the maximum velocity of quasi-particles.

This work identifies then three different regimes in the propagation of correlations determined by the divergences in the excitations spectrum. Just one regime is unbounded, for $\alpha < 1$, in agreement with the absence of bounds for these values of α. For $\alpha > 1$ the propagation is always bounded but a direct comparison to the bounds presented in Sec. 2.4 is not explicitly carried out.
This perfectly explains the propagation of correlations, it would be possible anyway to find different observables with a behavior that cannot be explained from the spectrum alone.

3.2.2 Quench from an initial product state

As we discussed for short-range interacting quantum systems, the bounds on the time evolution of local observables can be derived from the bounds on the norm of the commutator taking into account the correlations already present in the initial state. The dependence of the propagation on the initial state has been studied in Ref. [168]. As we found in Sec. 2.4 it is possible to bound the commutator between local observables if $\alpha > 1$. In this work Eisert et al. demonstrated that it is possible to have a lower bound on the propagation of correlations if the initial state is a product state. They show analytically that in such a state, the bound applies for $\alpha > 1/2$ while in the case of a generic initial state, it applies for $\alpha > 1$. They set the system in an initial product state and then they let it evolve under the LRI Hamiltonian

$$\mathcal{H} = \sum_{i \neq j} \frac{V}{|i-j|^{\alpha}} \sigma_i^z \sigma_j^z. \tag{3.3}$$

The time evolution of the $x - x$ spins correlations $\langle \sigma_0^x \sigma_\delta^x \rangle - \langle \sigma_0^x \rangle \langle \sigma_\delta^x \rangle$ are then evaluated using the exact expressions derived in Ref. [239]. In Fig. 3.4 the time evolution of correlations for different values of α is shown for the Ising model for the case where the initial state of the system is a product state. For $\alpha < 1/2$ the propagation of correlations is instantaneous, the activation of correlations takes place in the same way for all the values of the distance δ. This result is compatible to the bound on the time evolution starting from an initial product state. For $1/2 < \alpha < 1$, the spreading of correlations is not instantaneous but an activation time, depending on the distance, $t^\star(R)$ appears. For this range of values of α, $t^\star$ seems to scale faster-than-ballistic. For $\alpha > 1$ the propagation is ballistic over some tens of lattice sites and it then becomes slower-than-ballistic. These three regimes are similar to the ones found in Ref. [169] we briefly discussed above. Anyway, the fact that in this case the correlations in the initial state are zero, since we start from a product state, changes the ranges of values of α where these regimes occur by a factor $1/2$.
The importance of the initial state is something that have to be taken into account carefully. In fact, many times it has been assumed that the bound over the local operators is the same as the one on the observables. As we motivated in Sec. 2.1 and as it has been rigorously demonstrated in Ref. [240], the presence of correlations in the initial state matters in both long- and short-range interacting systems.

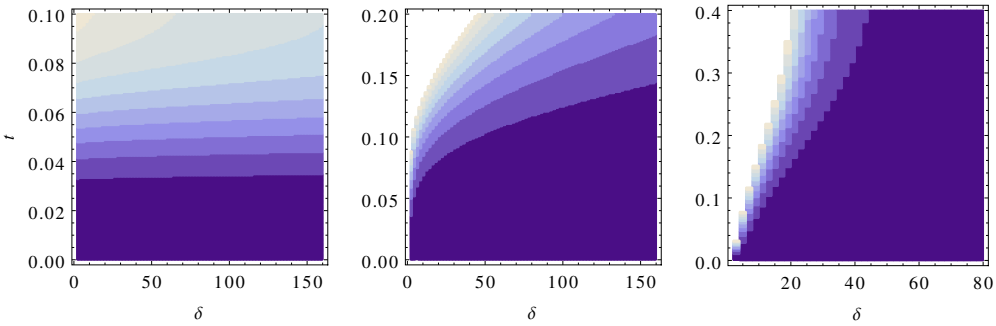

Figure 3.4: Time evolution of the spin-spin correlations for a system prepared in a product state and evolved in time under the Hamiltonian (3.3) with different values of α. The data are obtained evaluating the exact expressions of the correlation function presented in Ref. [239]. Left figure: time evolution for $\alpha = 1/4$. An instantaneous time evolution is found for small values of α. Correlations activate everywhere right after the application of the Hamiltonian. Central figure: time evolution for $\alpha = 3/4$. A faster-than-ballistic propagation is found for $1/2 < \alpha < 1$. This is due to the fact that the initial state is a product state and no correlations are present at the beginning. Right figure: rime evolution for $\alpha = 3/2$. A ballistic propagation is found over some tens of sites and then it becomes slower-than-ballistic. These three figures point out the dependence of the propagation on the initial state. Comparing them with the results presented in Fig. (3.3) we can see how the same three regimes are found but for different values of α depending on the initial state. Figure from Ref. [168].

3.2.3 Spin models in dimensions higher than one

Schachenmayer et al. in Ref. [172] studied the effect of the dimensionality using the Discrete Truncated Wigner Approximation (DTWA). An interesting introduction to this numerical method can be found in the same work and in references therein. The authors study the time evolution of one and two points correlations. They set the system in a product state and then let it evolve under the influence of the Ising or XY Hamiltonian. This is done in one dimensional systems, where a comparison between the results of DTWA and t-DMRG is possible. Then, they extend their approach to two dimensional systems, where t-DMRG is not available for long-range systems.

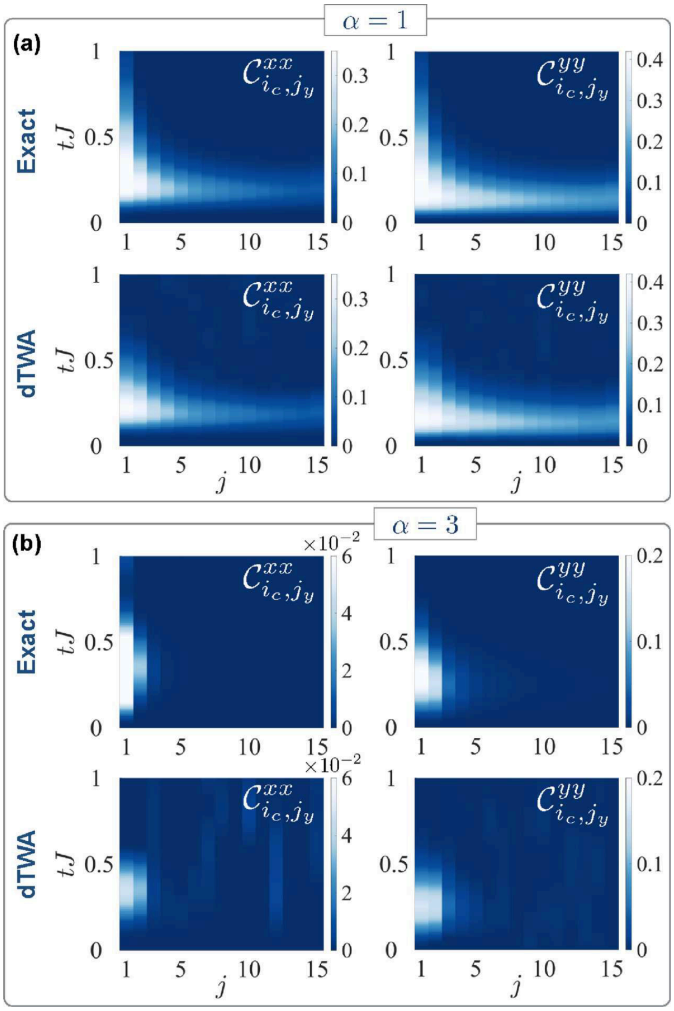

Figure 3.5: Time evolution of spin-spin correlations along different directions in one-dimensional Ising model for different values of α, $\alpha = 1$ upper panel and $\alpha = 3$ lower panel. For all the studied observables a comparison between the exact diagonalization and DTWA is presented for bi-dimensional system of sizes 31×31 finding consistent results between these two approaches. In this case the authors find a ballistic propagation for all studied cases. Figure from Ref. [172].

In Fig. 3.5 the time evolution of xx- and yy-spins correlations for a 2D systems are computed using the DTWA and then compared with the exact solutions for the Ising model. The two methods are again in agreement for the studied values of α. For $\alpha = 1$ the correlations show a rapid activation at all distances for both the observables. As we saw above, for small values of α it is possible to find fast propagating signals in correlation functions. For $\alpha = 3$ the situation is different and it is possible to see how distant spins remain uncorrelated over longer computational times meaning that the spreading of correlations in this case is bounded in some way.

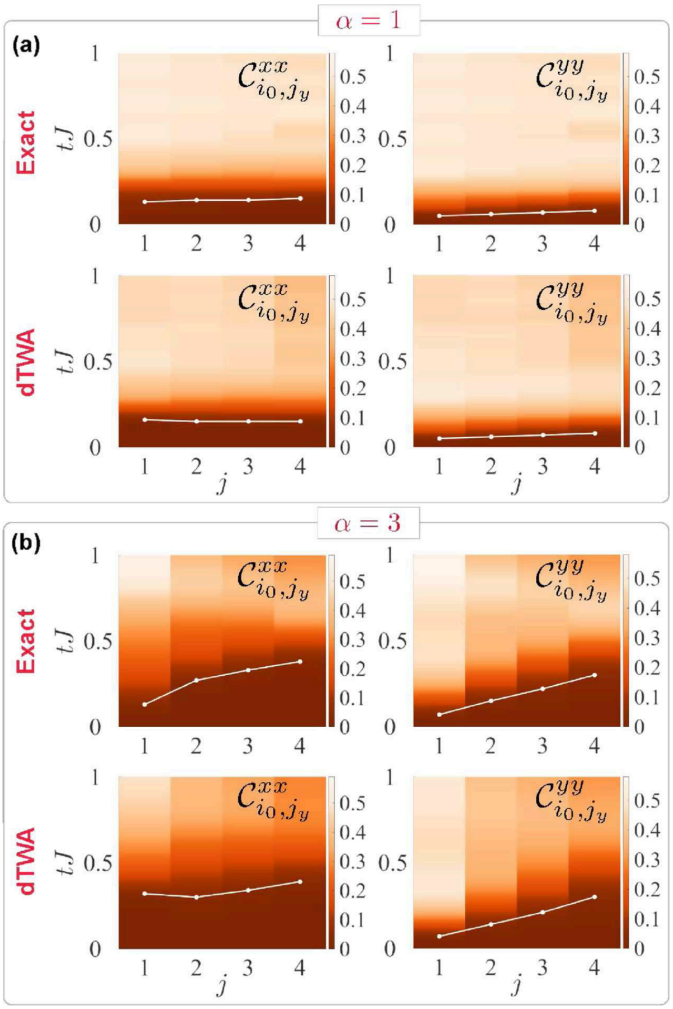

Figure 3.6: Time evolution of spin-spin correlations along different directions in bi-dimensional XY model for different values of α, $\alpha = 1$ upper panel and $\alpha = 3$ lower panel. For all the studied observables a comparison between the exact diagonalization and DTWA is presented for systems 4×5 finding consistent results between these two approaches. In this case, different regimes are found for different values of α: a ballistic propagation for $\alpha = 3$ and a faster-than-ballistic propagation for $\alpha = 1$. This becomes clearer looking at the white lines in all the plots. These represent the points where the correlation function reaches a values of 0.05 and they give information about the activation time $t^\star(R)$. Figure from Ref. [172].

In Fig. 3.6 the time evolution of the same quantities are plotted for different values of α in a 2D XY model. Again for the XY model, the agreement between the exact diagonalization and the DTWA results is perfect. For $\alpha = 1$, the propagation is fast and independent on the distance j. This effect is even clearer if we observe the white lines in the plots. They represent the values of t where the correlation function reaches the threshold $\mathcal{C}_{thres} = 0.05$ at fixed j. This is reached at the same time everywhere in the

system for $\alpha = 1$, pointing out an instantaneous propagation.
The same plots are shown for $\alpha = 3$ where, again, a good agreement between the DTWA and the exact diagonalization data is found. In this case a distance-dependent horizon is found. As before, the white lines represent the value of time where correlations reach $\mathcal{C}_{thres} = 0.05$ for different distances. There, the activation time depends on the distance. The light-cone is given by the values of τ where the correlation function reaches $\mathcal{C}_{thres}$ at different j. In Fig. 3.7 (a) the values of τ as function of j are plotted in log-log scale for one-dimensional and bi-dimensional systems for different α. In all the studied cases, the authors find a linear proportionality between the logarithm of the two studied quantities. The same analysis is repeated for the one-dimensional chain using the t-DMRG which gives results in fair agreement with the DTWA method. These both suggest a dependence of the form

$$\tau \propto j^{\eta}, \tag{3.4}$$

where η depends on α.
Repeating this study for different values of α, it is possible to determine the dependence of the parameter η on it, which is shown in Fig. 3.7. For one dimensional systems, the same can be done using t-DMRG. The parameters η extracted from DTWA and t-DMRG are in agreement, in particular for small values of α in one dimension. In two dimensions the results are only provided by the DTWA. The (b) and (c) panels show a clear difference in the behaviors of the horizon between one and two dimensional systems:

- In the one-dimensional case, the propagation is always local with $\eta > 0$ also when $\alpha < 1$, where we expect to find an instantaneous regime. The value η increases then as α grows becoming larger than 1 for $\alpha \sim 3$. This behavior is slightly different in the t-DMRG data, where η seems to saturate to 1 for $\alpha \sim 3$. The DTWA works better for small values of α and this explains this discrepancy between the two approaches in the region $2 \lesssim \alpha \lesssim 3$.

- In the two-dimensional case, three clear regions are found for different values of α. A region where the propagation is instantaneous, $\eta \approx 0$, for $\alpha < 2$. A region where the propagation is local but faster-than-ballistic for $2 < \alpha < 3$, where η grows from 0 to a value close to one. For $\alpha > 3$ a nearly ballistic region, where $\eta \sim 1$ and a linear light-cone appears.

It remains an open question to see how the dimensionality plays a key role for the XY model and just two regimes are found for $D = 1$ (a faster than ballistic and a ballistic one) while three regimes are found for $D = 2$. For $\alpha \lesssim 2$ the propagation is instantaneous, for $2 \lesssim \alpha \lesssim 3$ the propagation is algebraic and faster than ballistic and for $3 \lesssim \alpha$ the propagation is nearly ballistic.

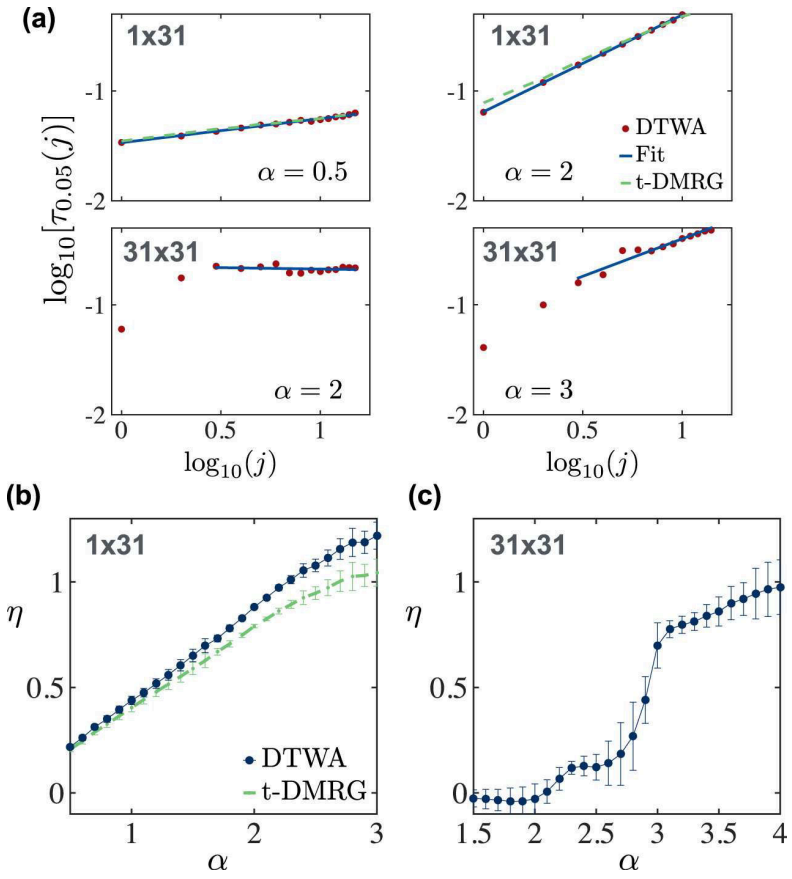

Figure 3.7: Study of the parameter η as function of α for the one-dimensional and bi-dimensional XY model. These values are computed using DTWA approach and for $D = 1$ they are compared to the ones extracted from t-DMRG. Upper panel: Log-Log plots of the function $\tau(R)$ as defined in Eq. (3.4) as function of j. It is possible to see how correlations are activated instantaneously for $\alpha = 1/2$ in $D = 1$ and for $\alpha = 2$ in $D = 2$. Using the same plots its is possible to find that for $\alpha = 2$ in $D = 1$ and for $\alpha = 3$ in $D = 2$ a faster-than-ballistic light-cone is found, $\eta < 1$. The dependence of η on α is computed using DTWA and t-DMRG for a one-dimensional system and they are presented in Figure (b). It is possible to see again how the agreement between the two is better for small values of α than for larger ones. Both of them predict a faster-than-ballistic spreading for all values of . For larger values the DTWA predicts a slower-than-ballistic propagation while the t-DMRG a ballistic one. The quantity η as function of α is then computed for a bi-dimensional system, in this case the DTWA is the only available numerical method. Three regions are found depending on α: for $\alpha \lesssim 2$ $\eta \sim 0$ which identifies an instantaneous signal appearing in the system. For $2 \lesssim \alpha \lesssim 3.5$ the parameter η increases almost from 0 to 1 determining a faster-than-ballistic propagation. For $3.5 \lesssim \alpha$ the value $\eta \sim 1$ correspondent to a ballistic propagation of correlations. Figure from Ref. [172].

3.2.4 Conclusion for the literature results

The discussion of these three very important works in the literature aims to point out the variety of results obtained by different methods for the propagation of correlations in long-range interacting quantum spin systems. The bounds on these models predict two different regimes (a bounded and an unbound regime) separated by the critical value $\alpha = D$. The numerical results show anyway a richer structure with an unbounded, an algebraic and a ballistic regimes separated by values of α that depend son different details. In Ref. [169] these different regimes have been connected to the microscopic theory through the quasi-particle approach, which shows different divergences.
If the initial state is a product state, these regimes are found for smaller values of α. Finally, the data from one and two dimensional XY systems, point out that the regimes found in one dimension are not found in two dimensions. This suggests that the study of one dimensional systems is not enough to understand the full physics of the out-of-equilibrium dynamics. It is worth stressing that most of these results were, however found from dynamics in relatively small systems. Their behavior in the thermodynamic limit still remains open.
In order to understand and clarify all these results coming from different models, a general theory valid for every dimension is needed. This will help to connect the different results from different systems and to connect the microscopic theory with the results of the different general bounds found in the literature. The development of this theory is the main topic of this chapter and it is the core of my work. The connection between the time evolution of correlations and the microscopic quantities, such as the energy spectrum, will be investigated.

3.3 Monte Carlo results for $D = 1$

Before to present our analytical work, let us discuss Monte Carlo results for the LRTI model, which form a basis for our study. These results have been obtained by G. Carleo in collaboration with me and they are published in a joint work, Ref. [23].
We will focus on the Long-Range Transverse Ising Model (LRTI)

$$\mathcal{H} = \frac{V}{2} \sum_{\mathbf{R} \neq \mathbf{R}'} \frac{\sigma^z_{\mathbf{R}} \sigma^z_{\mathbf{R}'}}{|\mathbf{R} - \mathbf{R}'|^\alpha} - h \sum_{\mathbf{R}} \sigma^x_{\mathbf{R}}, \tag{3.5}$$

where $\sigma^j_{\mathbf{R}}$ with $j \in \{x, y, z\}$ are the local Pauli matrices and $|\mathbf{R} - \mathbf{R}'|$ is the Cartesian distance between the two sites $\mathbf{R}$ and $\mathbf{R}'$ on the D-dimensional hypercubic lattice. .
We will study the time evolution of the correlations along the z direction

$$G_c^{\sigma\sigma}(R = |\mathbf{R} - \mathbf{R}'|, t) - G_c^{\sigma\sigma}(R = |\mathbf{R} - \mathbf{R}'|, t = 0) = \langle \sigma^z_{\mathbf{R}}(t) \sigma^z_{\mathbf{R}'}(t) \rangle_c - \langle \sigma^z_{\mathbf{R}}(0) \sigma^z_{\mathbf{R}'}(0) \rangle_c$$

for different values of α ranging from extremely long-range $\alpha \sim 0$ to $\alpha \to \infty$.
The t-VMC has already demonstrated to be an accurate method to describe the time-evolution of short-range interacting many-body quantum systems [22, 216]. We use it to

study the time-evolution of Hamiltonian (3.5), which is the first time this method has been used to study the effects of long-range interactions in the time evolution.
As we said, the t-VMC is based on a wave function of the Jastrow type,

$$|\Psi(t)\rangle = e^{\sum_k \lambda_k(t) O_k} |\Phi_0\rangle ,$$

where the operators O_l are the operators taken into account to describe the dynamics. For the LRTI chain, the operators O_k determining the time evolution are

$$O_k = \sigma^z_k \sigma^z_{-k},$$

already taken into the center of mass reference frame and $\sigma^z_k = \sum_R e^{-\imath Rk} \sigma^z_R$.
The equation of motion for the time dependent parameters $\lambda_k(t)$ can then be solved using this specific set of operators and then the time evolution of the wave-function is fully determined. This can be used to compute time averages and expectation values. The time evolution of these parameters is in fact given by a first order differential equation which can be solved using extremely stable tools allowing the exploration of large times.

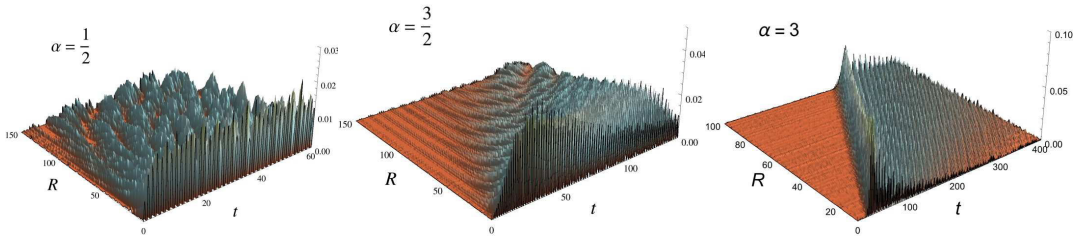

Figure 3.8: Time evolution of the spin-spin correlations following a quantum quench in a LRTI chain with different values of α. The initial state is the ground state of (3.5) in one dimension and we perform a quantum quench at fixed magnetic field. Different regimes are found for different values of α. For $\alpha < 1$ the propagation is instantaneous. For $1 < \alpha < 2$ the propagation exhibits a horizon which is algebraic but with a slower-than-ballistic behavior. Finally for $\alpha > 2$ the propagation is ballistic. The extremely long computation times accessible using the t-VMC with the large system sizes make possible to have a clearer characterization of these regimes than in the results of other methods. The large system size allows to see that the activation of correlation for $\alpha < 1$ takes place at the same time at any length. For $1 < \alpha < 2$, the long computation time allow to extract a clear value of the scaling of the horizon pointing out that it is slower-than-ballistic. For $\alpha > 2$ a linear interpolation of the correlation front allows a high precision of the value of the light-cone velocity that can be compared to analytic methods, see Sec. (3.6.1). Results obtained by G. Carleo in collaboration with my and published in a joint publication, Ref. [23].

In Fig. 3.8 the results for the time evolution of the spin-spin function

$$G^{\sigma\sigma}_c(R,t) = \langle \sigma^z_i(t) \sigma^z_{i+R}(t) \rangle_c - \langle \sigma^z_i(0) \sigma^z_{i+R}(0) \rangle_c$$

following a global quantum quench in the LRTI chain with different values of α are presented [23]. For $\alpha < 1$ the propagation of correlations is instantaneous and the correlations are activated everywhere in the system right after the quench. For $1 < \alpha < 2$ the propagation of correlations is non-instantaneous, but it is not ballistic, i.e. a non-linear light-cone appears. Finally, for $\alpha > 2$ a ballistic spreading of correlations is present, compatible with the fact that for large value of α the model is close to the behavior expected in short-range counterpart of Hamiltonian (3.5). These results are compatible with the ones found in [169] using the t-DMRG algorithm for a local quench. These results, however, significantly extend previous ones because the long computational times allow to extract more details from the numerical data. In particular, it is possible to see how the quasi-local regime has a clear slower-than-ballistic propagation of correlations, see also Fig. 3.9. For the instantaneous regime, a clear violation of locality is present and correlations are activated at every distance in an extremely short time.
The time scales accessible by these simulations are extremely large, order of hundreds of time cycles, while the ones accessible by the methods discussed before are of the order of ten at most. This allows us to extract precise results from these data, such as the velocity of the light-cone, that will be compared with the maximum group velocity of the excitations, or the shape of the light-cone for the quasi-local regime.
The initial state of the system is the ground state of the initial Hamiltonian and correlations are already present in the system before the quench. We find that the values of α separating these regimes are always larger than the ones presented in [168] for an initial product state.
The large computational times accessible using the t-VMC allow to extract the scaling of the correlation function in the quasi-local regime, $1 < \alpha < 2$, finding that it is slower than ballistic. The value of the light cone is extracted from the Monte Carlo results imposing a threshold ϵ to the correlation function. The activation time $t^\star$, defined as the moment where the correlation function reaches the value ϵ, depends algebraically on the distance R

$$t^\star \propto R^\beta.$$

For every value of ϵ we can then extract the value of β. We then take the limit $\epsilon \to 0$ repeating the previous procedure for smaller and smaller values of ϵ. We find then that the function $\beta(\epsilon)$ takes a finite value in this limit.

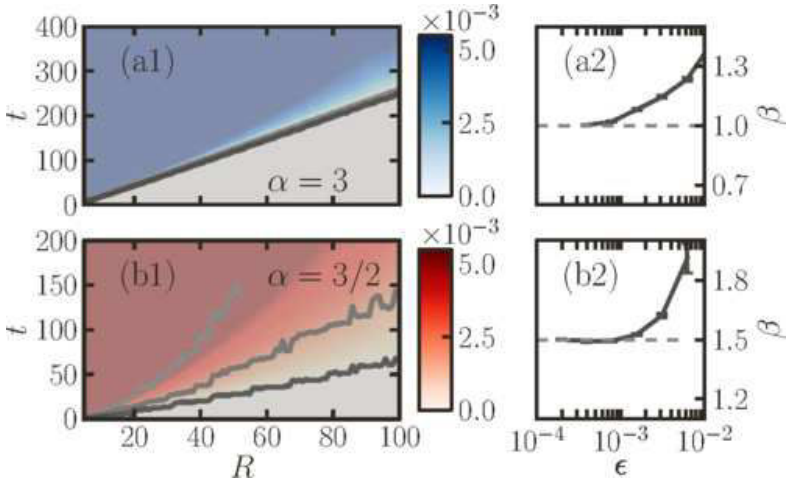

Figure 3.9: Values of the scaling parameter β of the horizon for $\alpha = 3$ (a1) and for $\alpha = 3/2$ (b1). These values are computed fitting the activation time $t^\star$ obtained imposing different thresholds ϵ to the correlation function computed using the t-VMC. For the ballistic case (a2) it is possible to see how $\beta \to 1$ as we take smaller and smaller ϵ. For $\alpha = 3/2$ (b2), the same method gives $\beta \to 3/2$ pointing out that the propagation is slower-than-ballistic. We will clarify this result using the quasi-particle picture in Sec. (3.6.2). in the same section we will detail also the ϵ method to extract the light-cone shape we briefly described here. Results obtained by G. Carleo in collaboration with me and published in a joint publication Ref. [23].

In Fig. 3.9 the results for a decreasing values of ϵ are presented for the $\alpha > 2$ region (upper panel) and for $1 < \alpha < 2$ region (lower panel). The coefficient β in the first case decreases to $\beta = 1$ as the threshold ϵ vanishes. It corresponds to a ballistic propagation. In the second case, the same procedure gives us a value of $\beta = 3/2$. It corresponds to a sub-ballistic propagation of correlations. The last result is quite surprising because the propagation is slower than ballistic instead of being faster as may be expected from the extended Lieb-Robinson bound, see Sec. 2.4.
We need then an analytic approach to clarify these questions:

- How is it possible to explain the propagation regimes from the microscopic point of view?
- How is it possible to characterize better the regimes found in the numerics? In particular: determining the velocity in the ballistic regime, finding the scaling of the light-cone in the quasi-local one and determining how locality is broken for $\alpha < 1$.

In the next chapter we study these points using the linear spin wave theory (LSWT). A similar approach is used to analyze the spectral properties in one dimension. Here we will extend the theory to the D-dimensional case and to include the full contribution of

the magnons to the correlation function under study. Finally we will extract analytic results where available characterizing the three regimes found and extending our analysis to generic dimensions.

3.4 Spin wave approximation

We want to start our discussion presenting a method to diagonalize Hamiltonian (3.5). From this point to the end of this chapter all the results presented have been derived directly by the author and published in Ref. [170]. In the case of a large magnetic field, the state of the system can be visualized as a strongly polarized state along the x-direction and small oscillations around it due to the long-range potential. These oscillations will be the fundamental excitations of the model and they are responsible for the spreading of correlations and other local observables.
Let us first briefly recall the quadratic approximation for the LRTI model, in order to write Hamiltonian (3.5) into a quadratic form we use linear spin wave theory (LSWT). We first rotate the reference axes around the free axis y by an arbitrary angle θ in order to find the minimum of the classical energy. In the rotated frame, the new spin operators read

$$\sigma^{x'}_{\mathbf{R}} = \cos\theta\,\sigma^{x}_{\mathbf{R}} - \sin\theta\,\sigma^{z}_{\mathbf{R}} \quad , \quad \sigma^{y'}_{\mathbf{R}} = \sigma^{y}_{\mathbf{R}} \quad , \text{and} \quad \sigma^{z'}_{\mathbf{R}} = \sin\theta\,\sigma^{x}_{\mathbf{R}} + \cos\theta\,\sigma^{z}_{\mathbf{R}},$$

and the Hamiltonian

$$\begin{aligned}\mathcal{H} \;=\; & \frac{V}{2}\sum_{\mathbf{R}\neq\mathbf{R}'} \frac{\cos^2\theta\,\sigma^{z'}_{\mathbf{R}}\sigma^{z'}_{\mathbf{R}'} + \sin^2\theta\,\sigma^{x'}_{\mathbf{R}}\sigma^{x'}_{\mathbf{R}'} - \sin\theta\cos\theta\left(\sigma^{x'}_{\mathbf{R}}\sigma^{z'}_{\mathbf{R}'} + \sigma^{z'}_{\mathbf{R}}\sigma^{x'}_{\mathbf{R}'}\right)}{|\mathbf{R}-\mathbf{R}'|^{\alpha}} \\ & -h\sum_{\mathbf{R}}\left(\sin\theta\,\sigma^{z'}_{\mathbf{R}} + \cos\,\theta\sigma^{x'}_{\mathbf{R}}\right).\end{aligned}$$

We then use the approximate Holstein-Primakoff transformation [241, 110]

$$\sigma^{z'}_{\mathbf{R}} \approx a^{\dagger}_{\mathbf{R}} + a_{\mathbf{R}} \qquad \text{and} \qquad \sigma^{x'}_{\mathbf{R}} = 2n_{\mathbf{R}} - 1 = 2a^{\dagger}_{\mathbf{R}}a_{\mathbf{R}} - 1, \tag{3.6}$$

valid for small bosonic occupation number $n_{\mathbf{R}} \ll 1$, and expand the Hamiltonian in the form $\mathcal{H} = \sum_{n\geq 0}\mathcal{H}_n$ where every $\mathcal{H}_n$ contains exactly n Holstein-Primakoff particle operators among $a_{\mathbf{R}}$, $a_{\mathbf{R}'}$, $a^{\dagger}_{\mathbf{R}}$, and $a^{\dagger}_{\mathbf{R}'}$. The zeroth-order term is the classical energy,

$$E_{\mathrm{cl}} = L^{D}\left[\left(\sum_{\mathbf{R}\neq\mathbf{R}'}\frac{V}{2|\mathbf{R}-\mathbf{R}'|^{\alpha}}\right)\sin^2\theta + h\cos\theta\right],$$

where L^D is the total number of lattice sites. The rotation angle θ is chosen to minimize the classical energy. It yields $\theta = \pi$ for anti-ferromagnetic exchange, $V > 0$ (The same result is anyway found for $V < 0$). The Hamiltonian computed for $\theta = \pi$ reads

$$\mathcal{H} = E_{\mathrm{cl}} + \frac{V}{2}\sum_{\mathbf{R}\neq\mathbf{R}'}\frac{\left(a^{\dagger}_{\mathbf{R}} + a_{\mathbf{R}}\right)\left(a^{\dagger}_{\mathbf{R}'} + a_{\mathbf{R}'}\right)}{|\mathbf{R}'|^{\alpha}} + 2h\sum_{\mathbf{R}}a^{\dagger}_{\mathbf{R}}a_{\mathbf{R}}.$$

This Hamiltonian belongs to the class of quadratic Hamiltonians that can be diagonalized using a Bogoliubov transformations. This procedure is generic and it can be applied to a large class of different models. In the following, we will describe this procedure for an operator of the class

$$\hat{\mathcal{H}} = \frac{1}{2}\sum_{\mathbf{R},\mathbf{R}'}\left[\mathcal{A}_{\mathbf{R},\mathbf{R}'}\left(\hat{a}^\dagger_{\mathbf{R}}\hat{a}_{\mathbf{R}'} + \hat{a}_{\mathbf{R}'}\hat{a}^\dagger_{\mathbf{R}}\right) + \mathcal{B}_{\mathbf{R},\mathbf{R}'}\left(\hat{a}_{\mathbf{R}}\hat{a}_{\mathbf{R}'} + \hat{a}^\dagger_{\mathbf{R}}\hat{a}^\dagger_{\mathbf{R}'}\right)\right], \tag{3.7}$$

where $\mathbf{R}$ and $\mathbf{R}'$ span the sites of a regular D-dimensional hypercubic lattice of unit lattice spacing. $\hat{a}_{\mathbf{R}}$ and $\hat{a}^\dagger_{\mathbf{R}}$ are, respectively, the annihilation and creation operators at site $\mathbf{R}$, with the usual bosonic commutation relations $[\hat{a}_{\mathbf{R}}, \hat{a}^\dagger_{\mathbf{R}'}] = \delta_{\mathbf{R},\mathbf{R}'}$, and the coefficients $\mathcal{A}_{\mathbf{R},\mathbf{R}'}$ and $\mathcal{B}_{\mathbf{R},\mathbf{R}'}$ are coupling amplitudes, containing both short- and long-range terms. For the LRTI model we have

$$\mathcal{A}_{\mathbf{R},\mathbf{R}'} = 2h\delta_{\mathbf{R},\mathbf{R}'} + \frac{V}{|\mathbf{R}-\mathbf{R}'|^\alpha} \qquad \mathcal{B}_{\mathbf{R},\mathbf{R}'} = \frac{V}{|\mathbf{R}-\mathbf{R}'|^\alpha}$$

A variety of systems can be described by Hamiltonian (3.7). Examples include weakly-interacting bosons and spin systems in strongly polarized states, see Refs. [242, 110]. Assuming translation invariance and parity symmetry, the coefficients $\mathcal{A}_{\mathbf{R},\mathbf{R}'}$ and $\mathcal{B}_{\mathbf{R},\mathbf{R}'}$ only depend on the Cartesian inter-site distance $R = |\mathbf{R}-\mathbf{R}'|$. This condition allows us to write Hamiltonian (3.7) in momentum space as

$$\hat{\mathcal{H}} = \frac{1}{2}\sum_{\mathbf{k}}\left[\mathcal{A}_{\mathbf{k}}\left(\hat{a}^\dagger_{\mathbf{k}}\hat{a}_{\mathbf{k}} + \hat{a}_{-\mathbf{k}}\hat{a}^\dagger_{-\mathbf{k}}\right) + \mathcal{B}_{\mathbf{k}}\left(\hat{a}_{-\mathbf{k}}\hat{a}_{\mathbf{k}} + \hat{a}^\dagger_{\mathbf{k}}\hat{a}^\dagger_{-\mathbf{k}}\right)\right], \tag{3.8}$$

where $\mathcal{A}_{\mathbf{k}}$, $\mathcal{B}_{\mathbf{k}}$, and $\hat{a}_{\mathbf{k}}$ are the discrete Fourier transforms of $\mathcal{A}_{\mathbf{R},\mathbf{R}'}$, $\mathcal{B}_{\mathbf{R},\mathbf{R}'}$, and $\hat{a}_{\mathbf{R}}$, respectively, defined as

$$f_{\mathbf{k}} \equiv \sum_{\mathbf{R}} f_{\mathbf{R}} \exp\left(i\mathbf{k}\cdot\mathbf{R}\right), \tag{3.9}$$

for any field $f_{\mathbf{R}}$. The previous equation defines also the Brillouin zone

$$\left\{\mathbf{k} = (k_1, k_2, \ldots, k_i, \ldots, k_N), k_i = \frac{2\pi n_i}{L}, n_i = 0, 1, \ldots, N-1\right\}.$$

The annihilation and creation operators $\hat{a}_{\mathbf{k}}$ and $\hat{a}^\dagger_{\mathbf{k}}$ fulfill the bosonic commutation rule $[\hat{a}_{\mathbf{k}}, \hat{a}^\dagger_{\mathbf{k}'}] = \delta_{\mathbf{k},\mathbf{k}'}$ and, due to parity symmetry, the coefficients $\mathcal{A}_{\mathbf{k}}$ and $\mathcal{B}_{\mathbf{k}}$ are real-valued. Hamiltonian (3.8) can now be diagonalized using the standard Bogoliubov transformation [7],

$$\hat{a}_{\mathbf{k}} = u_{\mathbf{k}}\hat{b}_{\mathbf{k}} + v_{\mathbf{k}}\hat{b}^\dagger_{-\mathbf{k}}, \tag{3.10}$$

where the functions $u_{\mathbf{k}}$ and $v_{\mathbf{k}}$ can be assumed to be real-valued without loss of generality, and to fulfill condition $u^2_{\mathbf{k}} - v^2_{\mathbf{k}} = 1$ to ensure the commutation relation $[\hat{b}_{\mathbf{k}}, \hat{b}^\dagger_{\mathbf{k}'}] = \delta_{\mathbf{k},\mathbf{k}'}$. Then, provided we choose

$$u_{\mathbf{k}} = \operatorname{sign}\left(\mathcal{A}_{\mathbf{k}}\right)\sqrt{\frac{1}{2}\left(\frac{|\mathcal{A}_{\mathbf{k}}|}{|E_{\mathbf{k}}|}+1\right)} \quad \text{and} \quad v_{\mathbf{k}} = -\operatorname{sign}\left(\mathcal{B}_{\mathbf{k}}\right)\sqrt{\frac{1}{2}\left(\frac{|\mathcal{A}_{\mathbf{k}}|}{|E_{\mathbf{k}}|}-1\right)}, \tag{3.11}$$

the Hamiltonian takes the quadratic form

$$\hat{\mathcal{H}} = \mathcal{E}_0 + \sum_{\mathbf{k}\neq 0} E_{\mathbf{k}} \hat{b}^\dagger_{\mathbf{k}} \hat{b}_{\mathbf{k}}, \tag{3.12}$$

where $\hat{b}_{\mathbf{k}}$ and $\hat{b}^\dagger_{\mathbf{k}'}$ represent the annihilation and creation operators of a quasi-particle of momentum $\mathbf{k}$, and

$$E_{\mathbf{k}} = \text{sign}\left(\mathcal{A}_{\mathbf{k}}\right) \sqrt{\mathcal{A}^2_{\mathbf{k}} - \mathcal{B}^2_{\mathbf{k}}} \tag{3.13}$$

is the quasi-particle dispersion relation. The quantity $\mathcal{E}_0$ is the zero-point energy, i.e. the energy of the vacuum of quasi-particles. Dynamical stability requires that the quasi-particle energy $E_{\mathbf{k}}$ is real-valued, i.e. $h\left(h + \mathcal{B}_{\mathbf{k}}\right) \geq 0$.
For the specific case of the LRTI model we have

$$\mathcal{A}_{\mathbf{k}} = 2h + VP\left(\mathbf{k}\right) \quad \text{and} \quad \mathcal{B}_{\mathbf{k}} = VP\left(\mathbf{k}\right), \tag{3.14}$$

where

$$P\left(\mathbf{k}\right) = \sum_{\mathbf{R}} \frac{e^{\imath \mathbf{k}\cdot\mathbf{R}}}{|\mathbf{R}|^\alpha} \tag{3.15}$$

is the Fourier transform of the long-range potential.
The energy spectrum is found using the Eq. (3.13) and it yields

$$E_{\mathbf{k}} = 2\sqrt{h\left(h + VP\left(\mathbf{k}\right)\right)}.$$

We now analyze how a quench protocol in the LRTI model can be described using quadratic Hamiltonians.

3.4.1 Quantum quench and correlation function

We focus our attention on the out-of-equilibrium dynamical properties of the system induced by a quantum quench. This protocol consists in preparing the system in some initial state $|\Psi_0\rangle$ at time $t = 0$ and let it evolve under the action of some final Hamiltonian $\mathcal{H}_\text{f}$. For instance, $|\Psi_0\rangle$ may be the ground state of another initial Hamiltonian $\mathcal{H}_\text{i}$. Here we assume that $\mathcal{H}_\text{i}$ and $\mathcal{H}_\text{f}$ are both generic quadratic bosonic Hamiltonians as Eq. (3.7). The quench consists then in an abrupt change of the amplitudes $\mathcal{A}_{\mathbf{R}}$ and $\mathcal{B}_{\mathbf{R}}$ from $\mathcal{A}^\text{i}_{\mathbf{R}}$ and $\mathcal{B}^\text{i}_{\mathbf{R}}$ to $\mathcal{A}^\text{f}_{\mathbf{R}}$ and $\mathcal{B}^\text{f}_{\mathbf{R}}$. Assuming that the quench $\mathcal{H}_\text{i} \to \mathcal{H}_\text{f}$ takes place on a time scale shorter than any characteristic dynamical time, the time evolution of the system for $t > 0$ is determined by the equation

$$|\Psi(t)\rangle = \mathrm{e}^{-i\mathcal{H}_\text{f} t} |\Psi_0\rangle, \tag{3.16}$$

where we set $\hbar = 1$. Quantum quenches constitute a controlled protocol to study out-of-equilibrium dynamics of correlated quantum systems and are now experimentally realized in cold-atom systems [48, 47, 214, 14, 243, 244, 245].
The post-quench dynamical properties of the system can be studied via the correlation

function of local observables. For the LRTI model, the natural observable operator is $\sigma^z_{\mathbf{R}} = \frac{1}{2}\left(a^\dagger_{\mathbf{R}} + a_{\mathbf{R}}\right)$ even if different choices are possible. This correlation function is connected trough a multiplying constant to the more general expectation value

$$G(\mathbf{R},t) = \langle\Psi(t)|(\hat{a}^\dagger_{\mathbf{R}} + \hat{a}_{\mathbf{R}})(\hat{a}^\dagger_{\mathbf{0}} + \hat{a}_{\mathbf{0}})|\Psi(t)\rangle. \tag{3.17}$$

Turning to Fourier space and taking the thermodynamic limit, it reads

$$\begin{aligned} G(\mathbf{R},t) \;=\; & \int \frac{d^D\mathbf{k}}{(2\pi)^D} e^{-i\mathbf{k}\cdot\mathbf{R}} \langle\Psi_0| \Big[\hat{a}^\dagger_{\mathbf{k}}(t)\hat{a}_{\mathbf{k}}(t) + \hat{a}_{-\mathbf{k}}(t)\hat{a}^\dagger_{-\mathbf{k}}(t) + \hat{a}_{-\mathbf{k}}(t)\hat{a}_{\mathbf{k}}(t) \\ & + \hat{a}^\dagger_{\mathbf{k}}(t)\hat{a}^\dagger_{-\mathbf{k}}(t)\Big] |\Psi_0\rangle \end{aligned} \tag{3.18}$$

where the time evolution of the operators is evaluated in the Heisenberg picture. In order to compute explicitly the correlation function $G(\mathbf{R},t)$, we first substitute the particle annihilation and creation operators by their expressions in terms of the quasi-particle ones associated to the final Hamiltonian,

$$\hat{a}_{\mathbf{k}}(t) = u^{\mathrm{f}}_{\mathbf{k}}\, \hat{b}^{\mathrm{f}}_{\mathbf{k}}(t) - v^{\mathrm{f}}_{\mathbf{k}}\, \hat{b}^{\mathrm{f}\dagger}_{-\mathbf{k}}(t), \tag{3.19}$$

found from the inverse of the Bogoliubov transform (3.10). We then substitute the quasi-particle operator at time t by its time evolution

$$\hat{b}^{\mathrm{f}}_{\mathbf{k}}(t) = \exp(-iE^{\mathrm{f}}_{\mathbf{k}}t)\, \hat{b}^{\mathrm{f}}_{\mathbf{k}}(0). \tag{3.20}$$

The initial value $\hat{b}^{\mathrm{f}}_{\mathbf{k}}(0)$ is determined imposing the continuity of the Bogoliubov transformation (3.10) associated to the initial and final Hamiltonians respectively, it yields

$$\hat{a}_{\mathbf{k}} = u^{\mathrm{i}}_{\mathbf{k}}\hat{b}^{\mathrm{i}}_{\mathbf{k}}(0) + v^{\mathrm{i}}_{\mathbf{k}}\hat{b}^{\mathrm{i}\dagger}_{-\mathbf{k}}(0) = u^{\mathrm{f}}_{\mathbf{k}}\hat{b}^{\mathrm{f}}_{\mathbf{k}}(0) + v^{\mathrm{f}}_{\mathbf{k}}\hat{b}^{\mathrm{f}\dagger}_{-\mathbf{k}}(0), \tag{3.21}$$

and

$$\hat{a}^\dagger_{\mathbf{k}} = u^{\mathrm{i}}_{\mathbf{k}}\hat{b}^{\mathrm{i}\dagger}_{\mathbf{k}}(0) + v^{\mathrm{i}}_{\mathbf{k}}\hat{b}^{\mathrm{i}}_{-\mathbf{k}}(0) = u^{\mathrm{f}}_{\mathbf{k}}\hat{b}^{\mathrm{f}\dagger}_{\mathbf{k}}(0) + v^{\mathrm{f}}_{\mathbf{k}}\hat{b}^{\mathrm{f}}_{-\mathbf{k}}(0). \tag{3.22}$$

We then find the relation

$$\hat{b}^{\mathrm{f}}_{\mathbf{k}}(0) = \left(u^{\mathrm{i}}_{\mathbf{k}}u^{\mathrm{f}}_{\mathbf{k}} - v^{\mathrm{i}}_{\mathbf{k}}v^{\mathrm{f}}_{\mathbf{k}}\right)\hat{b}^{\mathrm{i}}_{\mathbf{k}} - \left(u^{\mathrm{i}}_{\mathbf{k}}v^{\mathrm{f}}_{\mathbf{k}} - v^{\mathrm{i}}_{\mathbf{k}}u^{\mathrm{f}}_{\mathbf{k}}\right)\hat{b}^{\mathrm{i}\dagger}_{-\mathbf{k}}. \tag{3.23}$$

This expression allows us to write the correlation function $G(\mathbf{R},t)$ as a function of the position $\mathbf{R}$ and of the time t, and the initial quasi-particle operators $\hat{b}^{\mathrm{i}}_{\mathbf{k}}$ and $\hat{b}^{\mathrm{i}\dagger}_{\mathbf{k}}$. We then calculate the quantum average over the initial state $|\Psi_0\rangle$, which we assume to be the ground state of the initial Hamiltonian $\mathcal{H}_{\mathrm{i}}$, defined by $\hat{b}^{\mathrm{i}}_{\mathbf{k}}|\Psi_0\rangle = 0$ for any $\mathbf{k}$. After some straightforward algebra we find that the correlation function can be evaluated in the thermodynamic limit. It reads

$$\begin{aligned} G_{\mathrm{c}}(\mathbf{R},t) \;&\equiv\; G(\mathbf{R},t) - G(\mathbf{R},0) \\ &=\; \frac{1}{2}\int \frac{d^D\mathbf{k}}{(2\pi)^D}\mathcal{F}(\mathbf{k}) \left[\mathrm{e}^{-i\mathbf{k}\cdot\mathbf{R}} - \frac{\mathrm{e}^{i\left(\mathbf{k}\cdot\mathbf{R} - 2E^{\mathrm{f}}_{\mathbf{k}}t\right)} + \mathrm{e}^{i\left(\mathbf{k}\cdot\mathbf{R} + 2E^{\mathrm{f}}_{\mathbf{k}}t\right)}}{2}\right] \end{aligned} \tag{3.24}$$

where

$$\mathcal{F}(\mathbf{k}) = \frac{\mathcal{A}^{\mathrm{i}}_{\mathbf{k}}\mathcal{B}^{\mathrm{f}}_{\mathbf{k}} - \mathcal{A}^{\mathrm{f}}_{\mathbf{k}}\mathcal{B}^{\mathrm{i}}_{\mathbf{k}}}{\left(\mathcal{A}^{\mathrm{f}}_{\mathbf{k}} + \mathcal{B}^{\mathrm{f}}_{\mathbf{k}}\right) E^{\mathrm{i}}_{\mathbf{k}}}. \tag{3.25}$$

This expression can be interpreted using the Cardy-Calabrese picture [161]. It states that the correlations created following the quench can be understood as waves. Their spreading is described by the final dispersion relation $E^f_{\mathbf{k}}$ and the initial state, determining just the pre-factor $\mathcal{F}(\mathbf{k})$, which acts as an integral weight. Following the quasi-particle picture, the key quantity to understand the propagation of correlations is the group velocity of these excitations

$$\mathbf{V}_{\mathbf{k}} = \nabla_{\mathbf{k}} E^f_{\mathbf{k}}.$$

For the specific case of the LRTI model, we are interested in the time evolution of spin-spin correlations

$$G^{\sigma\sigma}_c(\mathbf{R}, t) = \langle \sigma^z_{\mathbf{R}}(t)\sigma^z_{\mathbf{R}'}(t)\rangle_c - \langle \sigma^z_{\mathbf{R}}(0)\sigma^z_{\mathbf{R}'}(0)\rangle_c$$

Using the transformations (3.6) we find

$$\langle \sigma^z_{\mathbf{R}}(t)\sigma^z_{\mathbf{R}'}(t)\rangle_c = \frac{1}{4}\langle \left(a^\dagger_{\mathbf{R}}(t) + a_{\mathbf{R}}(t)\right)\left(a^\dagger_{\mathbf{R}'}(t) + a_{\mathbf{R}'}(t)\right)\rangle = \frac{1}{4}G(\mathbf{R}, t)$$

where $G(\mathbf{R}, t)$ is defined in Eq. (3.17). Finally we get

$$G^{\sigma\sigma}_c(\mathbf{R}, t) = \frac{1}{4}G_c(\mathbf{R}, t) = \frac{1}{8}\int \frac{d^D\mathbf{k}}{(2\pi)^D}\mathcal{F}(\mathbf{k})\left[\mathrm{e}^{-i\mathbf{k}\cdot\mathbf{R}} - \frac{\mathrm{e}^{i\left(\mathbf{k}\cdot\mathbf{R} - 2E^{\mathrm{f}}_{\mathbf{k}}t\right)} + \mathrm{e}^{i\left(\mathbf{k}\cdot\mathbf{R} + 2E^{\mathrm{f}}_{\mathbf{k}}t\right)}}{2}\right] \tag{3.26}$$

and

$$\mathcal{F}(\mathbf{k}) = \frac{\left(h^{\mathrm{i}}V^{\mathrm{f}} - h^{\mathrm{f}}V^{\mathrm{i}}\right)P\left(\mathbf{k}\right)}{\left[h^{\mathrm{f}} + V^{\mathrm{f}}P\left(\mathbf{k}\right)\right]E^{\mathrm{i}}_{\mathbf{k}}}$$

where we used the expressions (3.24) and the values of the amplitudes $\mathcal{A}_{\mathbf{k}}$ and $\mathcal{B}_{\mathbf{k}}$ for the LRTI, Eq. (3.25).
These expressions define the time evolution of the spin-spin correlations as functions of distance and time following a global quantum quench in a generic LRTI model.

3.5 Spectral divergences and propagation of correlations

3.5.1 Divergence properties of the spectrum

Before analyzing the dynamical behavior of the correlation function $G_{\mathrm{c}}(\mathbf{R}, t)$ written above, it is worth discussing the divergences that appear in the various terms of Eq. (3.24) due to long-range interactions. This is motivated by the known dynamical behavior of short-range systems. There, the propagation of correlations following a quantum quench exhibits a *light-cone* structure in its space-time dynamics [158, 164]. It shows up in the form of a linearly increasing horizon, which can be interpreted as being generated by the contribution of the fastest quasi-particles defined by the final Hamiltonian $\mathcal{H}_{\mathrm{f}}$. For that class of Hamiltonians, the velocity defined by the horizon is then expected to be twice the

maximum group velocity of the quasi-particles [161]. This is expected to hold in general, including for long-range systems, whenever the post-quench Hamiltonian has excitations with well-defined, finite group velocities. In contrast, sufficiently long-range interactions can make the group velocity diverge and the propagation is not ballistic [23, 170, 169]. Divergences in the energy spectrum, not only in the group velocity, may further affect the dynamics of correlations. When $E^{\mathrm{f}}_{\mathbf{k}}$ diverges, at a finite $\mathbf{k}$ value, the space coordinate becomes irrelevant and the associated characteristic time $\tau \sim 1/E^{\mathrm{f}}_{\mathbf{k}}$ vanishes. This may yield instantaneous activation of correlations at arbitrary distance and, consequently the breaking of locality. Note that this scenario is not incompatible with the quasi-particle picture, since divergence of the energy $E^{\mathrm{f}}_{\mathbf{k}}$ at finite $\mathbf{k}$ implies divergence of the group velocity $\mathbf{V}_{\mathbf{k}} = \nabla_{\mathbf{k}} E^{\mathrm{f}}_{\mathbf{k}}$.
It is thus expected that the relevant divergences are those of the quasi-particle energy (3.13), and group velocity,

$$\mathbf{V}_{\mathbf{k}} = \nabla_{\mathbf{k}} E^{\mathrm{f}}_{\mathbf{k}} = \frac{h \nabla_{\mathbf{k}} P(\mathbf{k})}{\sqrt{h\left[h + P(\mathbf{k})\right]}} \sim \frac{\nabla_{\mathbf{k}} \mathcal{B}^{\mathrm{f}}_{\mathbf{k}}}{E^{\mathrm{f}}_{\mathbf{k}}}. \tag{3.27}$$

The parameter $\mathcal{B}_k$, which, according to Eq. (3.14) et Eq. (3.15), reads

$$\mathcal{B}^{\mathrm{f}}_{\mathbf{k}} = V^{\mathrm{f}} \sum_{\mathbf{R}\neq 0} \frac{\mathrm{e}^{i\mathbf{k}\cdot\mathbf{R}}}{|\mathbf{R}|^{\alpha}}, \tag{3.28}$$

may diverge in the infrared limit, depending on the value of the exponent α. Approximating the previous expression around $\mathbf{k} \approx 0$ we get

$$\mathcal{B}^{\mathrm{f}}_{\mathbf{k}} \sim \int dR \int d\Omega \frac{\mathrm{e}^{ikR\cos(\theta)}}{R^{\alpha-D+1}} \sim k^{\alpha-D} \qquad \text{and} \qquad \nabla_{\mathbf{k}} \mathcal{B}_{\mathbf{k}} \sim k^{\alpha-D-1}, \tag{3.29}$$

in the thermodynamic limit where Ω is the D dimensional solid angle and θ is the azimuthal angle with respect to $\mathbf{k}$, and $k = |\mathbf{k}|$. Typical behaviors of the energy and group velocity of the LRTI model for various values of α and dimensions $D = 2$ are shown in Fig. 3.10.
For $D + 1 < \alpha$ (right column in Fig. 3.10), both $\mathcal{B}_{\mathbf{k}}$ and $\nabla_{\mathbf{k}} \mathcal{B}_{\mathbf{k}}$ converge to a finite value in the infrared limit. Hence, both the energy and the group velocity are bounded for any value of the momentum $\mathbf{k}$. Note that the maximum group velocity is not necessary at $\mathbf{k} = 0$ as for instance in the example shown in the figure. In the same figure it is also possible to see how there are different maxima present in the structure. One is located in the infrared region and it is due to the long-range potentials and other two are located at finite values of the wave-vector. These maxima are located in a region of the spectrum where the long-range potential is not divergent and their value is always finite. They do not contribute to the determination of the front of correlations but to the internal structure of the correlation function.
For $D < \alpha < D + 1$ (central column in Fig. 3.10), $\mathcal{B}_{\mathbf{k}}$ is finite but $\nabla_{\mathbf{k}} \mathcal{B}_{\mathbf{k}}$ diverges in the infrared limit. Hence, the group velocity diverges, giving rise to infinitely fast modes,

while the energy is finite with a cusp around the origin. Writing $\mathcal{B}^{\mathrm{f}}_{\mathbf{k}} = \mathcal{B}^{\mathrm{f}}_0 + \mathcal{B}^{\mathrm{f}\prime}_0 |\mathbf{k}|^{\alpha - D}$, we find

$$|\mathbf{V}_{\mathbf{k}}| \approx \sqrt{\frac{h^{\mathrm{f}}}{h^{\mathrm{f}} + \mathcal{B}^{\mathrm{f}}_0}} \frac{(\alpha - D)\mathcal{B}^{\mathrm{f}\prime}_0}{|\mathbf{k}|^{D+1-\alpha}}. \tag{3.30}$$

For $\alpha < D$ (left column in Fig. 3.10), both $\mathcal{B}_{\mathbf{k}}$ and $\nabla_{\mathbf{k}}\mathcal{B}_{\mathbf{k}}$ diverge in the infrared limit. Hence, both the energy and the group velocity go to infinity. Writing $\mathcal{B}^{\mathrm{f}}_{\mathbf{k}} \approx \mathcal{B}^{\mathrm{f}}_0 / |\mathbf{k}|^{D-\alpha}$, we find the energy

$$E^{\mathrm{f}}_{\mathbf{k}} = \frac{2\sqrt{h^{\mathrm{f}}\mathcal{B}^{\mathrm{f}}_0}}{|\mathbf{k}|^{\frac{D-\alpha}{2}}} \tag{3.31}$$

and the group velocity

$$|\mathbf{V}_{\mathbf{k}}| = \frac{(D-\alpha)\sqrt{h^{\mathrm{f}}\mathcal{B}^{\mathrm{f}}_0}}{|\mathbf{k}|^{\frac{D-\alpha+2}{2}}}. \tag{3.32}$$

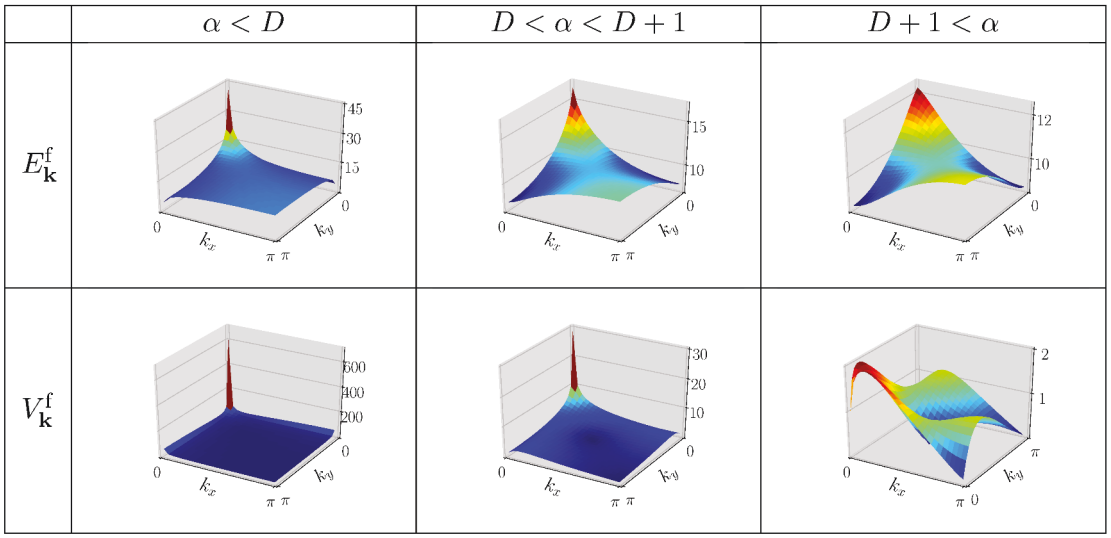

Figure 3.10: Energy (top panels) and modulus of the group velocity $V^{\mathrm{f}}_{\mathbf{k}} = |\mathbf{V}^{\mathrm{f}}_{\mathbf{k}}|$ (bottom panels) for a two-dimensional ($D = 2$) long-range system described by the dispersion relation (3.13) for a bi-dimensional Ising model for various values of the exponent α. For $\alpha < D$ (left panels), both the energy and the group velocity diverge in $\mathbf{k} = 0$. For $D < \alpha < D + 1$ (central panels) the energy is finite but shows a cusp around $\mathbf{k} = 0$, which corresponds to a divergent group velocity around the same point. For $D + 1 < \alpha$, both the energy and the group velocity are finite and well behaved. Note that the absolute maximum of the group velocity is located close to but not exactly at the origin $\mathbf{k} = 0$. Figure published in Ref. [170].

3.5.2 Propagation of correlations

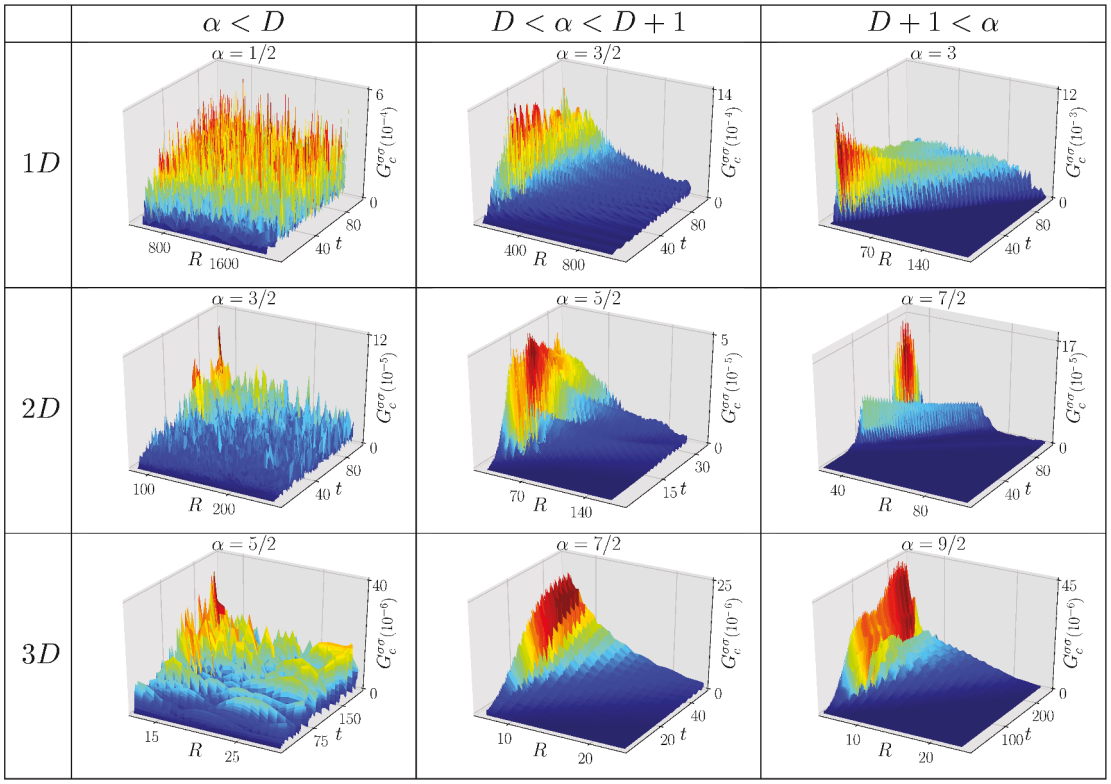

Figure 3.11: Space-time evolution of the spin-spin correlation function following quantum quenches in the LRTI model in various dimensions D (rows) and for different values of the exponent α (columns). For almost all cases, the quenches are from $V_\mathrm{i} = 1/2$ to $V_\mathrm{f} = 1$ for a fixed magnetic field $h = 2$. The only exception is for the 3D case with $\alpha = 5/2$ (left, bottom) where we used the quench $V_\mathrm{i} = 1/4 \to V_\mathrm{f} = 1/2$ and $h_\mathrm{i} = h_\mathrm{f} = 4$ in order to avoid dynamical instabilities. The linear system sizes are $L = 2^{12}$ in 1D, $L_x = L_y = 2^9$ in 2D, and $L_x = L_y = L_z = 2^6$ in 3D, with periodic boundary conditions. Distances are measured in units of the lattice constant and times in units of the inverse magnetic field. Figure published in Ref. [170].

We are now in the position to discuss how these divergences are connected to the spreading of correlations in the LRTI. Fig. 3.11 shows the space-time dynamics of the connected spin-spin correlation function $G_\mathrm{c}^{\sigma\sigma}(\mathbf{R}, t)$, defined in Eq. (3.26), for various values of the exponent α of the long-range exchange term and the different lattice dimensions $D = 1$, $D = 2$, and $D = 3$. The quench is performed by changing the value of V at fixed h in a LRTI model described by Hamiltonian (3.5). In particular we used $h_\mathrm{i} = h_\mathrm{f} = 2$ and $V_\mathrm{i} = 1/2 \to V_\mathrm{f} = 1$ for almost all the quenches. The only exception is the case $\alpha = 5/2$ and $D = 3$, where we use $h_\mathrm{i} = h_\mathrm{f} = 4$ and $V_\mathrm{i} = 1/2 \to V_\mathrm{f} = 1/4$ in order to ensure dynamical stability. For these values the dispersion relation $E_\mathbf{k}$ is always positive and

real-valued. Hence, the initial state $|\Psi_0\rangle$, i.e. the ground-state of the initial Hamiltonian, is the vacuum of the magnons. We checked that the condition $n_R \ll 1$ is fulfilled for every quench, allowing the description of the LRTI model by a quadratic Hamiltonian (3.8). The results are found by exact numerical integration of Eq. (3.24) using Eq. (3.25) for the LRTI. In Fig. 3.11, the complete evolution as a function of the position R and the time t is shown in 1D, while it is plotted along the diagonals $\mathbf{R} = (R, R)$ in 2D and $\mathbf{R} = (R, R, R)$ in 3D. The results show different behaviors depending on the respective values of α and D.
For $D + 1 < \alpha$, right-hand-side column in Fig. 3.11, a clear evidence of a strong form of locality, namely a light-cone, is present. While the correlations are significant for $t > R/V_{\mathrm{lc}}$, where V_{lc} is some velocity, they are instead strongly suppressed for $t < R/V_{\mathrm{lc}}$. For $D < \alpha < D + 1$, we still find evidence of locality with correlations appearing for $t > F(R)$, where F is some finite-valued function. This behavior is clear in 1D and 2D while, in 3D, finite lattice size effects hardly permits to determine the function F (see details below). For $\alpha < D$, the numerical data is compatible with a locality breakdown and instantaneous activation of the correlations. Still a very thin band with vanishing correlations is visible at short times. It is due to finite-size effects and their scaling actually confirms locality breakdown (see details below).
In the next sections we are going to study one by one these regimes and compare the data extracted from exact numerical integration to theoretical predictions derived from the analytic expression 3.26.

3.6 Regimes of propagation

3.6.1 Local regime $\alpha > D + 1$: comparison with Cardy-Calabrese picture.

Consider first the case where both the energy and the group velocity are bounded in the whole Brillouin zone for the LRTI Hamiltonian described in Sec. 3.4. This occurs for algebraically decaying interactions of the type Eq. (3.14) with $\alpha < D + 1$.
To study the evolution of the correlation function, it is worth separating the static and time-dependent components, and rewrite the correlation function (3.24) as

$$G_{\mathrm{c}}(\mathbf{R}, t) = g(\mathbf{R}, t) + g_\infty(\mathbf{R}, t), \tag{3.33}$$

where

$$g_\infty(\mathbf{R}) = \frac{1}{2} \int \frac{d^D\mathbf{k}}{(2\pi)^D} \mathrm{e}^{-i\mathbf{k}\cdot\mathbf{R}} \mathcal{F}(\mathbf{k}) \tag{3.34}$$

is the asymptotic thermalization value, and

$$g(\mathbf{R}, t) = -\frac{1}{2} \int \frac{d^D\mathbf{k}}{(2\pi)^D} \mathcal{F}(\mathbf{k}) \left[\frac{\mathrm{e}^{i\left(\mathbf{k}\cdot\mathbf{R} - 2E^{\mathrm{f}}_{\mathbf{k}} t\right)} + \mathrm{e}^{i\left(\mathbf{k}\cdot\mathbf{R} + 2E^{\mathrm{f}}_{\mathbf{k}} t\right)}}{2} \right] \tag{3.35}$$

is the time-dependent part. The latter contains the relevant evolution of the correlation function given by the post-quench dynamics. This contribution may be interpreted as

the spreading of two counter-propagating beams of quasi-particles that are represented by the two oscillating functions $e^{i\left(\mathbf{k}\cdot\mathbf{R}\mp 2E^{\mathrm{f}}_{\mathbf{k}}t\right)}$. Using the stationary-phase approximation, the main contribution to Eq. (3.35) is given by the points determined by

$$\nabla_{\mathbf{k}}\left(\mathbf{k}\cdot\mathbf{R}\mp 2E^{\mathrm{f}}_{\mathbf{k}}t\right)=0. \tag{3.36}$$

They define the separation and time-dependent condition

$$\frac{\mathbf{R}}{t}=\pm 2\nabla_{\mathbf{k}}E^{\mathrm{f}}_{\mathbf{k}}, \tag{3.37}$$

where the $\pm$ sign represents the two directions of the beams. This procedure can be interpreted as selecting the contribution to the correlation function (3.35) of the modes with a velocity equal to $\mathbf{R}/t$. Since the group velocity $\mathbf{V}_{\mathbf{k}}=\nabla_{\mathbf{k}}E^{\mathrm{f}}_{\mathbf{k}}$ is bounded for $\alpha > D+1$, it has a maximum value V_{M}. Then Eq. (3.37) has solutions only for $|\mathbf{R}|/t\leq V_{\mathrm{M}}$. This defines a ballistic (linear) horizon, that is a "light cone", in the $|\mathbf{R}|-t$ plane. Its slope gives the "light-cone" velocity V_{lc}, defined by

$$V_{\mathrm{lc}}=2\mathrm{Max}(V_{\mathbf{k}}). \tag{3.38}$$

The presence of a ballistic horizon in the out-of-equilibrium dynamics is thus directly connected to the presence of a finite maximal group velocity [161]. Equation (3.37) can also predict what happens for points outside the light-cone. If $|\mathbf{R}|/t$ exceeds the maximum value $2|\mathbf{V}_{\mathrm{M}}|$, then Eq. (3.37) has no solution. In this case the integration over the oscillating functions has no stationary point and the correlation functions is suppressed.
More precisely, for $|\mathbf{R}|/t < 2V_{\mathrm{M}}$ the contribution to the time-dependent part of the correlation function of the modes with parameter $\mathbf{v}=\mathbf{R}/t$ is given by the stationary-phase-approximation expression in generic dimension,

$$g(\mathbf{R},t)\simeq\sum_{\lambda\in\mathcal{S}_{\mathbf{v}}}\mathcal{W}\left(\mathbf{k}_{\lambda}\right)\cos\left(\mathbf{k}_{\lambda}\cdot\mathbf{R}\pm 2E^{\mathrm{f}}_{\mathbf{k}_{\lambda}}\right), \tag{3.39}$$

where the index λ spans the set $\mathcal{S}_{\mathbf{v}}$ of solutions of Eq. (3.37) for a fixed value of $\mathbf{R}/t$. The dimension-dependent quantity

$$\mathcal{W}\left(\mathbf{k}\right)=\left(\frac{2\pi}{t}\right)^{\frac{D}{2}}\frac{\mathcal{F}(\mathbf{k})}{\left[\det\mathcal{L}(\mathbf{k})\right]^{1/2}}, \tag{3.40}$$

where $(\mathcal{L}_D)_{ij}=\partial_{k_i}\partial_{k_j}E^{\mathrm{f}}_{\mathbf{k}}$ is the Hessian matrix of the final dispersion relation $E^{\mathrm{f}}_{\mathbf{k}}$, and it represents the weight associated to each contributing pair of modes. In practice, some of the modes with the velocity $\mathbf{R}/t$ may be insignificant if they have an extremely small weight $\mathcal{W}(\mathbf{k}_{\lambda})$ compared to the other modes with the same velocity. This circumstance, however, does not affect the horizon, as long as at least one mode has a significant weight. In the opposite case the effective spreading of correlations may be slower than the expected bound, Eq. (3.38) [23] and we will discuss it in details in the next chapter. The

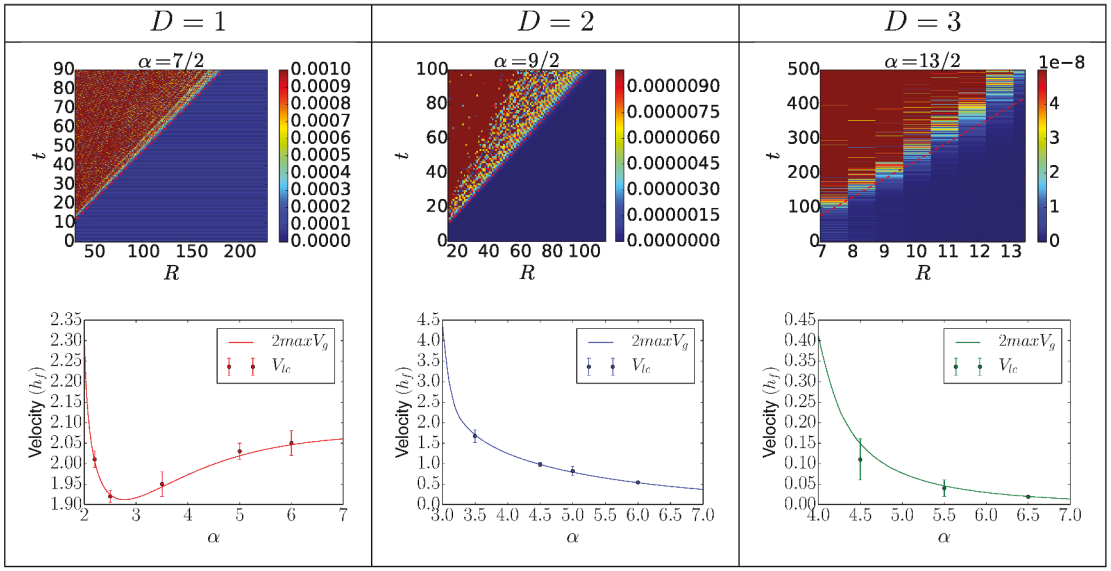

Figure 3.12: Dynamics of the spin-spin correlation function in the local regime ($D+1<\alpha$) in 1D (left column, $\alpha=5$), 2D (central column, $\alpha=7/2$), and 3D (right column, $\alpha=13/2$). The quenches are defined by the initial and final values $h_\mathrm{i}=h_\mathrm{f}=2$ and $V_\mathrm{i}=1\to V_\mathrm{f}=1/2$ in 1D and 2D, and $h_\mathrm{i}=h_\mathrm{f}=5$ and $V_\mathrm{i}=1/2\to V_\mathrm{f}=1/4$ in 3D. The linear system sizes are $L=2^9$ in 1D, $L_x=L_y=2^8$ in 2D, and $L_x=L_y=L_z=2^6$ in 3D. The top panel shows the space-time dynamics of the spin-spin correlation function (color plot) together with the line $R=V_\mathrm{lc}t$ (dashed red line)), where the light-cone velocity V_lc is fitted to the boundary of the local region. The lower panel shows the comparison of the fitted light-cone velocity V_lc with twice the maximum group velocity, $2\max\partial_k E_k^\mathrm{f}$, as computed from Eq. (3.13). Excellent agreement is found in all cases. Figure published in Ref. [170].

predictions of the theoretical model based on the quasi-particle picture point out that a linear ballistic light-cone structure have to be found in the propagation of correlations for $\alpha>D+1$. This is motivated by the fact that the velocity spectrum of the fundamental excitations is bounded and the maximum group velocity defines the light-cone velocity of propagations as predicted by the Cardy-Calabrese approach.

This expectation is confirmed by the numerics (see right column of Fig. 3.11). More precisely, we show in the upper panel of Fig. 3.12 the space-time dynamics of the correlation function, for various values of $\alpha>D+1$ and $D=1$, 2 or 3. They are similar to these of Fig. 3.11, except what we used a stronger contrast to enhance the difference between the correlated and uncorrelated regions. In this way we are sure that the colormap enhance just the correlation front and not the internal structure. This procedure is somehow similar to the ϵ method we will describe in the next section.

All the studied cases show a clear ballistic (light-cone-like) behavior of the correlation front in all dimensions. Fitting a linear function, $R=R_0+V_\mathrm{lc}t$, to the correlation front, we find the light-cone velocity V_lc. In the lower panels of Fig. 3.12 the values extracted

numerically are compared to the ones extracted from the spectrum. We find an excellent agreement for all the studied cases within the error-bars. The width of the error bars reflects the fact that the leaks outside the light-cone are algebraically decaying, Ref. [213] ans Sec. 2.1.3, and this makes more complicated to define the exact position of the correlation front. The good quantitative agreement between the numerics and the prediction of Eq. (3.38) confirms that the correlation front is mainly determined by the propagation of counter-propagating quasi-particles with the highest velocities, whenever they exist, as predicted by the Cardy-Calabrese scenario [161].

3.6.2 Quasi-local regime

Let us now turn to the case where the energy is finite but the group velocity diverges due to a cusp in the energy spectrum around $\mathbf{k} = 0$, which corresponds to $D < \alpha < D + 1$. It follows from Eq. (3.13) and the discussion of Sec. 3.5 that the dispersion relation of the post-quench Hamiltonian may be written

$$E^{\mathrm{f}}_{\mathbf{k}} = E_0 + V_0 |\mathbf{k}|^{1-\chi} \tag{3.41}$$

and the group velocity

$$|\nabla_{\mathbf{k}} E^{\mathrm{f}}_{\mathbf{k}}| = (1-\chi) V_0 |\mathbf{k}|^{-\chi}, \tag{3.42}$$

where $\chi = D + 1 - \alpha$.

Quasi-particle results Since the correlation horizon is expected to be determined by the contributions with largest velocity, namely $\mathbf{k} = 0$ in this case, we can write the correlation function (3.24) around that point as

$$\begin{aligned} G_{\mathrm{c}}(R,t) &\simeq \frac{1}{2}\int_0^\pi dk \cos(kR)\left[1 - \cos(2E_0 t + 2V_0 t k^{1-\chi})\right] \\ &= -\cos(2E_0 t)\int_0^\pi dk \cos(kR)\left[\cos\left(2V_0 t k^{1-\chi}\right) - 1\right] \\ &\quad + \sin(2E_0 t)\int_0^\pi dk \cos(kR)\sin\left(2V_0 t k^{1-\chi}\right). \end{aligned} \tag{3.43}$$

We then focus on the first integral and write it as a power series in t

$$\int_0^\pi dk \cos(kR)\left[\cos\left(2V_0 t k^{1-\chi}\right) - 1\right] = \sum_{n=1}^{\infty} \frac{(-1)^n (2V_0 t)^{2n}}{2n!} \int_0^\pi dk \cos(kR)\, k^{2n(1-\chi)}. \tag{3.44}$$

This new integral can be computed for every value of R. We find

$$\int_0^\pi dk \cos(kR)\, k^{2n(1-\chi)} = \pi^{1+2n(1-\chi)} \frac{{}_1F_2\left[\frac{1}{2}+n(1-\chi), \frac{1}{2}, (1-\chi)n+\frac{3}{2}, -\pi^2\frac{R^2}{4}\right]}{1+2n(1-\chi)},$$

where ${}_1F_2$ is the hypergeometric function defined by the vector $(1,2)$ [246]. For large values of R, we use the asymptotic limit of the latter, which yields

$$\int_0^\pi dk \cos(kR) k^{2n(1-\chi)} \simeq A_n^1(R) + B_n^1(R) \tag{3.45}$$

$$A_n^1(R) = \pi^{1+2n(1-\chi)} \frac{\sin(\pi R)}{\pi R} \tag{3.46}$$

$$B_n^1(R) = -\frac{\sin[\pi(\chi-1)n]\Gamma[1+2n(1-\chi)]}{R^{2(1-\chi)n+1}}. \tag{3.47}$$

We can evaluate simply the summation over n of the first term, and we find

$$\sum_{n=1}^{\infty} \frac{(-1)^n (2V_0 t)^{2n}}{2n!} A_n^1(R) = \frac{\left[1-\cos\left(2V_0\pi^{1-\chi}t\right)\right]\sin(\pi R)}{R}. \tag{3.48}$$

In the limit of large R and t the last term will go to zero leaving the correlation function unaffected. Inserting now B_n^1 in Eq. (3.44), we need to compute the sum over n. This is analytically possible just for $D=1$ and $\alpha = 3/2$, which corresponds to $\chi = 1/2$. For these values of the parameters we find

$$\cos(2E_0 t) \sum_{n=1}^{\infty} \frac{(-1)^n (2V_0 t)^{2n}}{2n!} \frac{\sin\left(\frac{\pi}{2}n\right)}{R^{n+1}} \Gamma[1+n] \tag{3.49}$$

$$= (-1)^{3/4} \pi \frac{2V_0 t}{R^{\frac{3}{2}}} \cos(2E_0 t) \left[\operatorname{erf}\left(\frac{\sqrt[4]{-1}V_0 t}{\sqrt{R}}\right) e^{\frac{\imath(2V_0 t)^2}{4R}} + \operatorname{erfi}\left(\frac{\sqrt[4]{-1}V_0 t}{\sqrt{R}}\right) e^{-\frac{\imath(2V_0 t)^2}{4R}} \right].$$

This function scales as $t/R^{3/2}$ multiplied by a smooth oscillating function.
The second term in Eq. (3.43) can be studied along the same lines. First we write it as a power series in t,

$$\sin(2E_0 t) \int_0^\pi dk \cos(kR) \sin\left(2V_0 t k^{1-\chi}\right)$$

$$= \sin(2E_0 t) \sum_{n=0}^{\infty} \frac{(-1)^n (2V_0 t)^{2n+1}}{(2n+1)!} \int_0^\pi \cos(kR) k^{(2n+1)(1-\chi)}. \tag{3.50}$$

The integral can again be expressed again as an hypergeometric function for every value of n

$$\int_0^\pi \cos(kR) k^{(2n+1)(1-\chi)}$$

$$= \pi^{1+2n(1-\chi)} \frac{{}_1F_2\left[\frac{\chi}{2} + (n+1)(1-\chi), \frac{1}{2}, 1 + \frac{\chi}{2} + (n+1)(1-\chi), -\pi^2 \frac{R^2}{4}\right]}{1+(1-\chi)(2n+1)} \tag{3.51}$$

Taking now the asymptotic value of this function in the large R limit we find

$$\int_0^\pi \cos(kR) k^{(2n+1)(1-\chi)} \simeq A_n^2(R) + B_n^2(R) \tag{3.52}$$

$$A_n^2(R) = \pi^{1+2n(1-\chi)} \frac{\sin(\pi R)}{\pi R} \tag{3.53}$$

$$B_n^2(R) = \frac{(-1)^{n+1} \cos\left[\frac{\pi\chi}{2}(2n+1)\right]\Gamma[1+(2n+1)(1-\chi)]}{R^{1+(1-\chi)(2n+1)}}. \tag{3.54}$$

As we demonstrated in Eq. (3.48), the summation of A_n^2 over n goes to zero as $1/R$ and hence does not affect the correlation function in that regime. We can plug B_n^2 in Eq. (3.51) and sum over n. As before, it is possible to perform these computations analytically in the case $D = 1$ and $\alpha = 3/2$ where it gives

$$\begin{aligned} &- \sin(2E_0 t) \sum_{n=0}^{\infty} \frac{\cos\left[\frac{\pi}{4}(2n+1)\right] \Gamma\left[1+\frac{1}{2}(2n+1)\right] (2V_0 t)^{2n+1}}{R^{1+\frac{1}{2}(2n+1)}(2n+1)!} \\ &= - \sin(2E_0 t) \frac{V_0 t}{R^{\frac{3}{2}}} \sqrt{\frac{\pi}{2}} \left[\cos\left(\frac{V_0^2 t^2}{R}\right) - \sin\left(\frac{V_0^2 t^2}{R}\right)\right]. \end{aligned}$$

Again, this term scales as $t/R^{3/2}$ and the oscillating functions do not affect this dominant behavior.
For $D = 1$ and $\alpha = 3/2$, the correlation function (3.24) thus scales as

$$G_c(R,t) \sim \frac{t}{R^{3/2}}. \tag{3.55}$$

Hence, the correlation horizon is algebraic, $t \sim R^{\beta}$. Note that the scaling (3.55) is slower than ballistic, in agreement with the Monte-Carlo results presented in Fig. 3.9. This is surprising because it may be expected that a divergent group velocity would allow faster-than-ballistic scaling. This idea is also consistent with extended Lieb-Robinson bounds, which are faster-than-ballistic see Sec. 2.4. Our exact analysis shows that interference effects between the contributing divergent modes strongly affect the correlation front and the known bounds are not saturated.

Numerical results for the scaling of the light-cone We derived the scaling of the correlation function explicitly for the case $D = 1$ and $\alpha = 3/2$. For other cases the computation is not tractable, with the previous approach. It is anyway important to study the behavior of the correlation horizon for different values of α and different dimensions D. We will do it here numerically, extracting this quantity from the data presented in Fig. 3.11. We impose then a threshold ϵ and we find the value of the activation time $t^\star$ when the correlation function reaches ϵ for every value of R

$$\bar{G}(t^\star, R) = \epsilon \tag{3.56}$$

In particular, we consider time-averaged correlation functions, $\bar{G}(t,R) = \frac{1}{t}\int_0^t d\tau G_c^{\sigma\sigma}(\mathbf{R},t)$, in order to minimize the effects of undesirable small time oscillations.

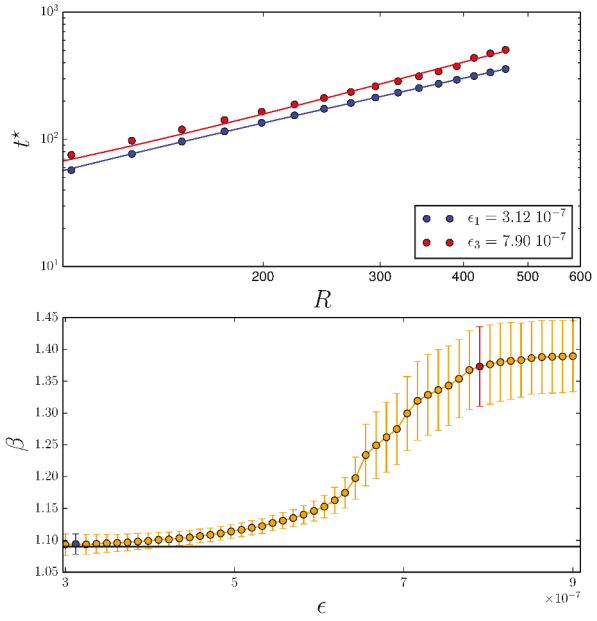

Figure 3.13: Top panel: $t^\star$ as function of R for different values of ϵ in log-log scale (points) with the fitted function (continuous lines). It is possible to see the algebraic dependence of $t^\star$ from R and the agreement between the fit and the numerical data. Bottom panel: Function $\beta(\epsilon)$ as extracted from fits to $t^\star(R) = R^\beta$ for different values of ϵ, the errors are due to the fit. It is possible to see that as ϵ becomes smaller $\beta(\epsilon)$ approaches a constant, black line. The points in red and blue correspond to the parameters obtained by the fit of the data of the same colors in the top panel. The data used for this analysis comes from a quench in a $D = 2$ model with $\alpha = 2.3$ and $h_i = h_f = 2$, $V_i = 1 \to V_f = 1/2$ and $L_x = L_y = 2^{11}$. Such system size is necessary to get a good fit in the large R region, where the algebraic regime is supposed to be found. Figure published in Ref. [170].

In the top panel of Fig. 3.13 the values of $t^\star$ as a function of R for $D = 2$ are shown for different values of ϵ in log-log scale. From the plot, it is clear that there is an algebraic dependence between these two quantities in the large R regime, as suggested by the analytic result for a specific case of $D = 1$ and $\alpha = 3/2$. We can then interpolate these points with a generic algebraic dependence of the type $t^\star(R) = t_0^\star + m * R^\beta$ for every values of ϵ. The limit $\epsilon \to 0^+$ will give us the correct and ϵ-independent scaling of the horizon, $\lim_{\epsilon\to 0} \beta(\epsilon)$. This limit can be found in the bottom panel of Fig. 3.13, where the value of the fitted parameter β is traced as function of ϵ for $\alpha = 2.3$. The minimal value of ϵ accessible is due to finite size of the lattice. We then extract the limit $\epsilon \to 0^+$ extrapolating the data for finite ϵ.

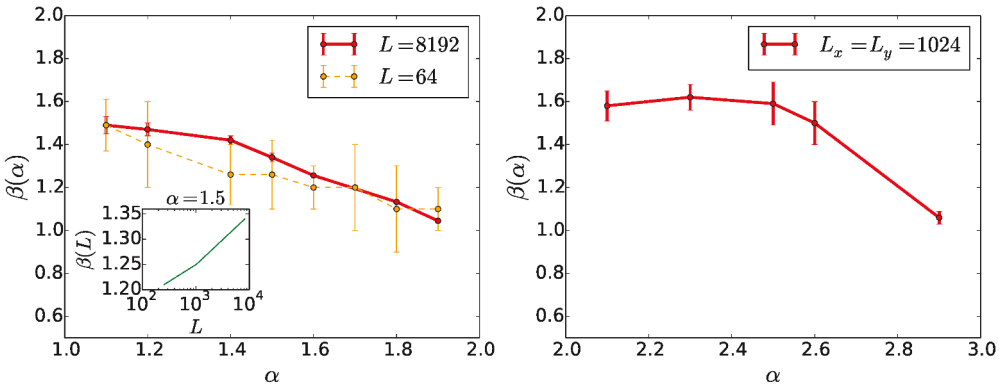

Figure 3.14: Values of the fit parameter β as a function of α for systems in dimensions $D = 1$ and $D = 2$. The data are obtained analyzing the time evolution of correlation in systems of length $L = 2^{13} = 8192$ and $L = 2^6 = 64$ for $D = 1$ and $L_x = L_y = 2^{10}$ for $D = 2$. The inset in the left figure presents the dependence of the parameter β on the system size L for the case of $\alpha = 3/2$ and $D = 1$. Figure published in Ref. [170].

In Fig. 3.14 the value of β as functions of α is plotted for $D = 1$ chains of different sizes and $D = 2$ systems. It is possible to see that $\beta \to 1$ as $\alpha \to D + 1$(see Ref. [172]). It means that a continuous crossover between the non ballistic, $D < \alpha < D + 1$, and the ballistic, $\alpha > D + 1$, regimes is present. On the other side, the transition at $\alpha = D$ between the non-local and the slower-than-ballistic regimes, is discontinuous. From our data, it is possible to extrapolate the two limits. For $D = 1$, we find $\beta = 1.52 \pm 0.02$ for $\alpha \to 1$ and $\beta = 1.01 \pm 0.08$ for $\alpha \to 2$. For $D = 2$, we find $\beta = 1.56 \pm 0.3$ for $\alpha \to 2$ and $\beta = 1.1 \pm 0.5$ and $\alpha \to 3$. This can be explained directly from the expression (3.24) and from the form of the spectrum. In the region $\alpha < D$ the dispersion relation is explicitly divergent, and this leads to the non-local regime, as discussed in (3.5). For all the values $\alpha > D$ the dispersion relation itself is not divergent and depends continuously on α, which means that the function β has to be continuous too. This motivates the discontinuity of the function β in $\alpha = D$ and its continuity in $\alpha = D + 1$.
We now discuss finite-size effects, which are important as we will see. In Fig. 3.14, we show a comparison with the values of the parameter β for two 1D systems of different sizes, namely $L = 2^{13} = 8192$ and $L = 2^6 = 64$. In spite of corresponding to system sizes that differ by more than two orders of magnitude, the results are quite close. In particular, they yield $\alpha \to 1$ and $\alpha \to 2$ limits that are consistent within error bars. Nevertheless, the results for the largest system are systematically above those found for the smallest system. In order to get more insight on finite-size effects, we have studied the behavior of β versus the system size for $\alpha = 3/2$ and $D = 1$. The results shown on the Inset of Fig. (3.14) show a systematic increase up to the largest system size we are able to compute. It shows that very large systems are necessary to reach the thermodynamic limit. However, the value of β we find for $L = 2^{13}$ is $\beta \simeq 1.34$, which is in fair agreement with the analytic prediction $\beta = 1.5$ (within 10% of the theoretical value). It is possible

to see how, increasing the system size, the value of β is increasing. The value expected value $\beta = 1.5$ is found in the Monte-Carlo results presented before.

3.6.3 Non-local regime

We consider finally the case where the quasi-particle energy spectrum (3.5) diverges. As discussed in Sec. 3.5 this is the case for $\alpha < D$, owing to the divergence of the Fourier transform of the potential (3.14). The dispersion relation around $k = 0$ takes then the form

$$E^{\mathrm{f}}_{\mathbf{k}} = \frac{e_0}{k^\gamma}, \tag{3.57}$$

where $e_0 = 2\sqrt{h^{\mathrm{f}}\mathcal{B}^{\mathrm{f}}_0}$ and $\gamma = \frac{D-\alpha}{2}$. Plugging this expression into Eq. (3.24) we find, again linearizing around $\mathbf{k} \approx 0$

$$G_{\mathrm{c}}(R,t) \sim \int_\Omega d\Omega \int_\epsilon^\pi dk k^{D-1+\gamma} e^{ikR\cos(\theta)} \left[1 - \cos\left(2e_0 t k^{-\gamma}\right)\right]. \tag{3.58}$$

The factor k^γ comes from the contribution of the weight $\mathcal{F} \sim 1/E^{\mathrm{i}}_{\mathbf{k}}$. Since the integral is dominated by the low-$\mathbf{k}$ components, the upper bound π of the integral is irrelevant. The lower bound $k = \epsilon$ holds for finite-size systems of linear length L and scales as $\epsilon \sim 1/L$. Hence, the limit $\epsilon \to 0$ is equivalent to the thermodynamic limit $L \to \infty$. We proceed by expanding the previous expression in powers of R and find

$$G_{\mathrm{c}}(R,t) \sim \sum_n \frac{i^n R^n}{n!} \int_\Omega d\Omega \cos^n(\theta) \lim_{\epsilon \searrow 0^+} \int_\epsilon^\pi dk k^{D-1+\gamma+n} \left[1 + \cos\left(\tau k^{-\gamma}\right)\right], \tag{3.59}$$

where we use the dimensionless time $\tau = 2e_0 t$. We can then integrate this expression term by term using the transformation $k \to q = k^{-\gamma}$ and find

$$\begin{aligned} &\int_{\frac{1}{\pi^\gamma}}^{L^\gamma} dq q^{-\frac{D+2\gamma+n}{\gamma}} \left[1 - \cos(\tau q)\right] \\ &= \frac{E_a\left(-iL^\gamma\tau\right) + E_a\left(iL^\gamma\tau\right) - E_a(-i\tau/\pi^\gamma) - E_a(i\tau/\pi^\gamma)}{2L^{D+n+\gamma}}, \end{aligned} \tag{3.60}$$

where $E_a(x)$ is the exponential integral function of order $a = \frac{D+2\gamma+n}{\gamma}$ [246]. In the above expression, the last two terms are bounded and the limit $L \to \infty$ can be taken without any problem after the summation. We thus focus on the first two terms, which contain the diverging energy contributions affecting locality. In the large L limit, we find

$$\frac{E_a\left(-iL^\gamma\tau\right) + E_a\left(iL^\gamma\tau\right)}{L^{D+n+\gamma}} \sim \frac{\sin\left(L^\gamma\tau\right)}{\tau} \frac{1}{L^{2\gamma+D}} \frac{1}{L^n}. \tag{3.61}$$

Plugging this expression into Eq. (3.59), we get

$$G_{\mathrm{c}}(R,t) \sim \lim_{L\to\infty} \frac{\sin\left(L^\gamma\tau\right)}{\tau} \frac{\int d\Omega e^{i\frac{R}{L}\cos(\theta)}}{L^{2\gamma+D}}. \tag{3.62}$$

The last equation shows that an algebraic divergence in the quasi-particles spectrum can lead to a signal which appears on a time scale $1/L^{\gamma}$ that goes to zero in the thermodynamic limit. Note that this time scale is directly connected to the divergence in the energy spectrum with the same exponent γ. This parameter depends on the specific model and the interaction decay exponent α. In our case $\gamma = \frac{D-\alpha}{2}$, notice that for free fermions, as stated in Ref. [165], we have $\gamma = \frac{D}{2} - \alpha$.
In this regime, the function $\sin(L^{\gamma}\tau)/\tau$ gives rise to a contribution of the type $\delta(\tau)$ to the correlation function at any distance. The same expression can be used to obtain the scaling of the correlation function itself, which yields to $G(\mathbf{R}, t) \sim 1/L^{\gamma+D}$. Moreover, these expressions show that the dominant contributions to the correlation function carry spherical symmetry despite the underlying lattice geometry. This will be important for our discussion of the correlation front in Sec 3.6.4. In the next section we will check all the analytic predictions made in this and in the last section.
We can compare our predictions with the ones extracted from our data. In particular the presence of a size-dependent time scale,

$$\tau \sim \frac{1}{L^{\gamma}} \sim \frac{1}{L^{\frac{D-\alpha}{2}}}. \tag{3.63}$$

can be directly checked. The latter determines the time of the first maximum of the correlation function for large distances. In Fig. 3.15(a) and (b) we plot the arrival time τ^* of the first maximum of the spin-spin correlation function at a distance equal to half the system size, $R = L/2$, as a function of L in 1D and 2D. Excellent agreement between the numerical data (points) and the predicted scaling (3.63) (dashed lines) is found for various values of $\alpha < D$ in both 1D and 2D. These results confirm the validity of the previous calculations.
Note that the same scaling can be found from the quasi-particle velocity. For power-law spectra as considered here, the group velocity scales as $V_k \sim E_k/k$, whose maximum is found for $k \sim 1/L$. Hence the time needed to reach half the system size, $L/2$, scales as $1/\max(E_k) \sim 1/L^{\frac{D-\alpha}{2}}$.

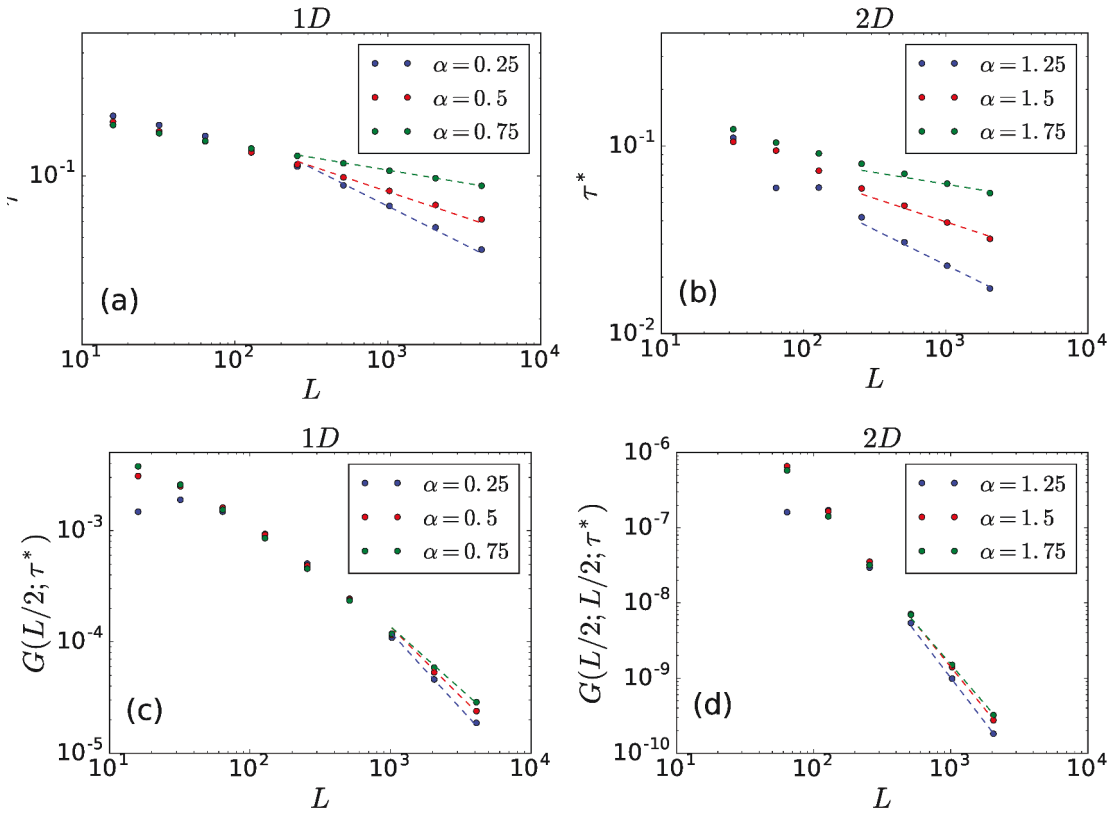

Figure 3.15: Activation time (upper panels) and amplitude (lower panels) of the spin-spin correlation function computed at $R = L/2$ in the non local regime ($\alpha < D$) for a 1D (left column) and 2D (right column) systems of different sizes. Note the log-log plot scales. The net decrease of the time of the first maximum for different values of α and L is the clear signature of locality breaking. The numerical data (points) are in good agreement with the analytical predictions (straight lines). The slopes of the straight lines is fixed by Eq. (3.63) and their intercepts have been found fitting the numerical data. Figure published in Ref. [170].

However, our analytic approach provides in addition the scaling of the amplitude of the correlation function at $t = \tau^*$. It yields

$$G_{\rm c}^{\sigma\sigma}(L/2, \tau^*) \propto \frac{\tau^*}{L^{2\gamma+D}} = \frac{1}{L^{\frac{3D-\alpha}{2}}} \tag{3.64}$$

Figures 3.15(c) and (d) compare numerical data (points) to the analytic prediction above (dashed lines) for the amplitude of the correlation function at $R = L/2$ and τ^*. Good agreement is found in both 1D and 2D and it further confirms our analytic predictions. Note that this result is a direct consequence of the interference between the fastest modes and cannot be found by the simplest independent quasi-particle approach.

3.6.4 Correlation front

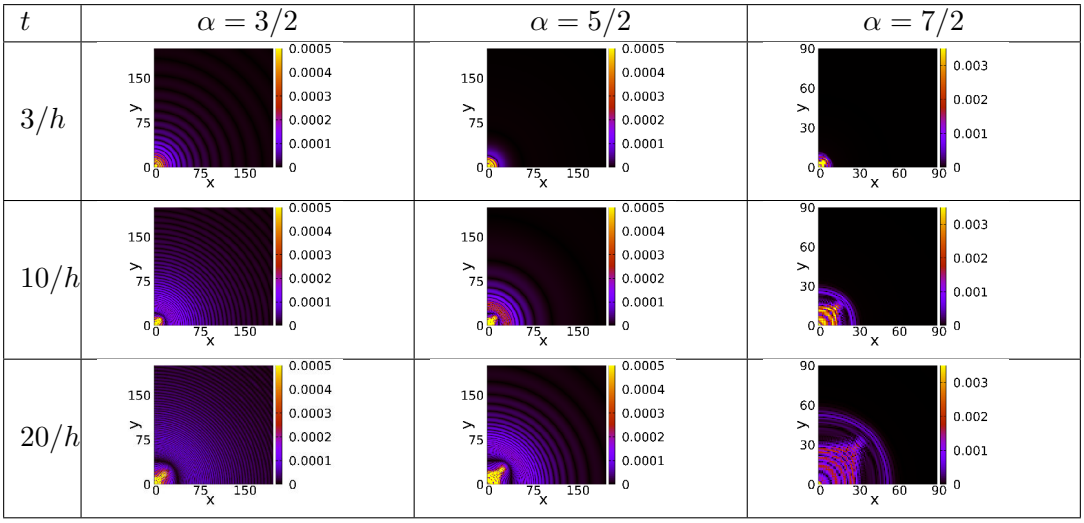

Figure 3.16: Correlation front at fixed times for the Spin-Spin correlation functions at fixed time for a bidimensional system. From left to right we find $\alpha = 3/2$, $\alpha = 5/2$ and $\alpha = 7/2$ in order to span all the possibles regimes. The correlation front shows clear spherical symmetry. Figure published in Ref. [170].

In this section we finally discuss the shape of the propagation front during the time evolution of the correlation function. For simplicity, we consider the two-dimensional case but the extension to higher dimensions D is straightforward. In Fig. 3.16 the correlation function $G_c^{\sigma\sigma}(\mathbf{R}, t)$, Eq. (3.26), for a quench in a $D = 2$ LRTI system is plotted as a function of the position $\mathbf{R}$ at various times t and for different values of the exponent α. In the instantaneous regime, $\alpha < D$, the correlation function is significantly different from zero for every value of $\mathbf{R}$ at any time t. Conversely, in the causal and quasi-causal regimes, for $\alpha > D$, correlations take a finite time to be activated. For $\alpha > D + 1$, a sharp edge is visible in the correlations and it evolves ballistically in time. In contrast, for $D < \alpha < D + 1$, the correlation front has a different scaling which is the signature of the quasi-locality. This is consistent with the discussion of Sec. 3.5 which points out that a non-ballistic propagation is present.
Let us now focus on the correlation pattern. For $\alpha < D$ the correlation function is spherically symmetric for large values of R while in the region close to the origin this symmetry is no longer present. This is in perfect agreement with Eq. (3.62) which predicts the correlation function in the large R region to be spherically symmetric. For $\alpha > D + 1$ there is a well-defined correlation front that spreads in the system and its symmetry is spherical despite the presence of the lattice. The symmetry of the front is due to the fact that the maximum group velocity is located very close to $\mathbf{k} = 0$, where the spectrum is spherically symmetric (see Fig. 3.10). The inner structure of the correlation function is determined by the other two local maxima, which are not in

the infrared region and whose contribution to the correlation function is not spherically symmetric, see Sec. 3.5 and Fig. 3.10. This contrasts with the behavior observed for the short-range Bose-Hubbard model, where the maximum group velocity is located at finite $\mathbf{k}$ and gives rise to a non spherical correlation front in 2D [216]. For the quasi-local regime $D < \alpha < D + 1$ we can use the same arguments used for the other two regimes. The divergence of the velocity is located at $\mathbf{k} = 0$ and it is not sufficient to destroy completely locality as discussed in Sec. 3.6.3 and a sort of locality, called quasi-locality, appears. Still, as for the other two regimes, the modes that dominate the horizon are located in the infrared region, whose form is dominated by the spherical symmetry of the long-range potential. This determines the spherical shape of the correlation function in the large R region. These considerations can be extended straightforwardly to any dimension higher than one because they only rely on the analysis of the symmetries of the energy spectrum and in particular around the point where is located the maximum group velocity.

3.7 Conclusions for the LRTI model

In this chapter we studied the time evolution of correlations in the LRTI model. We presented my analytical results for the dynamics of correlations and we compared them to accurate t-VMC data obtained by a collaborator.
The main result of this chapter is the fact that the spreading of correlations, depending on α, has a richer structure than the one predicted by general bounds [166, 163, 167]. We can then summarize the conclusion for our analysis of the LRTI model:

- For $\alpha < D$ no bound is present. In this case the spreading of correlations is instantaneous with a non-local propagation regime in the thermodynamic limit. From the microscopic point of view, this is due to the divergence of the energy spectrum E_k of the final Hamiltonian located at $k \approx 0$. In systems of finite linear size L this gives rise to a small time scale $\tau \sim 1/L^{\frac{D-\alpha}{2}}$ which vanishes as $L \to \infty$, see Sec. 3.6.3.

- For $D < \alpha < D + 1$ the presence of an algebraic bent light-cone $t^\star \propto R^\beta$ has been found and it is connected to a cusp in the energy spectrum E_k located at $k \approx 0$, see Sec. 3.6.2. The shape of the horizon can be analytically computed just for $D = 1$ and for $\alpha = 3/2$ but we checked numerically that this is true also for different values. The value of β as a function of α has been extracted for $D = 1$ and $D = 2$, finding that they are always slower-than-ballistic, $\beta > 1$.

- For $\alpha > D + 1$ we find a ballistic regime. It is connected to the presence of a finite maximum group velocity in the spectrum. In this case the propagation is ballistic and its velocity is given by the maximum group velocity multiplied by two, as predicted by the Cardy and Calabrese theorem.

- The shape of the light-cone for $D \geq 2$ is found to be spherical for $\alpha > D$, where a form of locality is present. For $\alpha < D$ no light-cone is present but the large R

part of the correlation function shows spherical symmetry. This is due to the fact that the large R region is strongly affected by the infrared behavior of the energy spectrum. In that region of the k-space, all the quantities get a spherical symmetry due to the syemmtry of the long-range potential.

The overall comparison between the general bounds presented in Sec. 2.4 and our data is good: where no bound is present ($\alpha < D$) the correlations are unbounded and where it is present ($\alpha > D$) we find a propagation of correlations restricted to a region of the space-time plane. The bounds predict anyway a logarithmic propagation for $D < \alpha < 2D$ and an algebraic faster-than-ballistic propagation from $\alpha > 2D$. We find a slower-than-ballistic propagation for $D < \alpha < D + 1$, confirmed by numerical and analytic computations [23, 170]. A ballistic spreading from $\alpha > D + 1$. Our results do not violate the general bounds on the long-range interactions. It is anyway impossible to guess the exact results found starting from the bounds. This points out that the microscopic analysis is still fundamental to describe the propagation of correlations. In particular: the spreading can be determined by the divergences in the energy spectrum. The weight of the quasi-particles in this case is important to characterize better the different regimes, but it does not change qualitatively the propagation. We will see in the next chapter that this integral weight can change drastically the time evolution of local observables despite the energy spectrum of the quasi-particles. This phenomenon appears in long-range interacting bosons on a lattice. Moreover, since the form of the weight depends on the observable, it is possible to have different observables with different propagation regimes pointing out a observable-dependent notion of locality in these systems.

4 Long-range Bose-Hubbard model

In this chapter we present my results on the long-range Bose-Hubbard chain. The Monte-Carlo data presented in Sec. 4.1 have been obtained by G. Carleo in collaboration with me. They have been published in a joint publication, Ref. [23] together with my analytical expressions, presented in Sec. 4.3.2. My results in Sec. 4.4 are preliminary and a deeper discussion will be published later.
In the last chapter we saw that the long-range transverse Ising (LRTI) model (3.5) exhibits three different regimes in its time evolution depending on the value α of long-range exchange $1/R^\alpha$. These three regimes can be predicted from the divergences of the energy spectrum of the fundamental excitations of the system (Sec. 3.5).
We want to investigate the validity of the previous results for different long-range interacting quantum systems. To do so, we study now the Long-Range Bose-Hubbard (LRBH) model

$$\mathcal{H} = -J \sum_{\langle i,j \rangle} \left(a_i^\dagger a_j + a_i a_j^\dagger \right) + \frac{U}{2} \sum_i n_i \left(n_i - 1 \right) + \frac{V}{2} \sum_{i \neq j} \frac{n_i n_j}{|i-j|^\alpha}, \tag{4.1}$$

where $\langle i, j \rangle$ constraints the hopping to the nearest-neighbor sites, the hopping energy is J, U is the on-site interaction strength, and V is the long-range interaction strength. The system is composed by bosonic particles, a_i ($a_i^\dagger$) is the destruction (creation) operator at site i. They fulfill the standard bosonic commutation relation

$$\left[a_i, a_j^\dagger \right] = \delta_{i,j}$$

and the number operator is $n_i = a_i^\dagger a_i$. This model can be realized in cold atomic experiments using the tools described in Sec. 1.3.2. This Hamiltonian describes bosonic particles on a lattice with short-range hopping and interaction potential

$$\mathcal{V}\left(|i-j| \right) = U \delta_{ij} + \frac{V}{|i-j|^\alpha}, \tag{4.2}$$

composed by a short-range (on-site) part and a long-range part that decays as a power law of exponent α.
We can briefly compare the form of the LRBH Hamiltonian to the one of the LRTI 3.5. The difference arises in the physical meaning of the long-range interactions. In the LRTI it represents a super-exchange term between distant spins. In this bosonic model the long-range part is a true potential between particles at large distances.
Another important difference between these two models is the dimension of their local Hilbert spaces. For the spin system this is bounded, while for the Bose-Hubbard model it

is not, see Sec. 1.3.2. The hypothesis of the local Hilbert space was fundamental for the rigorous demonstration of the Lieb-Robinson theorem presented in Sec. 2.1.2. From the mathematical point of view this means that all the bounds we presented for both short- and long-range interacting systems do not strictly hold for the Bose-Hubbard model. Anyway, it is clear that even if an infinite number of bosons can occupy the same site, this is physically impossible. The average number of particles in the ground state is in fact

$$\langle GS| n_i |GS\rangle .$$

The explicit form of this quantity is not known for generic values of the couplings J, U and V but it can be computed for some specific cases. For the Mott insulating state, $U \gg J$ and $V = 0$, the previous quantity is extremely easy to compute: in every site there are a number of particles equal to $\bar{n} \in \mathbb{N}$ which gives

$$\langle GS| n_i |GS\rangle = \bar{n}.$$

The dimension of the local Hilbert space is exactly one. During the time evolution the situation changes because the fundamental excitations of the systems are doblons, sites with $\bar{n} + 1$ particles, and holons, with $\bar{n} - 1$. Even there, the local Hilbert space is then limited to three states. It is then not unexpected that the Lieb-Robinson bound could work also in this case, see Sec. 2.3.2. Moreover, in the Mott insulating state, the correlations between sites are zero, it is a completely classical state. The condition of the bound 2.1.3 is satisfied for every local observable and, in fact, a ballistic propagation of correlations has been observed in Ref. [214] (see also Sec. 2.3.2).
For the superfluid phase, $J \gg U$ and $V = 0$, the wave-function is composed by completely delocalized and strong fluctuations of the average number of particles per site are present. The system in this regime is described as a coherent state

$$|GS\rangle = \prod_i e^{-\frac{|\alpha|^2}{2}} e^{\alpha a_i^\dagger} |0\rangle ,$$

where α is defined as

$$a |GS\rangle = \alpha |GS\rangle$$

where $\alpha \in \mathbb{C}$ because a is not a hermitian operator and its eigenvalues are complex. The modulus of α is fixed by the mean number of particles

$$\langle n\rangle = \langle GS| a_i^\dagger a_i |GS\rangle = |\alpha|^2.$$

We can project this on the Fock space to obtain the probability to have n_i particles per sites obtaining

$$P(n) = |\langle n, GS\rangle|^2 = \frac{\langle n\rangle^n}{n!} e^{-\langle n\rangle},$$

which decays rapidly as the average number of particles per sites $\langle n\rangle$ grows. We can then assume that the bounds we presented in 2.1.3 would work since the probability to span the unbounded Hilbert space during the time evolution is practically zero. The problem

in this state is the presence of extremely long-range correlations. As we discussed in Sec. 2.3.1.2, the superfluid has algebraically decaying correlations in its initial state. This violates explicitly the hypothesis of the theorem presented in Sec. 2.1.3. Despite that, a light-cone spreading of density-density correlations has been observed using t-VMC (see again Sec. 2.3.1.2) and it can be explained from the microscopic point of view using the Cardy-Calabrese approach, Sec. 2.2.
We want now to study the time evolution of different observables following a quantum quench in the long-range interaction coupling V. We will use a combined approach using t-VMC to access the time evolution and we compare its results to the quasi-particle approach. We will see how in this case the regimes of propagation are determined not just by the dispersion relation but also by the integral weight in k-space. This function is observable-dependent and we will show how different observables can exhibit different behaviors even if the dispersion relation of excitations is the same.

4.1 Monte Carlo results

As we did for the LRTI model, we start from the numerical results given by t-VMC, see Sec. 2.3.1.2. These simulations have been performed by G. Carleo in collaboration with me. They are published in a joint work, namely Ref. [23]. This algorithm has already been used to study the propagation of correlations in the standard Bose-Hubbard model, see Sec. 2.3.1 and Ref. [216], for quenches in the superfluid phase of the Bose-Hubbard model. It is possible to extend the same method to Hamiltonian 4.1 obtaining the time evolution of density-density correlations

$$G_C(R,t) = \langle n_R(t) n_0(t) \rangle_C - \langle n_R(0) n_0(0) \rangle_C \tag{4.3}$$

as function of R and t for quenches inside the superfluid regime. The subscript C indicates, as usual, the connected correlation function

$$\langle AB \rangle_C \equiv \langle AB \rangle - \langle A \rangle \langle B \rangle.$$

As we said, the wave function is of the Jastrow type [24], where we use $O_\alpha = n_k n_{-k}$

$$|\Psi(t)\rangle \propto e^{\sum_k \lambda_k(t) n_k n_{-k}} |\Phi_0\rangle ,$$

This wave function will take into account all the scattering of the type $n_k n_{-k}$ and the explicit time dependence is contained in the function $\lambda_k(t)$.

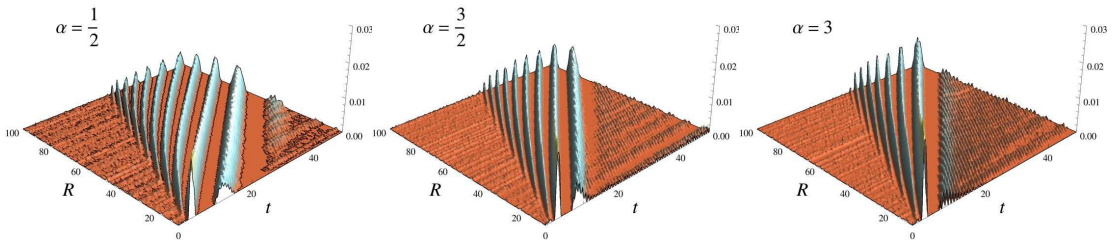

Figure 4.1: Time-evolution of the density-density correlations following a quantum quench in the LRBH model for $\alpha = 1/2$, $\alpha = 3/2$ and $\alpha = 3$. It is possible to see how correlations activate ballistically for every value of α. This is in contrast with the data presented, using the same numerical method in Sec. 3.2, for the LRTI. There three different regimes appear for the same values of α. This points out that the propagation is not a function of the long-range potential itself, defined by α, but a model-dependent microscopic analysis has to be carried out. Data obtained by G. Carleo in collaboration with me and published in a joint publication, Ref. [23].

The system is prepared in the ground state of the LRBH Hamiltonian (4.1) with parameters $J = 1$, $U_i = V_i$. A global quench $J = 1$, $U_f = V_f \neq V_i$ drives then the system out-of-equilibrium. The post-quench time evolution of the correlation function (4.3) is then studied for different values of α. In Fig. 4.1 the results are shown for $\alpha = 1/2$, $\alpha = 3/2$ and $\alpha = 3$. A ballistic propagation is found in all the studied cases for long times and large distances. The activation time $t^\star$ is finite and non-zero for every value of the distance. It is also linearly increasing with the distance, defining a constant light-cone velocity, $t^\star = R/v_{lc}$. This behavior is in contrast to the one found in the Ising model, where a ballistic spreading was found just for large values of α in both numerics and analytics.
Comparing now these results with the model-independent bounds discussed in Sec. 2.4 we can conclude that no violation is present. The propagation is in fact ballistic for small values of α where none of the state-of-the-art bound holds, meaning that every behavior of the correlation function can be accepted. For larger values of α, the bounds on the activation time are algebraic, i.e. $t^\star \propto R^\beta$, with $\beta \leq 1$. The ballistic propagation observed in the t-VMC data has exactly $\beta = 1$. The propagation is then slower than the one predicted by the bound and the latter is not violated.
As in the LRTI case, the general bounds are not able to predict the results found in the numerical data. As we did there, we will use the microscopic theory, i.e. the quasi-particle approach, to explain the numerical data.

4.2 The model and the excitation spectrum

As for the LRTI model, the analytic expressions and their interpretation are part of my work. They have been published, together with the t-VMC results, in Ref. [23].
Since the general bounds are unable to predict precisely the time evolution found in the

numerical data, we use again the microscopic theory. We will study quenches in the couplings U and V of Hamiltonian (4.1) in the superfluid regime, where U and V are small. In this regime the Hamiltonian can be approximated by a quadratic Hamiltonian where the excitations are Bogoliubov quasi-particles [7].

4.2.1 Bogoliubov approximation

The LRBH Hamiltonian describes bosons on a lattice with a nearest-neighbor hopping term with intensity J and and interaction potential already seen in Eq. (4.2). We can write the Hamiltonian in Fourier space using the translational invariance of the system. We define

$$a_R = \frac{1}{\sqrt{L}} \sum_k e^{-\imath kR} a_k$$
$$a_R^\dagger = \frac{1}{\sqrt{L}} \sum_k e^{\imath kR} a_k^\dagger$$

where L is the length of the chain, in order to preserve the form of the commutation relation in the k space

$$\left[a_k, a_q^\dagger\right] = \delta_{kq}.$$

We can then write the LRBH Hamiltonian in Fourier space as

$$\mathcal{H} = \sum_k \eta_k a_k^\dagger a_k + \frac{1}{2L} \sum_{q,k,p} \mathcal{V}(q) a_{k+q}^\dagger a_{p-q}^\dagger a_p a_k, \tag{4.4}$$

where $\eta_k = -2J\cos(k)$ is the nearest-neighbor hopping term where we set the lattice spacing to one, $a = 1$, and L is the length of the chain. In the previous equation we dropped a constant in the energy applying an energy shift. The function

$$\mathcal{V}(q) = U + V \sum_R \frac{e^{-\imath Rr}}{R^\alpha} \tag{4.5}$$

is the Fourier transform of the interaction potentials and contains a short-range interaction. The Fourier transform of the long-range potential depends on α.
As we discussed in Sec. 1.3, the ground state of a bosonic system with no interactions is the Bose-Einstein condensate. In the case where interactions are small we can then assume, as usually done, that the majority of the particles occupy the state at $k = 0$ and a small amount of them the other modes. The occupation of $k = 0$ mode is the macroscopic, we can write Hamiltonian (4.4) separating the different terms

$$a_0^\dagger \simeq a_0 \simeq \sqrt{N_0} \sim \sqrt{N},$$

where N_0 is the number of particles in the condensate.
The first term in Hamiltonian (4.4) will give a constant contribution because$\eta_{k=0} = -2J$

$$\sum_k \eta_k a_k^\dagger a_k = \eta_0 a_0^\dagger a_0 + \sum_{k\neq 0} \eta_k a_k^\dagger a_k = 2JN_0 + \sum_{k\neq 0} \eta_k a_k^\dagger a_k.$$

The same expansion can be computed for the long-range potential

$$\frac{1}{2L}\sum_{k,q,p}\mathcal{V}(q)a_{k-q}^{\dagger}a_{p+q}^{\dagger}a_p a_k \approx \frac{N_0}{2L}\sum_{k\neq 0}\Big[\mathcal{V}(k)\left(a_k^{\dagger}a_k + a_{-k}a_{-k}^{\dagger} + a_{-k}a_k + a_k^{\dagger}a_{-k}^{\dagger}\right) \tag{4.6}$$

$$+2\mathcal{V}(0)a_k^{\dagger}a_k\Big] + \frac{\mathcal{V}(0)N_0^2}{2L} \tag{4.7}$$

where we summed over k instead of over q in order to have the same label for the wave-vectors in both the one- and the two-body parts. We can then express the previous equation using the total number of particles N instead of the condensate one N_0 using the identity

$$N = N_0 + \sum_{k\neq 0}a_k^{\dagger}a_k \rightarrow N_0^2 \approx N^2 - 2N\sum_{k\neq 0}a_k^{\dagger}a_k.$$

Substituting this into Eq. (4.6) we obtain a quadratic Hamiltonian where now we have $\epsilon_k = 2J + \eta_k = 4J\sin^2(k/2)$

$$\mathcal{H} \simeq \frac{1}{2}\mathcal{V}(0)nN + \frac{1}{2L}\sum_{k\neq 0}\left\{[\epsilon_k + n\mathcal{V}(k)]\left(a_k^{\dagger}a_k + a_{-k}a_{-k}^{\dagger}\right) + n\mathcal{V}(k)\left(a_k^{\dagger}a_{-k}^{\dagger} + a_{-k}a_k\right)\right\}.$$

As we said in Sec. 1.3.1.1, the ground state of a non-interacting bosonic system is a condensate where all the particles occupy the zero mode. Hamiltonian (4.4) can then be rewritten in a general way as

$$\mathcal{H} = E_0 + \frac{1}{2}\sum_k\left[\mathcal{A}_k\left(a_k^{\dagger}a_k + a_{-k}a_{-k}^{\dagger}\right) + \mathcal{B}_k\left(a_k^{\dagger}a_{-k}^{\dagger} + a_{-k}a_k\right)\right], \tag{4.8}$$

where the quantities $\mathcal{A}_k$ and $\mathcal{B}_k$ are real-valued, and even functions of k, and the $a_k(a_k^{\dagger})$ are bosonic annihilation (creation) operators.
For the specific case of the LRBH we have

$$\mathcal{A}_k = \epsilon_k + n\mathcal{V}(k) \tag{4.9}$$

and

$$\mathcal{B}_k = n\mathcal{V}(k).$$

As before

$$\epsilon_k = 4J\sin^2\left(\frac{k}{2}\right)$$

is the free-boson dispersion relation, and the interaction potential in Fourier space is given in Eq. (4.5).
The Hamiltonian can then be diagonalized again using a Bogoliubov transformation $a_k = u_k b_k + v_k b_{-k}^{\dagger}$ [7] where

$$u_k = \sqrt{\frac{1}{2}\left(\mathcal{A}_k/\sqrt{\mathcal{A}_k^2 - \mathcal{B}_k^2} + 1\right)},$$

$$v_k = -\mathrm{sign}(\mathcal{B}_k)\sqrt{\frac{1}{2}\left(\mathcal{A}_k/\sqrt{\mathcal{A}_k^2 - \mathcal{B}_k^2} - 1\right)}.$$

The excitation spectrum is then given by

$$E_k = \sqrt{\mathcal{A}_k^2 - \mathcal{B}_k^2} = \sqrt{\epsilon_k \left[\epsilon_k + 2n\mathcal{V}(k)\right]},$$

and the Hamiltonian takes then the form of a free Hamiltonian for the operators b_k

$$\mathcal{H} = E_{GS} + \sum_k E_k b_k^\dagger b_k,$$

where E_{GS} is the vacuum energy of quasi-particles $b_k \left|GS\right\rangle = 0$ and the sum can be extended to all the values of k because for $k = 0$ the dispersion relation is zero. As we did in Sec. (3.4.1) for the LRTI model, which Hamiltonian takes the same form as this, the time evolution of different observables can be computed.

4.2.2 Time-evolution of observables

The system is prepared in the ground state of an initial Hamiltonian $\mathcal{H}_i$, defined by two functions $\mathcal{A}_k^i$ and $\mathcal{B}_k^i$, which corresponds to the vacuum of quasi-particles

$$b_k^i \left|0\right\rangle = 0 \quad \forall k.$$

The system is then driven out of equilibrium using a quantum quench. This is obtained using a sudden change $\mathcal{H}_i \to \mathcal{H}_f$, which triggers the time evolution

$$\left|\Psi\left(t\right)\right\rangle = e^{-\imath \mathcal{H}_f t} \left|0\right\rangle,$$

where we set $\hbar = 1$ as everywhere else. The quantum quench protocol, at the microscopic level, is obtained by a sudden change in the set of functions $\mathcal{A}_k^i$, $\mathcal{B}_k^i \to \mathcal{A}_k^f$, $\mathcal{B}_k^f$. The final Hamiltonian is then diagonalized by a different set of quasi-particle operators b_k^f $\left(b_k^{f\,\dagger}\right)$. The time evolution of post-quench operators is straightforward

$$\begin{aligned} b_k^f\left(t\right) &= b_k^f\left(0\right) e^{-\imath E_k^f t} \\ b_k^{f\,\dagger}\left(t\right) &= b_k^{f\,\dagger}\left(0\right) e^{\imath E_k^f t}. \end{aligned}$$

The initial conditions are $b_k^f\left(0\right)$ and $b_k^{f\,\dagger}\left(0\right)$ are fixed by the continuity of the operators $a_k\left(t\right)$ and $a_k^\dagger\left(t\right)$ at $t = 0$

$$\begin{aligned} u_k^i b_k^i\left(0\right) + v_k^i b_k^{i\,\dagger}\left(0\right) &= u_k^f b_k^f\left(0\right) + v_k^f b_k^{f\,\dagger}\left(0\right) = a_k\left(0\right) \\ u_k^i b_k^{i\,\dagger}\left(0\right) + v_k^i b_k^i\left(0\right) &= u_k^f b_k^{f\,\dagger}\left(0\right) + v_k^f b_k^f\left(0\right) = a_k^\dagger\left(0\right) \end{aligned}$$

which defines a relation between the initial and final quasi-particle operators. The previous relations allow to compute the time-evolution of the expectation value of every two-body observable.
The density-density correlation function is defined as

$$G_c^{dd}(R,t) = \langle n_R(t) n_0(t)\rangle_C - \langle n_R(0) n_0(0)\rangle_C.$$

In the Bogoliubov approximation we presented before, density-density correlation function takes the form

$$\langle n_R(t)n_0(t)\rangle_C = 2n\frac{1}{N}\sum_k e^{-\imath kR}\langle\Big[a_k^\dagger(t)a_k(t) + a_{-k}(t)a_{-k}^\dagger(t) + a_k^\dagger(t)a_{-k}^\dagger(t) + a_{-k}(t)a_k(t)\Big]\rangle.$$

This observable has the same form of spin-spin correlations once expressed as a function of magnons (see Sec. 3.4.1).
Rewriting all the particle operators as functions of quasi-particle ones, it is possible to explicit the time evolution

$$G_c^{dd}(R,t) = 2n_0\int_{-\pi}^{\pi} dk\frac{\mathcal{F}_2(k)}{2\pi}\cos(kR)\sin^2\left(E_k^f t\right) \tag{4.10}$$

where

$$\mathcal{F}_2(k) = \frac{\left(\mathcal{A}_k^f\mathcal{B}_k^i - \mathcal{A}_k^i\mathcal{B}_k^f\right)}{\left(\mathcal{A}_k^f + \mathcal{B}_k^f\right)E_k^i} = \frac{n\epsilon_k\left(\mathcal{V}^f(k) - \mathcal{V}^i(k)\right)}{\left(\epsilon_k + 2n\mathcal{V}^f(k)\right)E_k^i}.$$

We used the short-hand notation for the potential

$$\mathcal{V}^\lambda(k) = U^\lambda + V^\lambda\sum_R\frac{e^{-\imath Rk}}{R^\alpha},$$

where $\lambda = i,\ f$ for pre- or post-quench values of the couplings.
The function $\mathcal{F}_2$ depends explicitly on the observable studied. If we study the one-body correlation function, $g_1(R,t)$, defined as

$$g_1(R,t) = \langle a_R^\dagger(t)\,a_0(t)\rangle_C - \langle a_R^\dagger(0)\,a_0(0)\rangle_C,$$

we encounter a new function $\mathcal{F}_1$.
The time-evolution of particle operators can be written explicitly using the quasi-particle ones defined in the final Hamiltonian. The form taken by the dynamics of this observable makes clear that its spreading is still connected to the spreading of Bogoliubov particles,

$$g_1(R,t) = \langle a_R^\dagger a_0\rangle_C = \int_{-\pi}^{\pi} dk\frac{\mathcal{F}_1(k)}{2\pi}\cos(kR)\sin^2(E_k^f t), \tag{4.11}$$

where the pre-factor takes the observable-dependent form

$$\mathcal{F}_1(k) = \frac{\left(\mathcal{A}_k^f\mathcal{B}_k^i - \mathcal{A}_k^i\mathcal{B}_k^f\right)\mathcal{B}_k^f}{\left(E_k^f\right)^2 E_k^i}.$$

In conclusion, the LRBH model has two natural observables: density-density and the one-body correlation function. Both these observables can be interpreted in the same way: two counter-propagating beams of quasi-particles of phase E_k^f spread in the system after

a quantum quench. The difference between the two observables is the integral weight, $\mathcal{F}_2(k)$ for the density-density correlations, and $\mathcal{F}_1(k)$ for the function $g_1(R,t)$. These functions take into account the contribution to the specific observable of the different modes. These different weights represent the fact that not all the parts of the spectrum contribute at the same way to different observables. We will see in full details how this applies to locality and its breakdown in the LRBH model.

4.3 Correlation function and protection of locality

Let now discuss in full detail the time-evolution of the density-density correlations.

4.3.1 Comparison with Monte Carlo results.

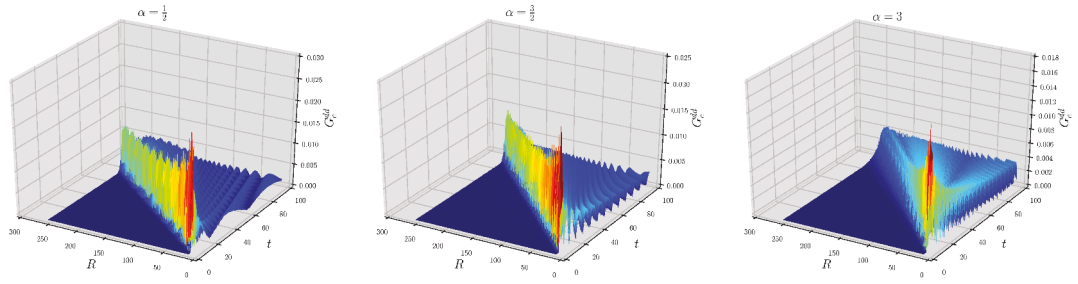

Figure 4.2: Time evolution of the density-density correlations following a quantum quench for the LRBH Hamiltonian with different values of α. The time evolution for all the studied values of the long-range couplings is ballistic in agreement with the results found in the t-VMC.

We start our microscopic analysis from the time evolution of the density-density correlations following a quantum quench. We study the time evolution for the same values of α already studied using Monte Carlo calculated by computing Eq. (4.10) using exact numerical integration. As in the t-VMC data, a ballistic spreading of correlations is found for every value of α, see again Fig. 4.2.
We can then take rewrite Eq. (4.10) as

$$G_c^{dd}(R,t) = n\int_{-\pi}^{\pi} dk \frac{\mathcal{F}_2(k)}{(2\pi)}\left[\cos(kR) - \frac{\cos\left(kR+2E_k^f t\right)+\cos\left(kR-2E_k^f t\right)}{2}\right] \quad (4.12)$$

$$= g_\infty(R) + \bar{g}(R,t). \quad (4.13)$$

We can then interpret this expression in the same way as we did for the LRTI model. The time-independent function $g_\infty(R)$ is the equilibration value and $\bar{g}(R,t)$ is the time dependent part responsible for the dynamics of the observable.
The interpretation based on the quasi-particle picture can give us useful hints on the

regime of propagation of correlations, as we saw in Sec. 3.5. We need now to analyze the energy spectrum of the model and its derivative, the group velocity, for different values of α.

4.3.2 Energy spectrum of excitations

We can start our microscopic analysis from the energy spectrum of the Bogoliubov excitations, which reads

$$E_k = \sqrt{\epsilon_k \left[\epsilon_k + 2n\mathcal{V}(k)\right]}.$$

ϵ_k is the short-range hopping part and $\mathcal{V}(k)$ is the Fourier transform of the interaction potential containing both short- and long-range part are written in Eq. (4.5). For $\alpha < 1$, the Fourier transform of the long-range potential is divergent around $k \approx 0$

$$\mathcal{V}(k) = U + \sum_R \frac{1}{R^\alpha} \approx \sum_R \frac{1}{R^\alpha}.$$

The sum has to be computed from $R = 1$ to $R = L$ and it gives a divergent value in the thermodynamic limit,

$$\mathcal{V}(k) \sim L^{1-\alpha}.$$

We can then express this values as a function of $k = \frac{2\pi}{L}$ and obtain

$$\mathcal{V}(k) \sim \frac{1}{k^{1-\alpha}}.$$

The pole of the long-range potential is not sufficient to have a divergent energy spectrum. In fact, the short-range hopping part goes to zero as

$$\epsilon_k = 4J \sin^2(k/2) \sim k^2,$$

and the dispersion relation is finite in the infrared limit

$$E_k = \sqrt{\epsilon_k \left(\epsilon_k + 2n\mathcal{V}(k)\right)} \approx \sqrt{k^2 \left(k^2 + 2nV_0 k^{-(1-\alpha)}\right)} \sim \sqrt{k^2 2nV_0 k^{-(1-\alpha)}} \sim k^{\frac{1+\alpha}{2}}. \tag{4.14}$$

In contrast, the group velocity of the excitations is divergent

$$V_k = \partial_k E_k \sim \partial_k k^{\frac{1+\alpha}{2}} \sim k^{\frac{\alpha-1}{2}} = \frac{1}{k^{|\frac{1-\alpha}{2}|}}.$$

In Fig. 4.3 the group velocity of the Bogoliubov quasi-particles is plotted for $\alpha = 1/2$. It is possible to see the divergence of this quantity in the infrared limit.

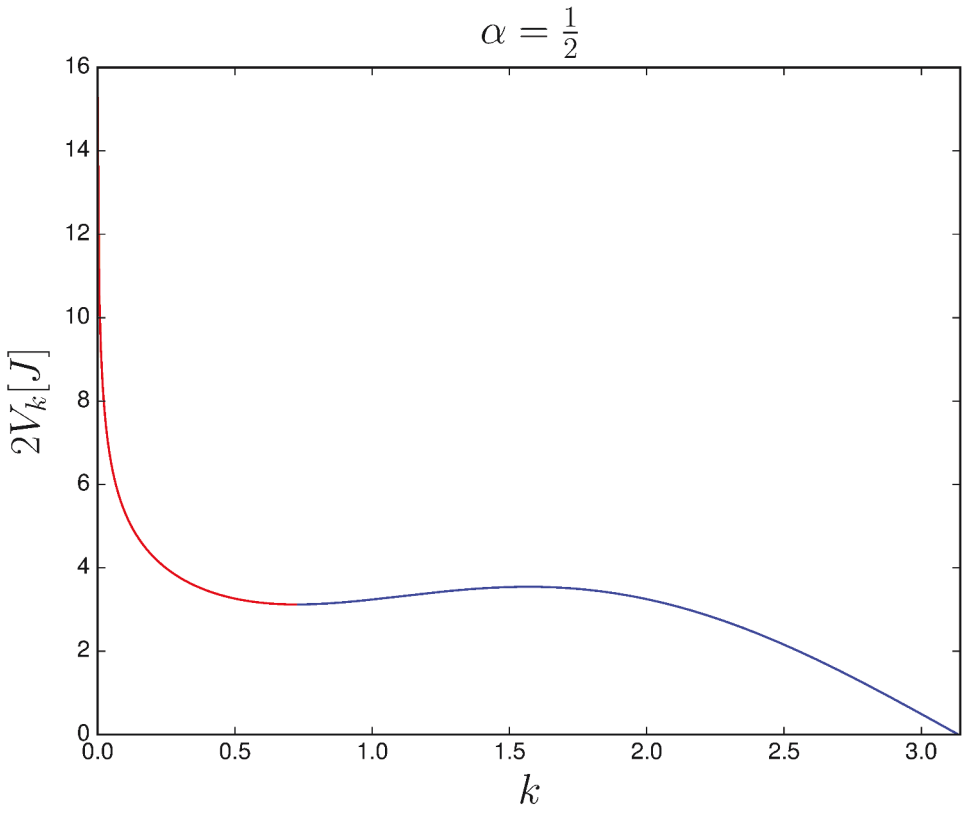

Figure 4.3: Group velocity of the Bogoliubov excitations for $\alpha < 1$. It is possible to see how the long-range interactions make it divergent around $k \approx 0$. The function is also non monotone as due to the shape of the short-range hopping ϵ_k which contributes to the local finite maximum locate at finite k.

This explains why a ballistic propagation is found for this observable for $\alpha > 1$. In see Sec. 3.6.1 we showed how a finite maximum velocity forces the correlation front to spread ballistically with a finite velocity.
For $\alpha < 1$ anyway a ballistic propagation is found in the t-VMC data and in the exact evaluation of Eq. (4.12). This cannot be explained considering just the energy spectrum. This quantity has in fact a divergent derivative around $k \approx 0$ which does not affect the propagation of correlations.
This very last observation is a key difference between the two models: in the LRTI model different regimes of propagation are determined by different divergences in the spectrum. In the LRBH model, the same ballistic propagation regime is found despite the changes in the quasi-particles spectrum. This points out that the analysis of the dispersion relation alone is not enough to explain the spreading of local observables.

4.3.3 Protection of locality

In this section we will explain in full detail why the density-density correlation function exhibits a linear light-cone even for $\alpha < 1$, i.e. where the group velocity is not bounded. This ballistic propagation is thus present even if the excitation spectrum contains modes with infinite velocity and this has been demonstrated to be sufficient to break locality in the LRTI model (see Sec. 3.6.2). To explain why the infinite velocities do not affect the propagation, we look at Eq. (4.10) which defines the density-density correlations. As we known, the effect of long-range interactions is stronger in the infrared region ($k \to 0^+$). A key ingredient that is not contained in the properties of the spectrum is the behavior in the infrared limit of the weight of the modes, namely the function

$$\mathcal{F}_2(k) = \frac{\left(\mathcal{A}_k^i \mathcal{B}_k^f - \mathcal{A}_k^f \mathcal{B}_k^i\right)}{\left(\mathcal{A}_k^f + \mathcal{B}_k^f\right) E_k^i} = \frac{n\left[\mathcal{V}^f(k) - \mathcal{V}^i(k)\right]\epsilon_k}{\left[\epsilon_k + 2n\mathcal{V}^f(k)\right] E_k^i}.$$

where we used again the short-hand notation

$$\mathcal{V}^\lambda(k) = U^\lambda + V^\lambda \sum_R \frac{e^{-\imath Rk}}{R^\alpha},$$

where λ can be i for the pre-quench values of the couplings and f for the post-quench values of the couplings.
For $\alpha < 1$ which is the case of interest in this section, we know that the long-range potential is divergent

$$\mathcal{V}(k) \sim \frac{1}{k^{1-\alpha}},$$

where we are interested just in its scaling in the infrared region.
In the same region, the function $\mathcal{F}_2(k)$ goes rapidly to zero due to the divergence in the long-range interactions

$$\mathcal{F}_2^{\alpha<1}(k) = \frac{n\left[\mathcal{V}^f(k) - \mathcal{V}^i(k)\right]\epsilon_k}{\left[\epsilon_k + 2n\mathcal{V}^f(k)\right] E_k^i} \approx \frac{\left(V^f - V^i\right) J}{2\sqrt{2nJV^i}} k^{\frac{3-\alpha}{2}}, \tag{4.15}$$

where $V^f \neq V^i \neq 0$ in order to have a non-zero leading order of the expansion.
If we compute the same quantity for $\alpha > 1$, we find that it goes to zero slower

$$\mathcal{F}_2^{\alpha>1}(k) \sim k.$$

This result can be easily obtained simply recalling that the potential $\mathcal{V}^\lambda(k) \sim \mathcal{V}_0^\lambda$ takes a finite value for $\alpha > 1$ because the mean value of the potential is finite. The previous result is then simply given by the ratio between $\epsilon_k \sim k^2$ and $E_k^i \sim k$. The comparison between the two cases $\alpha < 1$ and $\alpha > 1$ points out that long-range interactions reduce the contribution coming from the modes in the infrared region, the ones supposed to break locality. This can be used to motivate the fact that the contribution to the value of the observable coming from some parts of the spectrum is suppressed.

We are now going to make this argument more quantitative. We can study the time-dependent part $\bar{g}(R,t)$ of Eq. (4.12) in the limit where $R \to \infty$ and $t \to \infty$, keeping their ratio constant, $R/t = v$. In this limit, the integral in Eq. (4.12) can be evaluated using the stationary phase approximation, which gives

$$g_v(R,t) \approx \sum_\lambda \frac{1}{\sqrt{t}} \mathcal{W}_2(k^\star_\lambda) \cos\left(k^\star_\lambda R - 2E^f_{k^\star_\lambda} t\right). \tag{4.16}$$

The values $k^\star_\lambda$ are the solutions of the equation

$$\frac{R}{t} = 2\partial_k E_k$$

for a fixed ratio R/t, labeled by λ. In this case, multiple solutions appear for specific values of v because the spectrum is not monotonous. Physically, Eq. (4.16) represents the contribution of the modes with a defined velocity $v = R/t$ to the full correlation function. The weight of every $k^\star_\lambda$ is given by

$$\mathcal{W}_2(k) = \frac{\mathcal{F}_2(k)}{\sqrt{\partial^2_k E_k}}. \tag{4.17}$$

The function $\mathcal{W}_2(k)$ controls the contribution given by the different parts of the spectrum to the observable. The study of the variations of this function will be the key to understand the propagation of correlations.

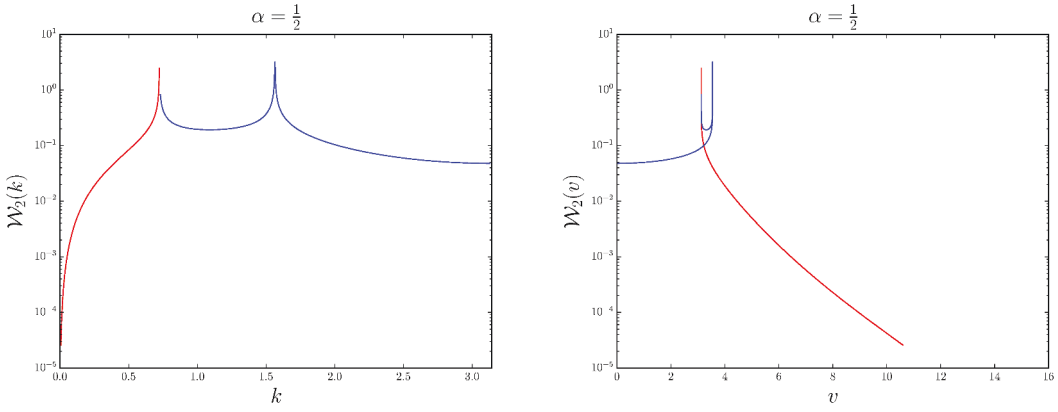

Figure 4.4: Plot of the function $\mathcal{W}_2(k)$ as function of k and as function of v. It is possible to see how a strong peak at finite velocity is present due to the finite maximum attained at finite values of k of the group velocity. The modes in the infrared region have an infinite velocity but their weight $\mathcal{W}$ is extremely small compared to the other modes. Since these modes do not affect the propagation we can neglect them in the time evolution and we can then say that the light-cone velocity is given by the maximum at finite velocity.

In Fig. 4.4 the function $\mathcal{W}_2$ is plotted as function of k (left panel) and as function of $v = 2\partial_k E_k$ (right panel). The letter is important in order to understand which group

velocity in the spectrum gives the larger contribution to the observable. In all the plots, we present in red the part of the spectrum located at $k \approx 0$, in this way it is possible to identify the contribution of the long-range potential.
From the previous plots it is possible to see how the contribution of the modes in the infrared region is extremely small. We can compute its scaling using the asymptotic we found before for the function $\mathcal{F}_2(k)$ and the dispersion relation in the infrared region

$$\begin{aligned}
&\mathcal{F}_2(k) \sim k^{\frac{3-\alpha}{2}}, \\
&E_k \sim k^{\frac{1+\alpha}{2}}, \\
&\partial_k^2 E_k \sim k^{-\frac{3-\alpha}{2}}.
\end{aligned}$$

We can then plug these expressions into the definition (4.17) to obtain the scaling

$$\mathcal{W}_2(k) \sim \frac{k^{\frac{3-\alpha}{2}}}{\sqrt{k^{-\frac{3-\alpha}{2}}}} = k^{\frac{3}{2}\left(\frac{3-\alpha}{2}\right)}. \tag{4.18}$$

The contribution of the modes located in the infrared region is then suppressed. Thanks to the divergence in the energy spectrum, the function $W_2(k)$ goes to zero much faster than $\mathcal{F}_2(k)$.
Since the quantity we are interested in is the velocity of the light-cone, the best choice is to express the function $\mathcal{W}_2$ as a function of the velocity instead of the momentum. This can be done analytically in the infrared region. We know the solution of the stationary phase equation in that limit, namely

$$\frac{R}{t} = v = 2\partial_k E_k = 2\partial_k k^{\frac{1+\alpha}{2}} \sim k^{-\frac{1-\alpha}{2}} \rightarrow k \sim v^{-\frac{2}{1-\alpha}}.$$

We can then plug the last relation into Eq. (4.18) to get the dependence of $\mathcal{W}_2$ on the velocity

$$\mathcal{W}_2(v) \sim [k(v)]^{\frac{3}{2}\left(\frac{3-\alpha}{2}\right)} \sim v^{-\frac{3}{1-\alpha}\left(\frac{3-\alpha}{2}\right)}.$$

The last equation points out that the contribution of the modes with a large velocity goes to zero as the velocity increases.
The analysis of the function $\mathcal{W}_2(k)$ outside the infrared region has two peaks. They correspond to the extremal points of the group velocity, where the second derivative of the dispersion relation goes to zero

$$\partial_k v_k = \partial_k^2 E_k \rightarrow 0.$$

This makes the denominator of Eq. (4.17) vanishing, giving to these extremal points a large contribution to the studied observable

$$\mathcal{W}_2(k) \sim \frac{1}{\sqrt{\partial_k^2 E_k}} \gg 1.$$

LRTI	$\alpha = 3$	LRBH	$\alpha = 1/2$	$\alpha = 3/2$	$\alpha = 3$
$v_c^{\text{t-VMC}}$	$0.3(7)\ h$	$v_c^{\text{t-VMC}}$	$3.(6)\ J$	$3.(5)\ J$	$3.(1)\ J$
v_c^{qp}	$0.3928\ h$	v_c^{qp}	$3.7408\ J$	$3.3893\ J$	$3.1772\ J$

Table 4.1: In this table we compare the velocity of the light-cone extracted from the Monte Carlo results with the one extracted from the quasi-particles approach. All the cases studied are one dimensional systems. For the LRTI model with $\alpha = 3$ and for the LRBH model for $\alpha = 3/2$ and $\alpha = 3$, the excitations have a finite group velocity. It is then possible to check how the velocity of the light-cone extracted from the numerics is compatible with the one computed with the quasi-particle picture. For the case $\alpha = 1/2$ in the LRBH a ballistic propagation is found in the Monte Carlo data. For the quasi-particles infinite velocity are present in the energy spectrum. Using the stationary phase approximation it is possible to find that the velocity that contributes to the observable is a finite group velocity located outside the infrared region. It is then possible to see how for this particular case the results of the quasi-particle picture and of the Monte Carlo can be compared. The difference between the two is compatible with the differences in the other cases, where the Cardy-Calabrese principle hold. This table can be found in the supplementary material of Ref. [23].

We can then see from Fig. (4.4) that the contribution of modes with large velocity is much smaller than the contribution coming from the modes located outside the infrared region. The difference between the contribution of the infrared region and the one of the extremal point, at least some orders of magnitude, makes the one of infinitely fast modes negligible in the summation of Eq. 4.16. The light-cone velocity observed in the numerical data is then given by

$$v_{lc} = 2 \max \partial_k E_k^f,$$

where the maximum is taken outside the infrared-region, blue line in Fig. 4.3. Since the contribution of the fast-modes in the long-range potential is negligible, compared to the rest of the spectrum, the velocity of the light-cone will be given by the finite maximum velocity located outside the infrared region. In Tab. (4.1), the comparison between the light-cone velocity extracted from the Monte Carlo data and the one obtained by the quasi-particle approach are presented. It is possible to see how the quasi-particles picture is able to predict the velocity of the light-cone with good accuracy where the Cardy-Calabrese works, LRTI and LRBH with $\alpha > 1$, and also where the analysis of the integral weight has to be taken into account, LRBH $\alpha < 1$.
Another interesting fact has to be pointed out now: the form of the function $\mathcal{F}_2$ is determined also by the initial state. The choice of a particular initial state can have then drastic changes in the dynamics. For example, in the case of a quench from a non-interacting Hamiltonian we get $\mathcal{F}_2 \sim$ const. In this case, the infinite velocities present in the spectrum have a finite contribution and the propagation is faster-than-ballistic.

The study of the density-density correlation function points out a dramatic difference

between the LRTI and LRBH model. In the LRTI model, the propagation is completely determined by the dispersion relation. In the LRBH model the analysis of the energy spectrum is not enough to infer the dynamics. In this case the pre-factor $\mathcal{F}_2(k)$ plays a crucial role to determine the regime of propagation itself. In this case the presence of infinite velocities in the spectrum is not enough to destroy the ballistic propagation, because the contribution of these modes is negligible. The final result is then a protection of locality: not only long-range interactions are not sufficient to destroy locality, but neither modes with infinite velocity are.
The result we presented points out another fact: the time-evolution have a dependence on the observable. The function $\mathcal{W}_2(k)$ is in fact proportional to the amplitude $\mathcal{F}_2(k)$, which form depends strictly on the specific observable. In the last section, we will try to investigate the time propagation of a different local operator, namely the $g_1(R,t)$ function, see Eq. (4.11). This is a natural observable for bosonic lattice models and it can be measured in standard cold atomic setups, see Sec. 1.3.2. This observable takes the same structure as the density-density correlations, with the same quasi-particles spreading giving the time evolution. The amplitude in the integral is anyway a different function $\mathcal{F}_1(k)$ which will determine a drastic change in the dynamics.

4.4 Time evolution of the one-body correlation function

We are now going to study the behavior of the $g_1(R,t)$ function following a quantum quench. At the present moment this is an ongoing work. The results presented here are just preliminary and they will be the topic of my next publications.
The function $g_1(R,t)$, see Eq. (4.11), takes the same form as the density-density correlation function in terms of quasi-particles. It can be written as two counter-propagating beams spreading with the dispersion relation of the final Hamiltonian. The contribution of every mode to the specific observable is encoded in the function $\mathcal{F}_1(k)$. This is different from the function $\mathcal{F}_2(k)$ of density-density correlations and it reads

$$\mathcal{F}_1(k) = \frac{\left(\mathcal{A}_k^f \mathcal{B}_k^i - \mathcal{A}_k^i \mathcal{B}_k^f\right) \mathcal{B}_k^f}{\left(E_k^f\right)^2 E_k^i},$$

where the amplitudes $\mathcal{A}_k$ and $\mathcal{B}_k$ are the same as those defined in Eq. (4.9). As we did in the previous section for the density-density correlations, we can interpret the time evolution of the one-body correlation function using the quasi-particles approach. The quasi-particle spectrum is left unchanged: it has an unbounded maximal group velocity for $\alpha < 1$ and finite maximum group velocity for $\alpha > 1$.
For $\alpha > 1$ the propagation has to be bounded: the fact that the fundamental excitations of the system spread with a finite velocity forces local observables to be bounded by a light-cone.
For $\alpha < 1$ an infinite velocity appears in the infrared region due to the divergence of the Fourier transform of the long-range potential. The fundamental excitations responsible for spreading of the $g_1(R,t)$ and of the density-density correlations are the same. The

weights $\mathcal{F}_1$ is completely different from $\mathcal{F}_2$ and this changes the dynamics. This can be again quantifies studying the correlation function in the stationary phase approximation. For $g_1(R,t)$, it can be written in the same general form as before

$$g_1(R,t) \approx \sum_\lambda \frac{1}{\sqrt{t}} \mathcal{W}_1(k^*_\lambda) \cos\left(k^\star_\lambda R - 2E^f_{k^\star_\lambda} t\right),$$

where now

$$\mathcal{W}_1(k) = \frac{\mathcal{F}_1(k)}{\sqrt{\partial_k^2 E_k^f}}. \tag{4.19}$$

It has to be noticed how the functions $\mathcal{W}_2(k)$ and $\mathcal{W}_1(k)$ depend specifically on the observable studied through the pre-factors $\mathcal{F}_2(k)$ and $\mathcal{F}_1(k)$. In Sec. 4.3.3 we described how the behavior of $\mathcal{W}_2(k)$ is able to protect locality suppressing the contribution to the density-density correlations coming from infinitely fast modes. We are going to do the same study for $g_1(R,t)$ demonstrating that this observable does not protect the locality. We need to evaluate Eq. (4.19) in the infrared limit. To do so, we expand the pre-factor $\mathcal{F}_1(k)$ for $\alpha < 1$ and $k \sim 0$ using the asymptotic formula $\mathcal{V}^\lambda(k) \sim V^\lambda k^{-(1-\alpha)}$

$$\mathcal{F}_1(k) = \frac{n^2 \epsilon_k \left(\mathcal{V}^f(k) - \mathcal{V}^i(k)\right) \mathcal{V}^f(k)}{\left(E^f_k\right)^2 E^i_k} \sim \sqrt{\frac{\mathcal{V}(k)}{\epsilon_k}} \sim k^{-\frac{3-\alpha}{2}}.$$

Remarkably, it turns out to be the inverse of $\mathcal{F}_2(k)$. The divergence of the dispersion relation is the same as before and its derivative is

$$\partial_k^2 E_k \sim k^{-\frac{3-\alpha}{2}}$$

We can then put all these pieces together to obtain the scaling of $\mathcal{W}_1(k)$ in the infrared limit,

$$\mathcal{W}_1(k) = \frac{\mathcal{F}_1(k)}{\sqrt{\partial_k^2 E_k^f}} \sim \frac{k^{-\frac{3-\alpha}{2}}}{k^{-\frac{1}{2}\left(\frac{3-\alpha}{2}\right)}} \sim k^{-\frac{1}{2}\left(\frac{3-\alpha}{2}\right)}.$$

This function diverges as $k \to 0$ and then quasi-particles in that region will affect strongly the time evolution. We can then compare this scaling with the one of the $\mathcal{W}_2(k) \sim k^{\frac{3}{2}\left(\frac{3-\alpha}{2}\right)}$ which gives completely different behaviors. The one coming from the density-density correlations are strongly suppressed in the density-density correlations, while these are extremely large in the $g_1(R,t)$.

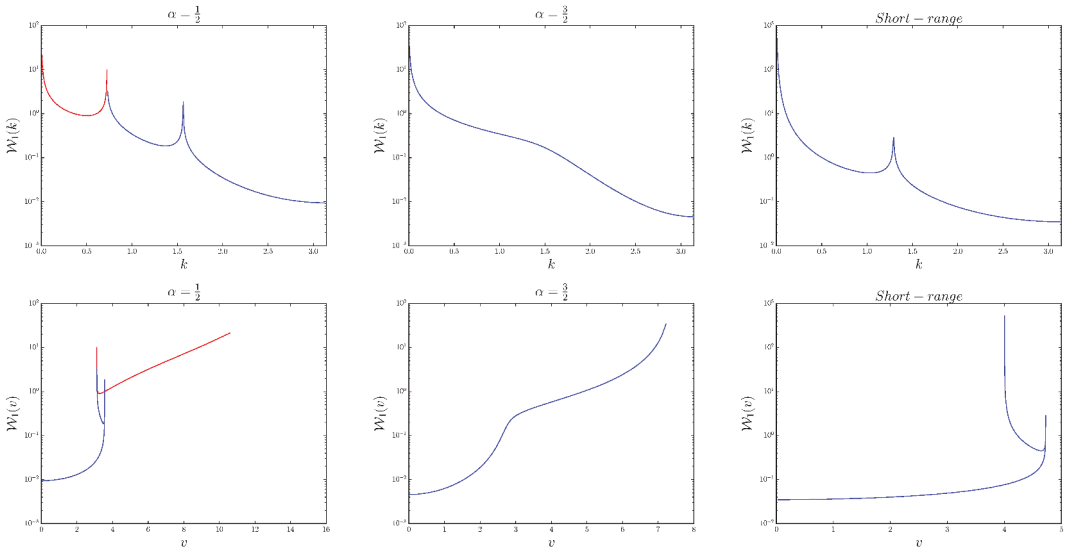

Figure 4.5: Upper panel: plots of the function $\mathcal{W}_1(k)$ for the $g_1(R,t)$ found for different cases: $\alpha = 1/2$, $\alpha = 3/2$ and a short-range model. Lower panel: the same quantities as before are plotted as function of the velocity of the quasi-particles. It is possible to see how the branch containing the infinite velocity, $k \approx 0$ region, has a huge weight for this observable. The effect of the different weight is faster-than-ballistic spreading of correlations in the time evolution of the observable.

In Fig. 4.5 the weights $\mathcal{W}_1(k)$ for the $g_1(R,t)$ are presented as function of k (upper row) and as function of $v = 2\partial_k E_k^f$ (lower row) for $\alpha = 1/2$, right column, $\alpha = 3/2$, central column, and a short-range model $V_i = V_f = 0$, left column. It is possible to see how, for $\alpha = 1/2$ and $\alpha = 3/2$, the function $\mathcal{W}_1(k)$ diverges in the infrared region for the long-range interactions. This means that the modes located in the $k \approx 0$ region give a large contribution to the observable. For $\alpha > 1$ and for the short-range model, the infrared region has an extremely large contribution to the observable, but in these cases no infinite velocity is present.

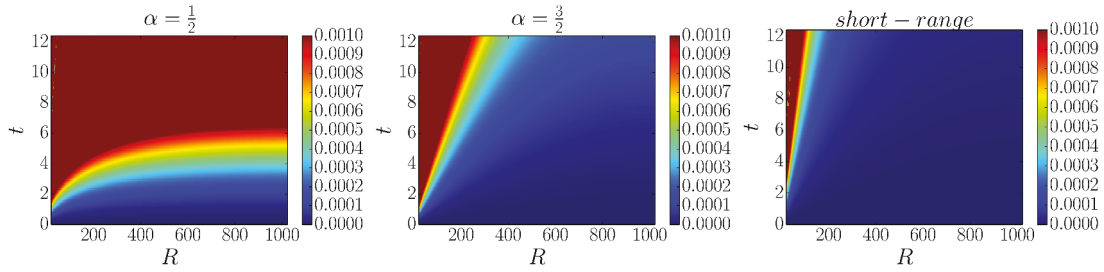

Figure 4.6: Time evolution of the function $g_1(R,t)$ for different values of $\alpha = 1/2$, $\alpha = 3/2$ and for a short-range model. In the $\alpha = 1/2$ case, a faster-than-ballistic propagation is found compatible with the presence of infinite velocities in the excitation spectrum. For $\alpha = 3/2$, where the velocity has a finite maximum group velocity attained at $k \approx 0$, the time evolution if ballistic as in the short-range case represented on the right, even if their velocities are different. This figure points out, how different observables can have different behaviors even if the quasi-particles have the same group velocity.

In Fig. 4.6 it is possible to see the time evolution of the $g_1(R,t)$ for $\alpha = 1/2$, $\alpha = 3/2$, and for the short-range version of the Hamiltonian, $V^f = V^i = 0$. While in the two figures on the right ($\alpha = 3/2$ and short-range case) it is possible to see a linear structure in the time evolution, on the figure on the left ($\alpha = 1/2$) this structure is absent. The correlation functions in this case is not bounded by a linearly increasing light-cone due to the divergent group velocity of some excitations. If we compare this case to the one already discussed in Sec. 3.6.2 for the LRTI model we can find some analogies. In both cases the presence of a cusp in the energy spectrum, finite dispersion relation and infinite velocity, leads to an algebraic light-cone $t^\star \propto R^\beta$. The main difference is anyway in the values of β: for the LRTI model the propagation was slower-than-ballistic, $\beta > 1$, while for the LRBH model it is faster-than-ballistic $\beta < 1$ (at least qualitatively). The parameter β is anyway extremely model dependent, as we saw in Sec. 3.1 3.2. The difference between the behaviors of the two models is not completely surprising.

This is an important point. In the derivation of the general bounds on the time evolution of local observables the explicit form of these operators has always been neglected. The operators are requested to be bounded in order to approximate them as constants

$$A \leq \|A\| \mathbb{I}.$$

This is a rather brutal bound and it completely destroys all the physical information to the dynamics coming from the operator. Using this argument, the only meaningful quantity used to describe the time evolution is the energy spectrum of the excitations. For short-range interactions the approximation was enough to describe the right behavior of the dynamics of the expectation values. This is anyway not surprising: short-range interactions impose clearly a bound over the propagation of correlations that cannot be nothing but linear.

When the long-range interactions come into play the situation drastically changes. In this case the spreading of correlations can take different shapes, from slower-than-ballistic to instantaneous. In the studied models, the bounds are not enough to describe the right propagation and the microscopic approach is still fundamental to predict the correct dynamics of correlations. In particular the microscopic analysis outlines a characteristic of the time evolution which is completely absent in the general bounds: the dependence on the observable. Two observables as the density-density correlations and the one-body correlation have different behaviors even if the quasi-particles responsible for their propagation have the same spectrum for both the observables.

5 Conclusions and outlook

In this manuscript we presented the results for the time evolution of correlations in long-range interacting quantum systems following a quantum quench. We compared two models: a spin model and a lattice boson model. Both of them are described by Hamiltonians containing long-range terms of the type $1/R^\alpha$. The spin model has a long-range spin exchange term while the bosonic one has long-range standard interactions. In the limits where these two Hamiltonians can be mapped onto quadratic bosonic Hamiltonians the time evolution could be solved analytically. Using these results we compute the exact time evolution of different observables and we compare it to the general Lieb-Robinson bounds extended to long-range interacting lattice Hamiltonians. In all the cases studied there, the real time evolution exhibits a more complex behavior than the one presented in these bounds.

For the spin system, we compare the results obtained in one dimension using the time-dependent variational Monte Carlo (t-VMC) algorithm to the ones obtained using the linear spin wave theory (LSWT), and an excellent agreement is found. We then extend this approach to arbitrary dimensions D. The time evolution of spin-spin correlations following a quantum quench takes different regimes depending on the value of α.

For $\alpha < D$, the dynamics is instantaneous: correlations are activated everywhere in the system right after the quench. This result can be described perfectly using the quasi-particle approach. The dispersion relation of the fundamental excitations of the system is divergent and it determines a characteristic activation time that vanishes in the thermodynamic limit. This vanishing activation time can be found also analytically integrating the modes with a divergent dispersion relation or using the indetermination principle. Computing the activation time in a finite system we are able to determine the finite-size scaling of this time and check it using the numerical results. Instantaneous propagation is in perfect agreement with the general bounds: for $\alpha < D$ no bound is present allowing for arbitrary fast propagation.

For $D < \alpha < D+1$, the time evolution follows an algebraically increasing horizon $t^\star \propto R^\beta$ with $\beta > 1$ which identifies a slower-than-ballistic propagation. In this case, the energy spectrum of the excitations is finite but its derivative, defining the group velocity of the excitations, is infinite. Using the quasi-particle approach it is possible to compute the contribution of these modes to the correlation function in some cases and to compute the scaling of the light-cone analytically. This exact computation confirms that the propagation is slower-than-ballistic even if infinite velocities are presents in the spectrum.

For $\alpha > D + 1$, the propagation of correlations is ballistic. The spectrum of excitations shows a finite maximum group velocity. This velocity determines the velocity of the light-cone of correlations in the same way as short-range interacting systems.

These results point out that the time evolution can be predicted simply looking at the

energy spectrum of excitations. This is an important fact: the energy spectrum of the quasi-particles can be determined in different ways, also experimentally. An analysis of the divergences in this case is reliable to determine qualitative and quantitative predictions on the time evolution.
The results obtained by the microscopic approach do not violate the general bounds for long-range interacting quantum systems found in the literature. Anyway, these bounds describe correctly the time evolution just for the case $\alpha < D$, where no bound is present and the time evolution observed is instantaneous. In the other two cases, the general bounds are respected but they are far from the results obtained by the real time evolution. The exact dynamics is then fundamental and our work provides a huge simplification in this sense: we determine the main quantity to describe the time evolution, the dispersion relation. It, however, assumes that it can be derived analytically.
We then switch to the interacting bosons. Mathematically, the interaction potential here takes the same form as the long-range spin-exchange previously studied, they both respect the same general bounds. However the physical meaning is completely different: in the previous case the spin exchange was representing a sort of "kinetic term" while here it is a real interaction potential.
We find both in Monte Carlo and analytic results, based on the Bogoliubov approach, a ballistic propagation of density-density correlations for any value of α. We can then try to interpret these results using the spectrum of the fundamental excitations. We find that the energy spectrum contains infinite velocities just if $\alpha < 1$. Despite these fast moving quasi-particles, the propagation of the density-density correlations is ballistic.
We explain that observation by studying the contribution to the observable coming from different modes. This naturally arises from the general form of the two-body correlations in the stationary phase limit. We find that the contribution coming from the modes with an infinite velocity is strongly suppressed due to long-range interactions. The time evolution is then completely unaffected by the presence of infinite velocities, which would determine non-ballistic propagation.
The importance of the previous results is that, for the first time, something different from the energy spectrum alone determines the time evolution. In this case, an observable-dependent quantity is crucial to determine the correct dynamics beyond the simple quasi-particle method based on the group velocity. The previous results is also sensible to the initial state, that can be chosen to enhance the presence of these infinite velocities breaking locality.
We then decide to study another observable, namely the one-body correlation function. The energy spectrum of the excitations is the same as before, it contains infinite group velocities for $\alpha < 1$. What changes from the two-body (density-density) correlations is the contribution of these modes: In the previous case it was vanishing while in this case it diverges. The effects of the infinite velocities are then not negligible for this specific observable and we then find an algebraic faster-than-ballistic propagation of correlations for $\alpha < 1$ and a ballistic propagation for $\alpha > 1$.
We demonstrated the presence of an observable-dependent dynamics which was not contained in the general bounds and it is still not taken into account by other methods than

the microscopic one presented here. This determines the need to use the microscopic approach to understand the real time evolution.
In the case of the bosonic system, as before, the dynamics does not violate the general bounds. Anyway, they are not just overestimating the time evolution, as in the spin model. Here the bounds seem to not be able to take into account the observable-dependence locality explained using the microscopic theory. This new dependence is well described by the microscopic approach which is, as before, the only way to explain the spreading of correlations in a precise way.

Many different directions can be considered to continue the exploration of the effects of long-range interactions on the time evolution. The first involves the ongoing work on the one-body correlation function in long-range bosonic systems. This work involves the correct understanding of the time evolution and the difference from density-density correlations for $\alpha < 1$. At the same time, it would be interesting to work directly on the bounds, trying to introduce the dependence on the observables we see in the quasi-particle picture.
From a more general point of view, we are working on the spreading of correlations in long-range interacting many body systems. We want to demonstrate that different structures with particular scalings appear during the dynamics. These structures have already been detected in numerical works on dynamics with short-range interactions. Using the quasi-particle picture it is possible to demonstrate that generic correlations have two or more structures with different parameters, velocities if they are linear and even scaling if they are algebraic. The presence and correct description of these structures may lead to a classification of these phenomena and a more precise understanding of the differences that appear in the numerical and experimental data.
After these works it would be interesting to explore the effect of long-range interactions on all the phenomena where the characteristic velocity of quasi-particles is important. Long-range interactions can in fact make this velocity divergent and this can change some phenomena as the relaxation of observables. These effects have already been measured in trapped ions experiments and they would open a new research line.

Bibliography

[1] K Huang. *Statistical Physics*. Wiley, New York, 1987.

[2] E Fermi. *Termodinamica*. Programma di matematica, fisica, elettronica. Bollati Boringhieri, 2. ed., 6. rist edition, 1988.

[3] V I Arnold, A Weinstein, and K Vogtmann. *Arnold V I Mathematical Methods Of Classical Mechanics*. Graduate Texts in Mathematics. Springer, 2nd edition, 1989.

[4] E Schrödinger. An undulatory theory of the mechanics of atoms and molecules. *Phys. Rev.*, 28:1049–1070, 1926.

[5] K B Davis, M O Mewes, M R Andrews, N J van Druten, D S Durfee, D M Kurn, and W Ketterle. Bose-einstein condensation in a gas of sodium atoms. *Phys. Rev. Lett.*, 75:3969–3973, 1995.

[6] M H Anderson, J R Ensher, M R Matthews, C E Wieman, and E A Cornell. Observation of bose-einstein condensation in a dilute atomic vapor. *Science*, 269(5221):198–201, 1995.

[7] N N Bogolyubov. On the theory of superfluidity. *J. Phys.(USSR)*, 11:23–32, 1947. [Izv. Akad. Nauk Ser. Fiz.11,77(1947)].

[8] J Bardeen, L. N. Cooper, and J. R. Schrieffer. Theory of superconductivity. *Phys. Rev.*, 108:1175–1204, 1957.

[9] R Kubo. Statistical-mechanical theory of irreversible processes. i. general theory and simple applications to magnetic and conduction problems. *Journal of the Physical Society of Japan*, 12(6):570–586, 1957.

[10] A Polkovnikov, K Sengupta, A Silva, and M Vengalattore. *Colloquium* : Nonequilibrium dynamics of closed interacting quantum systems. *Rev. Mod. Phys.*, 83:863–883, 2011.

[11] E Altman. Non equilibrium quantum dynamics in ultra-cold quantum gases. *ArXiv:1512.00870 [cond-mat.quant-gas]*, 2015.

[12] P L Kapitza. Dynamic stability of a pendulum when its point of suspension vibrates. *Soviet Phys. JETP*, 21:588–592, 1951.

[13] P L Kapitza. Pendulum with a vibrating suspension. *Usp. Fiz. Nauk*, 44:7–15, 1951.

[14] J Eisert, M Friesdorf, and C Gogolin. Qauntum manybody systems out of equilibrium. *Nature Physics*, 11(2):124–130, 2015.

[15] B Sutherland. *Beautiful Models: 70 Years of Exactly Solved Quantum Many-body Problems*. World Scientific Publishing Company, first edition edition, 2004.

[16] M Gaudin and J-S Caux. *The Bethe Wavefunction*. CUP, 2014.

[17] M Suzuki. *Quantum Monte Carlo Methods in Equilibrium and Nonequilibrium Systems: Proceedings of the Ninth Taniguchi International Symposium*. Springer Series in Solid-State Sciences 74. Springer-Verlag Berlin Heidelberg, 1 edition, 1987.

[18] U Schollwöck. The density-matrix renormalization group. *Rev. Mod. Phys.*, 77:259–315, 2005.

[19] G Vidal. Efficient classical simulation of slightly entangled quantum computations. *Phys. Rev. Lett.*, 91:147902, 2003.

[20] G Vidal. Efficient simulation of one-dimensional quantum many-body systems. *Phys. Rev. Lett.*, 93:040502, 2004.

[21] A J Daley, C Kollath, U Schollwöck, and G Vidal. Time-dependent density-matrix renormalization-group using adaptive effective hilbert spaces. *Journal of Statistical Mechanics: Theory and Experiment*, 2004(04):P04005, 2004.

[22] G Carleo, F Becca, M Schiró, and M Fabrizio. Localization and glassy dynamics of many-body quantum systems. *Scientific Report*, 2:243, 2012.

[23] L Cevolani, G Carleo, and L Sanchez-Palencia. Protected quasilocality in quantum systems with long-range interactions. *Phys. Rev. A*, 92:041603, 2015.

[24] E Feenberg. *Theory of Quantum Fluids*. Pure and Applied Physics 31. Academic Press Inc.,U.S, 1969.

[25] I Bloch, J Dalibard, and S Nascimbene. Quantum simulations with ultracold quantum gases. *Nature Physics*, 8(4):267–276, 2012.

[26] C N Cohen-Tannoudji. Nobel lecture: Manipulating atoms with photons. *Rev. Mod. Phys.*, 70:707–719, 1998.

[27] D J Griffiths. *Introduction to Electrodynamics*. Pearson Education, 4th edition, 2012.

[28] P S Epstein. The stark effect from the point of view of schroedinger's quantum theory. *Phys. Rev.*, 28:695–710, 1926.

[29] W Ketterle and N J Van Druten. Evaporative cooling of trapped atoms. volume 37, pages 181 – 236. Academic Press, 1996.

[30] T Jacqmin, B Fang, T Berrada, T Roscilde, and I Bouchoule. Momentum distribution of one-dimensional bose gases at the quasicondensation crossover: Theoretical and experimental investigation. *Phys. Rev. A*, 86:043626, 2012.

[31] T Schumm, S Hofferberth, L M Andersson, S Wildermuth, S Groth, I Bar-Joseph, J Schmiedmayer, and P Kruger. Matter-wave interferometry in a double well on an atom chip. *Nature Physics*, 1(1):57–62, 2005.

[32] W Ketterle, D S Durfee, and D M Stamper-Kurn. Making, probing and understanding bose-einstein condensates. *eprint arXiv:cond-mat/9904034*, 1999.

[33] M Inguscio, W Ketterl, and C Salomon. Ultra-cold fermi gases: Proceedings of the international school of physics 'enrico fermi'. 2008.

[34] M Lewenstein, A Sanpera, and V Ahufinger. *Ultracold Atoms in Optical Lattices: Simulating quantum many-body systems*. Oxford University Press, 2012.

[35] L Pitaevskii and S Stringari. *Bose-Einstein condensation*. The International Series of Monographs on Physics. Oxford University Press, USA, 2003.

[36] L Pitaevski and S Strigari. *Bose-Einstein condensation*. 2003.

[37] S Giorgini, L P Pitaevskii, and S Stringari. Theory of ultracold atomic fermi gases. *Rev. Mod. Phys.*, 80:1215–1274, 2008.

[38] M Renderia, W Zwerger, and M Zwierlein. *The BEC-BCS crossover ad the Unitary Fermi Gas*, volume 86. Springer, 2012.

[39] T E Drake, Y Sagi, R Paudel, J T Stewart, J P Gaebler, and D S Jin. Direct observation of the fermi surface in an ultracold atomic gas. *Phys. Rev. A*, 86:031601, 2012.

[40] C Chin, R Grimm, P Julienne, and E Tiesinga. Feshbach resonances in ultracold gases. *Rev. Mod. Phys.*, 82:1225–1286, 2010.

[41] M Baranov, L Dobrek, K Góral, L Santos, and M Lewenstein. Ultracold dipolar gases a challenge for experiments and theory. *Physica Scripta*, 2002(T102):74, 2002.

[42] R Blatt and C F Roos. Quantum simulations with trapped ions. *Nature Physics*, 8(4):277–283, 2012.

[43] A Griesmaier, J Werner, S Hensler, J Stuhler, and T Pfau. Bose-einstein condensation of chromium. *Phys. Rev. Lett.*, 94:160401, 2005.

[44] K Góral, L Santos, and M Lewenstein. Quantum phases of dipolar bosons in optical lattices. *Phys. Rev. Lett.*, 88:170406, 2002.

[45] N R Cooper, E H Rezayi, and S H Simon. Vortex lattices in rotating atomic bose gases with dipolar interactions. *Phys. Rev. Lett.*, 95:200402, 2005.

[46] M A Baranov, K Osterloh, and M Lewenstein. Fractional quantum hall states in ultracold rapidly rotating dipolar fermi gases. *Phys. Rev. Lett.*, 94:070404, 2005.

[47] P Richerme, Z-X Gong, A Lee, C Senko, J Smith, M Foss-Feig, S Michalakis, A V Gorshov, and C Monroe. Non-local propagation of correlations in quantum systems with long-range interactions. *Nature*, 511(7508):198–201, 2014.

[48] P Jucevic, B P Lanyon, P Hauke, C Hempel, P Zoller, R Blatt, and C F Roos. Quasiparticle engineering and entanglement propagation in a quantum many-body system. *Nature*, 511(7508):202–205, 2014.

[49] H L F Essler, H Frahm, F Gohmann, A Klumper, and V E Korepin. *The one-dimensional Hubbard model*. Cambridge University Press, 2005.

[50] V E Korepin, N M Bogoliubov, and A G Izergin. *Quantum inverse scattering method and correlation functions*. Cambridge monographs on mathematical physics. Cambridge University Press, 1993.

[51] T Giamarchi. *Quantum Physics in One Dimension*. The international series of monographs on physics 121. Clarendon; Oxford University Press, illustrated edition edition, 2004.

[52] C Kollath, U Schollwöck, and W Zwerger. Spin-charge separation in cold fermi gases: A real time analysis. *Phys. Rev. Lett.*, 95:176401, 2005.

[53] B Paredes and J I Cirac. From cooper pairs to luttinger liquids with bosonic atoms in optical lattices. *Phys. Rev. Lett.*, 90:150402, 2003.

[54] A Recati, P O Fedichev, W Zwerger, and P Zoller. Spin-charge separation in ultracold quantum gases. *Phys. Rev. Lett.*, 90:020401, 2003.

[55] G Boéris, L Gori, M D Hoogerland, A Kumar, E Lucioni, L Tanzi, M Inguscio, T Giamarchi, C D'Errico, G Carleo, G Modugno, and L Sanchez-Palencia. Mott transition for strongly interacting one-dimensional bosons in a shallow periodic potential. *Phys. Rev. A*, 93:011601, 2016.

[56] B Paredes, A Widera, V Murg, O Mandel, S Folling, I Cirac, G V Shlyapnikov, T W Hansch, and I Bloch. Tonks-girardeau gas of ultracold atoms in an optical lattice. *Nature*.

[57] H Moritz, T Stöferle, M Köhl, and T Esslinger. Exciting collective oscillations in a trapped 1d gas. *Phys. Rev. Lett.*, 91:250402, 2003.

[58] T Kinoshita, T Wenger, and D S Weiss. Observation of a one-dimensional tonks-girardeau gas. *Science*, 305(5687):1125–1128, 2004.

[59] C Schori, T Stöferle, H Moritz, M Köhl, and T Esslinger. Excitations of a superfluid in a three-dimensional optical lattice. *Phys. Rev. Lett.*, 93:240402, 2004.

[60] B L Tolra, K M O'Hara, J H Huckans, W D Phillips, S L Rolston, and J V Porto. Observation of reduced three-body recombination in a correlated 1d degenerate bose gas. *Phys. Rev. Lett.*, 92:190401, 2004.

[61] P W Anderson. Absence of diffusion in certain random lattices. *Phys. Rev.*, 109:1492–1505, 1958.

[62] B Damski, J Zakrzewski, L Santos, P Zoller, and M Lewenstein. Atomic bose and anderson glasses in optical lattices. *Phys. Rev. Lett.*, 91:080403, 2003.

[63] R Roth and K Burnett. Ultracold bosonic atoms in two-colour superlattices. *Journal of Optics B: Quantum and Semiclassical Optics*, 5(2):S50, 2003.

[64] R Roth and K Burnett. Phase diagram of bosonic atoms in two-color superlattices. *Phys. Rev. A*, 68:023604, 2003.

[65] J E Lye, L Fallani, M Modugno, D S Wiersma, C Fort, and M Inguscio. Bose-einstein condensate in a random potential. *Phys. Rev. Lett.*, 95:070401, 2005.

[66] D Clément, A F Varón, M Hugbart, J A Retter, P Bouyer, L Sanchez-Palencia, D M Gangardt, G V Shlyapnikov, and A Aspect. Suppression of transport of an interacting elongated bose-einstein condensate in a random potential. *Phys. Rev. Lett.*, 95:170409, 2005.

[67] N Bilas and N Pavloff. Propagation of a dark soliton in a disordered bose-einstein condensate. *Phys. Rev. Lett.*, 95:130403, 2005.

[68] C Fort, L Fallani, V Guarrera, J E Lye, M Modugno, D S Wiersma, and M Inguscio. Effect of optical disorder and single defects on the expansion of a bose-einstein condensate in a one-dimensional waveguide. *Phys. Rev. Lett.*, 95:170410, 2005.

[69] N Bilas and N Pavloff. Anderson localization of elementary excitations in a one-dimensional bose-einstein condensate. *The European Physical Journal D - Atomic, Molecular, Optical and Plasma Physics*, 40(3):387–397, 2006.

[70] T Schulte, S Drenkelforth, J Kruse, W Ertmer, J Arlt, K Sacha, J Zakrzewski, and M Lewenstein. Routes towards anderson-like localization of bose-einstein condensates in disordered optical lattices. *Phys. Rev. Lett.*, 95:170411, 2005.

[71] T Schulte, S Drenkelforth, J Kruse, R Tiemeyer, K Sacha, J Zakrzewski, M Lewenstein, W Ertmer, and J J Arlt. Analysis of localization phenomena in weakly interacting disordered lattice gases. *New Journal of Physics*, 8(10):230, 2006.

[72] R C Kuhn, C Miniatura, D Delande, O Sigwarth, and C A Müller. Localization of matter waves in two-dimensional disordered optical potentials. *Phys. Rev. Lett.*, 95:250403, 2005.

[73] T Paul, P Leboeuf, N Pavloff, K Richter, and P Schlagheck. Nonlinear transport of bose-einstein condensates through waveguides with disorder. *Phys. Rev. A*, 72:063621, 2005.

[74] S Lellouch and L Sanchez-Palencia. Localization transition in weakly interacting bose superfluids in one-dimensional quasiperdiodic lattices. *Phys. Rev. A*, 90:061602, 2014.

[75] P Lugan, D Clément, P Bouyer, A Aspect, M Lewenstein, and L Sanchez-Palencia. Ultracold bose gases in 1d disorder: From lifshits glass to bose-einstein condensate. *Phys. Rev. Lett.*, 98:170403, 2007.

[76] L Sanchez-Palencia and M Lewenstein. Disordered quantum gaes under control. *Nature Physics*, 6(2):87–95, 2010.

[77] T. Claeson and P. Delsing (Eds.). Condensation and coherence in condensed systems. 2001.

[78] W Hofstetter, J I Cirac, P Zoller, E Demler, and M D Lukin. High-temperature superfluidity of fermionic atoms in optical lattices. *Phys. Rev. Lett.*, 89:220407, 2002.

[79] A Koetsier, D B M Dickerscheid, and H T C Stoof. Bec-bcs crossover in an optical lattice. *Phys. Rev. A*, 74:033621, 2006.

[80] T Stöferle, H Moritz, K Günter, M Köhl, and T Esslinger. Molecules of fermionic atoms in an optical lattice. *Phys. Rev. Lett.*, 96:030401, 2006.

[81] M Köhl, H Moritz, T Stöferle, K Günter, and T Esslinger. Fermionic atoms in a three dimensional optical lattice: Observing fermi surfaces, dynamics, and interactions. *Phys. Rev. Lett.*, 94:080403, 2005.

[82] K Günter, T Stöferle, H Moritz, M Köhl, and T Esslinger. Bose-fermi mixtures in a three-dimensional optical lattice. *Phys. Rev. Lett.*, 96:180402, 2006.

[83] S Ospelkaus, C Ospelkaus, O Wille, M Succo, P Ernst, K Sengstock, and K Bongs. Localization of bosonic atoms by fermionic impurities in a three-dimensional optical lattice. *Phys. Rev. Lett.*, 96:180403, 2006.

[84] B. Douçot, M. V. Feigel'man, L. B. Ioffe, and A. S. Ioselevich. Protected qubits and chern-simons theories in josephson junction arrays. *Phys. Rev. B*, 71:024505, 2005.

[85] A Kitaev. Anyons in an exactly solved model and beyond. *Annals of Physics*, 321(1):2 – 111, 2006. January Special Issue.

[86] O Kinouchi and M Copelli. Optimal dynamical range of excitable networks at criticality. *Nat Phys*, 2(5):348–351, 2006.

[87] A Micheli, G K Brennen, and P Zoller. A toolbox for lattice-spin models with polar molecules. *Nat Phys*, 2(5):341–347, 2006.

[88] R B Laughlin. Anomalous quantum hall effect: An incompressible quantum fluid with fractionally charged excitations. *Phys. Rev. Lett.*, 50:1395–1398, 1983.

[89] L Jacak, P Sitko, K Wieczorek, and A Wójs. *Quantum Hall Systems: Braid Groups, Composite Fermions, and Fractional Charge (International Series of Monographs on Physics 119)*. International Series of Monographs on Physics 119. Oxford University Press, USA, 2003.

[90] N K Wilkin and J M F Gunn. Condensation of "composite bosons" in a rotating bec. *Phys. Rev. Lett.*, 84:6–9, 2000.

[91] B Paredes, P Fedichev, J I Cirac, and P Zoller. $\frac{1}{2}$-anyons in small atomic bose-einstein condensates. *Phys. Rev. Lett.*, 87:010402, 2001.

[92] N R Cooper, N K Wilkin, and J M F Gunn. Quantum phases of vortices in rotating bose-einstein condensates. *Phys. Rev. Lett.*, 87:120405, 2001.

[93] K W Madison, F Chevy, W Wohlleben, and J Dalibard. Vortex formation in a stirred bose-einstein condensate. *Phys. Rev. Lett.*, 84:806–809, 2000.

[94] R N Palmer and D Jaksch. High-field fractional quantum hall effect in optical lattices. *Phys. Rev. Lett.*, 96:180407, 2006.

[95] A S Sørensen, E Demler, and M D Lukin. Fractional quantum hall states of atoms in optical lattices. *Phys. Rev. Lett.*, 94:086803, 2005.

[96] E J Mueller. Artificial electromagnetism for neutral atoms: Escher staircase and laughlin liquids. *Phys. Rev. A*, 70:041603, 2004.

[97] D Jaksch and P Zoller. Creation of effective magnetic fields in optical lattices: the hofstadter butterfly for cold neutral atoms. *New Journal of Physics*, 5(1):56, 2003.

[98] M Greiner, O Mendel, T Esslinger, T W Hansch, and I Bloch. Quantum phase transition from a superfluid to a mott insulator in a gas of ultracold atoms. *Nature*, 415(6867):39–44, 2002.

[99] I Bloch. Ultracold quantum gases in optical lattices. *Nature Phsysics*, 1:23–30, 2005.

[100] J Hecker Denschlag, J E Simsarian, H Haffner, C McKenzie, A Browaeys, D Cho, K Helmerson, S L Rolston, and W D Phillips. A bose-einstein condensate in an optical lattice. *Journal of Physics B: Atomic, Molecular and Optical Physics*, 35(14):3095, 2002.

[101] T Stöferle, H Moritz, C Schori, M Köhl, and T Esslinger. Transition from a strongly interacting 1d superfluid to a mott insulator. *Phys. Rev. Lett.*, 92:130403, 2004.

[102] E Haller, R Hart, M J Mark, J G Danzl, L Reichsollner, M Gustavsson, M Dalmonte, G Pupillo, and H-C Nagerl. Pinning quantum phase transition for a luttinger liquid of strongly interacting bosons. 466(7306):597–600, 2010.

[103] M Greiner, I Bloch, O Mandel, T W Hänsch, and T Esslinger. Exploring phase coherence in a 2d lattice of bose-einstein condensates. *Phys. Rev. Lett.*, 87:160405, 2001.

[104] M Greiner and S Folling. Condensed-matter physics: Optical lattices. *Nature*, 453(7196):736–738, 2008.

[105] J Hubbard. Electron correlations in narrow energy bands. *Proceedings of the Royal Society of London A: Mathematical, Physical and Engineering Sciences*, 276(1365):238–257, 1963.

[106] T Esslinger. Fermi-hubbard physics with atoms in an optical lattice. *Annual Review of Condensed Matter Physics*, 1(1):129–152, 2010.

[107] I Bloch. Quantum coherence and entanglement with ultracold atoms in optical lattices. *Nature*, 453(7198):1016–1022, 2008.

[108] M Lewenstein, A Sanpera, V Ahufinger, B Damski, A Sen(De), and U Sen. Ultracold atomic gases in optical lattices: mimicking condensed matter physics and beyond. *Advances in Physics*, 56(2):243–379, 2007.

[109] D Jaksch and P Zoller. The cold atom hubbard toolbox. *Annals of Physics*, 315(1):52 – 79, 2005. Special Issue.

[110] A Auerbach. *Interacting electrons and quantum magnetism*. Graduate texts in contemporary physics. Springer-Verlag, 1994.

[111] A V Gorshkov, A M Rey, A J Daley, M M Boyd, J Ye, P Zoller, and M D Lukin. Alkaline-earth-metal atoms as few-qubit quantum registers. *Phys. Rev. Lett.*, 102:110503, 2009.

[112] M Lewenstein, L Santos, M A Baranov, and H Fehrmann. Atomic bose-fermi mixtures in an optical lattice. *Phys. Rev. Lett.*, 92:050401, 2004.

[113] A B Kuklov and B V Svistunov. Counterflow superfluidity of two-species ultracold atoms in a commensurate optical lattice. *Phys. Rev. Lett.*, 90:100401, 2003.

[114] J Wehr, A Niederberger, L Sanchez-Palencia, and M Lewenstein. Disorder versus the mermin-wagner-hohenberg effect: From classical spin systems to ultracold atomic gases. *Phys. Rev. B*, 74:224448, 2006.

[115] P Rabl, A J Daley, P O Fedichev, J I Cirac, and P Zoller. Defect-suppressed atomic crystals in an optical lattice. *Phys. Rev. Lett.*, 91:110403, 2003.

[116] M Popp, J-J Garcia-Ripoll, K G H Vollbrecht, and J I Cirac. Ground-state cooling of atoms in optical lattices. *Phys. Rev. A*, 74:013622, 2006.

[117] M Popp, J-J Garcia-Ripoll, K G H Vollbrecht, and J I Cirac. Cooling toolbox for atoms in optical lattices. *New Jour of Phys*, 8(8):164, 2006.

[118] A Griessner, A J Daley, D Jaksch, and P Zoller. Fault-tolerant dissipative preparation of atomic quantum registers with fermions. *Phys. Rev. A*, 72:032332, 2005.

[119] H Häffner, C F Roos, and R Blatt. Quantum computing with trapped ions. *Physics Reports*, 469(4):155 – 203, 2008.

[120] R Blatt and D Wineland. Entangled states of trapped atomic ions. *Nature*, 453(1008):1008–1015, 2008.

[121] J I Cirac and P Zoller. Quantum computations with cold trapped ions. *Phys. Rev. Lett.*, 74:4091–4094, 1995.

[122] D Porras and J I Cirac. Effective quantum spin systems with trapped ions. *Phys. Rev. Lett.*, 92:207901, 2004.

[123] M Johanning, A F Varón, and C Wunderlich. Quantum simulations with cold trapped ions. *Journal of Physics B: Atomic, Molecular and Optical Physics*, 42(15):154009, 2009.

[124] R Islam, E E Edwards, K Kim, S Korenblit, C Noh, H Carmichael, G-D Lin, L-M Duan, C-C Joseph Wang, J K Freericks, and C Monroe. Onset of a quantum phase transition with a trapped ion quantum simulator. *Nature Communications*, 2:377, 2011.

[125] K Kim, S Korenblit, R Islam, E E Edwards, M-S Chang, C Noh, H Carmichael, G-D Lin, L-M Duan, C C Joseph Wang, J K Freericks, and C Monroe. Quantum simulation of the transverse ising model with trapped ions. *New Journal of Physics*, 13(10):105003, 2011.

[126] S Sachdev. *Quantum Phase Transitions*. Cambridge University Press, 2001.

[127] H J Metcalf and P van der Straten. *Laser cooling and trapping*. Graduate texts in contemporary physics. Springer, corrected edition, 1999.

[128] J Reichel and V Vuletic. *Atom Chips*. Wiley-VCH, 2011.

[129] R Folman, P Krüger, D Cassettari, B Hessmo, T Maier, and J Schmiedmayer. Controlling cold atoms using nanofabricated surfaces: Atom chips. *Phys. Rev. Lett.*, 84:4749–4752, 2000.

[130] A L Gaunt, T F Schmidutz, I Gotlibovych, R P Smith, and Z Hadzibabic. Bose-einstein condensation of atoms in a uniform potential. *Phys. Rev. Lett.*, 110:200406, 2013.

[131] A Ramanathan, K C Wright, S R Muniz, M Zelan, W T Hill, C J Lobb, K Helmerson, W D Phillips, and G K Campbell. Superflow in a toroidal bose-einstein condensate: An atom circuit with a tunable weak link. *Phys. Rev. Lett.*, 106:130401, 2011.

[132] M Taglieber, A-C Voigt, T Aoki, T W Hänsch, and K Dieckmann. Quantum degenerate two-species fermi-fermi mixture coexisting with a bose-einstein condensate. *Phys. Rev. Lett.*, 100:010401, 2008.

[133] F Schreck, L Khaykovich, K L Corwin, G Ferrari, T Bourdel, J Cubizolles, and C Salomon. Quasipure bose-einstein condensate immersed in a fermi sea. *Phys. Rev. Lett.*, 87:080403, 2001.

[134] S Will, T Best, U Schneider, L Hackermuller, D-S Luhmann, and I Bloch. Time-resolved observation of coherent multi-body interactions in quantum phase revivals. *Nature*, 465(7295):197–201, 2010.

[135] C N Weiler, T W Neely, D R Scherer, A S Bradley, M J Davis, and B P Anderson. Spontaneous vortices in the formation of bose-einstein condensates. *Nature*, 455(7215):948–951, 2008.

[136] G Lamporesi, S Donadello, S Serafini, F Dalfovo, and G Ferrari. Spontaneous creation of kibble-zurek solitons in a bose-einstein condensate. *Nature Physics*, 9(10):656–660, 2013.

[137] W H Zurek. Cosmological experiments in superfluid helium? *Nature*, 317(6037):505–508, 1985.

[138] J Eisert, M Cramer, and M B Plenio. *Colloquium* : Area laws for the entanglement entropy. *Rev. Mod. Phys.*, 82:277–306, 2010.

[139] W S Bakr, A Peng, M E Tai, R Ma, J Simon, J I Gillen, S Fölling, L Pollet, and M Greiner. Probing the superfluid–to–mott insulator transition at the single-atom level. *Science*, 329(5991):547–550, 2010.

[140] J F Sherson, C Weitenberg, M Endres, M Cheneau, I BLoch, and S Kuhr. Single-atom-resolved flourescence imaging of an atomic mott insulator. *Nature*, 467(7311):68–72, 2010.

[141] R Bücker, A Perrin, S Manz, T Betz, Ch Koller, T Plisson, J Rottmann, T Schumm, and J Schmiedmayer. Single-particle-sensitive imaging of freely propagating ultracold atoms. *New Journal of Physics*, 11(10):103039, 2009.

[142] R Bucker, J Grond, S Manz, T Berrada, T Betz, C Koller, U Hohenester, T Schumm, A Perrin, and J Schmiedmayer. Twin-atom beams. *Nature Physics*, 7(8), 2011.

[143] C Gross, H Strobel, E Nicklas, T Zibold, N Bar-Gill, G Kurizki, and M K Oberthaler. Atomic homodyne detection of continuous variable entanglement twin-atom states. *Nature*, 480(7376):219–223.

[144] B Lücke, M Scherer, J Kruse, L Pezzé, F Deuretzbacher, P Hyllus, O Topic, J Peise, W Ertmer, J Arlt, L Santos, A Smerzi, and C Klempt. Twin matter waves for interferometry beyond the classical limit. *Science*, 334(6057):773–776, 2011.

[145] T Berreda, S van Frank, R Bücker, T Schumm, J F Schaff, and J Schmiedmayer. Integrated mach zehnder interferometer for bose einstein condensates. *Nature communication*, 4, 2013.

[146] C Gross, T Zibold, E Nicklas, J Esteve, and M K Oberthaler. Nonlinear atom interferometer surpasses classical precision limit. *Nature*, 464(7292):1165–1169, 2010.

[147] M F Riedel, Y Li, T W Hänsch, A Sinatra, and P Treutlein. Atom-chip-based generation of entanglement for quantum metrology. *Nature*, 464(7292):1170–1173, 2010.

[148] M Gring, M Kuhnert, T Langen, T Kitagawa, B Rauer, M Schreitl, I Mazets, D A Smith, E Demler, and J Schmiedmayer. Relaxation and prethermalization in an isolated quantum system. *Science*, 337(6100):1318–1322, 2012.

[149] M Kuhnert, R Geiger, T Langen, M Gring, B Rauer, T Kitagawa, E Demler, D Adu Smith, and J Schmiedmayer. Multimode dynamics and emergence of a characteristic length scale in a one-dimensional quantum system. *Phys. Rev. Lett.*, 110:090405, 2013.

[150] T Langen, M Gring, M Kuhnert, B Rauer, R Geiger, D Adu Smith, I E Mazets, and J Schmiedmayer. Prethermalization in one-dimensional bose gases: Description by a stochastic ornstein-uhlenbeck process. *The European Physical Journal Special Topics*, 217(1):43–53, 2013.

[151] D Adu Smith, M Gring, T Langen, M Kuhnert, B Rauer, R Geiger, T Kitagawa, I Mazets, E Demler, and J Schmiedmayer. Prethermalization revealed by the relaxation dynamics of full distribution functions. *New Journal of Physics*, 15(7):075011, 2013.

[152] J Berges, S Borsányi, and C Wetterich. Prethermalization. *Phys. Rev. Lett.*, 93:142002, 2004.

[153] C-L Hung, V Gurarie, and C Chin. From cosmology to cold atoms: Observation of sakharov oscillations in a quenched atomic superfluid. *Science*, 341(6151):1213–1215, 2013.

[154] S Sachdev, K Sengupta, and S M Girvin. Mott insulators in strong electric fields. *Phys. Rev. B*, 66:075128, 2002.

[155] J Simon, W S Bakr, R Ma, M E Tai, P M Preiss, and M Greiner. Quantum simulation of antiferromagnetic spin chains in an optical lattice. *Nature*, 472(7343):307–312, 2011.

[156] F Meinert, M J Mark, E Kirilov, K Lauber, P Weinmann, A J Daley, and H-C Nägerl. Quantum quench in an atomic one-dimensional ising chain. *Phys. Rev. Lett.*, 111:053003, 2013.

[157] F Meinert, M J Mark, E Kirilov, K Lauber, P Weinmann, M Gröbner, A J Daley, and H-C Nägerl. Observation of many-body dynamics in long-range tunneling after a quantum quench. *Science*, 344(6189):1259–1262, 2014.

[158] E H Lieb and D W Robinson. The finite group velocity of quantum spin systems. *Comm. Math. Phys.*, 28(3):251–257, 1972.

[159] A Einstein, B Podolsky, and N Rosen. Can quantum-mechanical description of physical reality be considered complete? *Phys. Rev.*, 47:777–780, 1935.

[160] A Fine. Hidden variables, joint probability, and the bell inequalities. *Phys. Rev. Lett.*, 48:291–295, 1982.

[161] P Calabrese and J Cardy. Time dependence of correlation functions following a quantum quench. *Phys. Rev. Lett.*, 96:136801, Apr 2006.

[162] P Di Francesco, P Mathieu, and D Senechal. *Conformal Field Theory.* (Graduate Texts in Contemporary Physics). Springer, 1996.

[163] M B Hastings. Locality in Quantum Systems. *arXiv:1008.5137 [math-ph]*, 2010.

[164] M B Hastings and T Koma. Spectral gap and exponential decay of correlations. *Communications in Mathematical Physics*, 265(3):781–804, 2006.

[165] D M Storch, M van den Worm, and M Kastner. Interplay of soundcone and supersonic propagation in lattice models with power law interactions. *New Journal of Physics*, 17(6):063021, 2015.

[166] M Foss-Feig, Z-X Gong, C W Clark, and A V Gorshkov. Nearly linear light cones in long-range interacting quantum systems. *Phys. Rev. Lett.*, 114:157201, 2015.

[167] T Matsuta, T Koma, and S Nakamura. Improving the Lieb-Robinson bound for long-range interactions. *ArXiv e-prints*, April 2016.

[168] J Eisert, M van den Worm, S R Manmana, and M Kastner. Breakdown of quasilocality in long-range quantum lattice models. *Phys. Rev. Lett.*, 111:260401, 2013.

[169] P Hauke and L Tagliacozzo. Spread of correlations in long-range interacting quantum systems. *Phys. Rev. Lett.*, 111:207202, 2013.

[170] L Cevolani, G Carleo, and L Sanchez-Palencia. Spreading of correlations in exactly solvable quantum models with long-range interactions in arbitrary dimensions. *New Journal of Physics*, 18(9):093002, 2016.

[171] M Van Regemortel, D Sels, and M Wouters. Information propagation and equilibration in long-range kitaev chains. *Phys. Rev. A*, 93:032311, 2016.

[172] J Schachenmayer, A Pikovski, and A M Rey. Dynamics of correlations in two-dimensional quantum spin models with long-range interactions: a phase-space monte-carlo study. *New Journal of Physics*, 17(6):065009, 2015.

[173] A S Buyskikh, M Fagotti, J Schachenmayer, F H L Essler, and A J Daley. Entanglement growth and correlation spreading with variable-range interactions in spin and fermionic tunnelling models. *ArXiv:1601.02106*, 2016.

[174] J V Neumann. Beweis des ergodensatzes und desh-theorems in der neuen mechanik. *Zeitschrift für Physik*, 57(1):30–70, 1929.

[175] S Goldstein, L J Lebowitz, R Tumulka, and N Zanghì. Long-time behavior of macroscopic quantum systems. *The European Physical Journal H*, 35(2):173–200, 2010.

[176] P Mazur. Non-ergodicity of phase functions in certain systems. *Physica*, 43(4):533 – 545, 1969.

[177] A Peres. Ergodicity and mixing in quantum theory. i. *Phys. Rev. A*, 30:504–508, 1984.

[178] J Cardy. Thermalization and revivals after a quantum quench in conformal field theory. *Phys. Rev. Lett.*, 112:220401, 2014.

[179] P Reimann. Foundation of statistical mechanics under experimentally realistic conditions. *Phys. Rev. Lett.*, 101:190403, 2008.

[180] T Kinoshita, T Wenger, and D S Weiss. A quantum newton's cradle. *Nature*, 440(7086):900–903, 2006.

[181] M D Girardeau. Decay of magnetization in the one-dimensional xy model. *Physics Letters A*, 30(8):442 – 443, 1969.

[182] M D Girardeau. Relaxation of localized magnetization in the one-dimensional xy model. *Physics Letters A*, 32(2):67 – 68, 1970.

[183] E Barouch, B M McCoy, and M Dresden. Statistical mechanics of the XY model. i. *Phys. Rev. A*, 2:1075–1092, 1970.

[184] T Barthel and U Schollwöck. Dephasing and the steady state in quantum many-particle systems. *Phys. Rev. Lett.*, 100:100601, 2008.

[185] M Cramer and J Eisert. A quantum central limit theorem for non-equilibrium systems: exact local relaxation of correlated states. *New Journal of Physics*, 12(5):055020, 2010.

[186] P Jordan and E Wigner. Über das paulische äquivalenzverbot. *Zeitschrift für Physik*, 47(9):631–651, 1928.

[187] M Rigol, V Dunjko, v Yurovsky, and M Olshanii. Relaxation in a completely integrable many-body quantum system: An *Ab Initio* study of the dynamics of the highly excited states of 1d lattice hard-core bosons. *Phys. Rev. Lett.*, 98:050405, 2007.

[188] E T Jaynes. Information theory and statistical mechanics. *Phys. Rev.*, 106:620–630, 1957.

[189] M A Cazalilla. Effect of suddenly turning on interactions in the luttinger model. *Phys. Rev. Lett.*, 97:156403, 2006.

[190] A Iucci and M A Cazalilla. Quantum quench dynamics of the luttinger model. *Phys. Rev. A*, 80:063619, 2009.

[191] S Sotiriadis and P Calabrese. Validity of the gge for quantum quenches from interacting to noninteracting models. *Journal of Statistical Mechanics: Theory and Experiment*, 2014(7):P07024, 2014.

[192] S Sotiriadis and G Martelloni. Equilibration and gge in interacting-to-free quantum quenches in dimensions $d > 1$. *Journal of Physics A: Mathematical and Theoretical*, 49(9):095002, 2016.

[193] J-S Caux and F H L Essler. Time evolution of local observables after quenching to an integrable model. *Phys. Rev. Lett.*, 110:257203, 2013.

[194] J De Nardis, L Piroli, and J-S Caux. Relaxation dynamics of local observables in integrable systems. *Journal of Physics A: Mathematical and Theoretical*, 48(43):43FT01, 2015.

[195] M Brockmann, B Wouters, D Fioretto, J De Nardis, R Vlijm, and J-S Caux. Quench action approach for releasing the néel state into the spin-1/2 xxz chain. *Journal of Statistical Mechanics: Theory and Experiment*, 2014(12):P12009, 2014.

[196] F H L Essler and M Fagotti. Quench dynamics and relaxation in isolated integrable quantum spin chains. *Journal of Statistical Mechanics: Theory and Experiment*, 2016(6):064002, 2016.

[197] M Fagotti. On conservation laws, relaxation and pre-relaxation after a quantum quench. *Journal of Statistical Mechanics: Theory and Experiment*, 2014(3):P03016, 2014.

[198] M Fagotti, M Collura, F H L Essler, and P Calabrese. Relaxation after quantum quenches in the spin-$\frac{1}{2}$ heisenberg xxz chain. *Phys. Rev. B*, 89:125101, 2014.

[199] M Kollar and M Eckstein. Relaxation of a one-dimensional mott insulator after an interaction quench. *Phys. Rev. A*, 78:013626, 2008.

[200] M Eckstein and M Kollar. Near-adiabatic parameter changes in correlated systems: influence of the ramp protocol on the excitation energy. *New Journal of Physics*, 12(5):055012, 2010.

[201] B Bertini and M Fagotti. Pre-relaxation in weakly interacting models. *Journal of Statistical Mechanics: Theory and Experiment*, 2015(7):P07012, 2015.

[202] E Kaminishi, T Mori, T N Ikeda, and M Ueda. Entanglement pre-thermalization in a one-dimensional bose gas. *Nature Physics*, 11(12):1050–1056, 2015.

[203] E H Lieb and W Liniger. Exact analysis of an interacting bose gas. i. the general solution and the ground state. *Phys. Rev.*, 130:1605–1616, 1963.

[204] E H Lieb. Exact analysis of an interacting bose gas. ii. the excitation spectrum. *Phys. Rev.*, 130:1616–1624, 1963.

[205] M Girardeau. Relationship between systems of impenetrable bosons and fermions in one dimension. *Journal of Mathematical Physics*, 1(6):516–523, 1960.

[206] A D Cronin, J Schmiedmayer, and D E Pritchard. Optics and interferometry with atoms and molecules. *Rev. Mod. Phys.*, 81:1051–1129, 2009.

[207] M Rigol. Breakdown of thermalization in finite one-dimensional systems. *Phys. Rev. Lett.*, 103:100403, 2009.

[208] S Trotzky, Y-A Chen, A Flesch, I P McCulloch, U Schwollwock, J Eisert, and I Bloch. Probing the relaxation towards equilibrium in an isolates strongly correlated one-dimensional bose gas. *Nature*, 8(4):325–330, 2012.

[209] S Fölling, S Trotky, P Cheinet, M Feld, R Saers, A Widera, T Muller, and I Bloch. Direct observation of second-order atom tunneling. *Nature*, 448(7157), 2006.

[210] J Sebby-Strabley, M Anderlini, P S Jessen, and J V Porto. Lattice of double wells for manipulating pairs of cold atoms. *Phys. Rev. A*, 73:033605, 2006.

[211] M Cramer, A Flesch, I P McCulloch, U Schollwöck, and J Eisert. Exploring local quantum many-body relaxation by atoms in optical superlattices. *Phys. Rev. Lett.*, 101:063001, 2008.

[212] A Flesch, M Cramer, I P McCulloch, U Schollwöck, and J Eisert. Probing local relaxation of cold atoms in optical superlattices. *Phys. Rev. A*, 78:033608, Sep 2008.

[213] S Bravyi, M B Hastings, and F Verstraete. Lieb-robinson bounds and the generation of correlations and topological quantum order. *Phys. Rev. Lett.*, 97:050401, 2006.

[214] M Cheneau, P Barmettler, D Poletti, M Endres, P Schausz, T Fukuhara, C Gross, I Bloch, C Kollath, and S Kuhr. Light-cone like spreading of correlations in a quantum many-body system. *Nature*, 481(7382):484–487, 2012.

[215] S R Manmana, S Wessel, R M Noack, and A Muramatsu. Time evolution of correlations in strongly interacting fermions after a quantum quench. *Phys. Rev. B*, 79:155104, 2009.

[216] G Carleo, F Becca, L Sanchez-Palencia, S Sorella, and M Fabrizio. Light-cone effect and supersonic correlations in one- and two-dimensional bosonic superfluids. *Phys. Rev. A*, 89:031602, 2014.

[217] J De Nardis, B Wouters, M Brockmann, and J-S Caux. Solution for an interaction quench in the lieb-liniger bose gas. *Phys. Rev. A*, 89:033601, 2014.

[218] B Nachtergaele and R Sims. Lieb-robinson bounds and the exponential clustering theorem. *Communications in Mathematical Physics*, 265(1):119–130, 2006.

[219] E F Krause. *Taxicab Geometry: an adventure in non-Euclidean geometry.* Dover Publications, 1987.

[220] L Bonnes, F H L Essler, and A M Läuchli. "light-cone" dynamics after quantum quenches in spin chains. *Phys. Rev. Lett.*, 113:187203, 2014.

[221] G De Chiara, S Montangero, P Calabrese, and R Fazio. Entanglement entropy dynamics of heisenberg chains. *Journal of Statistical Mechanics: Theory and Experiment*, 2006(03):P03001, 2006.

[222] P Calabrese, F H L Essler, and M Fagotti. Quantum quench in the transverse-field ising chain. *Phys. Rev. Lett.*, 106:227203, 2011.

[223] E Barouch and B M McCoy. Statistical mechanics of the XY model. iii. *Phys. Rev. A*, 3:2137–2140, 1971.

[224] J M Zhang, C Shen, and W M Liu. Quantum quench dynamics of the bose-hubbard model at finite temperatures. *Phys. Rev. A*, 83:063622, Jun 2011.

[225] A M Läuchli and C Kollath. Spreading of correlations and entanglement after a quench in the one-dimensional bose hubbard model. *Journal of Statistical Mechanics: Theory and Experiment*, 2008(05):P05018, 2008.

[226] M Collura, P Calabrese, and F H L Essler. Quantum quench within the gapless phase of the spin $-\frac{1}{2}$ heisenberg xxz spin chain. *Phys. Rev. B*, 92:125131, 2015.

[227] C Kollath, A M Läuchli, and E Altman. Quench dynamics and nonequilibrium phase diagram of the bose-hubbard model. *Phys. Rev. Lett.*, 98:180601, 2007.

[228] R P Feynman. Space-time approach to non-relativistic quantum mechanics. *Rev. Mod. Phys.*, 20:367–387, 1948.

[229] J L Cardy and D C Lewellen. Bulk and boundary operators in conformal field theory. *Physics Letters B*, 259(3):274 – 278, 1991.

[230] P Calabrese and J Cardy. Quantum quenches in 1+1 dimensional conformal field theories. *Journal of Statistical Mechanics: Theory and Experiment*, 2016(6):064003, 2016.

[231] M Srednicki. Entropy and area. *Phys. Rev. Lett.*, 71:666–669, 1993.

[232] M A Cazalilla and J B Marston. Time-dependent density-matrix renormalization group: A systematic method for the study of quantum many-body out-of-equilibrium systems. *Phys. Rev. Lett.*, 88:256403, 2002.

[233] H Bethe. Zur theorie der metalle. *Zeitschrift für Physik*, 71(3):205–226, 1931.

[234] F Pellegrini, S Montangero, G E Santoro, and R Fazio. Adiabatic quenches through an extended quantum critical region. *Phys. Rev. B*, 77:140404, Apr 2008.

[235] S Yamada, M Okumura, T Imamura, and M Machida. Direct extension of the density-matrix renormalization group method toward two-dimensional large quantum lattices and related high-performance computing. *Japan Journal of Industrial and Applied Mathematics*, 28(1):141–151, 2011.

[236] F Verstraete and J I Cirac. Continuous matrix product states for quantum fields. *Phys. Rev. Lett.*, 104:190405, 2010.

[237] L Cevolani and L Sanchez-Palencia. In preparation. 2017.

[238] T Langen, R Geiger, M Kuhnert, B Rauer, and J Schmiedmayer. Local emergence of thermal correlations in an isolated quantum many-body system. *nature Physics*, 9(10):640–643.

[239] M van den Worm, B C Sawyer, J J Bollinger, and M Kastner. Relaxation timescales and decay of correlations in a long-range interacting quantum simulator. *New Journal of Physics*, 15(8):083007, 2013.

[240] M Kastner. Entanglement-enhanced spreading of correlations. *New Journal of Physics*, 17(12):123024, 2015.

[241] T Holstein and H Primakoff. Field dependence of the intrinsic domain magnetization of a ferromagnet. *Phys. Rev.*, 58:1098–1113, Dec 1940.

[242] A L Fetter and J D Walecka. *Quantum Theory of Many-Particle Systems*. Dover Books on Physics. Dover Publications, 2003.

[243] S Trotzky, P Cheinet, S Fölling, M Feld, U Schnorrberger, A M Rey, A Polkovnikov, E A Demler, M D Lukin, and I Bloch. Time-resolved observation and control of superexchange interactions with ultracold atoms in optical lattices. *Science*, 319(5861):295–299, 2008.

[244] T Langen, R Geiger, and J Schmiedmayer. Ultracold atoms out of equilibrium. *Annual Review of Condensed Matter Physics*, 6(1):201–217, 2015.

[245] R Geiger, T Langen, I E Mazets, and J Schmiedmayer. Local relaxation and light-cone-like propagation of correlations in a trapped one-dimensional bose gas. *New Journal of Physics*, 16(5):053034, 2014.

[246] M Abramowitz and I A Stegun. *Handbook of mathematical functions*. NBS, 1972.

université PARIS-SACLAY

ÉCOLE DOCTORALE
Ondes et Matière (EDOM)

Titre : Localité et dynamique hors equilibre dans systemes quantiques avec interaction de longue porté

Mots clés : *Dynamique-hors-de-l'equilibre, Propagation des correlatons, Atoms ultra froids, Systèmes quantiques fortement corrélés*

Résumé : Cette thèse présente une étude des propagations des corrélations dans les systèmes avec interaction de longue portée. La dynamique des observables locales ne peut pas être décrite avec les méthodes utilisées pour la physique statistique à l'équilibre et les approches complètement nouvelles doivent être développées. Différentes bornes sur l'évolution temporelle des corrélations ont été dérivées, mais la dynamique réelle trouvée dans des données expérimentales et numériques est beaucoup plus compliquée avec différents régimes de propagation. Une approche plus spécifique est donc nécessaire pour comprendre ces phénomènes. Nous présentons une méthode analytique pour décrire l'évolution temporelle d'observables génériques dans des systèmes décrits par des hamiltoniens quadratiques avec interactions de courte et longue portée. Grâce ces expressions, la propagation des observables peut être interprétée comme la propagation des excitations du système. Nous appliquons cette méthode générique à un modèle de spins et on obtient trois régimes différents. Ils peuvent être directement expliqués qualitativement et quantitativement par les divergences du spectre des excitations. Le résultat le plus important est le fait que la propagation, là où elle n'est pas instantanée, est au plus balistique, voir plus lente, alors les bornes permettent une propagation significativement plus rapide. On applique les mêmes expressions analytiques à un système de bosons sur un réseau avec interaction de longue et courte portée. Nous étudions les corrélations à deux corps qui ont un comportement toujours balistique et les corrélations à un corps qui ont un comportement plus riche. Cet effet peut être expliqué en calculant la contribution aux deux observables des différentes excitations qui déterminent les parties du spectre contribuant à l'observable. Ces résultats démontrent que la propagation des observables n'est pas déterminée uniquement par le spectre des excitations mais également par des quantités qui dépendent de l'observable et qui peuvent changer complètement le régime de propagation.

Title : Out-Of-Equilibrium Dynamics and Locality in long-range Many-Body Quantum Systems

Keywords : *Out-of-equilibrium dynamics, Spreading of correlations, Ultra-Cold atoms, Strongly correlated quantum systems*

Abstract : In this thesis we present our results on the propagation of correlations in long-range interacting quantum systems. The dynamics of local observables in these systems cannot be described with the standard methods used in equilibrium statistical physics and completely new methods have to be developed. Several bounds on the time evolution of correlations have been derived for these systems. However the propagation found in experimental and numerical results is completely different and several regimes are present depending on the long-range character of the interactions. Here we present analytical expressions to describe the time evolution of generic observables in systems where the Hamiltonian takes a quadratic form with long- and short-range interactions. These expressions describe the spreading of local observables as the spreading of the fundamental excitations of the system. We apply these expressions to a spin model finding three different propagation regimes. They can be described qualitatively et quantitatively by the divergences in the energy spectrum. The most important result is that the propagation is at most ballistic, but it can be also significantly slower, where the general bounds predict a propagation faster than ballistic. This points out that the bounds are not able to describe properly the propagation, but a more specific approach is needed. We then move to a system of lattice bosons interacting via long-range interactions. In this case we study two different observables finding completely different results for the same interactions: the spreading of two-body correlations is always ballistic while the one of the one-body correlations ranges from faster-than-ballistic to ballistic. Using our general analytic expressions we find that different parts of the spectrum contribute differently to different observables determining the previous differences. This points out that an observable-dependent notion of locality, missing in the general bounds, have to be developed to correctly describe the time evolution.

Université Paris-Saclay
Espace Technologique / Immeuble Discovery
Route de l'Orme aux Merisiers RD 128 / 91190 Saint-Aubin, France